

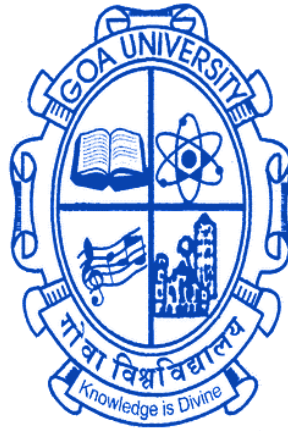
Triple-Oxygen and Hydrogen Isotope based Climate Reconstruction using Ice Core Records from Coastal Dronning Maud Land, East Antarctica

A Thesis submitted in partial fulfilment for the Degree of

DOCTOR OF PHILOSOPHY

IN THE SCHOOL OF EARTH, OCEAN, AND ATMOSPHERIC SCIENCES

GOA UNIVERSITY



By

TARIQ EJAZ

National Centre for Polar and Ocean Research

Headland Sada, Vasco da Gama, Goa, India-403804

&

School of Earth, Ocean, and Atmospheric Sciences

Goa University

Taleigao Plateau, Goa, India-403206

JANUARY 2023

DECLARATION

I, Tariq Ejaz, hereby declare that this thesis represents work that has been carried out by me and that it has not been submitted, either in part or full, to any other University or Institution for the award of any research degree.

Place: Goa University

Date: 15/03/2024

Tariq Ejaz





CERTIFICATE

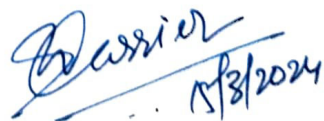
I hereby certify that the above Declaration of the candidate, Tariq Ejaz is true, and the work was carried out under my supervision.



Dr. Thamban Meloth
Research Supervisor
Director
National Centre for Antarctic & Ocean Research
Vasco-da-Gama, Goa 403 804



Dr. Kotha Mahender
Research co-supervisor
Professor
Dept. of Earth Science
Goa University
Taleigao, Goa 403 206



Acknowledgments

My deepest pleasure is to express my sincere gratitude to my supervisor, **Dr. Thamban Meloth, Director**, National Centre for Polar and Ocean Research, for his invaluable guidance, consistent support, and patience throughout my Ph.D. Research. His vast knowledge and wealth of experience helped me in my daily life and academic achievements. My journey in the Ice Core lab would not be complete without his motivation and inspiration.

I would also like to thank my co-supervisor, **Prof. Kotha Mahender**, whose continuous guidance have been of essential importance during my doctorate work. I thank **Dr. Waliur Rahaman** for his encouragement, guidance, and support throughout the research. I am grateful for his fruitful suggestions that improved my scientific knowledge and skills. I want to mention my immense thank to **Prof. G. N. Nayak**, Goa University, and **Dr. Sushant S. Naik**, National Institute of Oceanography, my DRC members, for constructive discussions and suggestions.

I acknowledge the **National Centre for Polar and Ocean Research** for providing academic and administrative support. I would like to convey my heartfelt gratitude to the former Director, of NCPOR, **Dr. M. Ravichandran**, Secretary, Ministry of Earth Science (MoES), for his support and encouragement during my research journey. I thank **Mr. Mirza Javed Beg**, **Dr. Rahul Mohan**, and **Dr. Laluraj CM** for their positivity and support, which helped my research and improved my social life. Ministry of Earth Sciences (MoES), Government of India, sincerely acknowledged for funding through the project “PACER-Cryosphere and Climate”. HRDG-CSIR is acknowledged for the NET/JRF fellowship. I am grateful to Vice-chancellor, Registrar, Dean, and all

Earth Science Department staff at Goa University for the doctorate thesis and all possible support. My sincere thanks to all the scientists and staff members of the NCPOR family.

My special thanks to Mr. Prashant Redkar, Mr. Ashish Painginkar, and Dr. Mahalinganathan for their immense support in ice core processing and analysis. I am grateful to my colleagues for the scientific support and technical assistance during the processing and analyses in the Ice Core Laboratory. My Special thanks to Mohammad Tarique, Alok Kumar Sinha, Mohammad Nuruzzama, Ashutosh Acharya, Vikram Goel, Syed Salim, Sunil Oulkar, Rahul Dey, Priyesh Prabhat, Ankit Pramanik, Bhanu Pratap, Lathika, Ajit Tapendre Singh, Milind Mutnale, Gautami Samui, Runa Antony, Kaveri Kumbar, Riya Naik, Aritri Sanyal, Kamini Meshram, Lavkush Patel, Girija Kalyani, Sibin Simon, Gayathri Eledath, and Shivam Sundram for motivation and support throughout the processes. I would like to thank Mohd Zuhair, Farooq Jafri, Naushad Ali, Masood Alam, Arisha Iqbal, Aditi Chatterjee, Rahul Mohan Bind, Mohammad Hammad, and Syed Hussian for their motivation.

Finally, I thank my parents, Shri Ejaz Ahmad, and Smt. Naushaba Khatoon, my grandparent, Late Haji Manzoor Ahmad, and Smt. Tahira Khatoon, my uncles Siraj Ahmad and Niyaz Ahmad, and my younger brothers Sharim Ejaz, Laraib Niyaz, and the rest of the family for their support and encouragement.

Tariq Ejaz

Dedicated to all my teachers and mentors

Abstract

Antarctic ice sheet is one of the most critical climate archives. The ice core records retrieved from the ice sheet plays a critical role in understanding the past climate on an annual to decadal timescale. Major climatic oscillations like El Niño Southern Oscillation (ENSO), Pacific Decadal Oscillation (PDO), Interdecadal Pacific Oscillation (IPO) and their phase relation with the Southern Annular Mode (SAM) largely control Antarctic climate variability. However, the relative roles of these climate modes remain elusive, particularly in the backdrop of global warming. To investigate the role of these climate modes in the Antarctic temperature variability, this study used a well-dated and annually resolved new ice core (IND33) collected as part of the Indian Scientific Expedition to Antarctica along with published ice core records (DML07, DML05, and DML17) of stable water isotopes ($\delta^{18}\text{O}$, δD) for the past two centuries (1809–2013 CE) from Dronning Maud Land (DML) in East Antarctica. The Principal Component Analysis (PCA) performed on the ice core records of the DML region unveils that the first principal component explaining the maximum variability ($\sim 32\%$) in $\delta^{18}\text{O}$ records is related to late spring to summer (Nov–Dec–Jan) temperature rather than the mean annual temperature. This indicates that reconstructed annual temperature based on Antarctic ice core $\delta^{18}\text{O}$ records in the DML region could be biased toward the temperature of the months/seasons of higher precipitation with low-moderate wind speed, which are suitable for better preservation of the ice core signals. This study reconstructed the DML temperature record of the past two centuries (1809–2019 CE) at an annual resolution based on the $\delta^{18}\text{O}$ ice core record (1809–1993 CE) combined with the recent ERA5 surface air temperature record (1994–2019 CE). The reconstructed temperature anomaly record reveals a significant cooling trend in the 19th century during 1809–1907 CE at a rate of $-0.164 \pm 0.045^\circ\text{C decade}^{-1}$ followed by a

warming trend from the mid-20th to early 21st century (1942–2019 CE) at a rate of $+0.452 \pm 0.056^{\circ}\text{C decade}^{-1}$. This long-term warming trend since the 1940s coincides with the increase in ENSO events and its strong anti-phase relation with SAM, suggesting an increasing influence of SAM–ENSO coupling in modulating the DML temperature in recent decades.

Sea ice around the Antarctic continent is a critical component other than temperature, which regulates the global ocean-climate system. The Sea Ice Concentration (SIC) records of various oceanic sectors of Antarctica available since 1979 reveal dramatic changes in recent years; however, there is no consensus yet on its drivers of changes and their future projections. The lack of long-term SIC records has impeded the quantification of sea ice variability, trends, and various forcing factors and mechanisms. This study found that the second principal component, PC2, which elucidates ($\sim 27\%$) variability in the $\delta^{18}\text{O}$, is related to the SIC in the proximal oceanic sector of the DML region. Therefore, an attempt has been made to reconstruct a long-term SIC record (1809–1993 CE) for the Western Indian Ocean Sector (WIOS) of Antarctica based on the PC2 variability derived from the $\delta^{18}\text{O}$ ice core record. This long-term SIC record reveals a significant decline during 1830–1884 CE with a rate of $0.58\% \pm 0.12\% \text{ decade}^{-1}$, followed by a moderate increase during 1927–1993 CE with a rate of $0.24\% \pm 0.11\% \text{ decade}^{-1}$. Modern satellite-derived SIC records reveal an unprecedented increase of $2.59 \pm 0.86\% \text{ decade}^{-1}$ during 1994–2014 CE over the last two centuries as determined by the ice core-derived SIC record. The combined satellite and ice core based SIC record (1809–2019 CE) also reveals a significant increase in interannual variability at the ENSO band and decadal variability at the PDO band (16–32 years) in the last few decades. This investigation suggests that wind-driven sea-ice dynamics associated with switching phases of SAM and remote teleconnections of

Pacific oscillations largely control the interannual to decadal sea ice variability in this region.

The Sea Surface Temperature (SST) is another important factor that significantly influences sea ice variability. SST in the Southern Ocean is a crucial climate parameter to understand the impact of recent climate change on the Antarctic cryosphere region. In the absence of high-resolution long-records of SST from the Southern Ocean, several hypotheses related to Southern Ocean warming in recent decades and its impact on the cryosphere region still need to be tested. This study reconstructed a long-term SST record (1809–2013 CE) of the Western Indian Ocean sector of Antarctica (WIOS) using an annually resolved deuterium excess (*d-excess*) record of a 101.4m long ice core (IND-33). The spatial correlation between *d-excess* and ERA-5 SST anomaly records during 1979–2013 CE clearly shows that ice core *d-excess* records in the coastal DML region are primarily related to past SST variability in the WIOS region. A similar correlation was also observed between an isotope enabled atmospheric general circulation model (ECHAM5-wiso) derived *d-excess* and SST variation over this region. This study found that *d-excess* and SST are strongly correlated and stable over a long period; thus, *d-excess* records can be used to reconstruct long-term (1809–2013 CE) annual SST anomaly records for the WIOS region. The reconstructed SST anomaly (SSTA) record during 1809–2013 CE, combined with the available ERA-5 data, shows a slightly increasing trend ($+0.004 \pm 0.001^{\circ}\text{C decade}^{-1}$) during 1809–1969 CE. However, a significant declining trend in SST anomaly ($-0.028 \pm 0.009^{\circ}\text{C decade}^{-1}$) is found during 1981–2014 CE. The investigation of the reconstructed SST reveals a dominant cyclicality of 40 years throughout the record suggesting a dominant influence of Pacific Decadal Oscillation (PDO) in variability at

the decadal scale over the WIOS region. However, a recent decline in SST anomaly over the WIOS region reveals a strong anti-phase relation with SAM index during 1979–2015 CE. Such a relationship suggests that the recent decline in SST anomaly is related to the accumulation of wind-derived sea ice concentration over the WIOS region during the positive shift in SAM.

Additionally, this study investigated the spatial variability of triple oxygen and hydrogen isotopes in the DML region of East Antarctica. Surface snow transects derived from stable isotopes showed similar isotopic variation to that observed in the ECHAM5-wiso model-derived isotopic record. Surface snow cores and model output suggest a decrease in heavier isotopes as precipitation events along the coast fractionate heavier isotopes. A rapid decline in temperature with elevation and continentality causes $\delta^{18}\text{O}$ and δD to decrease monotonically in the mountain region. High-precision triple oxygen isotope measurements have enabled the derivation of $^{17}\text{O-excess}$, a novel proxy, which is strongly controlled by relative humidity. The $^{17}\text{O-excess}$ from surface snow shows a decreasing trend while moving from coast to inland and is inversely correlated with relative humidity. The relative humidity is an essential atmospheric component that modulates the Antarctic precipitation, sea ice variability, and ice sheet mass balance. Therefore, an attempt has been made to reconstruct the relative humidity based on the $^{17}\text{O-excess}$ ice core record. The reconstructed relative humidity shows the influence of interannual-decadal climate variabilities such as ENSO and IPO. However, the SAM has a more significant role in controlling wind-related variability in the relative humidity of the DML region. A positive SAM results in the strengthening of westerly wind and a reduction in relative humidity. This doctoral thesis uses novel and traditional proxy records of ice core from Antarctica, thus providing an excellent insight into the

past changes in East Antarctic climate, sea ice, sea surface temperature, and their modulation by various climate modes and oscillations.

Keywords: Antarctica, ice core, $\delta^{18}\text{O}$, *d-excess*, *¹⁷O-excess*, surface air temperature, Sea ice, sea surface temperature, relative humidity, ENSO, PDO, IPO, SAM.

Contents

Introduction.....	11
1.1 Antarctic ice sheet- Earth's climate archive	11
1.2 Antarctica in a Changing Climate	14
1.3 Proxy climate records from Antarctic ice cores	15
1.3.1 Stable Water Isotopes and Precipitation.....	16
1.3.2 The <i>d-excess</i> (deuterium excess) and <i>¹⁷O-excess</i> record: second-order proxies.	17
1.3.3 Chemical records in ice cores.....	18
1.3.4 Snow/ice accumulation.....	19
1.4 Antarctic climate: variability and forcing factors	20
1.4.1 Sea ice variability in the different sectors of the Southern Ocean.....	21
1.4.2 Antarctic temperature variability and forcing factors.....	22
1.4.3 Southern Ocean climate variability and teleconnections.....	24
1.4.4 Relative humidity and moisture sources in Southern Ocean.....	25
1.5 Objectives of the study	27
1.6 Outline of the thesis.....	27
Material and Methods	30
2.1 Study Area.....	30
2.1.1 Dronning Maud Land region, East Antarctica.....	30
2.1.2 Ice core and snow cores from the DML region	32
2.1.3 Technical details of ice/snow core drilling system.....	33
2.2 Processing (core cutting and sub-sampling) of ice core and snow cores	35
2.3 Analysis of ice core and snow core samples	37
2.3.1 Stable isotopes analysis using Isotope Ratio Mass Spectrometer (IRMS).....	37
2.3.2 Analysis of stable isotopes using Triple Isotope Water Analyzer (TIWA).....	38
2.3.3 Isotope calibration and normalization for deriving <i>¹⁷O-excess</i>	42
2.3.4 Data processing to derive <i>¹⁷O-excess</i>	43
2.3.5 Major ion analysis	44

2.4 Chronology of the IND33 ice core	45
2.6 An overview of the data sources, statistical methods, and toolbox used in this study	51
2.6.1 ERA5 reanalysis data	51
2.6.2 ECHAM5-wiso model data.....	51
2.6.3 Climate Indices and ice core data	52
2.7 Statistical methods and tools	53
2.7.1 Principal Component Analysis (PCA)	53
2.7.2 Time series analysis	54
Rapid warming over East Antarctica since 1940s caused by increasing influence of ENSO and SAM.....	56
3.1 Introduction.....	56
3.2 Results and Discussion	58
3.2.1 Variability in $\delta^{18}\text{O}$ Records from DML Region and Implications on Temperature Trends	58
3.2.2 Role of ENSO, IPO, and SAM on Temperature Variability during the Last Two Centuries	68
3.3 Conclusions.....	81
Sea ice variability and trends in the Western Indian Ocean Sector of Antarctica during the past two centuries and its response to climatic mode.....	82
4.1 Introduction.....	82
4.2 Results and Discussion	86
4.2.1 Accumulation rates at the IND33 core site	86
4.2.2 Ice core $\delta^{18}\text{O}$ records from the DML	87
4.2.3 Factors controlling the $\delta^{18}\text{O}$ variability in DML ice core records	91
4.2.3.1 $\delta^{18}\text{O}$ –temperature variability in the ice core record.....	92
4.2.3.2 $\delta^{18}\text{O}$ –sea ice variability in the DML ice core record.....	98
4.2.4 Sea ice trends and variability in the Western Indian Ocean Sector (WIOS) ...	104
4.2.5 Influence of SAM and ENSO teleconnections on sea ice dynamics	107
4.3 Conclusions.....	118
Sea surface temperature variability over the western Indian Ocean sector of Antarctica during the past two centuries and its linkages to tropical-extratropical climate modes.....	120

5.1 Introduction.....	120
5.2 Results and Discussion.....	123
5.2.1 Temporal variation in $\delta^{18}\text{O}$, δD , and <i>d-excess</i> records.....	123
5.2.2 Factors controlling the variability in <i>d-excess</i> and its relation to oceanic evaporation	126
5.2.3 Role of tropical variability and its control on SSTA over the WIOS region...	133
5.2.4 Role of SAM in controlling the SST variability over the WIOS region	136
5.3 Conclusions	139
Spatio-temporal variability of triple water isotopes in high accumulation regions of East Antarctica.....	141
6.1 Introduction	141
6.2 Results and Discussion.....	143
6.2.1 Spatial distribution of triple water isotopes in Antarctica and factors controlling their variability	143
6.2.2 Spatial variation in the ^{17}O - <i>excess</i> record over the DML region	147
6.2.3 Temporal variation of ^{17}O - <i>excess</i> in ice core record and controlling factors..	150
6.2.4 Reconstruction of relative humidity and its role in Antarctic climate variability	152
6.2.5 Relative humidity variability and influence of different climate modes	157
6.3 Conclusion.....	159
Summary and Future Perspectives	162
7.1 Surface air temperature of the DML region during the past two centuries.....	162
7.2 Sea ice concentration, trends, and variability during the last two centuries	163
7.3 Sea surface temperature variability in WIOS and control of different climate modes	164
7.4 Spatial and temporal variability of triple water isotopes in coastal East Antarctica	165
7.5 Future Perspectives	166
Bibliography	167
List of Publications	202
Conference Presentations.....	202

List of Figures

Figure 1.1 Map of Antarctica with ice surface elevation	12
Figure 1.2 Cumulative ice sheet mass change and contribution to sea level.....	13
Figure 1.3 Regional isotope composites from the different Antarctic ice cores and slopes of the reconstructed temperature during the past century.....	24
Figure 2.1 Location map of the study area and surrounding oceanic sectors in East Antarctica.....	31
Figure 2.2 Ice core drilling conducted from the central DML region (location: 71° 30' 36" S and 10° 09' 36" E; elevation: 1470 m).....	34
Figure 2.3 Drilling of snow cores was performed with a Kovacs Mark IV device with a 14 cm barrel diameter and snow cutters.....	35
Figure 2.4 Ice core retrieval and sample processing at National Centre for Polar and Ocean Research (NCPOR).....	36
Figure 2.5 Stable Isotope Ratio Mass Spectrometer (IRMS) at NCPOR, Goa.....	38
Figure 2.6 Triple Isotope Water Analyzer (TIWA-45EP) instrument at NCPOR ice core lab facility.....	42
Figure 2.7 Ion Chromatograph (IC) instrument for cation and anion analysis housed in a Class-100 clean room at NCPOR, Goa.....	45
Figure 2.8 Chronology of IND33 ice core using stable isotope and major ions.....	46
Figure 2.9 Demonstration of annual layer counting based on the seasonal signal resolved $\delta^{18}\text{O}$ and ionic records of IND33 ice core within a depth interval (0–10 m).....	49

Figure 2.10 Comparison of age-depth models based on manual counting of annual layers and StratiCounter method.....	50
Figure 2.11 Principal Component Analysis of multiple ice cores from the DML region...	53
Figure 3.1 Annual $\delta^{18}\text{O}$ record of ice cores used in this study.....	60
Figure 3.2 Correlation of PC1 with annual and seasonal ERA5 surface air temperature.....	63
Figure 3.3 RACMO2 model monthly averaged precipitation and ERA5 monthly averaged surface wind speed.....	65
Figure 3.4 Correlation of PC1 with seasonal ERA5 surface air temperature.....	66
Figure 3.5 Reconstructed surface air temperature of DML region and trend analysis.....	68
Figure 3.6 The power spectrum, wavelet, and scaled averaged variance analysis of reconstructed surface air temperature anomaly.....	70
Figure 3.7 Cross wavelets transform analysis of surface air temperature anomaly with SOI and IPO.....	71
Figure 3.8 Surface air temperature anomaly during strong El Niño and La Niña years.....	73
Figure 3.9 Spatial temperature variability during El Niño and La Niña year.....	74
Figure 3.10 Spatial variation of heat flux anomaly over the DML region during ENSO events.....	76

Figure 3.11 Mean Sea Level Pressure (MSLP) correlates with surface air temperature during positive and negative SAM indices.....78

Figure 3.12 Correlation of SAM index with surface air temperature and wavelet coherence analysis between SAM and SOI.....80

Figure 4.1 Annual variation in accumulation rate and $\delta^{18}\text{O}$ records of the IND33 ice core.....87

Figure 4.2 Ice core $\delta^{18}\text{O}$ record and anomaly in the selected $\delta^{18}\text{O}$ record from the DML region.....88

Figure 4.3 Comparison of ECHAM5-wiso model $\delta^{18}\text{O}$ record in precipitation and measured ice core $\delta^{18}\text{O}$ records.....90

Figure 4.4 $\delta^{18}\text{O}$ ice core records from ice cores used in the present study and their correlation with ERA5 surface air temperature.....93

Figure 4.5 PC1 correlation with ERA5 annual surface air temperature.....94

Figure 4.6 Correlation of PC1 with surface air temperature and temperature reconstruction.....97

Figure 4.7 Seasonal backward wind trajectories analysis for the DML region.....99

Figure 4.8 Spatial plots describing the correlation and mechanism for sea ice variability with $\delta^{18}\text{O}$ record.....101

Figure 4.9 Correlation plots of PC2 with sea ice and reconstruction of sea ice concentration of WIOS.....103

Figure 4.10 Sea ice variability and trends in WIOS, East Antarctica.....	105
Figure 4.11 Time series analysis for the reconstructed sea ice concentration record.....	106
Figure 4.12 Correlation and time series analysis of sea ice concentration with SAM indices.....	109
Figure 4.13 Surface winds and sea ice anomaly plots during the positive SAM years.....	110
Figure 4.14 Sea ice correlation with SOI and surface air temperature.....	112
Figure 4.15 Sea ice correlation with ERA5 annual SST.....	113
Figure 4.16 Spatial anomaly plots of surface air temperature and sea ice concentration during El Niño and La Niña.....	114
Figure 4.17 Heat flux anomaly plots during El Niño (low sea ice) and La Niña (high sea ice) years.....	115
Figure 4.18 Wavelet coherence analysis of SAM and SOI.....	117
Figure 5.1 Annual variability of (a) $\delta^{18}\text{O}$ and δD records and (b) <i>d-excess</i> record from IND-33 ice core, derived from measured $\delta^{18}\text{O}$ and δD ice core record (1809–2013 CE).....	124
Figure 5.2 Correlation of δD with $\delta^{18}\text{O}$ ice core records used in this study and comparison of <i>d-excess</i> record.....	125
Figure 5.3 Correlation of ice core and ECHAM5-wiso model-based <i>d-excess</i> record with sea surface temperature and influence of wind drifted sea ice.....	128
Figure 5.4 Reconstructed SSTA based on the <i>d-excess</i> ice core record.....	129

Figure 5.5 Power spectrum and wavelet transform analysis of reconstructed SSTA.....131

Figure 5.6 Temporal and spatial demonstration of maximum/minimum SSTA observed in the last century related to El Niño /La Niña, respectively.....132

Figure 5.7 Spatial correlation of ERA5 SST with Nino3.4 and PDO.....134

Figure 5.8 Cross wavelet transform analysis of reconstructed SSTA with Nino3.4 and PDO.....135

Figure 5.9 Correlation of sea ice concentration with reconstructed SSTA over the WIOS.....136

Figure 5.10 Spatial and wavelet coherence plots show a possible mechanism for variation in SSTA over the WIOS.....138

Figure 6.1 Spatial variation of stable isotopes in ECHAM5-wiso model and surface snow core transect.....146

Figure 6.2 Relationship between $\delta^{17}\text{O}$ and $\delta^{18}\text{O}$ in DML surface snow core transect and the variation of ^{17}O -excess (per meg).....148

Figure 6.3 Correlation of relative humidity (%) with (a) d -excess (per mil) and (b) ^{17}O -excess (per meg).....149

Figure 6.4 Annual variation of the ^{17}O -excess (per meg) in the IND33 ice core.....151

Figure 6.5 (a) Correlation of IND33 ice core ^{17}O -excess record with ERA5 Relative Humidity (%). (b) Linear regression of ^{17}O -excess with ERA5 Relative Humidity (%) during 1979-2013 CE.....152

Figure 6.6 (a) Reconstructed relative humidity for the past two centuries (1809-2013 CE) based on the ^{17}O -excess record. Spatial correlation of reconstructed relative humidity with (b) ERA5 Total Precipitation and (c) NSIDC sea ice concentration during 1979-2013 CE.....154

Figure 6.7 (a) Reconstructed relative humidity (%) (1809-2013 CE) based on the linear regression equation derived from the correlation plot between ^{17}O -excess and ERA5 relative humidity (%). (b) Spectral analysis of reconstructed relative humidity (%). (c) Wavelet transform analysis of reconstructed relative humidity (%).....156

Figure 6.8 Spatial correlation of ERA5 relative humidity with (a) SOI, (b) IPO, and (c) SAM during 1979-2013 CE.....158

List of Tables

Table 2.1 Technical details of the drilling system.....33

Table 2.2 HL1 standard measured for stable isotopes in TIWA-45EP instrument during the ice core sample analysis.....40

Table 2.3 CDML1 standard measured for stable isotopes in TIWA-45EP instrument during the ice core sample analysis.....41

Table 2.4 Repeated measurement of unknown sample for stable isotopes in TIWA-45EP.....42

Table 2.5 USGS standards measured during the analysis of ice/snow core samples.....44

Table 2.6 Ice core records are used for principal component analysis.....54

Table 2.7 Eigenvalue and variability for principal components.....54

Table 2.8 Contribution of the variables (%) from selected ice cores.....54

Chapter 1

Introduction

Since the industrial revolution (1850 CE), global temperature has increased by ~ 0.6 - 0.8 °C. Further, the model projections predict another $\sim 2 - 3$ °C increase in global temperature by the end of this century, which will severely adversely impact the global climate (IPCC, 2013). It is now well established that the anthropogenic release of greenhouse gases from burning fossil fuels is one of the major factors responsible for recent climate change (Leduc et al., 2016; Overpeck and Cole, 2006). However, it is still not very clear what are the tipping points in global climate related to such dramatic changes. Therefore, it is important to understand the causes and mechanisms of Earth's climate variations in the past and use this knowledge to improve the uncertainties in the model projections and better plan climate mitigation. One of the best archives to study the past climate is the Antarctic ice sheet which directly preserves the climate records of the past several thousands of years (Etheridge et al., 1996; Lüthi et al., 2008; Yan et al., 2019).

1.1 Antarctic ice sheet- Earth's climate archive

Antarctica is the southernmost and most remote continent on the planet Earth. It serves as a natural laboratory due to its pristine nature and minimal anthropogenic influence. Antarctica covers an area of about four times the size of India, with 98% of the land covered by thick ice sheets. The continent can be broadly divided into East, and West Antarctica, separated by a mountain range called the Trans-Antarctic Mountain range stretching between the Weddell Sea and the Ross Sea (Figure.1.1). The Antarctic ice sheet is divided into three parts: the East Antarctic Ice Sheet (EAIS), the West Antarctic

Ice Sheet (WAIS), and the Antarctic Peninsula Ice Sheet (APIS). Each of these ice sheets has its unique characteristics. The WAIS is grounded well below sea level and therefore considered the Marine Ice Sheet. Warm ocean waters threaten to melt the WAIS at its base because the West Antarctic Ice Sheet (WAIS) is in a region of rapid warming. This rapid warming is a significant threat to WAIS stability and would raise sea levels by 3.3 m if it melted utterly (Bamber et al., 2009). However, the EAIS has a much higher potential to contribute to the global sea level rise; if melted completely, it would raise the global sea level by 53m (Fretwell et al., 2013). The result of the combined satellite observations and modeling of Antarctic surface mass balance has reported a mass loss of $2,720 \pm 1,390$ billion tonnes between 1992 and 2017, corresponding to an increase of 7.6 ± 3.9 millimeters in mean sea level (Figure 1.2) (Shepherd et al., 2018).

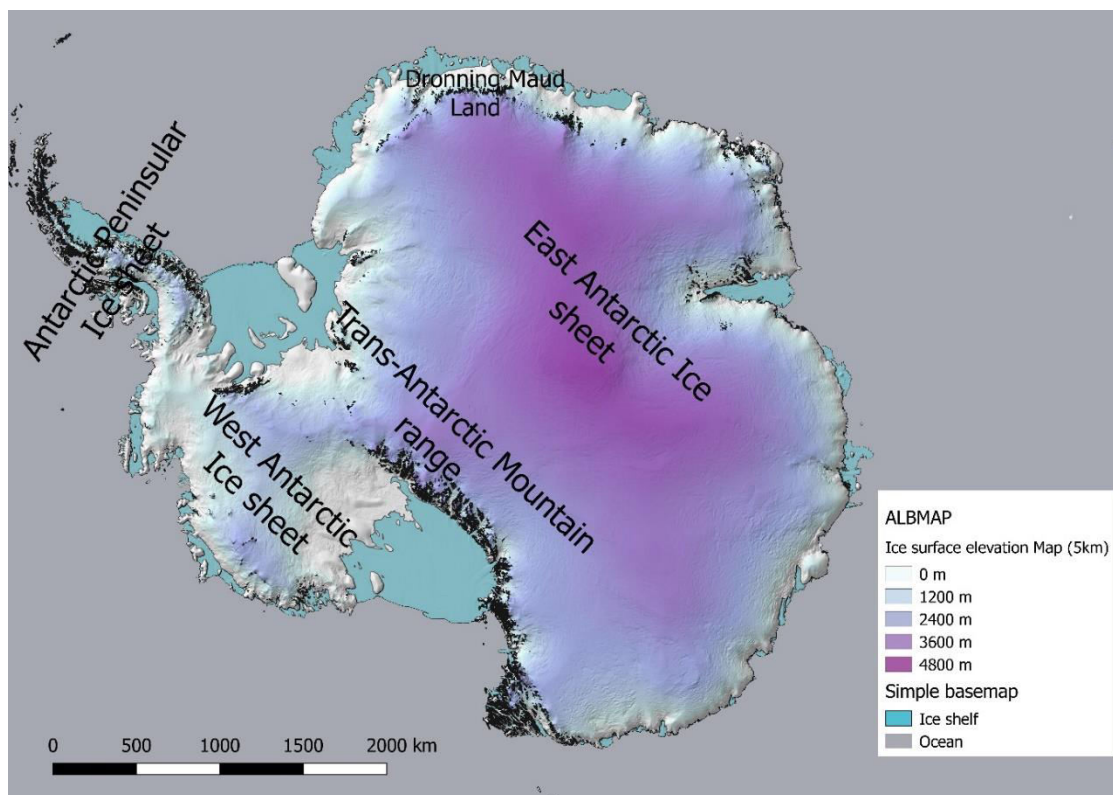


Figure 1.1. Map of Antarctica with ice surface elevation.

The map and the ice surface elevation model show the primary division of the Antarctic ice sheet Bamber et al. (2009). The map was created with QGIS 2.18.7 using Quantarctica (version 3.2).

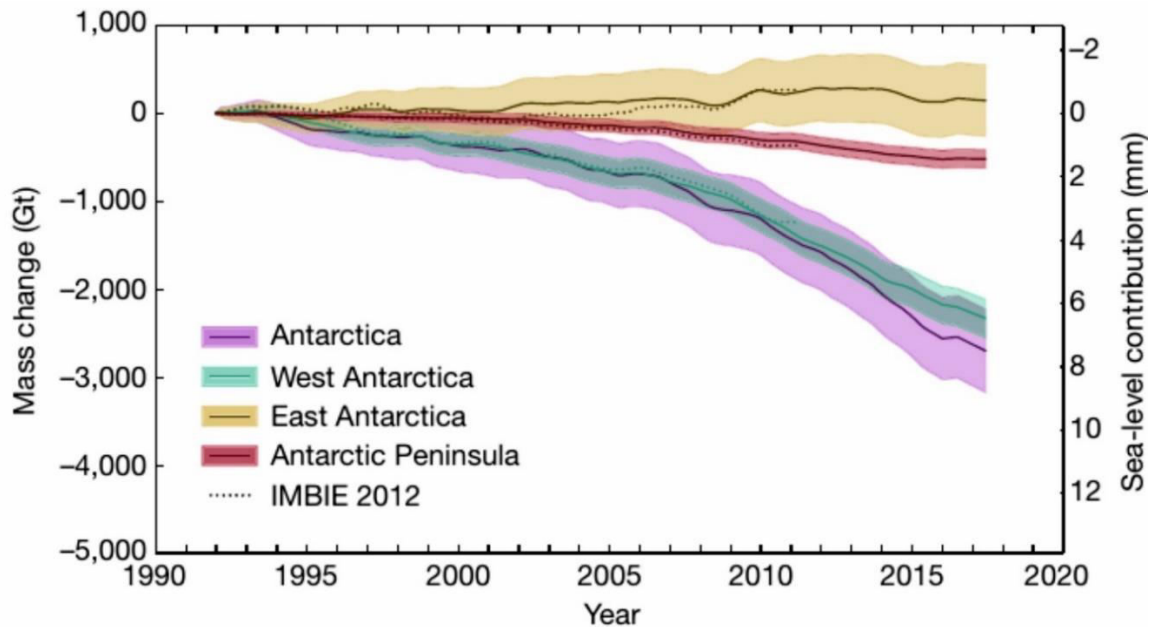


Figure 1.2. Cumulative ice sheet mass change and contribution to sea level.

Mass change in the Antarctic Ice sheet and its corresponding contribution to global sea level change (Shepherd et al., 2018).

The Antarctic ice sheet is considered one of the essential natural climate archives, preserving past climate information. Due to the extreme coldness of the continent, any snowfall on this continent gets accumulated and preserved. In the event of continuous snowfall on ice sheets, previous years' snowfall is compacted due to the increasing load above. The annual mean surface temperatures of the Antarctic remain below freezing, which means that the yearly snow cannot complete its ablation cycle. Thus, the snow accumulation history remains uninterrupted in the ice sheet. If we drill and recover an ice core at such places, the ice core can be used as the time machine that allows us to investigate past climate. The ice cores are usually retrieved by drilling vertically downwards into an ice sheet using an electro-mechanical drilling system.

There has been substantial advancement in drilling technologies, ice-sheet analysis, and understanding of the records preserved within polar ice sheets after the first effort to analyze polar ice over 90 years ago (Sorge, 1933). As part of further improvement in ice core drilling techniques, a Norwegian-British-Swedish collaborative team successfully drilled a 100 m ice core in Queen Maud Land, Antarctica (Schytt, 1954; Swithinbank, 1957). The first deep Antarctic ice core was recovered from the lake Vostok site in East Antarctica after about twelve years of effort. The Leningrad Mining Institute conducted the drilling operation and retrieved a 3623 m long ice core spanning 420 kyr (Petit et al., 1999). These successful efforts led to the formation of the EPICA (European Project for Ice Coring in Antarctica) consortium, which used a collaborative approach to deep ice drilling (Jouzel, 2013). Afterward, several ice cores were retrieved from different regions of Antarctica; however, most available records are at decadal to multi-decadal temporal resolution. Due to extremely low snow accumulation rates in inland Antarctica, most of the deep ice cores collected from the polar plateau cannot provide annually resolved climate records. The long-term ice core records comparable to the instrumental records on an annual to seasonal scale are very limited in numbers, except in a few coastal Antarctic sites, where high accumulation exists.

1.2 Antarctica in a Changing Climate

The impact of recent climate change on Antarctica is poorly understood due to a lack of long-term high-resolution climate records. Instrumental temperature records with a reasonable spatial coverage scale have been available only since 1958 (Nicolas and Bromwich, 2014). The resolution of continuous Spatio-temporal records of Antarctic climate has been known since the beginning of the satellite era in 1979s. However, these climate records are too short to discern long-term trends and variability at the decadal to multi-decadal scale (Turner et al., 2005). The Antarctic ice core

provides high-resolution climate records beyond instrumental records. Since the 1950s, several deep ice cores have been retrieved from Antarctica to reconstruct past climate records to understand climate variability and long-term changes at various time scales. In a recent study, Stenni et al. (2017) compiled stable isotope water records from 112 Antarctic ice cores with a temporal coverage of the past 2000 years. However, most ice cores were selected from higher elevation sites with lower accumulation rates, providing a relatively long-term climate record.

The coastal regions of Antarctica typically receive significantly higher precipitation than the interior plateau and, therefore, are ideal for assessing the annual to decadal climate variability (Curran et al., 2003; Goursaud et al., 2019; Turner et al., 2019). Coastal ice cores from Antarctica are sensitive enough to register even short-term fluctuations and changes in climate parameters such as accumulation, temperature, sea ice, dust influx, solar activity, and volcanic events (Abram et al., 2013; Laluraj et al., 2020; Laluraj et al., 2011; Masson-Delmotte et al., 2008; Mulvaney et al., 2012; Rahaman et al., 2016; Schneider et al., 2004; Thamban et al., 2010).

1.3 Proxy climate records from Antarctic ice cores

Precipitation in the form of snow deposited on the surface of an ice sheet records past climatic conditions and atmospheric composition, which are gradually compacted with a growing load of snow over time. Information regarding past climate is stored in chemical species present in surface snow, trapped gas bubbles in ice matrix, and stable water isotope composition of the snow. Analyzing these high-resolution chemical, stable isotope, and trapped gas records provides a detailed reconstruction of the past climate. These records illustrate the climatic changes on a local, regional, and global scale. While the gas records provide a direct reconstruction of past atmospheric

concentration, its chemical and isotopic compositions are essentially proxy records of climate. This study focused mainly on the stable isotopic record and chemical ions from ice cores from coastal Antarctica. A brief overview of a few of the proxies used in this thesis is given below.

1.3.1 Stable Water Isotopes and Precipitation

The stable isotopic composition of Antarctic snow and ice samples is commonly used to decipher past environmental conditions. After Dansgaard (1964) quantified the stable isotopic fractionation of rainwater during the evaporation-condensation process, this technique became the most valuable proxy for reconstructing past climate. Isotopic ratios of oxygen and hydrogen are strongly correlated with mean annual surface temperature according to the isotope-temperature relationship derived from Dansgaard (1964). Additionally, the stable isotope record of the Antarctic ice cores shows a strong seasonality effect due to the different precipitation types during the two seasons. This seasonality in the stable water isotopes enables us to date the ice core records by counting the annual layers (Eichler et al., 2000). Therefore, in the present study, stable water isotopes are used to establish both the ice core chronology and to reconstruct the past climate record.

However, due to the extremely minimal variation in isotopic ratios, all measurements are performed with respect to the internationally accepted standards such as Vienna Standard Mean Oceanic Water (V-SMOW) provided by International Atomic Energy Agency (IAEA, Vienna). The isotope ratios are expressed in delta notation (δ) and are used to quantify stable isotopes as relative ratios to internationally accepted standards. As a result, the delta (δ) of ^2H (D), ^{18}O , and ^{17}O for a given sample can be calculated using the following equations:

$$\delta D = \left(\frac{(^2\text{H}/^1\text{H})_{\text{Sample}}}{(^2\text{H}/^1\text{H})_{\text{VSMOW}}} - 1 \right) \times 1000 \quad (\text{i})$$

$$\delta^{18}\text{O} = \left(\frac{(^{18}\text{O}/^{16}\text{O})_{\text{Sample}}}{(^{18}\text{O}/^{16}\text{O})_{\text{VSMOW}}} - 1 \right) \times 1000 \quad (\text{ii})$$

$$\delta^{17}\text{O} = \left(\frac{(^{17}\text{O}/^{16}\text{O})_{\text{Sample}}}{(^{17}\text{O}/^{16}\text{O})_{\text{VSMOW}}} - 1 \right) \times 1000 \quad (\text{iii})$$

All the delta (δ) values are reported per mil (‰) or parts per thousand.

1.3.2 The *d-excess* (deuterium excess) and *¹⁷O-excess* record: second-order proxies.

The second-order parameter deuterium excess (*d-excess* = $\delta D - 8 \cdot \delta^{18}\text{O}$), derived as a kinetic fractionation component (non-equilibrium fractionation) and primarily associated with the temperature at moisture sources, can be used to describe changes in temperature at moisture sources and relative humidity (Merlivat and Jouzel, 1979). Different diffusion velocities of HDO and H₂¹⁸O are mainly responsible for the non-equilibrium components. In contrast to equilibrium fractionation, the slower-moving molecules of H₂¹⁸O have insufficient time to reach equilibrium, leading to significant deviations from the equilibrium state. Therefore, the fractionation ratios of two isotopes ($\delta^{18}\text{O}$ and δD) show deviations from ~1:8 ratios, generally observed in equilibrium conditions. The deviation of the typical isotopic ratios (i.e., 1:8) between $\delta^{18}\text{O}$ and δD is defined as *d-excess* (Dansgaard, 1964) and can be calculated by the equation:

$$d - excess = \delta D - 8 \cdot \delta^{18}\text{O} \quad (\text{iv})$$

It is well known that the extent of non-equilibrium fractionation during evaporation is influenced by several factors, including the relative humidity gradient above the surface, the air and surface water temperatures, and evaporative cooling (Cappa et al., 2003; Merlivat and Jouzel, 1979). As a result, variations in the sea ice conditions, sea surface temperatures, winds, and relative humidity significantly influence *d-excess* records in ice cores.

Recent advancements in analytical techniques allow us to measure the isotopic ratio $^{17}\text{O}/^{16}\text{O}$ in ice/snow core records, and that enables us to obtain $\delta^{17}\text{O}$ with high precision. Further, the $^{17}\text{O-excess}$ is derived from the measured record of $\delta^{18}\text{O}$ and $\delta^{17}\text{O}$ based on the equation shown below:

$$^{17}\text{O-excess} = \ln((\delta^{17}\text{O}/1000 + 1)) - 0.528 * \ln((\delta^{18}\text{O}/1000) + 1) \quad (\text{v})$$

In this equation (equation-v), the constant value of 0.528 represents the slope of the Global Meteoric Water Line (GMWL) (Barkan and Luz, 2007; Luz and Barkan, 2010). The equilibrium fractionation of liquids during evaporation and diffusive fractionation results in a deviation from GMWL (Barkan and Luz, 2007; Landais et al., 2008; Risi et al., 2010b). Since the $^{17}\text{O-excess}$ variation is smaller than $\delta^{18}\text{O}$, it is expressed in per meg or ppm (10^{-6}). In contrast to *d-excess*, this new proxy is not affected by the temperature at the source but rather by changes in relative humidity (Barkan and Luz, 2007; Landais et al., 2010). Therefore, it can be used as a robust proxy for reconstructing relative humidity.

1.3.3 Chemical records in ice cores

An important proxy component of the Antarctic ice core that stores valuable climate information is the deposition of chemical ions. Furthermore, they preserve

information about the nearby source region in coastal Antarctica (Laluraj et al., 2014; Mahalinganathan and Thamban, 2016; Rahaman et al., 2016). Several chemical ions in the coastal Antarctic ice core are significantly related to the sea ice in the nearby oceanic sector (Abram et al., 2010; Thomas et al., 2019). Chemical species that have been analyzed more frequently in the ice core include the major cations sodium (Na^+), magnesium (Ca^+), calcium (Ca^+), ammonium (NH_4^+), and potassium (K^+). In contrast, major anions include chloride (Cl^-), sulfate (SO_4^{2-}), and nitrate (NO_3^{2-}). Most major chemical ions display excellent seasonal variations and can be used to establish high-resolution ice core chronologies. Some major ions, such as sodium and sulfate, are used to derive a second-order parameter called non-sea-salt sulfate (nssSO_4^{2-}) in the record, which is used as markers of historical volcanic eruption events (Ejaz et al., 2021; Sigl et al., 2014; Sigl et al., 2015).

1.3.4 Snow/ice accumulation

The Antarctic ice sheet has a continuous record of snow accumulation over several thousands of years. Therefore, it plays a crucial role in retaining specific chemical components over long periods. However, the accumulation rate over the Antarctic ice sheet is dominantly controlled through precipitation events. Antarctica's coastal regions receive the most precipitation ($\sim 1\text{m}/\text{year}$), whereas the inland regions mostly have records of low precipitation ($\sim 5\text{cm}/\text{year}$). Therefore, the Antarctic coastal area is considered ideal for retrieving high-resolution climate records (seasonal to annual scale). Furthermore, these seasonally-annually resolved climate records can easily be compared with instrumental or satellite-based climate parameters and can be used to reconstruct past climate beyond instrumental records.

1.4 Antarctic climate: variability and forcing factors

Several tropical teleconnections and climate modes influence the Antarctic climate variability and changes within nearby oceanic sectors. El Niño Southern Oscillation (ENSO) is one of them and is predominantly associated with anomalous shifts in sea surface temperature (SST) over the tropical Pacific. ENSO is related to the ocean-atmospheric variability over the tropical Pacific and strongly influences global climate variability (Alexander et al., 2002; Karoly, 1989; Trenberth et al., 1998). Recent studies have suggested that global climate extremes could be amplified by the combined influence of ENSO and Pacific Decadal Oscillation (PDO) (Goodwin et al., 2016; Gregory and Noone, 2008; Wang et al., 2014), depending on their phase relationships. The PDO is believed to be a long-lived ENSO-like variability and a leading mode of SST variation over the North Pacific Ocean (Mantua et al., 1997). This also influences the Southern Hemisphere SST on a decadal time scale. A recent study from Wang et al. (2019) shows ENSO–PDO's coupled influence, which further modulates SST over the Atlantic Ocean sector. Due to Southern Hemispheric teleconnections, the Antarctic climate is sensitive to these tropical changes (Turner, 2004). However, it is not yet well understood how such changes in tropical oscillations and associated climate extremes influence Antarctic climate through space and time, particularly in the backdrop of continuing global warming since the industrial era ~1850 Common Era (CE).

Several attempts have been made based on model simulations and proxy records for reconstructing the long-term ENSO-PDO records. Results of long-term predictions of ENSO in Coupled Model Inter-comparison Project phase-5 (CMIP5) show contradictory results (Chen et al., 2017; Chen and Majda, 2017). Several attempts have been made based on tree rings (MacDonald and Case, 2005; Mann et al., 2009) and corals (Chakraborty et al., 2012; Cobb et al., 2003; Urban et al., 2000) to understand

decadal to centennial-scale variability of ENSO and PDO. These records show good agreement in shorter reconstructions; however, they differ in the case of longer records (D'Arrigo et al., 2005). In addition, a few essential caveats are attached to tree ring-based reconstruction, such as changes in sample depth, tree size, and chronology, some of which coincide with variance changes. Hence, they often misrepresent climate signals (Fowler et al., 2012). Further, such ENSO reconstructions are mostly from the ENSO regions in the tropics/subtropics and, therefore, may not necessarily reflect changes in ENSO influencing beyond the Niño regions. Since the ice core records from the coastal Antarctic register the annual variability, therefore, can be used to understand the influence of ENSO-related teleconnection.

1.4.1 Sea ice variability in the different sectors of the Southern Ocean

Sea ice cover over the Antarctic region is another critical component extensively controlled by the variations in ocean-atmosphere circulations (Carleton, 1989; Ferrari et al., 2014). Changes in sea ice cover in the Southern Ocean strongly influence the energy-mass balance and change in a temperature gradient, which further modulates heat exchange between ocean and atmosphere (Deb et al., 2017; Raphael, 2003; Simmonds et al., 2003). This consequently impacts the regional climate variations over Antarctica. Recent studies show a significant increasing trend in Antarctic sea ice cover associated with the westerly wind forcing due to the modulation of SAM (Holland and Kwok, 2012; Liu et al., 2004; Marshall, 2003; Spence et al., 2010); ENSO-PDO (Kwok and Comiso, 2002a; Yu et al., 2017); stratospheric ozone depletion (Marshall et al., 2004; Sigmond and Fyfe, 2014; Thompson et al., 2011) and increased basal melting of ice shelves due to rising SST over the southern ocean (Bintanja et al., 2013). Several studies have highlighted the regional variations of sea ice cover over Antarctica's Atlantic and Pacific Ocean sectors. Recent studies show a significant increase in sea ice

extent over the Indian Ocean sector during 1979–2015 CE (Deb et al., 2017; Jena et al., 2018). Sea ice variation in the Indian Ocean sector modulates the global climate in several ways through bottom water formation (Ohshima et al., 2013; Yabuki et al., 2006), relatively large meridional circulation, and acting as a carbon sink (Sloyan, 2006). Therefore, the modulation of sea ice cover over the Indian Ocean sector of Antarctica needs to be quantified on a longer time scale.

1.4.2 Antarctic temperature variability and forcing factors

The variation in Antarctica's surface air temperature and the surrounding oceanic sectors play an essential role in understanding Antarctic glaciology, oceanography, chemistry, and biology (Convey, 2003; Cook et al., 2005; Meredith and King, 2005; Scambos et al., 2017; Turner et al., 2017). Therefore, estimating long-term and high-resolution (annual) temperature records from the Antarctic continent is essential. Using stable water isotope calibrations, Goose et al. (2012) presented the first composite of Antarctic temperature by averaging the seven standardized temperature records. After that, several studies have attempted to reconstruct the Antarctic temperature for the last 2000 years based on the compilation of ice core records from different regions of Antarctica (PAGES 2k Consortium, 2013; Stenni et al., 2017). However, it was found that most of the ice core records were from the higher elevation, and very few were available from the Antarctic coast. Based on the reconstructed temperature from the stable isotopic ice core record, a significant warming trend was observed along the West Antarctic Ice Sheet (WAIS), Antarctic Peninsula (AP), and Dronning Maud Land (DML) coasts (Figure 1.3). The surface temperature of the WAIS, AP, and DML coast shows a significant rise in temperature with a rate of 0.97 ± 0.75 °C, 1.99 ± 1.7 °C, and 0.97 ± 0.73 °C 100yr^{-1} , respectively (Stenni et al., 2017) (Figure 1.3). This shows the deviation of the DML coast climate from the

rest of East Antarctica, as most of East Antarctica has shown a cooling trend in the last century. However, the DML coast has very few long-term high resolutions of ice core records to critically investigate the long-term climate variability on inter-annual to decadal timescale.

The Southern Annular Mode (SAM) is recognized as one of the most dominant modes of climate variability in the southern hemisphere (Marshall, 2003); the positive phase of SAM is associated with low-pressure anomalies over Antarctica and high-pressure anomalies over mid-latitudes and vice-versa (Abram et al., 2014; Marshall, 2003; Marshall et al., 2006; Thompson and Wallace, 2000; Turner et al., 2005). The SAM generally shows a dipole response to the East Antarctic and Antarctic Peninsula temperature; a strong correlation between temperature and SAM is observed across the Antarctic Peninsula during the positive SAM, and the opposite is observed in East Antarctica (Kwok and Comiso, 2002a; Marshall, 2007; Thompson and Solomon, 2002). Therefore, shifting SAM to a positive phase in the last several decades, we expect cooling across East Antarctica. However, studies from the Dronning Maud Land (DML) region of East Antarctica show the absence of such long-term cooling; instead warming trend was observed in the last century (Naik et al., 2010; Stenni et al., 2017). Therefore, obtaining more spatially distributed and temporally extended proxy records from the DML region is imperative for a better understanding the processes and factors involved in the SAM-temperature relationships.

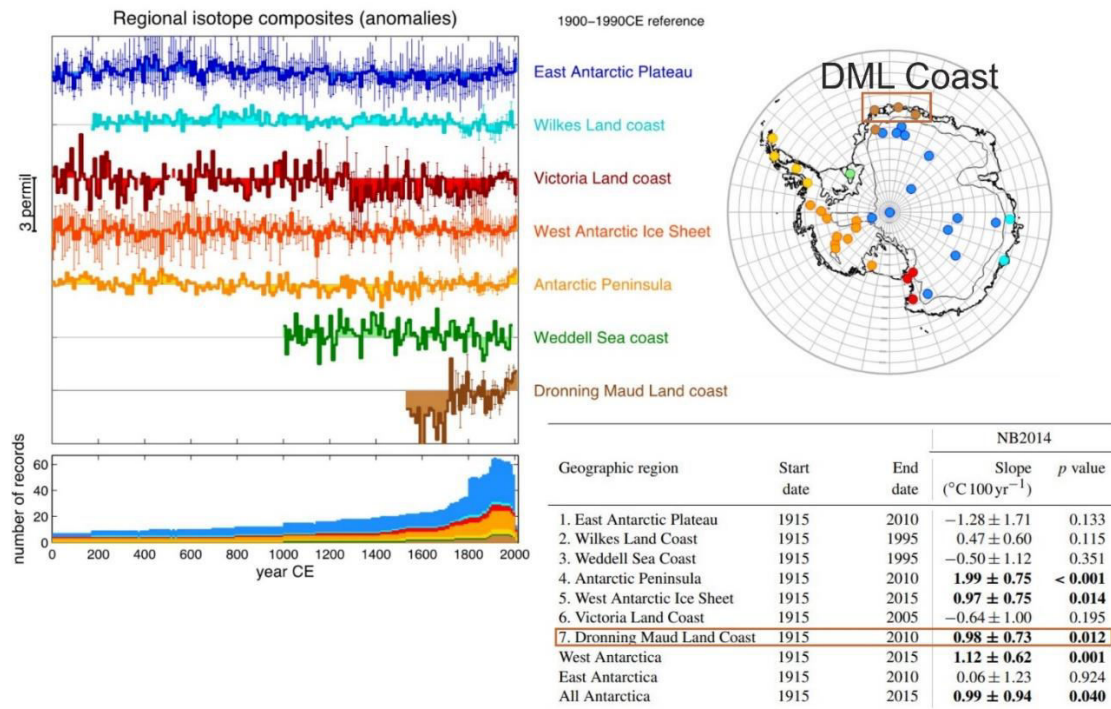


Figure 1.3. Regional isotope composites from the different Antarctic ice cores and slopes of the reconstructed temperature during the past century (Stenni et al., 2017).

Reconstructed temperature shows a significant warming trend in the WAIS, AP, and DML coast regions. At the same time, the East Antarctic Plateau, Weddell Sea Coast, and Victoria Land Coast have shown a cooling trend in the past century.

1.4.3 Southern Ocean climate variability and teleconnections

Over the past few decades, the Southern Ocean has experienced rapid changes with widespread climate impacts. Besides its contribution to the global circulation of heat, freshwater, and nutrients, the Southern Ocean also impacts climate, ecology, and human lives via its crucial role in ocean productivity and the biogeochemical and carbon cycle. Despite all this, the Southern Ocean is one of the least studied regions on Earth, leading to substantial uncertainties associated with estimates of future Southern Ocean processes and their consequences for the world (IPCC, 2013). Some studies have used different ice core records of *d-excess* to reflect the past sea surface temperature (SST) condition during glacial-interglacial changes (Stenni et al., 2004; Stenni et al., 2001;

Stenni et al., 2010; Vimeux et al., 2001). There is a dominant influence on the Southern Ocean due to tropical variations associated with ENSO and PDO. These processes modulate the southern hemisphere's SSTs on an annual-decadal scale. It has been found in a recent study that ENSO-PDO influences SST over the Atlantic Ocean sector in a coupled manner (Wang et al., 2019). Surface energy flux modulated by ENSO-related atmospheric teleconnections dominates SST and sea-ice variability over the Southern Ocean. There is a lack of quantitative information regarding the ENSO-PDO-related variation of SST over Antarctica's Western Indian Ocean sector (WIOS) and its possible impact on sea ice variation. Therefore, it is important to understand the long-term variability of the sea surface temperature of the Southern Ocean and its possible teleconnection in this oceanic sector of Antarctica. This study attempts to decipher the high-resolution (annual) SST variation based on the ice core-derived *d-excess* record and related teleconnection to tropical/extra-tropical climate modes.

1.4.4 Relative humidity and moisture sources in the Southern Ocean

The *d-excess* record in the ice/snow core has frequently been interpreted as a proxy for moisture source conditions because it is sensitive to temperature and humidity during evaporation. Model studies suggested that the effect of SST changes at evaporation can overwhelm signals of relative humidity changes in the *d-excess* record of the Polar region (Vimeux et al., 2001). This interpretation, however, is complicated by the fact that *d-excess*, even in equilibrium conditions, is not a conservative tracer (Jouzel and Merlivat, 1984; Kavanaugh and Cuffey, 2003; Masson-Delmotte et al., 2008; Petit et al., 1999; Uemura et al., 2012). Therefore, attempts have been made to use a derived proxy *¹⁷O-excess* for understanding the changes in the relative humidity both spatially and temporally. Both theoretical and experimental evidence shows that an excess of ¹⁷O ($^{17}\text{O-excess} = \ln((\delta^{17}\text{O}/1000 + 1)) - 0.528 * \ln((\delta^{18}\text{O}/1000) +$

1)) in meteoric water is due to the evaporation of ocean water into undersaturated air and is inversely correlated with relative humidity (Barkan and Luz, 2007; Luz and Barkan, 2010; Risi et al., 2010a). While going through the equilibrium fractionation process, the heavy isotopologues (H_2^{17}O and H_2^{18}O) were preferentially removed relative to H_2^{16}O and depleted the vapor in $\delta^{17}\text{O}$ and $\delta^{18}\text{O}$. However, the heaviest isotopologues (H_2^{18}O) more preferentially fractionate from water vapor, resulting in more positive ^{17}O -excess values. The ^{17}O -excess record is ideally suited to understand relative humidity changes since it is insensitive to evaporation temperatures and less susceptible to equilibrium fractionation during snow formation than the d -excess record. The relative humidity has large-scale implications in understanding the Antarctic precipitation, sea ice variability, and ice sheet mass balance. Therefore, it is important to reconstruct the relative humidity of the DML region beyond the instrumental record.

In the present thesis, triple oxygen (^{18}O , ^{17}O , ^{16}O) and hydrogen (^1H , ^2H) isotopic records from high accumulation ice cores were used to reconstruct climatic variables such as surface air temperature, sea ice concentration, sea surface temperature, and relative humidity for the past two centuries. Further, spatial variability of isotopes in the DML region is studied along the transects from coast to inland. Efforts were made to understand the influence of possible climate modes and oscillations in controlling the variability of surface air temperature, sea ice concentration, sea surface temperature, and total cloud cover.

1.5 Objectives of the study

Objectives of this doctoral study:

1. To undertake a high-resolution reconstruction of Antarctic climate variability during the past few centuries using various isotope proxy records in an ice core from coastal Dronning Maud Land.
2. To study the past evolution of Antarctic climate variability and its linkages to tropical/ extra-tropical climatic modes using ice core proxy records and climate reanalysis data.
3. To understand the spatial variability of triple-oxygen isotopes in modern snow along a transect in Antarctica to delineate the processes and its paleoclimatic implications.

1.6 Outline of the thesis

This thesis comprises seven chapters. The content of each chapter is as follows:

Chapter 1 describes the importance and significance of the proposed work based on the available literature and gaps in knowledge. The chapter also briefly introduces the Antarctic ice core and possible proxies used for understanding the past climate. A brief overview of past climate changes and the evolution of different climate variables, particularly in the backdrop of the global warming period, is provided in this chapter. Finally, it also highlights the data gaps and their importance for a better understanding of climate systems and possible influence from tropical regions.

Chapter 2 provides a detailed overview of the study region (Dronning Maud Land region of East Antarctica) and its importance for paleoclimatic reconstructions. This chapter also describes the theoretical and experimental basis for the thesis. Two

types of samples, viz. Ice cores and surface snow core samples from coast to inland were used for paleoclimatic reconstruction. A detailed description of ice/snow core processing (cutting and sub-sampling) is provided in this chapter. Further, the analytical techniques used in the stable isotope and chemical ion measurements are described in detail. Additionally, this chapter covers the supporting/reanalysis data sources, statistical methods, and toolbox used in this study.

Chapter 3 focuses on reconstructing annual surface air temperature for the past two centuries using stable isotope records of ice cores from the DML region of East Antarctica. This chapter also provides the mechanism(s) and controlling factors of surface air temperature variability in the DML region.

Chapter 4 of the thesis uses stable isotope records from multiple ice cores and focuses on a novel method for estimating the sea ice record in the proximal oceanic sector of the DML region. This chapter provides the longest reconstructed sea ice record from the Western Indian Ocean Sector (WIOS) on an annual scale resolution. Further, an impact of different climate modes/tropical teleconnections and their related mechanism in controlling the sea ice variability is provided in this chapter.

Chapter 5 estimates the sea surface temperature of the WIOS region based on a high-resolution *d-excess* record from the IND33 ice core. This chapter presents the most extended annual SST record of the WIOS region annually. A detailed description of various forcing factors/climate teleconnections and their related mechanism in controlling the SST variability is provided in this chapter.

Chapter 6 provides the spatial distribution of stable isotopes from both snow cores and model-based records. This chapter provides the first data on spatial variability in triple isotopes of oxygen and hydrogen isotopes (δD , $\delta^{18}O$, and $\delta^{17}O$) in modern snow

along a transect in the DML region. For the first time in DML, a second-order proxy, i.e., ^{17}O -excess, is derived from the measured data and used to reconstruct the relative humidity for the past two centuries.

Chapter 7 summarizes the principal conclusions drawn from this thesis work. Furthermore, this chapter provides a brief outline highlighting future research/study scope.

Chapter 2

Material and Methods

This chapter contains a detailed overview of the study region (Dronning Maud Land region of East Antarctica) and its importance for paleoclimatic reconstructions. Further, a detailed description of the theoretical and experimental related studies forming the basis of the thesis is provided in this chapter. To achieve the scientific objectives of this thesis, two types of samples, viz. ice cores and surface snow core samples retrieved from the DML region of East Antarctica, were used. This chapter also describes the various methodologies used in the sample processing (ice/snow core cutting and sub-sampling) and analytical details of stable isotope and chemical ion measurements. The methodology used in establishing a robust chronology of the ice core is described in this chapter.

2.1 Study Area

2.1.1 Dronning Maud Land region, East Antarctica

The region of Dronning Maud Land (DML) covers between 20°W to 45°E, and its coastal region largely faces the Atlantic sector of the Southern Ocean. Several ice shelves surround the DML's coastal section, a characteristic feature of this region (Figure 2.1). Currently, Dronning Maud Land has 12 research stations. These include the Norwegian Troll and Tor stations; the Russian Novolazarevskaya Station; the South African SANAE IV; the Swedish Wasa; the Finnish Aboa; the German Neumayer-Station III and Kohnen; the Indian Maitri station; the Japanese Showa Station and Dome Fuji Station; and the Belgian Princess Elisabeth Station. These research stations are connected with a multinational collaborative air transport network known as Dronning

Maud Land Air Network Project (DROMLAN). In this region, the westerly winds play a crucial role in bringing moisture from the proximal oceanic sector to the coastal part. Further, it is known that the coastal Antarctic region receives more precipitation than its interior plateau. Thus, coastal sites are excellent locations for observing annual and decadal climate variability (Curran et al., 2003; Goursaud et al., 2019; Turner et al., 2019). Therefore, a high-resolution (seasonal to annual) ice core record can be very helpful for reconstructing past climatic records based on the calibration of ice core records with instrumental records.

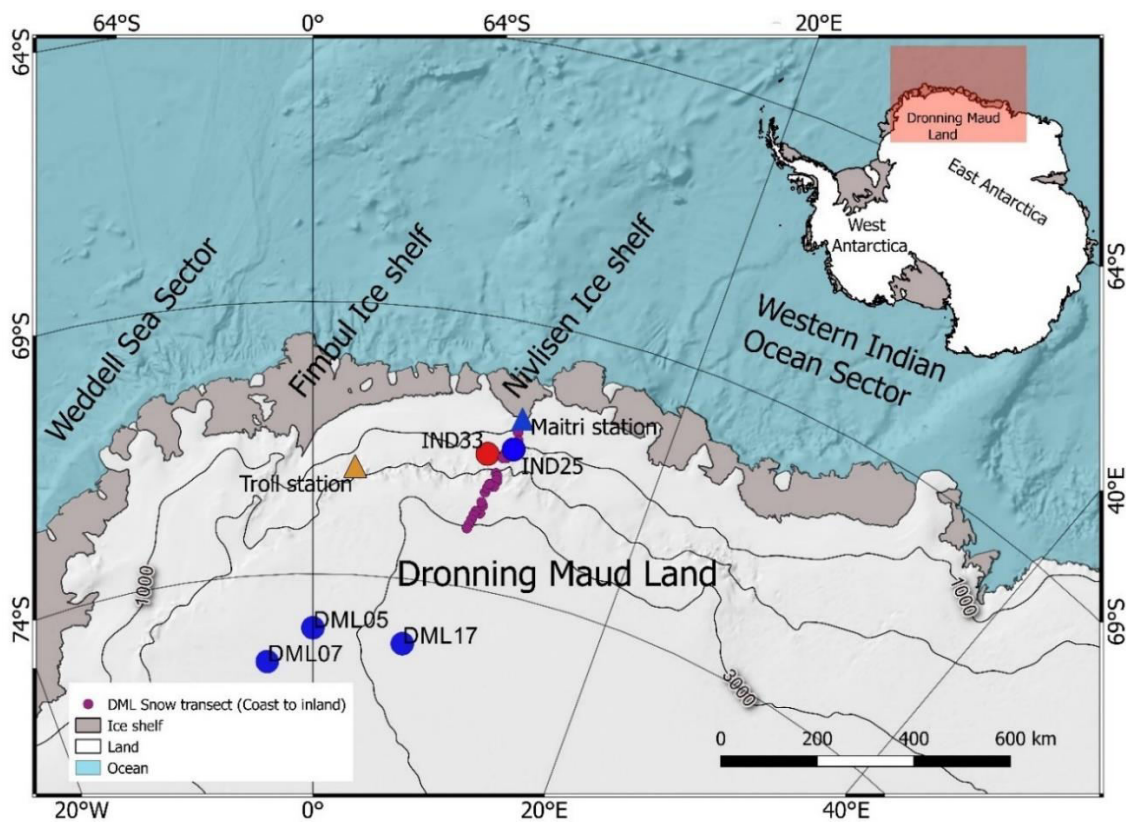


Figure 2.1. Location map of the study area and surrounding oceanic sectors in East Antarctica

The location of ice cores and snow cores used in the present study is shown in this map. The filled red circle represents the location of the newly retrieved IND33 ice core, while blue circles denote other published ice core records of IND25, DML07, DML05, and DML17 (Graf et al., 2002) used in this study. The snow cores transect (coast to inland) used in the present study is shown in purple circles.

2.1.2 Ice core and snow cores from the DML region

This study has used a suite of snow cores along a coast-to-inland transect for understanding the environmental processes and ice cores for reconstructing the regional climate variability. A new coastal ice core record (IND-33/B8; hereafter IND33) with a total length of 101.4 m was retrieved using an electro-mechanical drill during the 33rd Indian Scientific Expedition to Antarctica (ISEA) in the austral summer of 2013–14 from the central DML region (location: 71° 30' 36" S and 10° 09' 36" E; elevation: 1470 m) (Figure 2.1). The ice core drilling site was selected based on ground penetrating radar (GPR) data collected during the 28th ISEA and satellite data that contained information on the accumulation, ice flow velocity, and flow direction. With the logistics support of Maitri station, an over snow traverse was undertaken using several tracked snow vehicles. The entire drilling operations were carried out during the night hours to reduce the warmth and direct sunlight potentially hazardous to the drilling operations. The typical ambient temperatures during working hours varied between -25° and -20° Celsius, with strong catabatic winds at night. The drilling camp activities are depicted in Figure 2.2. Drilling activities were completed simultaneously, with all ice cores being labeled, packed in LDPE rolls, and stored in custom-made EPP (Expanded Polypropylene) ice core boxes. The drilling touched 101.4 m depth, and the operations were stopped due to multiple technical/logistic reasons. Accordingly, the camp was closed, and all types of machinery were packed properly in the drilling container for future missions. These EPP boxes were safely placed in deep snow pits and covered with snow till they were taken to the expedition vessel for final transport to NCPOR, Goa.

2.1.3 Technical details of ice/snow core drilling system

Ice core drilling was conducted using an electro-mechanical ice core drilling system (Type D-2 by GeoTecs). The drilling system is capable of recovering ice core with a diameter of 9.44 cm and core length of about 80cm in a single run. The outer diameter of the core barrel is 10.16 cm, and the length is 1.99 m. Two types of cutters are placed with rake angles of 35 and 40. The other technical details related to the ice core drilling system are provided in Table 2.1.

Table 2.1. Technical details of the drilling system

Drilling Components	Specifications
Core mount (shoe)	Three types with pitches 2, 3, and 4mm
Outer barrel Jacket	Diameter: 12.5 cm; Length: 2.09 m
Anti-torque system	Leaf spring blades (3 pcs) made of spring steel
Blade dimensions	length: 63.2 cm, width: 2 cm, thickness: 2.5 cm
Drive unit	DC Motor (100V/350 W/ 4000 rpm)
Reducer	Harmonic drive system with 1:80 reduction gear ratio
Winch unit model	Model W-MDL; Load: 100 kg
Armored cable diameter	5.7 mm
Drill Motor	DC Servo motor (87 V/11A/ 800 W/ 1,750 rpm)
Drill Mast	Height: 3.56 m (at the center of Pulley), made of aluminum
Pulley diameter	31.3 cm.

Many parameters affect the drilling system's performance, but the most important are the type of firn/ice and the surface/borehole temperature. The drilling system was designed for ice but drilled coastal ice sheets are comparatively warm, making optimal core recovery challenging.

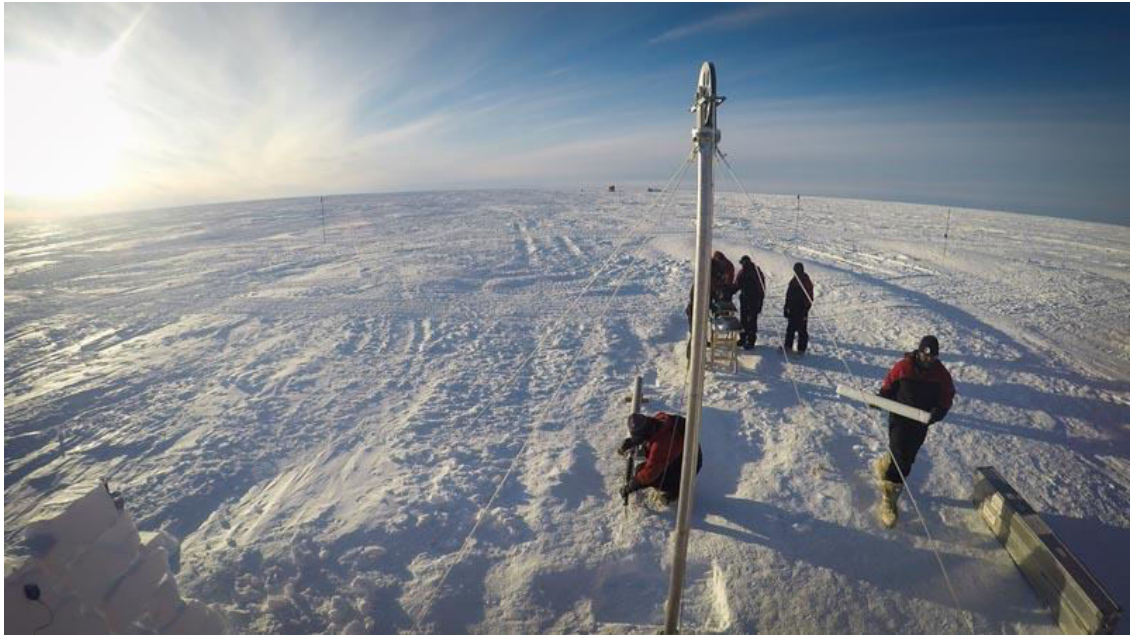


Figure 2.2. Ice core drilling conducted from the central DML region (location: 71° 30' 36" S and 10° 09' 36" E; elevation: 1470 m).

Snow cores along a transect from coast to inland in DML (a total of 25 snow cores, each ~1 meter long and 14 cm diameter) were retrieved using a KOVACS Mark-IV hand-drill during 2008–09 (Figure 2.3). The length of the core barrel was about 1.2m. A simple push-lock mechanism connected the torque handle with the barrel on the top portion. The core cutters are present at the bottom end of the barrel and capable of coring through the snowpack. The bottom end of the barrel was fitted with stainless steel core catchers to prevent the core from sliding out. At a time, this device can core an effective length of 1m of snow. Snow core samples were collected at intervals of 10km from the DML coast to the inland region, covering 300km and elevations up to 2800 m a.s.l. The retrieved snow cores were sealed immediately in high-density polyethylene bags to avoid contamination.



Figure 2.3. Drilling of snow cores was performed with a Kovacs Mark IV device with a 14 cm barrel diameter and snow cutters.

Afterward, the samples were packed in EPP boxes and stored in a refrigerated container at -20°C until transported to the National Centre for Polar and Ocean Research (NCPOR), Goa, India, where they were stored at the in-house Ice Core Laboratory maintained at -20°C .

2.2 Processing (core cutting and sub-sampling) of ice core and snow cores

The ice core processing laboratory at NCPOR is maintained at -15°C and enabled with core cutting/sub-sampling of ice/snow cores. A vertical bandsaw ice core cutter was used to slice the ice cores into two sections, with one section archived for future research (Figure 2.4c). The other half section of the ice core was decontaminated by carefully removing the outer layers using microtome blades. The sub-sampled

sections (5cm) were further cut into different parts for stable isotopes of water (oxygen and hydrogen), trace elements, atmospheric dust, and major ion measurements (Figure 2.4d). The outer section of the sub-sampled core is used for stable isotopic measurement, whereas the interior section is used for trace elements, atmospheric dust, and major ion measurement to avoid contamination (shown in Figure 2.4b). Each subsample was sealed in contamination-free LDPE containers for stable isotope, ionic, trace metal, and particle quantification analysis. However, in the present thesis, only stable isotopes and major ions were used to understand the climate variabilities.

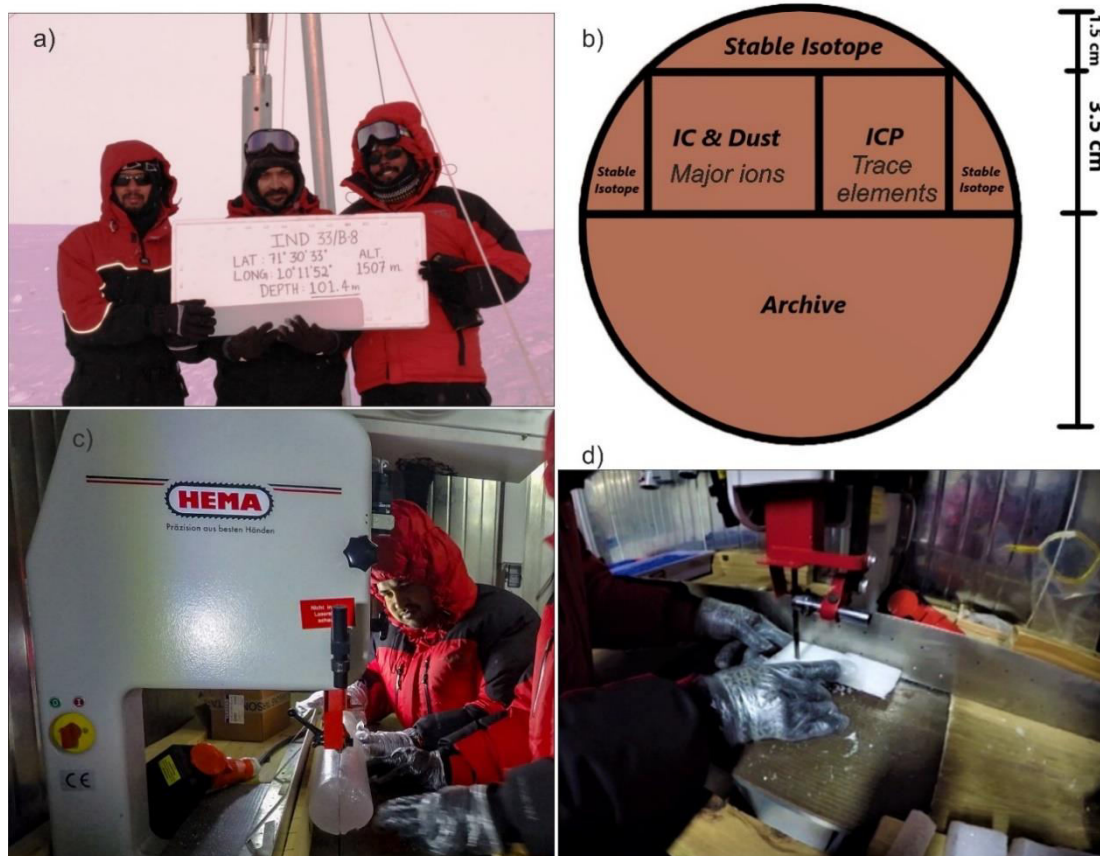


Figure 2.4. Ice core retrieval and sample processing at National Centre for Polar and Ocean Research (NCPOR).

(a) The IND33 ice core field photo. (b) Ice core sub-sampling plan utilized for different types of analysis based on the cross-section shown in the figure. (c) Ice core cutting using a vertical bandsaw cutter. (d) sub-sampling of ice at 5cm intervals.

2.3 Analysis of ice core and snow core samples

2.3.1 Stable isotopes analysis using Isotope Ratio Mass Spectrometer (IRMS)

The stable isotopic ratios of melted ice core samples were measured using an ‘Isoprime’ Isotope Ratio Mass Spectrometer (GV Instruments, UK) at the NCPOR laboratory (Figure 2.5). The details of the $\delta^{18}\text{O}$ measurements have already been discussed elsewhere (Thamban et al., 2013). Briefly, the method of equilibration of water samples with CO_2 gas (Epstein and Mayeda, 1953) was used to determine $\delta^{18}\text{O}$ values. The isotopic composition is expressed per mil (‰) with respect to the international standard VSMOW. We measured $\delta^{18}\text{O}$ values in our in-house laboratory standard CDML1 (Naik et al., 2010) several times at regular intervals during the analysis of these ice core samples. The isotopic composition of the in-house standard was calibrated against the VSMOW/SLAP standards (Coplen et al., 1996). External precision of the $\delta^{18}\text{O}$ measurements was better than 0.1‰ (n=137, 1 σ standard deviation) based on several repeat measurements of the in-house standard CDML1 during the analysis.



Figure 2.5. Stable Isotope Ratio Mass Spectrometer (IRMS) at NCPOR, Goa.

2.3.2 Analysis of stable isotopes using Triple Isotope Water Analyzer (TIWA)

Traditional water isotope analysis performed using IRMS technology requires extensive sample preparation and a skilled, experienced operator. Further, oxygen and hydrogen ratios are separately processed, with ^{17}O being particularly cumbersome for IRMS. Recent advances like the cavity-enhanced laser absorption technique measure all three isotopes simultaneously, directly from water-based samples. Accordingly, all new ice/snow core samples were analyzed for oxygen and hydrogen isotopic ratios at National Centre for Polar and Ocean Research using OA-ICOS (off-axis integrated cavity output spectroscopy) laser absorption spectrometer, known as Triple Isotope Water Analyzer (TIWA-45EP from Los Gatos Research, USA) (Figure 2.6). This

instrument can simultaneously report all the stable isotopes of water ($\delta^2\text{H}$, $\delta^{17}\text{O}$, $\delta^{18}\text{O}$). This enabled us to derive the second-order proxies, such as *d-excess* and *¹⁷O-excess* (described in the details in the following section). The oxygen and hydrogen isotopic ratios were determined with high accuracy. The melted ice core samples were introduced in TIWA-45EP without sample conversion through PAL, HTC-xt auto-injector (CTC Analytics) equipped with a heated (≈ 85 °C) injector block (LGR) (Berman et al., 2013). Using Hamilton 1.2 μL , zero dead volume syringe, samples were injected into the injector block and evaporated for direct isotope analysis. Measurements were completed at a speed of ~ 90 s per individual injection. To remove the sample-to-sample memory, a total of nine injections were made, in which the first three injections were removed. The last six injections were averaged to produce a single, high-throughput (HT) sample measurement. One commercially available working standard from LGR1C and two laboratory standards (CDML1 and HL1) with known isotopic composition, spanning the entire range of our sample measurements (-46.19 ‰ to -19.49 ‰ for $\delta^{18}\text{O}$ and -362.85 ‰ to -154.0 ‰ for δD) were analyzed routinely as reference waters after every five ice core samples to check the instrument performance. Laboratory standards are calibrated on VSMOW/SLAP scale. The external precision obtained using our laboratory standard (CDML1 and HL1) for $\delta^{18}\text{O}$ was ± 0.046 ‰ and ± 0.068 ‰, respectively and for δD was ± 0.32 ‰ and ± 0.23 ‰ ($n=30$, 1σ standard deviation) (Table 2.2 and Table 2.3). Replicate analyses performed based on ten samples yield repeatability of ± 0.76 ‰ for δD and ± 0.09 ‰ for $\delta^{18}\text{O}$ (Table 2.4). All the raw instrumental OA-ICOS data were processed in LGR post-analysis software. Any measured injection with water number density outside the manufacturer's suggested range of $2\text{-}4.5 \times 10^{16}$ H_2O molecules/ cm^3 was discarded. Injections with incomplete evaporations were detected by examining the standard deviation of the

measured water number density (σ_{meas}) as reported by the instrument (Berman et al., 2013). Processed raw data directly gives $\delta^{18}\text{O}$ and δD , which are further used to yield deuterium excess (Dansgaard, 1964). However, for deriving the ^{17}O -excess, a more precise measurement is required for $\delta^{18}\text{O}$ and $\delta^{17}\text{O}$.

Table 2.2. HL1 standard measured for stable isotopes in TIWA-45EP instrument during the ice core sample analysis.

Standard	δD (per mil)	$\delta^{18}\text{O}$ (per mil)	$\delta^{17}\text{O}$ (per mil)
HL1	-362.534	-46.121	-24.627
HL1	-362.481	-46.119	-24.632
HL1	-362.514	-46.097	-24.616
HL1	-362.644	-46.224	-24.593
HL1	-362.603	-46.194	-24.632
HL1	-362.639	-46.127	-24.630
HL1	-362.632	-46.129	-24.632
HL1	-362.453	-46.067	-24.608
HL1	-363.030	-46.252	-24.703
HL1	-361.587	-45.868	-24.476
HL1	-362.643	-46.141	-24.658
HL1	-362.579	-46.130	-24.624
HL1	-362.536	-46.053	-24.646
HL1	-362.523	-46.090	-24.628
HL1	-362.408	-46.154	-24.709
HL1	-362.556	-46.130	-24.648
HL1	-362.665	-46.144	-24.646
HL1	-362.504	-46.062	-24.527
HL1	-362.704	-46.199	-24.655
HL1	-362.602	-46.120	-24.691
HL1	-362.729	-46.177	-24.652
HL1	-362.770	-46.169	-24.645
HL1	-362.850	-46.213	-24.695
HL1	-362.572	-46.118	-24.635
HL1	-362.676	-46.146	-24.602
HL1	-362.699	-46.152	-24.648
HL1	-362.687	-46.158	-24.654
HL1	-362.775	-46.108	-24.672
HL1	-362.821	-46.178	-24.671
HL1	-362.914	-46.177	-24.694
1σ stdev	0.238	0.069	0.048

Table 2.3. CDML1 standard measured for stable isotopes in TIWA-45EP instrument during the ice core sample analysis.

Standard	δD (per mil)	$\delta^{18}\text{O}$ (per mil)	$\delta^{17}\text{O}$ (per mil)
CDML1	-215.656	-26.938	-14.267
CDML1	-215.151	-26.969	-14.313
CDML1	-215.232	-26.944	-14.349
CDML1	-215.782	-26.915	-14.279
CDML1	-215.124	-26.914	-14.223
CDML1	-215.431	-26.963	-14.335
CDML1	-215.216	-26.937	-14.338
CDML1	-215.780	-26.893	-14.189
CDML1	-215.574	-26.925	-14.161
CDML1	-215.183	-26.923	-14.269
CDML1	-215.403	-26.945	-14.243
CDML1	-215.480	-26.906	-14.241
CDML1	-215.286	-26.893	-14.275
CDML1	-215.409	-26.984	-14.085
CDML1	-215.336	-26.959	-14.291
CDML1	-214.672	-26.930	-13.998
CDML1	-214.840	-26.906	-14.237
CDML1	-215.726	-26.965	-14.424
CDML1	-214.904	-26.921	-14.356
CDML1	-214.695	-26.869	-14.175
CDML1	-214.937	-26.870	-14.256
CDML1	-215.187	-26.850	-14.362
CDML1	-215.299	-26.830	-14.249
CDML1	-215.605	-26.839	-14.252
CDML1	-215.471	-26.830	-14.305
CDML1	-215.425	-26.956	-14.231
CDML1	-214.619	-26.902	-14.236
CDML1	-214.884	-26.836	-14.358
CDML1	-215.350	-26.835	-14.289
CDML1	-215.396	-26.947	-14.193
1σ stdev	0.323	0.046	0.086

Table 2.4. Repeated measurement of unknown sample for stable isotopes in TIWA-45EP.

Standard	δD (per mil)	$\delta^{18}O$ (per mil)	$\delta^{17}O$ (per mil)
R1	-223.553	-28.617	-15.198
R1	-222.786	-28.552	-15.221
R1	-223.285	-28.548	-15.289
R1	-223.557	-28.463	-15.121
R1	-222.520	-28.379	-15.310
R1	-222.088	-28.348	-15.159
R1	-221.571	-28.337	-15.122
R1	-221.890	-28.425	-15.322
R1	-221.908	-28.444	-15.170
R1	-221.717	-28.443	-15.315
1σ stdev	0.767	0.092	0.080

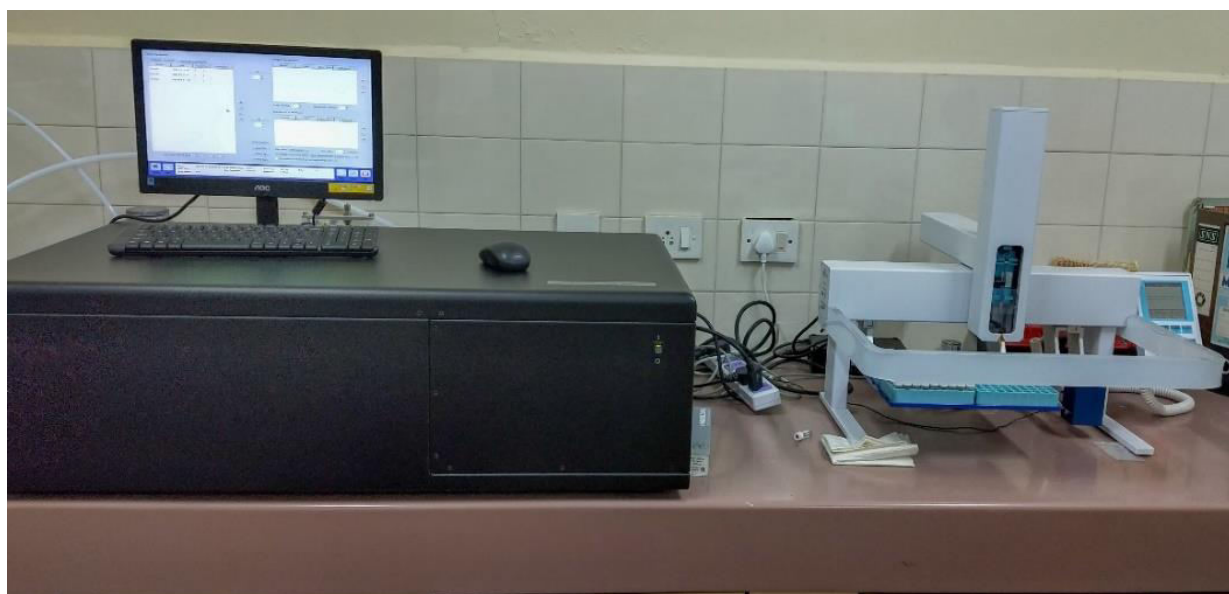


Figure 2.6. Triple Isotope Water Analyzer (TIWA-45EP) instrument at NCPOR ice core lab facility.

2.3.3 Isotope calibration and normalization for deriving ^{17}O -excess

A total of three commercially available working standards from USGS with known isotopic composition were analyzed after every ten samples during the entire period of analysis to ensure that the instrument was performing as expected. The oxygen and

hydrogen isotopic ratios ($^{18}\text{O}/^{16}\text{O}$, $^{17}\text{O}/^{16}\text{O}$, and $^2\text{H}/^1\text{H}$) were normalized using two international water standards, Vienna Standard Mean Ocean Water (VSMOW) and Standard Light Antarctic Precipitation (SLAP), following the procedure described in Schoenemann et al. (2013).

2.3.4 Data processing to derive ^{17}O -excess

The value reported for the ^{17}O -excess is much smaller (up to per meg or 0.001‰ or ppm) as compared to traditional $\delta^{18}\text{O}$ and $\delta^{17}\text{O}$ (reported in per mil or ‰). Due to this, the ^{17}O -excess values may be subject to significant uncertainty if either $\delta^{18}\text{O}$ or $\delta^{17}\text{O}$ measurements have slight variations. Therefore, this study uses a filter based on mass-dependent fractionation coefficient ($\theta = \ln(\delta^{17}\text{O} + 1)/\ln(\delta^{18}\text{O} + 1)$) to have quality-controlled data for deriving ^{17}O -excess (Tian et al., 2018). For kinetic transport, the fractional factor was found to be 0.511 ± 0.005 , while for equilibrium processes, it was 0.530 ± 0.001 (Barkan and Luz, 2005). Additionally, previous studies have demonstrated that almost all ^{17}O -excess values of global precipitation (e.g., rainfall, snowfall, and ice) fall within the range of -100 to $+100$ per meg (Li et al., 2015; Luz and Barkan, 2010; Pang et al., 2015; Steen-Larsen et al., 2014). During data processing, measurements with fractionation factors outside the 0.506 and 0.530 range and ^{17}O -excess values observed outside the range (-100 to $+100$ per meg) were removed from the analysis to reduce uncertainty. In the following step, the filtered data were used to obtain the ^{17}O -excess value for ice/snow core samples. Three USGS standards (USGS45, USGS47, and USGS46) were analyzed to check the instrument's stability and measurement precision. The precision of the measured standards is shown in Table 2.5.

Table 2.5. USGS standards were measured during the analysis of ice/snow core samples.

Standards	$\delta^{18}\text{O}$ (per mil) measured	$\delta^{18}\text{O}$ assigned	1 σ stdev	$\delta^{17}\text{O}$ (per mil) measured	$\delta^{17}\text{O}$ assigned	1 σ stdev
USGS45 (n=48)	-2.270	-2.38	0.021	-1.182	-1.19	0.016
USGS47 (n=38)	-19.797	-19.8	0.063	-10.475	-10.47	0.041
USGS46 (n=49)	-29.812	-29.8	0.067	-15.834	-15.85	0.043

2.3.5 Major ion analysis

The outer layers of the samples were cleaned using ceramic knife and placed under a laminar flow bench, housed in the -15 °C processing facility. Samples were melted in the Class-100 clean room facility immediately prior to the analysis. The melted samples were analysed simultaneously for both cations and anions using two separate Reagent Free-Ion Chromatographs. Major ions such as sodium (Na^+), (Cl^-), and sulfate (SO_4^{2-}) were analysed to use as supporting data for the establishment chronology of the IND33 ice core. Further, sodium (Na^+) and sulfate (SO_4^{2-}) ions were used to quantify the non-sea-salt sulfate [$\text{nssSO}_4^{2-} = \text{SO}_4^{2-} - 0.252 * (\text{Na}^+)$] in the record, which was used as markers of historical volcanic eruption events (tie points) to improve chronological constraints on the IND33 core. An ion-exchange chromatograph (Dionex DX-2500) with CS17 column was used to analyze cations (Na^+), whereas anions (Cl^- , SO_4^{2-}) were analyzed using Dionex ICS-2000 with AS11-HC analytical column (Figure 2.7) (Laluraj et al., 2011; Rahaman et al., 2016; Thamban et al., 2010). The instrumental detection limits of the Ion Chromatography system for the measurements of Na^+ , Cl^- and SO_4^{2-} is up to $2 \mu\text{g l}^{-1}$. Analytical precision and

accuracy determined based on several replicate analyses of samples and standards were better than 5%.



Figure 2.7. Ion Chromatograph (IC) instrument for cation and anion analysis housed in a Class-100 clean room at NCPOR, Goa.

2.4 Chronology of the IND33 ice core

An accurate age model is a prerequisite for any high-resolution ice core-based climate studies. Therefore, we made a rigorous effort to establish an accurate chronology. The chronology of the IND33 ice core was established in three steps (Figure 2.8). A first-order chronology was established based on the manual counting of annual layers in the $\delta^{18}\text{O}$ record. The primary handle in the manual layer counting was the seasonal signals in the $\delta^{18}\text{O}$ record, i.e., summer maxima and winter minima (Figure 2.8a). The excellent sampling resolution of this core enabled us to identify the seasonal signals and

differentiate annual layers. In the second step, nssSO_4^{2-} the record is plotted with the first-order chronology, and the known volcanic events were identified based on the prominent peaks in the nssSO_4^{2-} record (Figure 2.8b).

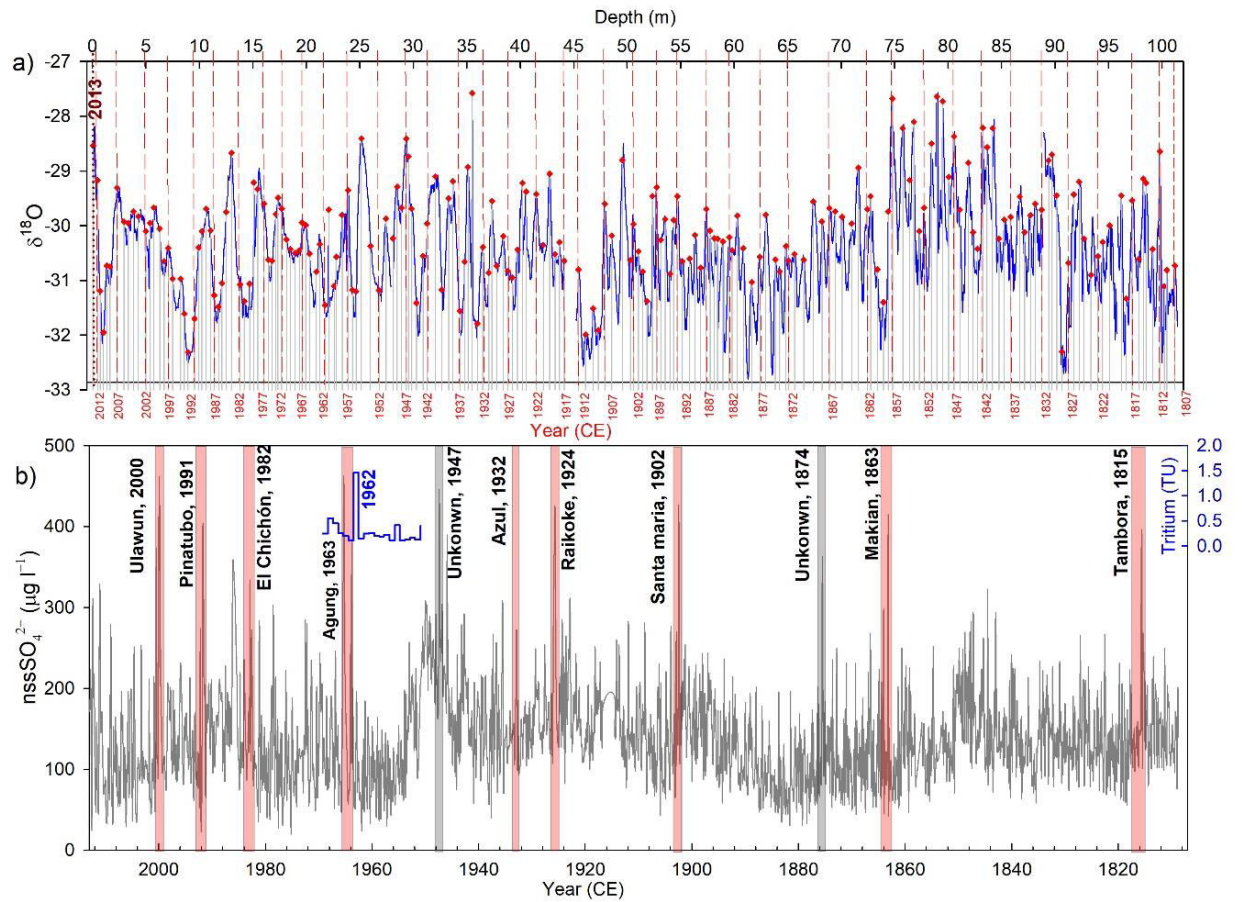


Figure 2.8. Chronology of IND33 ice core using stable isotope and major ions.

(a) The $\delta^{18}\text{O}$ profile of IND33 ice core. Red points and the vertical grey lines indicate annual layers identified based on the summer peaks in the $\delta^{18}\text{O}$ record. For better clarity, we have only shown our layer counting every five years with vertical red lines marked with the assigned year on the x-axis. (b) The non-sea salt sulfate (nssSO_4^{2-}) concentration profile of the IND33 ice core shows anomalously high peaks, which correspond to historical volcanic events. The peak in the tritium profile corresponds to the year of the major nuclear bomb testing event. The red shaded bars indicate the known historical volcanic events, whereas the grey shaded bars indicate the unknown volcanic events.

A total of nine known volcanic events were identified, including Ulawun (2000), Pinatubo (1991), El Chichón (1982), Agung (1963), Azul (1932), Raikoke (1924), Santa Maria (1902), Makian (1863) and Tambora (1815). In addition, two peaks were observed marked in a grey shade; however, we did not find any match with any known events reported in the literature. To further improve the chronology with an absolute age marker, tritium (^3H) concentrations were measured in selected sections (a total of 20 discrete samples) using an Ultra Low-Level Liquid Scintillation Spectrometer at the National Institute of Hydrology (NIH, Roorkee, India). The tritium profile shows an anomalous peak at ~ 22.25 m depth. The measured section of the IND33 ice core coincides with the well-known tritium peak of the most extensive nuclear bomb testing, "Tsar Bomba" in 1961, observed in all compiled tritium records ranges between 1961 and 1962 (Cauquoin et al., 2016). Thus considering a few months lag due to long-range transport, and it finally gets registered its signal in the Antarctic snow/ice sheet, the age of this layer is assigned as 1962 (Figure 2.8b). The tie points based on the volcanic events and the nuclear bomb testing event provide us with an independent handle to improve the accuracy of the ice core chronology. The chronology for the entire record, particularly the ages corresponding to the sub-sampling depths, was derived based on the linear interpolations between two annual layers. However, age-depth relationships generally follow non-linear relations (Peter and Carl, 2004). Therefore, linear interpolation between ages for individual sample depth and tuning the chronology with the tie points could introduce uncertainty in the ice core age model.

Additionally, isotope diffusion, wind-induced redistribution and scouring, sublimation, and condensation may introduce complexities in ice core $\delta^{18}\text{O}$ record, especially at sites or intervals of lower accumulation (Münch et al., 2016) which might

introduce uncertainty in annual layer counting based on the $\delta^{18}\text{O}$ record. To circumvent this problem and reduce the uncertainty associated with manual counting, we have used ionic records of Na^+ and Cl^- , which are less prone to such post-depositional processes and have shown strong seasonal signals; higher sea salt spray caused higher ionic concentrations during sea ice formation in winter and opposite during summer season. Finally, we compute the first-order chronology, ionic records (Na^+ and Cl^-) in-depth scale, and tie points in the MATLAB-based StratiCounter program to get the final age-depth model after non-linear optimization. This program works based on the statistical framework of Hidden Markov Models and the Expectation-Maximization algorithm (Winstrup et al., 2012), which was developed for annual layer counting in paleoclimate archives. This algorithm-based StratiCounter program has already been tested for the NEEM ice cores from Greenland and established their chronology with better accuracy (Sigl et al., 2015). The sampling resolution of the IND33 ice core was sufficiently high enough (~ 8 to 10 samples per year) to identify the seasonal signal in these ionic records and for automated annual layer counting in the StratiCounter software (Winski et al., 2019). For detailed illustration purposes, the measured ionic species and $\delta^{18}\text{O}$ record of the topmost section (0–10m depth) of the core, clearly depicting the annual cycles, is shown in Figure 2.9. The StratiCounter program accounts for all these chronological constraints and provides an age-depth model based on non-linear iterative optimization. Hence, chronology derived based on this method using the StratiCounter program is more robust and accurate.

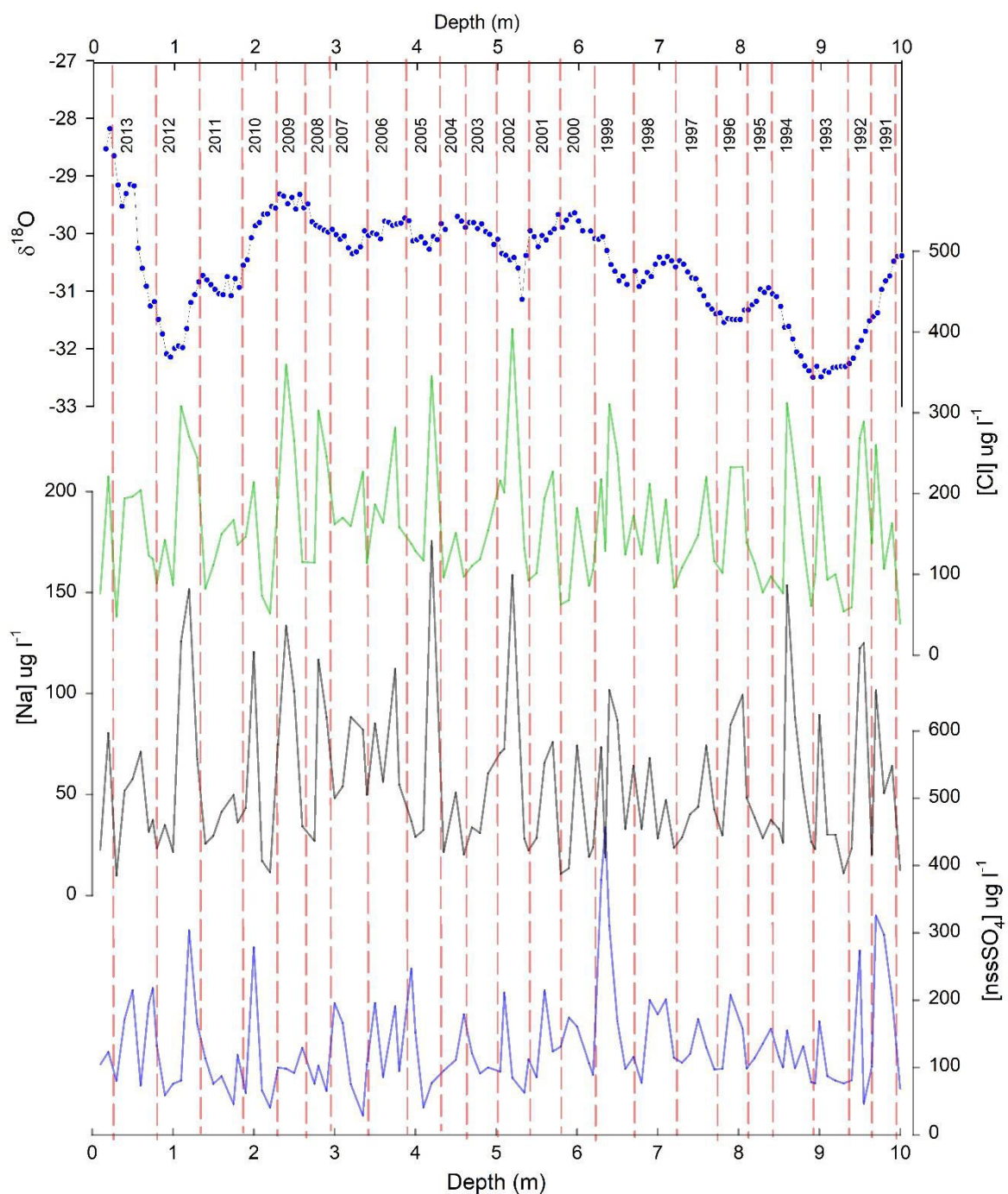


Figure 2.9. Demonstration of annual layer counting based on the seasonal signal resolved $\delta^{18}\text{O}$ and ionic records of IND33 ice core within a depth interval (0–10 m).

In the topmost section of the $\delta^{18}\text{O}$ record, ionic records such as Chloride (green), Sodium (black), and non-sea salt sulfate (blue) concentration show clear annual cyclicity. Vertical red dashed lines show the annual peak position based on the data shown.

To quantify the uncertainty of the chronology, the ages of the known volcanic events reported in the literature are compared with those derived from the automated StratiCounter program. All the ages of these known volcanic events derived from both methods agree within ± 1 year of uncertainty. Further, an excellent agreement was found between the chronology determined from manual layer counting and the chronology derived from the StratiCounter. The average difference between the ages derived from the manual layer counting and the StratiCounter is less than one year. Based on several constraints, the chronology is established for the entire core that represents the ice core record of 1809–2013 CE with an uncertainty of ± 1 year (Figure 2.10).

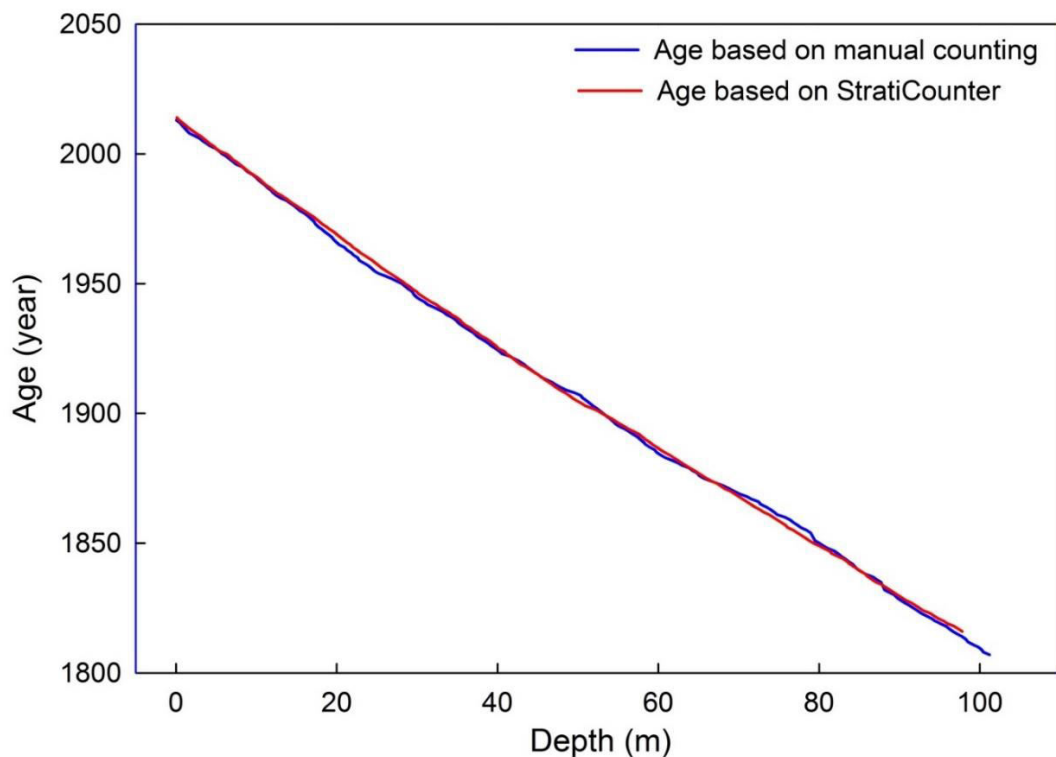


Figure 2.10. Comparison of age-depth models based on manual counting of annual layers and StratiCounter method.

2.6 An overview of the data sources, statistical methods, and toolbox used in this study

2.6.1 ERA5 reanalysis data

The European Reanalysis V5 (ERA5) represents the ECMWF's (European Centre for Medium-Range Weather Forecasts) fifth generation of climate and weather reanalysis for the seven decades (1950–recent). The datasets for ERA5 are generated using the ECMWF model forecast system coupled with 4D-Var data assimilation. In this study, ERA5 reanalysis data (Hersbach et al., 2020) available from 1979 at a resolution of $0.5^\circ \times 0.5^\circ$ latitude-longitude were used to investigate the role of different climate parameters in controlling stable isotopic variability in these ice core records and to reconstruct the past climate records beyond 1979. The monthly averaged data of ERA5 can be downloaded from Copernicus Climate Change Service (<https://cds.climate.copernicus.eu/cdsapp#!/dataset/reanalysis-era5-single-levels-monthly-means?tab=overview>).

2.6.2 ECHAM5-wiso model data

The Max Planck Institute for Meteorology has developed the ECHAM5 (European Central Hamburg Model) for predicting the atmosphere's general circulation. Simulations based on this model, when coupled with stable water isotopes, are called "ECHAM5-wiso". Model outputs are available for both long-term time scales (Steiger et al., 2017) and on a recent satellite time scale (Werner et al., 2018). The long-term model simulation is available from 1871–2011 CE at a spatial resolution of 1 degree (T106). The boundary conditions used in the long-term ECHAM5-wiso simulations were interpolated HadISST fields. These model simulations were based on the bulk formula available from Hoffmann et al. (1998), which includes both equilibrium and non-equilibrium effects of water isotope fractionation during evaporation from oceanic

surfaces. Model outputs are available in *NetCDF* (.nc files) and can be downloaded from (<https://zenodo.org/record/1249604#.YuoR5nZByUI>). ECHAM5-wiso model data was used in this study to understand the spatial variability of stable isotopes.

2.6.3 Climate Indices and ice core data

To understand the role of ENSO and its influences, long-term Southern Oscillation Index (SOI) data available from NOAA has been used in this study (<https://www.ncdc.noaa.gov/teleconnections/enso/indicators/soi/>) (Ropelewski and Jones, 1987). We also employ a long-term Interdecadal Pacific Oscillation (IPO) index available online (<https://psl.noaa.gov/data/timeseries/IPOTPI/tpi.timeseries.ersstv5.data>) (Henley et al., 2015). The Marshall SAM Index (Marshall, 2003) is combined here with the Reanalysis 20CRV2c SAM Index (Gong and Wang, 1999) to have a longer SAM record comparable to our target time window (1809–2019 CE). The Marshall SAM index on the annual scale can be downloaded from the link provided (<http://www.nerc-bas.ac.uk/public/icd/gjma/newsam.1957.2007.seas.txt>), whereas the Reanalysis 20CRV2c SAM Index is available online (https://psl.noaa.gov/data/20thC_Rean/timeseries/monthly/SAM/sam.20crv2c.long.data). The DML05, DML07, DML17, and IND25 ice core data used in this study are available at the PAGES 2k repository (<http://pastglobalchanges.org/science/wg/2k-network/data>).

2.7 Statistical methods and tools

2.7.1 Principal Component Analysis (PCA)

The Principal Component Analysis (PCA) is a statistical technique commonly used to extract the common signal from proxy records of various climate parameters and their

controlling factors. The main purpose of this method is to reduce multidimensional datasets with many variables to simpler variability without losing any relevant information. This study uses PCA to extract the common signal from multiple $\delta^{18}\text{O}$ ice core records selected from the DML region. The scree plot showing the eigenvalue and biplot for the principal components is shown in Figure 2.11. The principal component with eigen value >1 is significant and can be used to extract useful information. The implementation of principal component analysis in this study was facilitated through the utilization of XLSTAT software. The details of PCA performed on the ice cores are provided in Table 2.6, Table 2.7, and Table 2.8.

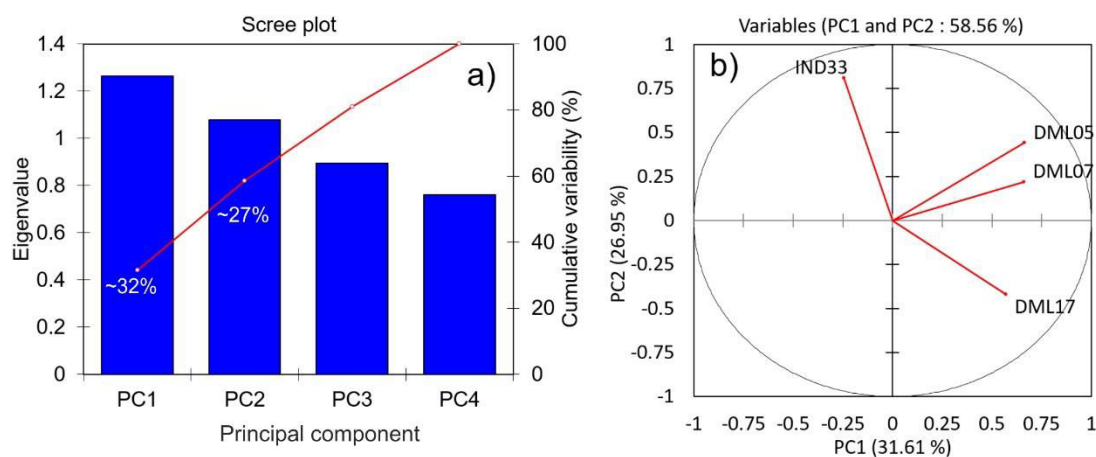


Figure 2.11. Principal Component Analysis of multiple ice cores from the DML region.

(a) Scree plot showing the eigenvalue of principal components. The principal component with an eigenvalue >1 is significant. The red line shows the cumulative % of the variation. Based on the eigenvalue, PC1 and PC2 are found to be significant. (b) Biplot for principal component analysis explains $\sim 60\%$ variability for PC1 and PC2. It also reveals that IND33 dominates the PC2, whereas the inland DML records dominate the PC1.

Table 2.6. Ice core records are used for principal component analysis.

$\delta^{18}\text{O}$ (per mil)					
Ice core	Time interval (CE)	Minimum	Maximum	Mean	Std. deviation
DML07	1809-1993	-47.85	-41.69	-45.02	1.28
DML17	1809-1993	-50.42	-42.76	-46.66	1.32
DML05	1809-1993	-49.68	-40.64	-45.12	1.54
IND33	1809-1993	-32.70	-27.68	-30.47	0.91

Table 2.7. Eigenvalue and variability for principal components.

	PC1	PC2	PC3	PC4
Eigenvalue	1.26	1.08	0.89	0.76
Variability (%)	31.61	26.95	22.37	19.06

Table 2.8. Contribution of the variables (%) from selected ice cores.

Ice core	PC1	PC2
DML07	34.64	4.47
DML17	25.66	16.45
DML05	34.92	18.12
IND33	4.77	60.97

2.7.2 Time series analysis

Several statistical analyses, such as power spectrum, wavelet transform, and scaled average variance analysis, have been performed using MATLAB codes to better understand the variability and distinguish ocean-atmospheric climate oscillations in the proxy records obtained from the ice core. The details regarding the time series analysis are provided below.

Power spectrum analysis: A Fortran 90 program (REDFIT) (Schulz and Mudelsee, 2002) is used to test if peaks in the spectrum of a time series are significant against the red noise background from a first-order autoregressive (AR1) process. A Matlab code of this program available online (<https://www.marum.de/Prof.-Dr.-michael-schulz.html#software>) is used to determine the significant periodicities against the red noise.

Wavelet analysis: Wavelet analysis decomposes the proxy-based ice core record into the time-frequency domain. The wavelet transform can be used to analyze time series that contain non-stationary power at many different frequencies. Wavelet transforms analysis enables us to identify the modes of variability and how those modes vary with time (Torrence and Compo, 1998). Statistical significance was estimated against a red noise model. A cross-wavelet analysis highlights the common highest power in two-time series and is used to analyze the covariance of two-time series. Statistical significance is estimated against a red noise model. This wavelet analysis was performed using the Matlab code available (<http://grinsted.github.io/wavelet-coherence/>).

Scaled average variance analysis: Scale-averaged variance analysis was performed on the time series record to examine the fluctuations in the record over a specific frequency band. Consequently, ENSO and PDO-driven temperature variability and changes were extracted within their respective frequency band. The analysis was carried out using Matlab codes available online at <http://paos.colorado.edu/research/wavelets/>.

Chapter 3

Rapid warming over East Antarctica since 1940s caused by increasing influence of ENSO and SAM

3.1 Introduction

The ice cores retrieved from different regions of Antarctica can be classified as low-resolution (decadal to centennial-scale over low accumulation regions), long-term records (Dansgaard et al., 1993; EPICA community members, 2004; Jouzel et al., 2007; Petit et al., 1999; Stenni et al., 2004) and high-resolution (seasonally to annually resolved over high accumulation regions), short-term records (Divine et al., 2009; Nardin et al., 2021; Schneider et al., 2017; Thamban et al., 2020). In recent years, studies have highlighted the importance of high-resolution ice core-based temperature records to improve climate models and better projections for future climate (PAGES 2k Consortium, 2013; Stenni et al., 2017). The high-resolution satellite-based temperature record for Antarctica has been available only since the beginning of 1979, and few stations-based instrumental records since ~1950 (Turner et al., 2020), which are too short to discern the long-term temperature variability. Based on a compilation of multiple (n=112) ice core water isotope records from Antarctica, Stenni et al. (2017) have reconstructed the surface air temperature of Antarctica for the past two millennia. However, only a few long-term ice core records with annual or better resolution were available from the DML region for their compilation; hence such temperature reconstruction for this region might have considerable uncertainty. Coastal Antarctica is a region of higher precipitation and accumulation (Naik et al., 2010; Thomas et al., 2017; Turner et al., 2019) and hence are ideal sites for the reconstruction of high-resolution climate records to resolve sub-annual to decadal climate variability related to temperature, precipitation, sea ice, dust, and solar cycles (Abram et al., 2007; Laluraj et

al., 2020; Laluraj et al., 2010; Laluraj et al., 2014; Masson-Delmotte et al., 2008; Mulvaney et al., 2012; Rahaman et al., 2019; Rahaman et al., 2016). Therefore, more stable water isotope records are needed from this region to reduce the uncertainty of the temperature reconstructions and improve our current knowledge of the long-term temperature variability, changes, and controlling factors.

The oxygen isotope ratios ($\delta^{18}\text{O}$) in ice core records have been widely used to reconstruct past temperatures (Dansgaard et al., 1969; Picciotto et al., 1960) and to infer the changes in moisture sources for precipitation (Noone and Simmonds, 2002). Several studies have demonstrated that the $\delta^{18}\text{O}$ proxy records show a profound influence of large-scale atmospheric circulation patterns around Antarctica on interannual to decadal and multi-decadal scales (Goodwin et al., 2016; Okumura et al., 2012; Yuan et al., 2018). Anomalous changes in sea surface temperature (SST) over the tropical Pacific associated with the El Niño Southern Oscillation (ENSO) and decadal to interdecadal Pacific oscillations significantly contribute to Antarctic temperature (Goodwin et al., 2016; Rahaman et al., 2019). Even with their distant origin in the equatorial Pacific, the ENSO strongly influences the southern extra-tropical and Antarctic climate via atmospheric teleconnections generated by Rossby wave trains (Ding et al., 2011; Jin and Kirtman, 2009; Turner, 2004). Further, Southern Annular Mode (SAM) has been demonstrated as the most dominant mode of climate variability in the Southern Hemisphere (Marshall, 2003); the positive phase of SAM is associated with low-pressure anomalies over Antarctica and high-pressure anomalies over mid-latitudes and vice-versa (Abram et al., 2014; Marshall, 2003; Marshall et al., 2006; Thompson and Wallace, 2000; Turner et al., 2005). The SAM generally shows a dipole response to the East Antarctic and Antarctic Peninsula temperature; a strong correlation between temperature and SAM is observed across the Antarctic Peninsula during the positive

SAM, and the opposite is found in East Antarctica (Kwok and Comiso, 2002b; Thompson and Solomon, 2002). Therefore, the shifting of SAM to a positive phase in the last several decades is expected to contribute to cooling across East Antarctica. However, studies from the Dronning Maud Land (DML) region of East Antarctica do not show any significant trends before 1900 CE; a significant warming trend has been observed in the last century (Stenni et al., 2017). Therefore, obtaining more spatially distributed long-term proxy records from the DML region is necessary to investigate the processes and factors that controlled the temperature variability and its trend in this part of Antarctica. Further, such studies will help improve our understanding of the influence of climatic modes and Pacific oscillations on the Antarctic temperature variability in response to the recent global warming.

This study envisages extracting temperature signals from multiple ice core $\delta^{18}\text{O}$ records and reconstructing the temperature of the past two centuries using a newly retrieved high-resolution ice core record along with other available $\delta^{18}\text{O}$ records from the DML region. Such spatially distributed high-resolution records from the DML region have enabled us to assess the interannual to decadal variability in temperature during the past two centuries and investigate factors contributing to these changes.

3.2 Results and Discussion

3.2.1 Variability in $\delta^{18}\text{O}$ Records from DML Region and Implications on Temperature Trends

The temporal variations of $\delta^{18}\text{O}$ in the IND33 ice core are shown in (Figure 3.1a). This new ice core from the coastal DML region offers a high resolution (seasonal-annual scale) record of $\delta^{18}\text{O}$; higher values are observed in summer and lower values in winter. The $\delta^{18}\text{O}$ values of the IND33 ice core range from -27.6‰ to -32.70‰ with a mean value of $-30.47\text{‰} \pm 0.89\text{‰}$. To better understand regional climate variability on

a longer time scale, we have selected three ice core records (DML05, DML07, and DML17) from the inland region of DML, which are in close proximity to the IND33 record. The annual $\delta^{18}\text{O}$ variability in DML ice cores is shown in (Figure 3.1b, c, d). Although these ice cores show large variability, they don't show a discernible common trend. The three inland ice cores from DML are close to each other within a few 100 km distances and show mean $\delta^{18}\text{O}$ values ranging from -45‰ to -46.7‰ (Graf et al., 2002). The ice cores in this study were selected based on the following criteria: (i) ice core records should have a common time interval of at least past two centuries with a time resolution of at least annual or better, (ii) the top part of the record should have a reasonable number of overlapping years with the available instrumental/reanalysis data for calibration with confidence (iii) the region from where the cores were selected should come under the significant influence of ENSO and SAM.

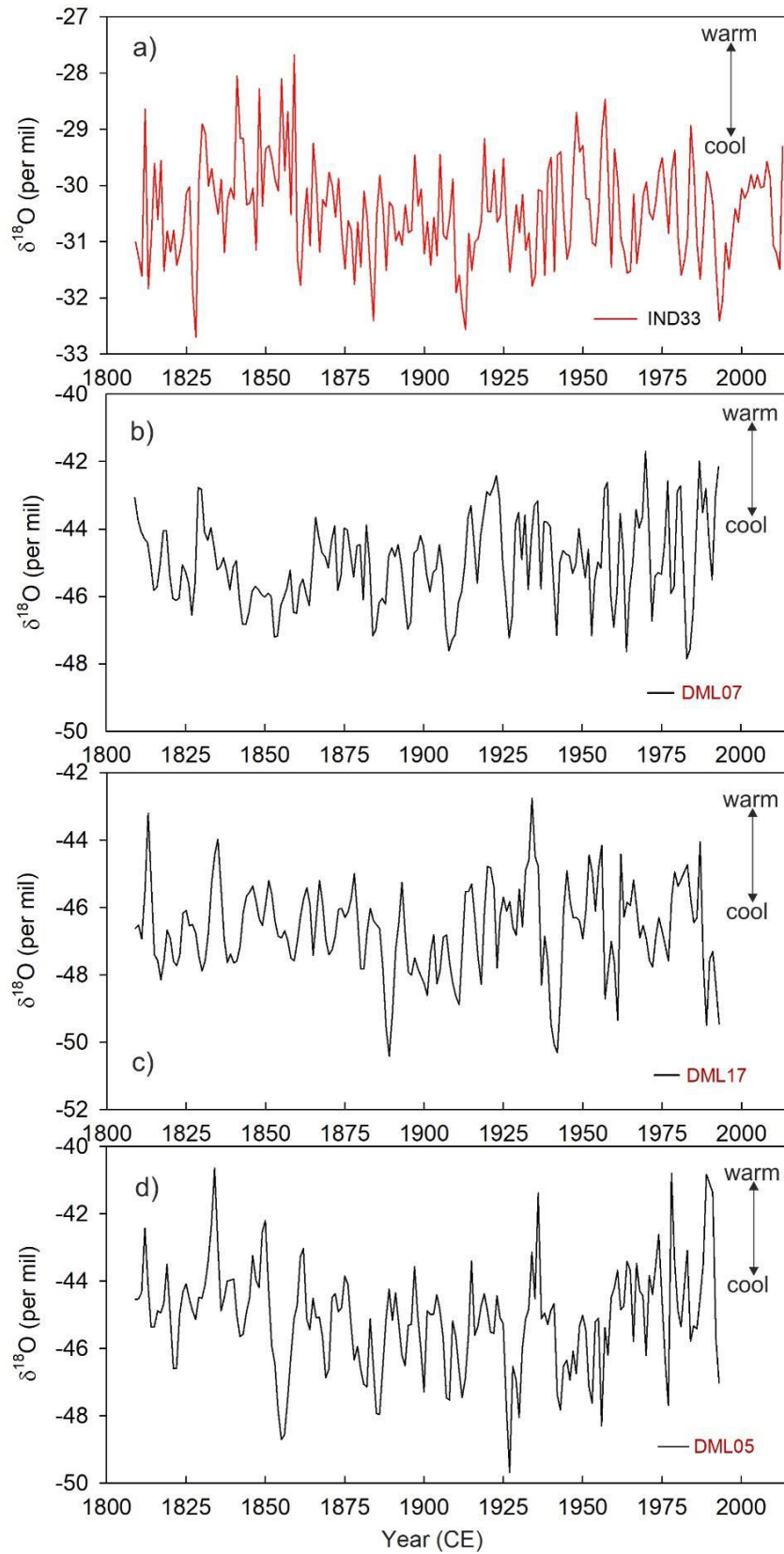


Figure 3.1 Annual $\delta^{18}\text{O}$ record of ice cores used in this study.

(a) IND33 ice core $\delta^{18}\text{O}$ record (1809–2013 CE) is compared with the DML ice core records (b) DML07, (c) DML17, and (d) DML05 of their common time interval (1809–2013 CE).

Several studies have demonstrated that $\delta^{18}\text{O}$ records in ice cores are influenced by several factors, such as temperature (Petit et al., 1999; Stenni et al., 2017), sea ice variability (Ejaz et al., 2021), precipitation (Fujita and Abe, 2006), and post-depositional changes related to exchange of water vapor between surface snow and atmosphere through diffusion (Landais et al., 2017). As a result, the $\delta^{18}\text{O}$ records represent a composite signal of various meteorological parameters and post-depositional processes and hence cannot be directly used to decipher climate variability. A previous study from this region has observed that the selected $\delta^{18}\text{O}$ ice core records are only weakly correlated with ERA5 annual surface air temperature (Ejaz et al., 2021). Therefore, principal component analysis (PCA) was performed on these four $\delta^{18}\text{O}$ records within their common time window (details provided in chapter 2) to deconvolute different climate signals embedded in the $\delta^{18}\text{O}$ records and finally to extract a common temperature signal which is representative over a large region of DML.

The $\delta^{18}\text{O}$ record in the ice core is influenced by several other factors, such as temperature, sea ice concentration, precipitation, and winds. However, surface air temperature is the dominant factor among the meteorological parameters that explain maximum variability in $\delta^{18}\text{O}$ ice core records from Antarctica (Masson-Delmotte et al., 2008; Rahaman et al., 2019). Therefore, the first principal component (PC1), which explains maximum variability (~32%), is dominantly related to the air temperature (Rahaman et al., 2019). Further, the second principal component (PC2), explains ~27% variability of $\delta^{18}\text{O}$ record is related to sea ice variability (Ejaz et al., 2021). The other

principal components, such as PC3 and PC4, are not significant (eigenvalues <1); therefore, they were not considered for further investigation. This study carried out a more rigorous investigation based on Pearson correlation analysis between PC1 and annual/seasonal surface air temperature shown in Figure 3.2. PC1 is found to be weakly correlated with the ERA5 annual surface air temperature averaged across the grid box over the DML region (71.5°S to 75.5°S ; 11.0°E to 5°W) from 1979 to 1993 CE ($r=0.33$, $p>0.05$) (Figure 3.2a).

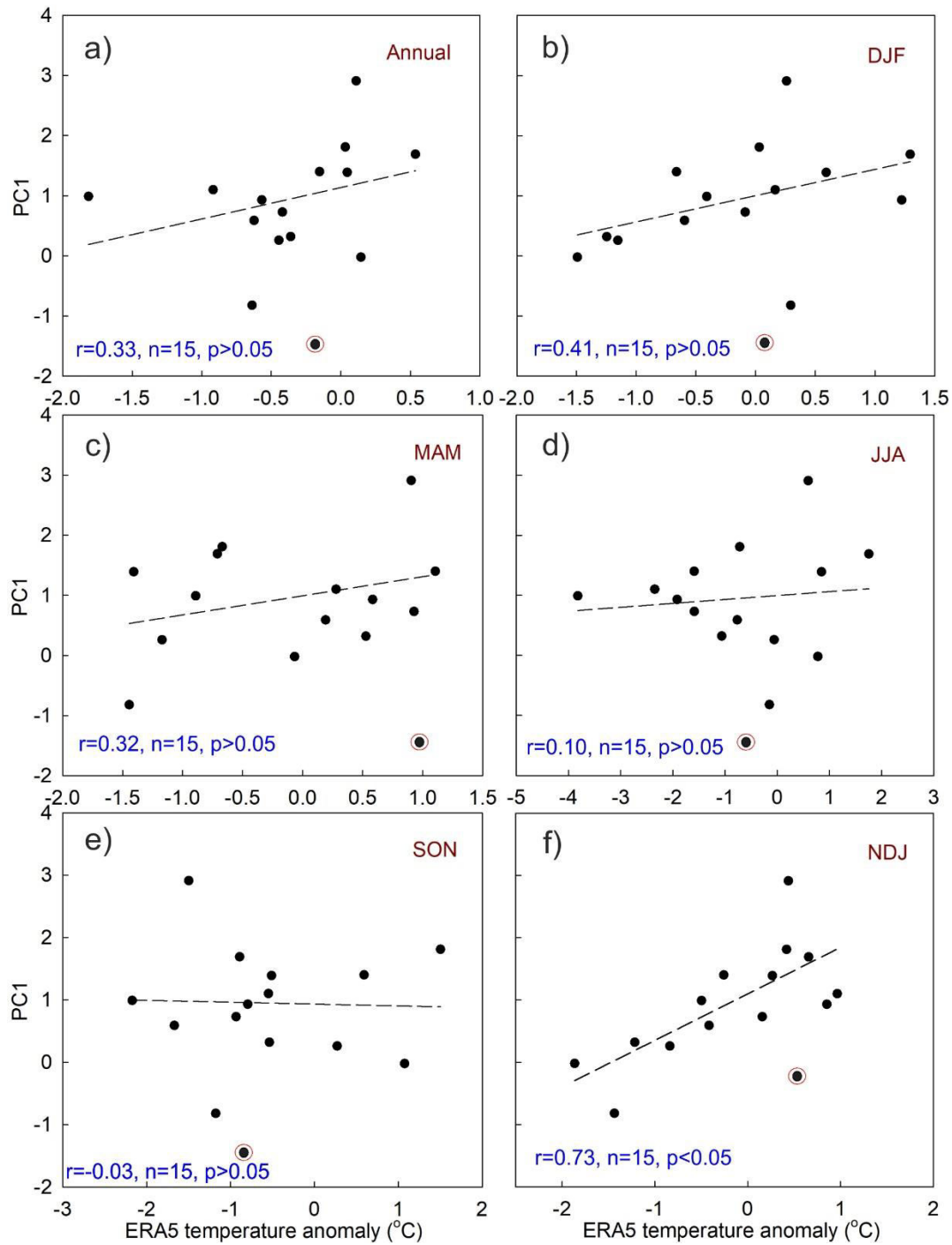


Figure 3.2 Correlation of PC1 with annual and seasonal ERA5 surface air temperature.

(a) PC1 correlation with ERA5 annual surface air temperature anomaly averaged over the DML region (71.5°S to 75.5°S; 11.0°E to 5°W). PC1 correlation with ERA5 surface air temperature anomaly averaged over the DML region during (b) Summer (DJF), (c) Autumn (MAM), (d) Winter (JJA), (e) Spring (SON), and (f) Late-spring to summer (NDJ). The strong correlation between PC1 and ERA5 surface air temperature ($r=0.73$, $p<0.05$, 1979–1993 CE, lag=1year) is observed during late spring to summer (NDJ).

The correlation between PC1 and temperature is not found to be significant during summer (DJF) and autumn (MAM) (Figure 3.2b, c). However, the ERA5 surface air temperature shows a strong correlation with PC1 ($r= 0.73$, $p<0.05$, lag = 1 year) during the late spring to summer (NDJ) season for the period 1979–1993 CE (Figure 3.2f). It is interesting to note that such a strong temperature correlation is not observed during winter (JJA) and spring (SON) seasons (Figure 3.2d-e), possibly due to strong cyclonic activity and blowing wind causing reworking and redistribution of accumulated snow (Mills et al., 2019; Mott et al., 2018). Our ERA5 seasonal temperature PC1 correlation analysis shows a significant correlation mainly observed during the season of reduced surface wind speed. In contrast, correlation is not observed during the season of high surface wind speed (winter) due to the intense reworking of freshly deposited snow in cyclonic activity. The maximum correlation is observed during the late spring to the summer season (NDJ) when accumulation was reasonably higher (Figure 3.3a), and wind speed was lower to moderate (Figure 3.3b) and thus suitable for better preservation of climate signals in the deposited snow/ice sheet.

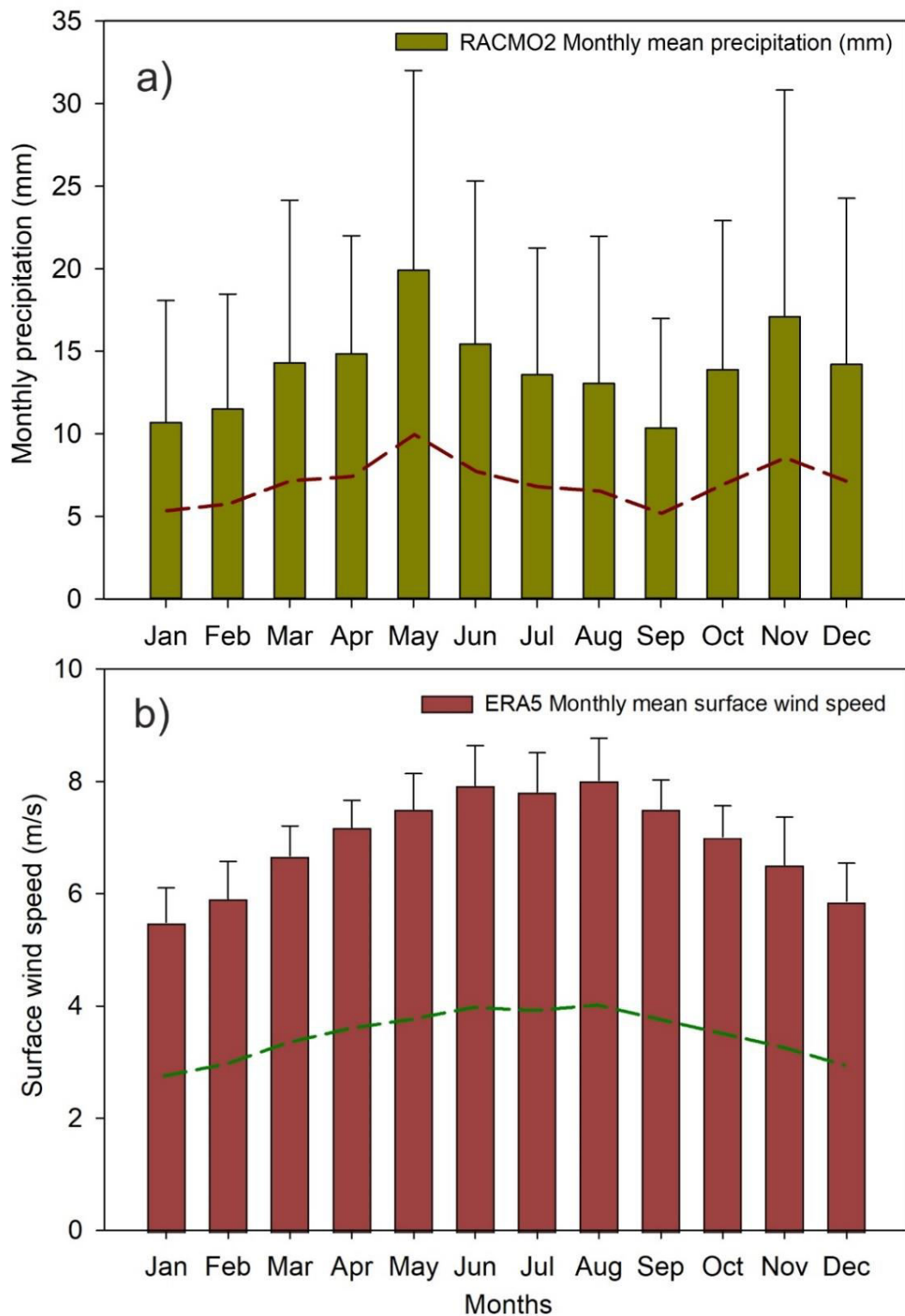


Figure 3.3 RACMO2 model monthly averaged precipitation and ERA5 monthly averaged surface wind speed.

(a) RACMO2 (van Wessem et al., 2018) model aggregate monthly precipitation over the DML region (71.5°S to 75.5°S ; 11.0°E to 5°W) from 1979–2013 CE. (b) ERA5 monthly averaged surface wind speed (m/s) over the DML region (71.5°S to 75.5°S ;

11.0°E to 5°W) from 1979–2013 CE. Error bar (1σ) represents precipitation and wind speed fluctuations during the representative month for the due period. Red and green dotted lines are drawn from the center of the bar plot to show precipitation and wind patterns during the different seasons. During April-May-June and October-November-December, the DML region is experiencing periods of high precipitation. In the case of surface wind patterns over the DML region, a high-speed wind during the winter caused freshly deposited snow to be reworked, but a low-speed wind during the summer resulted in less snow reworking.

The spatial correlation between PC1 and ERA5 surface air temperature during the NDJ season establishes a robust relation (Figure 3.4a). The spatial correlation is significant over the DML region during 1979–1993 CE. Therefore, for the reconstruction of the DML temperature, we have used the regression equation derived from the correlation between the PC1 and NDJ temperature anomaly.

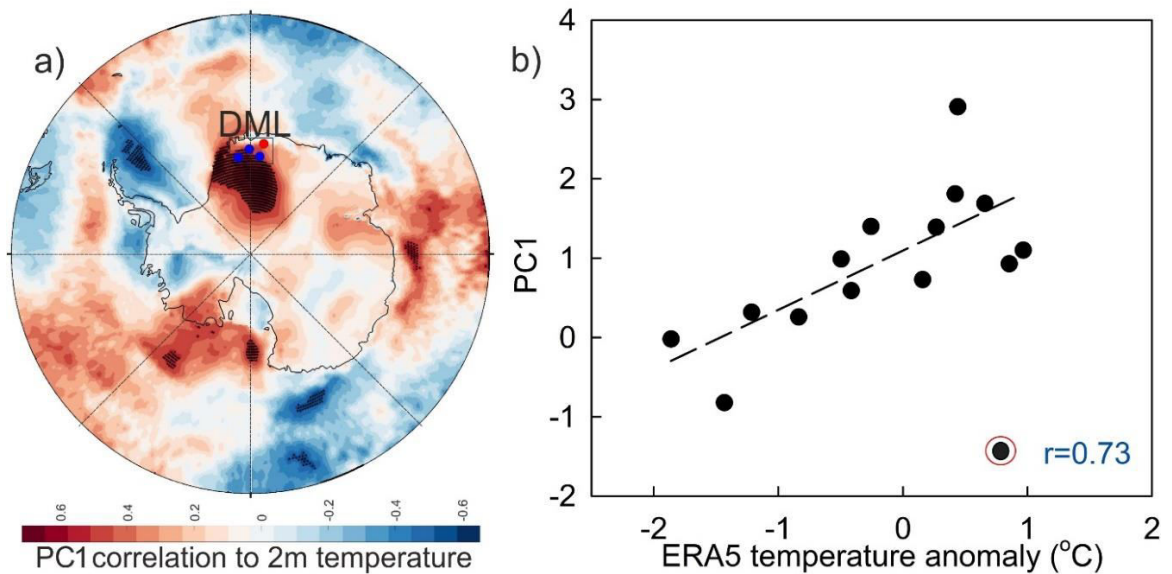


Figure 3.4. Correlation of PC1 with seasonal ERA5 surface air temperature.

(a) Spatial Correlation of Principal Component 1 (PC1) with seasonal (Nov-Dec-Jan) ERA5 surface air temperature record for the period of 1979–1993 CE. Stippling indicates statistically significant correlations (95% confidence level). (b) PC1 shows a significant correlation with seasonal (Nov-Dec-Jan) ERA5 2m temperature anomaly averaged over the DML region (71.5°S to 75.5°S; 11.0°E to 5°W) ($r= 0.73$, $n=15$, $p<0.05$, 1979–1993 CE, lag = ~ 1 year).

The temperature anomaly record (1809–1993 CE) of the DML region is reconstructed based on the linear regression equation derived from PC1 and the ERA5 NDJ temperature correlation (Figure 3.4b). Further, the ERA5 surface air temperature anomaly for the DML region (1994–2019 CE) is combined with our reconstructed ice core temperature record to determine the recent trend in the temperature record. The combined record of reconstructed and reanalysis ERA5 temperature anomaly records for the past two centuries (1809–2019 CE) enables us to determine the long-term trend in the DML temperature anomaly (Figure 3.5) and the influence of climate modes on temperature variability. To discern the significant long-term trend, a Mann-Kendall test (Kendall, 1975) was conducted and determined the breaking points of the trends in the temperature record. Accordingly, two significant trends have been identified in the DML temperature record (Figure 3.5). The reconstructed temperature record revealed a significant cooling trend during 1809–1907 CE ($n=98$, $p<0.05$) with a rate of -0.164 ± 0.045 °C decade⁻¹, followed by a significant warming trend with a rate of $+0.452 \pm 0.056$ °C decade⁻¹ during 1942–2019 CE ($n=77$, $p<0.05$). A recent study has shown that, during the past two decades (1998–2016 CE), a more rapid increase in the temperature ($+1.1 \pm 0.7$ °C decade⁻¹) has been observed in western Dronning Maud Land (Medley et al., 2018). Our study is also consistent with the rapid warming trend in recent decades. Therefore, it is essential to identify the potential drivers and their role in controlling the DML temperature trends and variability in the past two centuries.

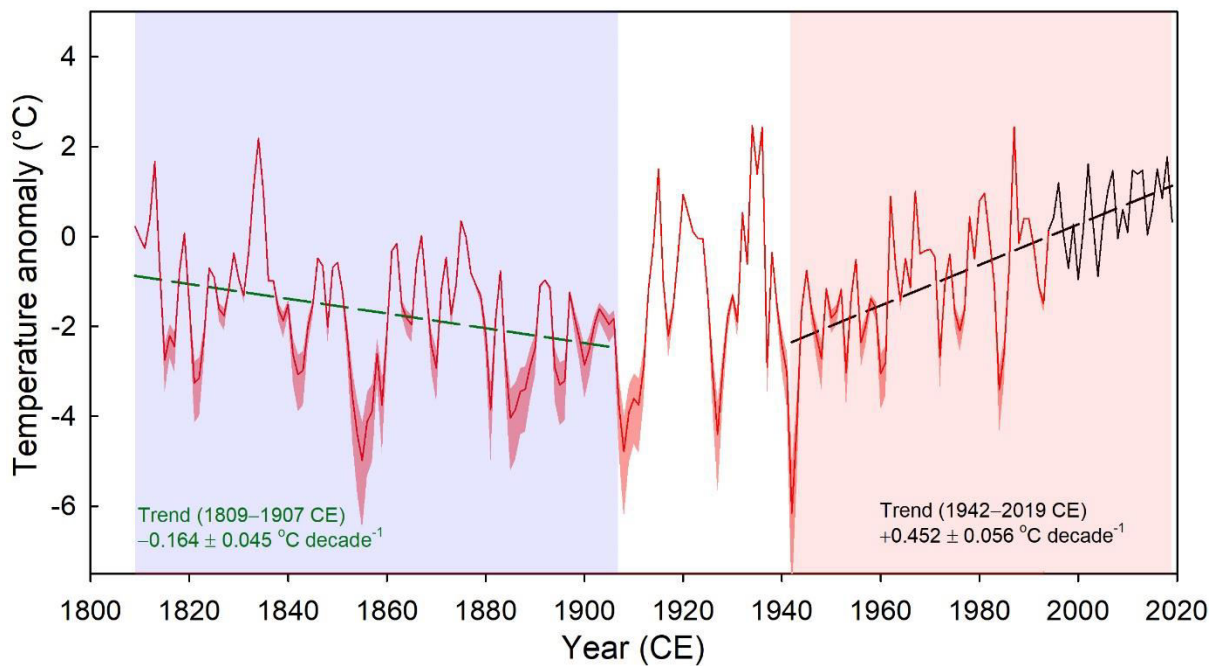


Figure 3.5. Reconstructed surface air temperature of DML region and trend analysis.

Trend analysis of the reconstructed surface air temperature anomaly record of the DML region, East Antarctica. The temperature anomaly was calculated based on the linear regression equation derived from the correlation between PC1 and ERA5 temperature anomaly (NDJ). The reconstructed mean annual surface air temperature anomaly demonstrates a significant ($p < 0.05$) declining trend during 1809–1907 CE and a significant ($p < 0.05$) increasing trend during 1942–2019 CE. The reconstructed temperature anomaly curve is shown in the red line (1807–1993 CE), while the black curve denotes the ERA5 2m temperature anomaly record for 1994–2019 CE. The red color shade represents the error envelope on the reconstructed temperature, and the dashed straight lines indicate trend lines.

3.2.2 Role of ENSO, IPO, and SAM on Temperature Variability during the Last Two Centuries

Tropical Pacific oscillations such as ENSO, IPO, and their teleconnections to Antarctica in space and time, particularly in the recent global warming, are not well understood. To identify dominant periodicities associated with the climate modes and their temporal evolutions during the past two centuries, a spectral analysis (Schulz and Mudelsee, 2002) was performed on the temperature anomaly record (Figure 3.6a)

(1809–2019 CE). The spectral analysis revealed significant (95% χ^2 level) periodicities of 5.2 and 15 years (Figure 3.6b). Further, a continuous wavelet analysis of the temperature record was performed to understand the influence of ENSO and IPO on DML temperature during the past two centuries and their temporal evolution (Figure 3.6c). Morlet wavelet transform (Torrence and Compo, 1998) is used to analyze non-stationary climate signals in the temperature record, which enable us to identify significant (at 95% significance level) periodicities and their links to ENSO and IPO. This highlights the maximum power of lower frequencies in the decadal band (12–18 years) during 1830–1870 CE and 1910–1950 CE, whereas, after the 1930s, high-frequency ENSO signals within the (2–8 years) band become more prominent. The variance at the ENSO band shows an increasing trend in the last century (Figure 3.6d), which is consistent with the earlier report from East Antarctica (Rahaman et al., 2019).

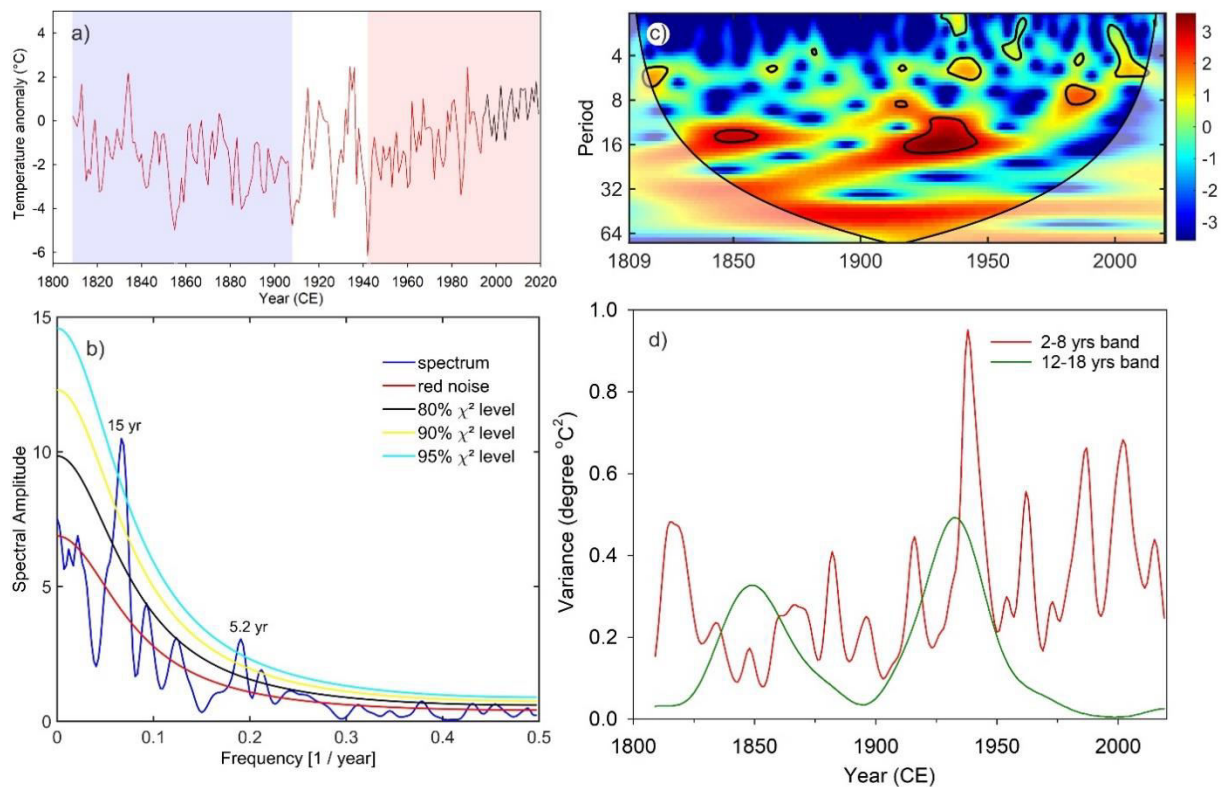


Figure 3.6. The power spectrum, wavelet, and scaled averaged variance analysis of reconstructed surface air temperature anomaly.

(a) Reconstructed temperature anomaly record combined with ERA5 surface air temperature anomaly records (1809–2019 CE). (b) Spectral analysis of temperature anomaly shows significant periodicities of 15 and 5.2 years (95% χ^2 level). (c) Wavelet analysis of the temperature anomaly record highlights significant periodicities in the color band. (d) Scaled average variance analysis at two bands, namely, 2–8 years and 12–18 years frequency bands.

In order to deconvolute the signals of ENSO and IPO, bandpass filters were applied at 2–8 years and 12–18 years bands (Figure 3.7a–b). The bandpass filtered temperature record at 12–18 years band shows anti-phase relation with that of the IPO index throughout the record (except for 1890–1920, and 1960–1980 CE). This anti-phase relation between temperature and IPO was more prominent from 1920–1950 CE. A cross-wavelet analysis (Grinsted et al., 2004) between the DML temperature anomaly record and the Southern Oscillation Index (SOI) reveals the highest common power at

2–8 years band (Figure 3.7c). This shows a systematic increase from lower to higher frequencies at the ENSO band in the 20th century. This is consistent with the earlier reports of increasing ENSO activity and its influence on the Antarctic temperature (Otto-Bliesner et al., 2016; Rahaman et al., 2019; Schmidt et al., 2012; Yeh et al., 2018). Cross-wavelet analysis between DML temperature and IPO shows a strong anti-phase relation between 1920–1950 CE (Figure 3.7b).

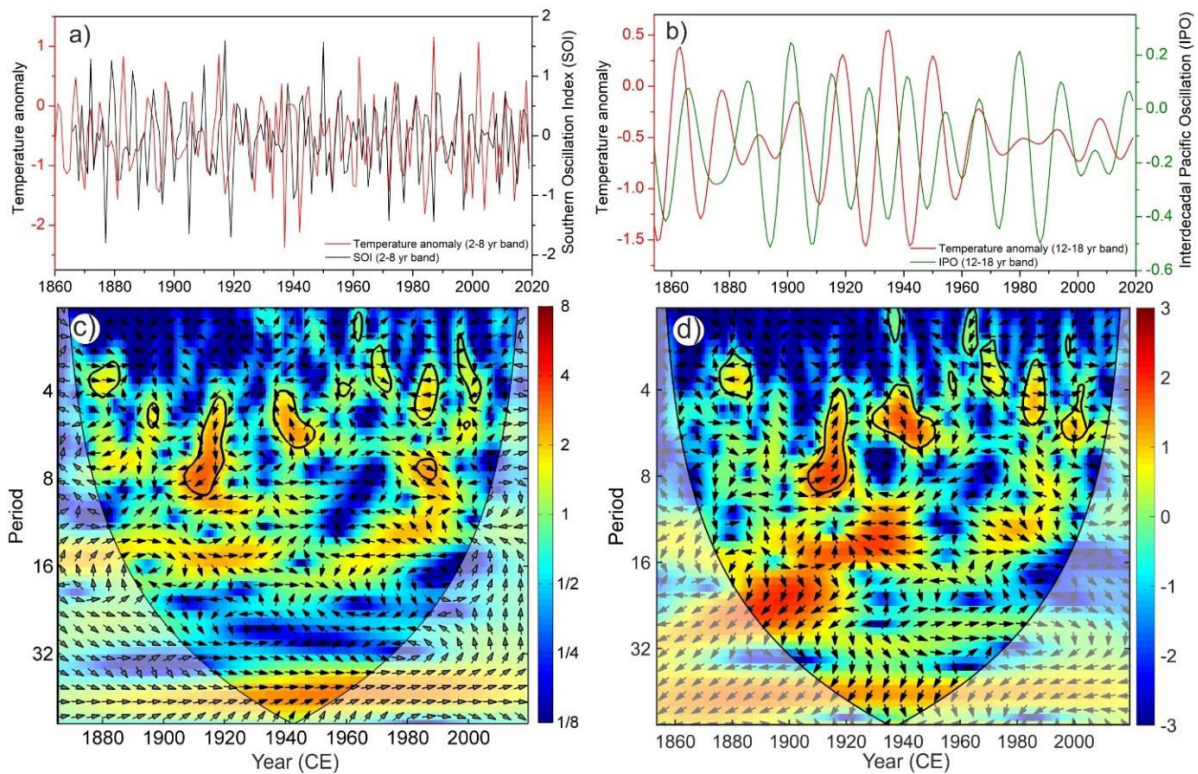


Figure 3.7. Cross wavelets transform analysis of surface air temperature anomaly with SOI and IPO.

Annual variability in temperature anomaly record with (a) SOI (1866–2019 CE) (Ropelewski and Jones, 1987), (b) IPO (1854–2019 CE) (Mantua and Hare, 2002). Cross-wavelet analysis of DML temperature anomaly with (c) SOI and (d) IPO. The thick black line depicts the cone of influence. The relative phase relationship is shown as arrows (with in-phase pointing right, anti-phase pointing left, temperature leading SOI or PDO by 90° pointing straight down and vice versa).

To understand the role of ENSO in modulating the temperature over the DML region, it is important to investigate the spatial variability of temperature during the El Niño (warm) and La Niña (cool) phases. Accordingly, we have used the ERA5 2m temperature anomaly for strong El Niño (1987, 1997, 2002, and 2016) and La Niña phases (1989, 1999, 2000, and 2010) to highlight the temperature variability during ENSO events. During the El Niño events, the spatial anomaly plots show an increase in surface temperature over the DML region (Figure 3.8 a,b,c,d). In contrast, it shows reduced surface temperature over the DML region during the La Niña events (Figure 3.8 e,f,g,h).

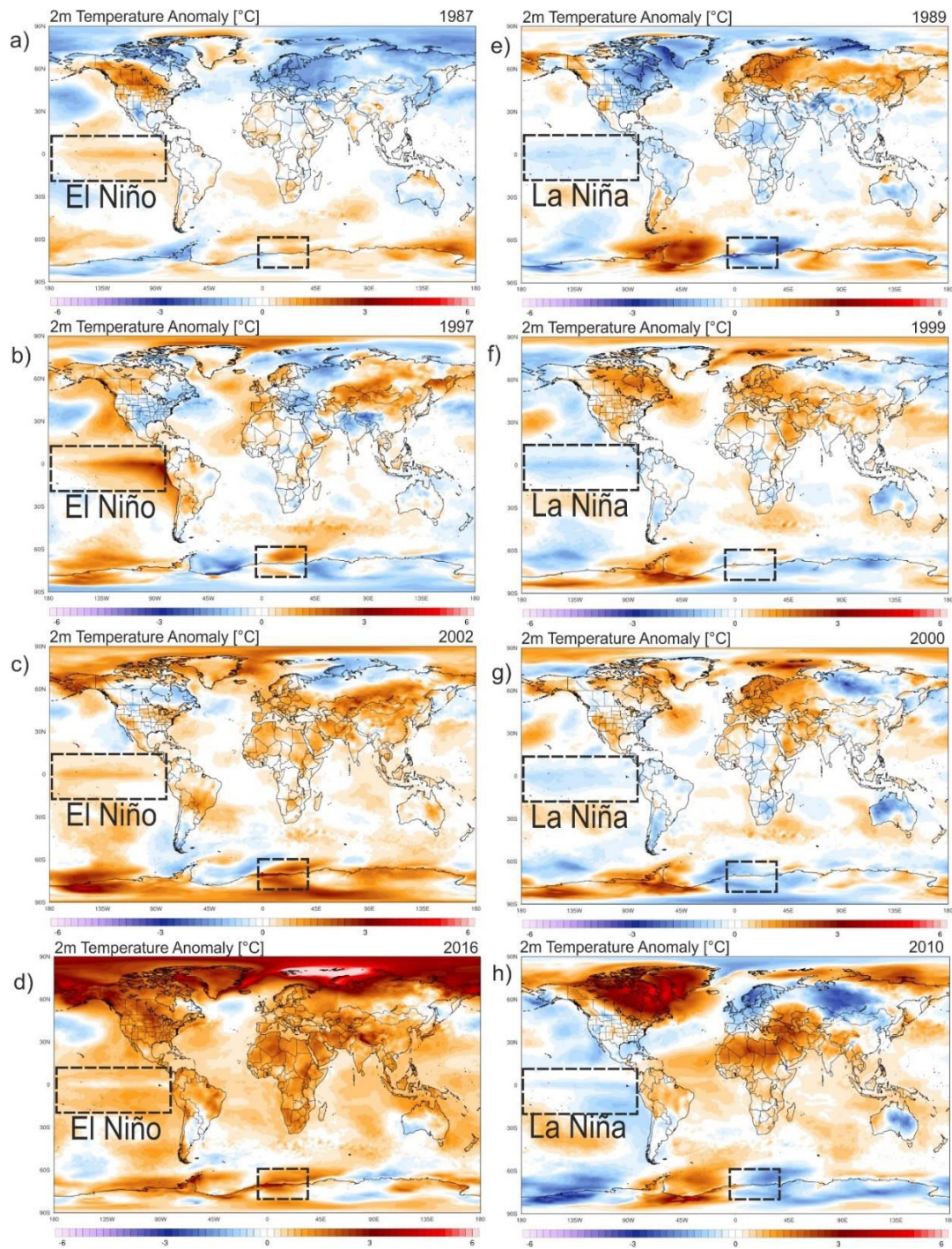


Figure 3.8. Surface air temperature anomaly during strong El Niño and La Niña years. *Spatial anomaly plots of ERA5 2m temperature during strong El Niño events (1987, 1997, 2002, and 2016) (a-d) and La Niña events (1989, 1999, 2000, and 2010) (e-h). During El Niño events (a-d), the anomaly plots show an increase in 2m temperature. In contrast, the La Niña events (e-h) highlight decreasing 2m temperature over the DML region of east Antarctica.*

The spatial composite anomaly record of mean surface ERA5 temperature during El Niño years also shows a strong positive anomaly over the DML region, indicating a significant increase in temperature during these events (Figure 3.9a). Similarly, during the La Niña years, the composite temperature anomaly record shows effective cooling across the DML region (Figure 3.9b).

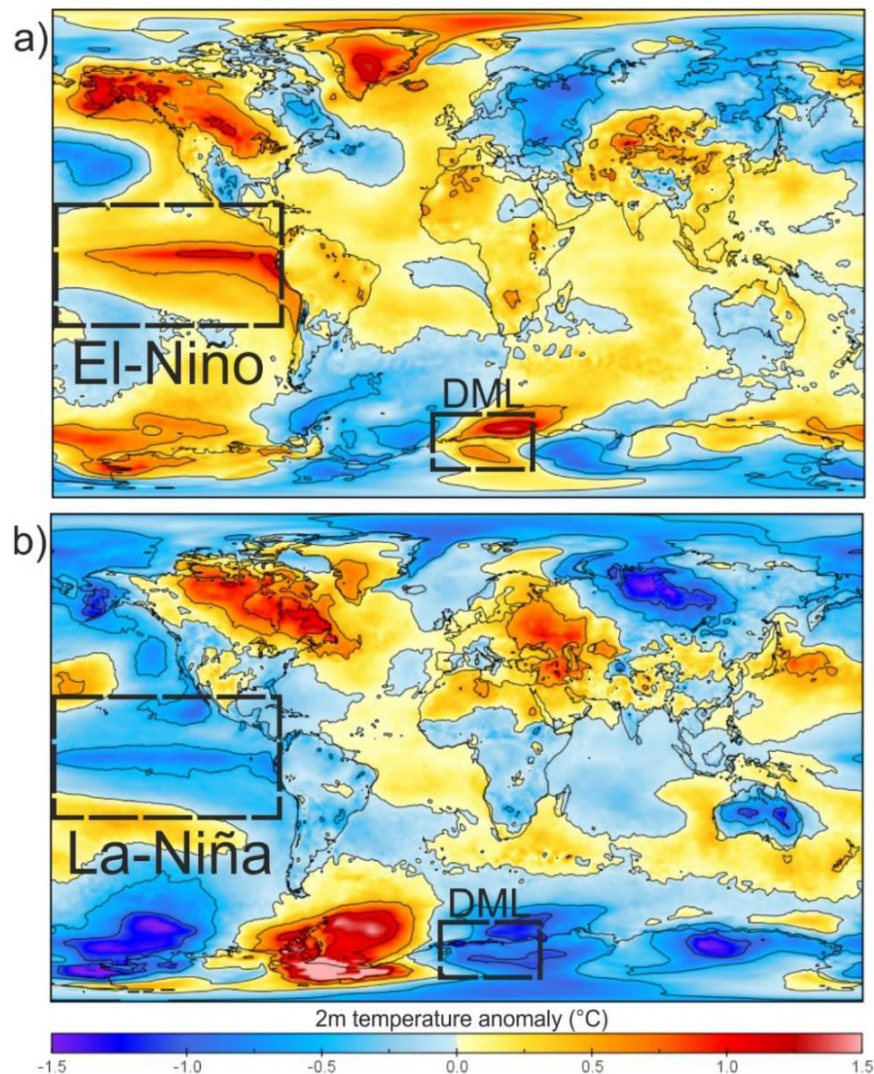


Figure 3.9. Spatial temperature variability during El Niño and La Niña year.

The composite ERA5 surface air temperature anomaly map for the (a) El Niño and (b) La Niña years. During El Niño years, the ERA5 surface air temperature anomaly shows a positive anomaly, while the opposite is observed during La Niña years over the DML region.

The teleconnections between the tropical Pacific and Antarctica are determined by the well-established dynamics of Rossby wave trains (Hoskins and Ambrizzi, 1993; Lachlan-Cope and Connolley, 2006). The atmospheric signature of this wave train is reflected in the Pacific South American (PSA) pattern during ENSO events (Li et al., 2021; Mo and Higgins, 1998). Rossby wave trains are caused by convective heating of the tropical atmosphere (Ding et al., 2012; Fogt et al., 2011; Li et al., 2021) and propagate with alternating highs and lows in the atmosphere, curved poleward and eastward towards Antarctica (Clem and Fogt, 2013). Once reaching Antarctica, they interact with the Amundsen Sea Low (ASL) and further combine into interannual variability, which is influenced by SAM (Clem et al., 2016). Nonetheless, it is also essential to understand the heat transfer during the El Niño and La Niña years to better understand the mechanism behind the temperature variability in the DML region. Towards this, we have used the vertical integral of the northward heat flux during El Niño and La Niña years. The anomaly plots of vertical heat flux (W m^{-2}) show strong positive anomalies over the DML region during the La Niña years (Figure 3.10a), suggesting increased northward transport of heat (Isaacs et al., 2021). While during the El Niño years, we observed a strong negative heat flux over the DML region (Figure 3.10b), suggesting a strong tropical heat transfer towards the DML region during El Niño events. This highlights the role of ENSO and its atmospheric teleconnections in modulating the temperature variability in the DML region of east Antarctica.

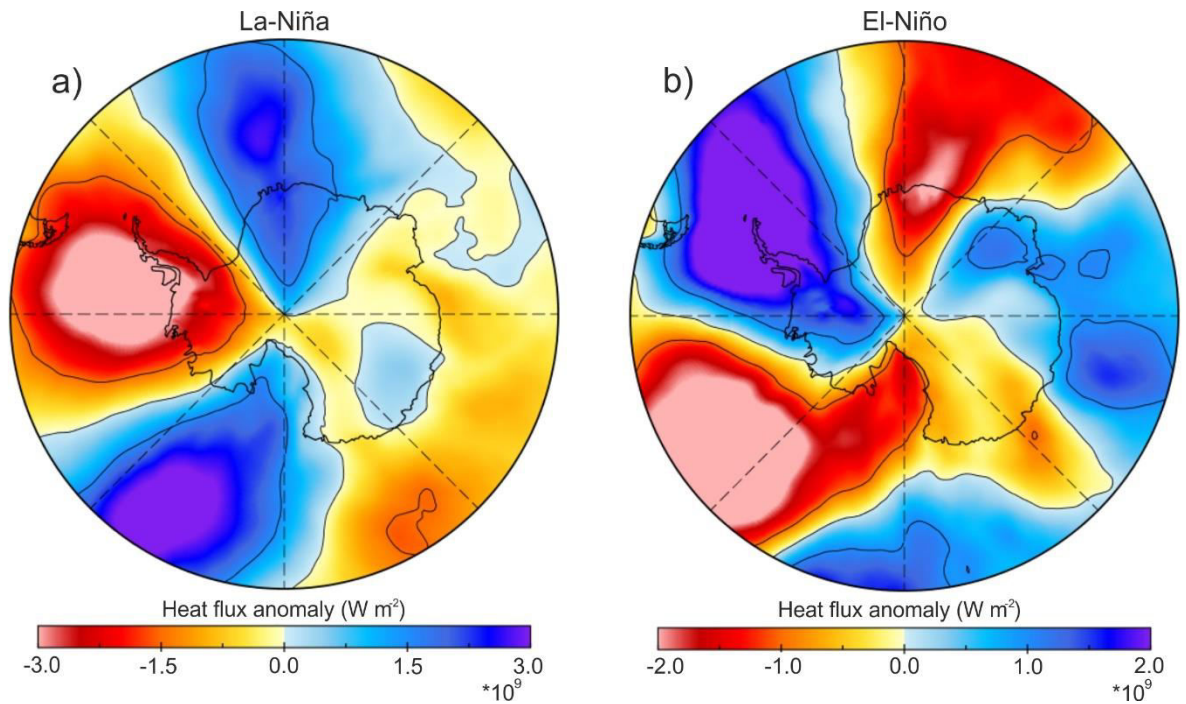


Figure 3.10. Spatial variation of heat flux anomaly over the DML region during ENSO events.

Heat flux anomaly during El-Niño and La-Niña years. Panel (a) and (b) show composite anomaly plots of the ERA5 vertical integral of the northward heat flux ($W m^{-2}$) for the La Niña years and El Niño years, respectively, during 1979–2019 CE. The negative anomaly of the vertical integral of the northward heat flux ($W m^{-2}$) suggests heat transfer from north to south. It indicates an increase in temperature over the DML region of East Antarctica and vice versa.

SAM is the primary climate mode in the Southern Hemisphere; hence, it is important to understand how it influenced DML temperature variability. In addition to the Rossby wave trains, ENSO signals are transmitted to the Antarctic region through a coupled interaction with SAM (Clem and Fogt, 2013). It is, therefore, necessary to understand the SAM-ENSO coupled interaction and its possible impact on surface air temperatures over the DML region. SAM is derived as the leading mode of Empirical Orthogonal Function (EOF) of Mean Sea Level Pressure (MSLP) between 20°S and 75°S (Lim and Hendon, 2015; Marshall et al., 2012). Accordingly, to understand the role of SAM-ENSO coupled interaction and its influence on the surface air temperature

of the DML region, we have used MSLP during the positive and negative SAM (pSAM and nSAM) years and correlated with ERA5 surface air temperature during the El Niño and La Niña years. During pSAM and El Niño years, MSLP is inversely related to ERA5 surface air temperatures, whereas a strong positive correlation is observed during the La-Niña years (Figure 3.11a-b). Furthermore, during nSAM and El-Niño years, MSLP is strongly correlated with the surface air temperature, whereas it is inversely related during La-Niña years (Figure 3.11c-d). In the above case, we have observed two modes of SAM-ENSO interactions; (i) pSAM/La Niña and nSAM/El Niño are in-phase (Figure 3.11b-c) and (ii) pSAM/El Niño and nSAM/La Niña are anti-phase (Figure 3.11a-d). There is a possibility of stronger teleconnections between ENSO and the Southern Pacific, based on the above in-phase pattern observed in case (i) and found to be consistent with earlier studies (Fogt and Bromwich, 2006; Fogt et al., 2011).

In contrast, the teleconnections became significantly weaker in the case of (ii) when there was an anti-phase relation (Fogt et al., 2011). Previous studies observed that periodic break out of anticyclonic waves occurs more frequently during the La Niña phase, generating high zonal wind anomalies that propagate the low-pressure anomalies poleward (60° S) during the pSAM years (Clem and Fogt, 2013). On the other hand, reverse conditions are often prevalent during El Niño events, which lead to positive pressure anomalies over the higher latitude and nSAM phases (Clem and Fogt, 2013). Therefore, our study supports the additional role of coupled interaction of SAM-ENSO in regulating the surface air temperature over the DML region.

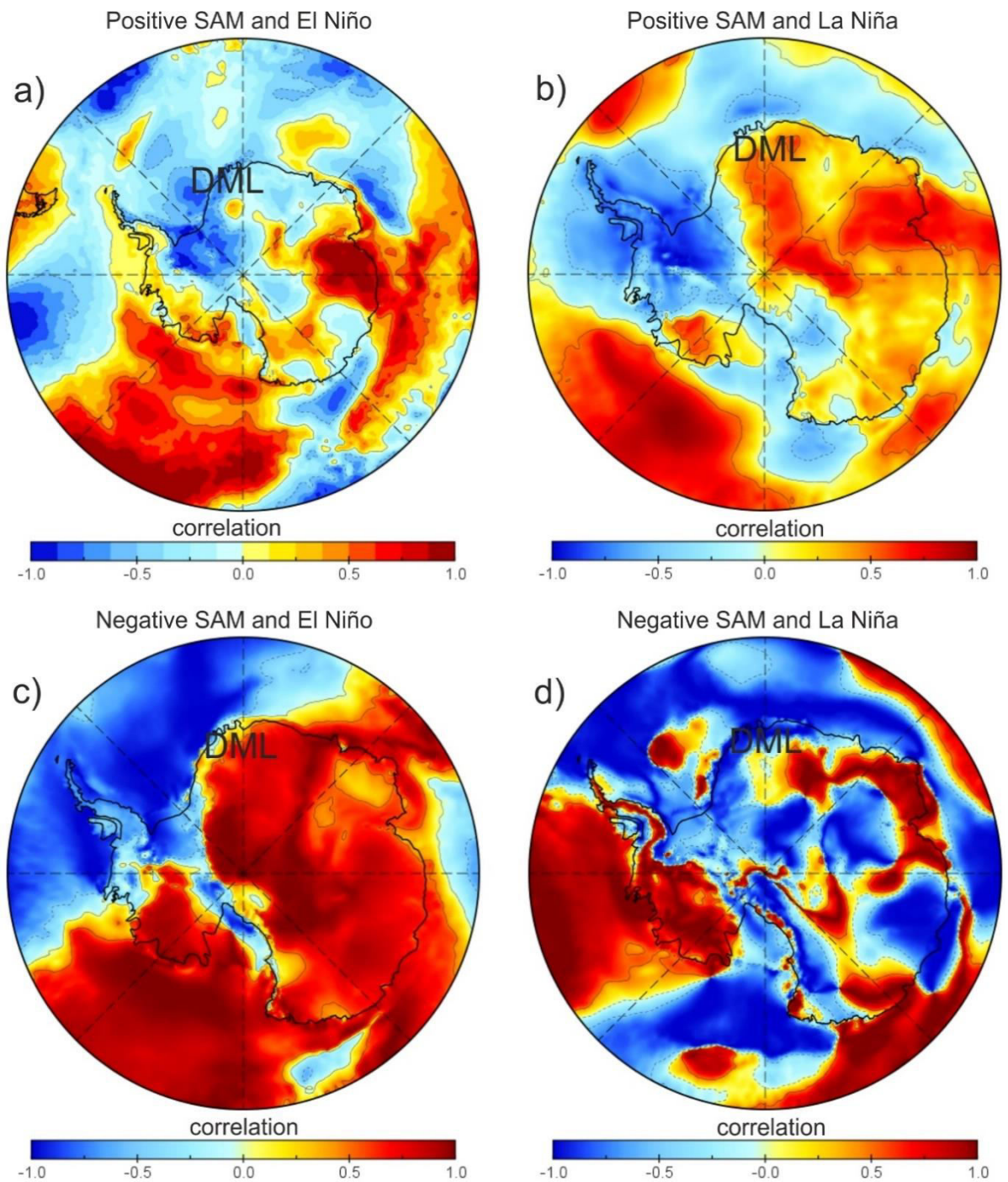


Figure 3.11. Mean Sea Level Pressure (MSLP) correlates with surface air temperature during positive and negative SAM indices.

MSLP during the Positive SAM (pSAM) years is correlated with ERA5 surface air temperature during (a) El Niño Years and (b) La Niña Years. MSLP during the negative SAM (nSAM) years is correlated with ERA5 surface air temperature during (c) El Niño Years and (d) La Niña Years.

The Marshall SAM index (Marshall, 2003), regressed with ERA5 reanalysis of annual surface air temperature for 1957–2019 CE, highlights a positive correlation across the western and central DML (Figure 3.12a). To understand the influence of the SAM-temperature relationship on a longer time scale, we have combined the Marshall SAM Index with the reanalysis 20CRV2c SAM index for an extended SAM record and compared it with the DML temperature record (Figure 3.12b). It is noteworthy that this extended SAM record shows its highest values and increasing trend in recent decades, similar to the temperature anomaly record shown in Figure 3.12c. This indicates that the warming trend since the 1940s is concomitant with the shifting of SAM to a positive phase. Such a positive shift could be attributed to the warming trend in the eastern DML for the last seven decades.

Further, a wavelet coherency between SAM–SOI records (1851–2019 CE) shows significant anti-phase relation between SAM at the decadal band since ~1940, which coincides with the warming trend in the DML region (Figure 3.12e). Compared to this, significant in-phase relation at 12–18 years band during 1880–1920 CE coincides with the cooling trend (Figure 3.12e). Therefore, we suggest that SAM–ENSO phase relation influence the DML surface air temperature variability at annual to multi-decadal scales.

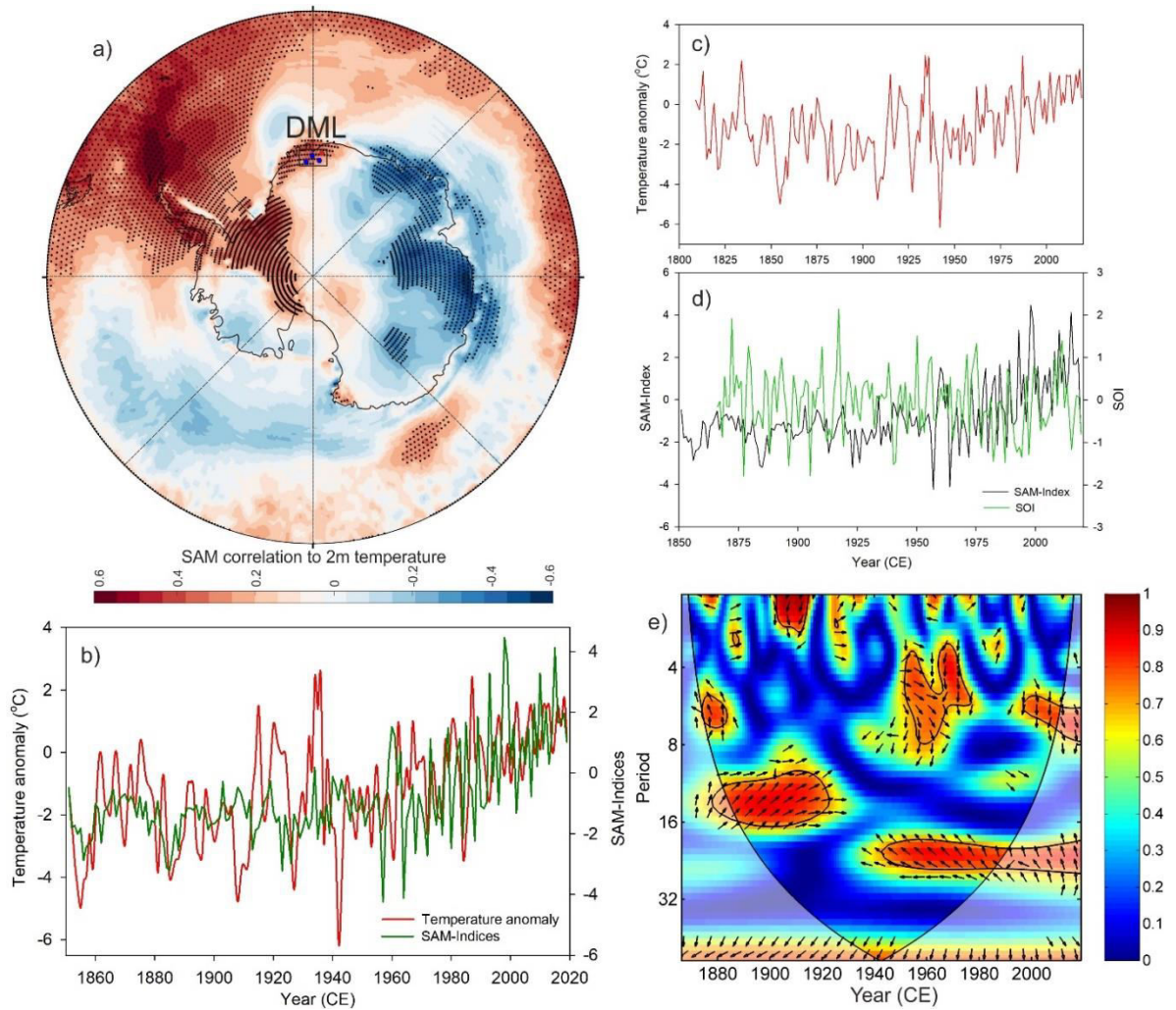


Figure 3.12. Correlation of SAM index with surface air temperature and wavelet coherence analysis between SAM and SOI.

(a) Spatial correlation of Marshall SAM Index (Marshall, 2003) with ERA5 reanalysis surface air temperature during (1957–2019 CE). Stippling indicates statistically significant correlations (95% confidence level). (b) The Marshall SAM Index combined with the long-term 20CRV2c SAM record (Gong and Wang, 1999) is compared with the DML temperature anomaly record. The reconstructed DML temperature anomaly record broadly follows the combined SAM records during their respective time intervals. (c) Annual reconstructed temperature anomaly record (1809–1993 CE) is combined with ERA5 reanalysis surface temperature (1994–2019 CE). (d) The SAM Index record is compared with the SOI record (Ropelewski and Jones, 1987). (e) Wavelet coherence between the combined SAM and SOI records (1851–2019 CE). The black contours indicate 95% of confidence, based on a red noise model. The thick black line indicates the cone of influence. The relative phase relationship is shown as arrows

(with in-phase pointing right, anti-phase pointing left, SAM leading SOI 90° pointing straight up and vice versa).

3.3 Conclusions

A high-resolution $\delta^{18}\text{O}$ record (1809–2013 CE) retrieved from a coastal region integrated with published ice core records from Dronning Maud Land (DML) in East Antarctica was used to investigate the factors that influenced oxygen isotope variability during the last two centuries. A principal component analysis (PCA) of the $\delta^{18}\text{O}$ records was performed to extract the surface air temperature signal and reconstruct the temperature record of the DML region from 1809–1993 CE. The reconstructed surface air temperature record (1809–1993 CE) combined with ERA5 reanalysis temperature anomaly record 1994–2019 CE was used to investigate the long-term trends, variability, and its link to various climate modes like SAM, ENSO, and IPO. The reconstructed DML temperature anomaly record shows a significant cooling trend at a rate of $-0.164 \pm 0.045 \text{ }^\circ\text{C decade}^{-1}$ during 1809–1907 CE, followed by a significant warming trend at a rate of $+0.452 \pm 0.056 \text{ }^\circ\text{C decade}^{-1}$ during the recent decades (1942–2019 CE). Our study revealed that ENSO coupled with SAM are the primary factors that modulate the surface air temperature variability in the DML region. Although the temperature signals at the ENSO band were persistent during the past two centuries, an increased shift from low (12–18 years band) to high-frequency (2–8 years band) oscillations was observed since the 1940s. We suggest that the shifting of SAM to a positive phase, coupled with increasing influences of ENSO in this part of Antarctica, has resulted in such dramatic warming of the DML region in recent decades.

Chapter 4

Sea ice variability and trends in the Western Indian Ocean Sector of Antarctica during the past two centuries and its response to climatic mode

4.1 Introduction

Recent climate change and its impact on Antarctica are poorly understood due to the lack of a network of long-term high-resolution climate records. Instrumental temperature records with a reasonable spatial coverage scale have been available only since 1958 (Nicolas and Bromwich, 2014). Although high-resolution, continuous Spatio-temporal records of Antarctic climate have been available since the beginning of the satellite era in 1979, these are too short to discern long-term trends and variability at annual to multi-decadal scales (Turner et al., 2005). Antarctic ice cores provide high-resolution climate records, which can go beyond instrumental records. To understand past climate variability and long-term changes at various time scales, several deep ice cores have been retrieved since the 1950s from Antarctica to reconstruct high-resolution climate records.

Coastal Antarctica typically receives higher precipitation than the interior plateau; therefore, coastal ice cores are ideal for assessing the annual to decadal climate variability (Curran et al., 2003; Goursaud et al., 2019; Naik et al., 2010; Turner et al., 2019). Coastal ice cores from Antarctica are sensitive enough to register and preserve even short-term fluctuations and changes in climate parameters such as accumulation, temperature, sea ice, dust influx, solar activity, and volcanic events (Abram et al., 2007; Masson-Delmotte et al., 2008; Mulvaney et al., 2012; Naik et al., 2010; Rahaman et al., 2016; Schneider et al., 2004; Thamban et al., 2006). Nevertheless, reconstruction of these parameters based on the ice core records is often complicated due to the non-linear

relation between proxies and non-stationary climate signals, as well as the influence of multiple factors that operate on a more local/regional scale, especially in the coastal regions (Abram et al., 2013). Therefore, challenges remain to deconvolute the climate signals from the ice core proxy records and to recognize forcing factors that influence Antarctic climate variability.

Among the Antarctic climate variables, sea ice is one of the least studied but critical components of the ocean and climate system. Changes in sea ice cover in the Southern Ocean strongly influence the energy-mass exchange processes and change in temperature gradient which further modulates heat exchange between ocean and atmosphere (Deb et al., 2017; Raphael, 2003; Simmonds and Xingren, 1993). Sea ice variations can modulate global ocean circulations and climate through changes in bottom water formation (Ohshima et al., 2013; Yabuki et al., 2006) and the storage capacity of atmospheric CO₂ into ocean deep abyss (Sloyan, 2006). Satellite records available since 1979 show that the Antarctic sea ice has been undergoing dramatic changes in various oceanic sectors (Eayrs et al., 2019). However, there is no consensus yet on the drivers that control sea ice variability and changes (Hobbs et al., 2016; Jones et al., 2016).

Sea ice cover over the Antarctic region is mainly controlled by variations in ocean-atmosphere circulations (Carleton, 1989; Ferrari et al., 2014). Recent studies show a significant increasing trend in Antarctic sea ice cover associated with the strengthening of westerlies due to the shifting of the Southern Annular Mode (SAM) to the positive mode (Holland and Kwok, 2012; Liu et al., 2004; Marshall, 2003; Spence et al., 2010); El Niño Southern Oscillation (ENSO)-SAM teleconnections and interdecadal variability of Pacific Decadal Oscillation (PDO) (Kwok and Comiso, 2002b; Yu et al., 2017); stratospheric ozone depletion (Marshall et al., 2004; Sigmond

and Fyfe, 2014; Thompson et al., 2011) and increased basal melting of ice shelves due to rising in SST over the Southern Ocean (Bintanja et al., 2013). Recent studies have shown a significant increase in sea ice cover in the Indian Ocean sector from 1979–2015 CE (Deb et al., 2017; Jena et al., 2018). The available satellite sea ice record is insufficient to discern long-term trends and variability; thus, it is difficult to understand whether this recent variability and changes are part of the long-term cyclicity. To address these questions, it is important to have annually resolved long-term sea ice records of various oceanic sectors.

Several chemical species measured in ice cores have been used as a proxy for reconstructing long-term SIC records. However, their concentrations could also be affected by several factors other than the SIC, such as changes in moisture source conditions, wind pattern, and transportation pathways, distance from the moisture sources, number of successive precipitation events of the moisture parcel during the transportation and post-depositional changes related to species migration in firn/ice (Thomas et al., 2019). In addition, some of the chemical proxies have been used to reconstruct SIC based on the relationship between the ionic concentration records with the satellite SIC record; however, their relationship is not consistent, and sometimes they even show opposite relations in different oceanic sectors of Antarctica (Thomas et al., 2019). For example, ice core sea salt sodium (Na^+) records show a positive correlation in the west Antarctic sectors (Sneed et al., 2011) and the Weddell Sea sector in east Antarctica (Rahaman et al., 2016). However, this relationship is not consistent in other sites (Abram et al., 2013). Several ice cores accumulation records from Antarctic Peninsula and the West Antarctic ice sheet suggest a strong inverse correlation with sea ice (Porter et al., 2016; Thomas and Bracegirdle, 2015); however, it is poorly correlated with chemical species at the same sites (Abram et al., 2010). Therefore, more

observations and reconstructions are required to understand the precise mechanism related to the variations of chemical species with sea ice. An organic aerosol component such as methanesulfonic acid (MSA) is used as a potential sea ice proxy. Coastal ice cores show statistically significant correlations between MSA and sea ice (Abram et al., 2010; Foster et al., 2006; Thomas and Abram, 2016; Welch et al., 1993; Xiao et al., 2015). However, several caveats are attached with the application of MSA as a sea ice proxy, and more site-specific observations are needed to understand the process that controls the sea ice formations (Röthlisberger et al., 2010).

It has been suggested that sea ice variability may affect stable water isotope records from coastal ice cores, mainly from Antarctic Peninsula, West Antarctica, and the Ross Sea region (Holloway et al., 2016; Thomas et al., 2013). Stable water isotope ice core records were also used to understand the sea ice variability during the last interglacial period (Holloway et al., 2017; Holloway et al., 2016). Though few coastal ice cores have been studied, however, so far, limited efforts have been made to reconstruct past sea ice conditions in the proximal oceanic sectors based on these ice core records.

In the present study, we have reconstructed past sea ice concentration (SIC) records based on a newly retrieved high-resolution ice core $\delta^{18}\text{O}$ record (1809–2013 CE) together with available records from Droning Maud Land (DML), east Antarctica. We provide an annually resolved longest SIC record (1809–1993 CE) of Antarctica's Western Indian Ocean Sector (WIOS). The reconstructed SIC record combined with that of the satellite-based record has enabled us to discern the long-term trend and variability during the past two centuries (1809–2019 CE). This long-term SIC record will offer an opportunity to investigate forcing factors/drivers contributing to the variability and changes at interannual to multi-decadal time scales.

4.2 Results and Discussion

4.2.1 Accumulation rates at the IND33 core site

Age-depth relationship and density profiles of the IND33 ice core were used to calculate annual accumulation rates at the core site. The accumulation rate in the IND33 ice core site shows large variability (Figure 4.1); it ranges from 114 to 726 kg m⁻² a⁻¹ with an average of $388 \pm 113(1\sigma)$ kg m⁻² a⁻¹. The temporal variability in accumulation rates reveals relatively higher values until 1910 CE and a discernible decreasing trend (1910–2013 CE) (Figure 4.1). The mean accumulation rate of the IND33 ice core falls within the reported range from DML and is comparable with the published records from this region (Divine et al., 2009; Thomas et al., 2017). The annually resolved $\delta^{18}\text{O}$ record does not show any significant relation with the accumulation ($r=0.0014$, $n=205$, $p>0.05$) (Figure 4.1). This indicates that $\delta^{18}\text{O}$ papers from the coastal DML sites did not undergo significant post-depositional processes. Hence, these records can be used to reconstruct the past climate of the DML region.

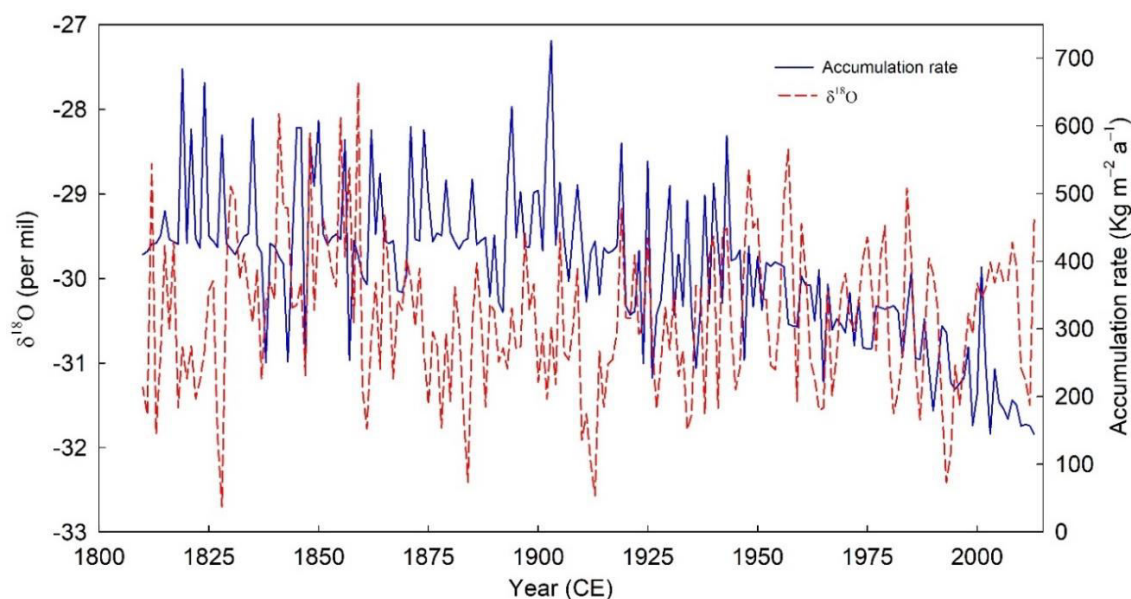


Figure 4.1. Annual variation in accumulation rate and $\delta^{18}\text{O}$ records of the IND33 ice core.

4.2.2 Ice core $\delta^{18}\text{O}$ records from the DML

The $\delta^{18}\text{O}$ values of the IND33 ice core range from -27.6‰ to -32.7‰ with a mean value of $-30.5 \pm 0.9\text{‰}$. The $\delta^{18}\text{O}$ profile reveals large variability in the coastal DML record with an increasing trend approximately from -32 to -28‰ during 1809–1860 CE and thereafter decreased to -32.5‰ during 1884/1885 CE (Figure 4.2a). It is important to note that $\delta^{18}\text{O}$ record showed a monotonous increase in the 20th century. To have a regional perspective, we have compared our record with the three ice core records (DML05, DML07, and DML17) from the inland DML region. Although the $\delta^{18}\text{O}$ anomaly records of these selected cores show considerable variations, overall, they follow a similar trend with a positive shift during ~1930–1993 CE (Figure 4.2b). Further, a composite anomaly in these records also shows a long-term declining trend which ended in the early 20th century, followed by a discernible increasing trend with higher amplitude variations (Figure 4.2b). We have also plotted a composite anomaly without an IND33 record that follows a similar pattern (Figure 4.2c).

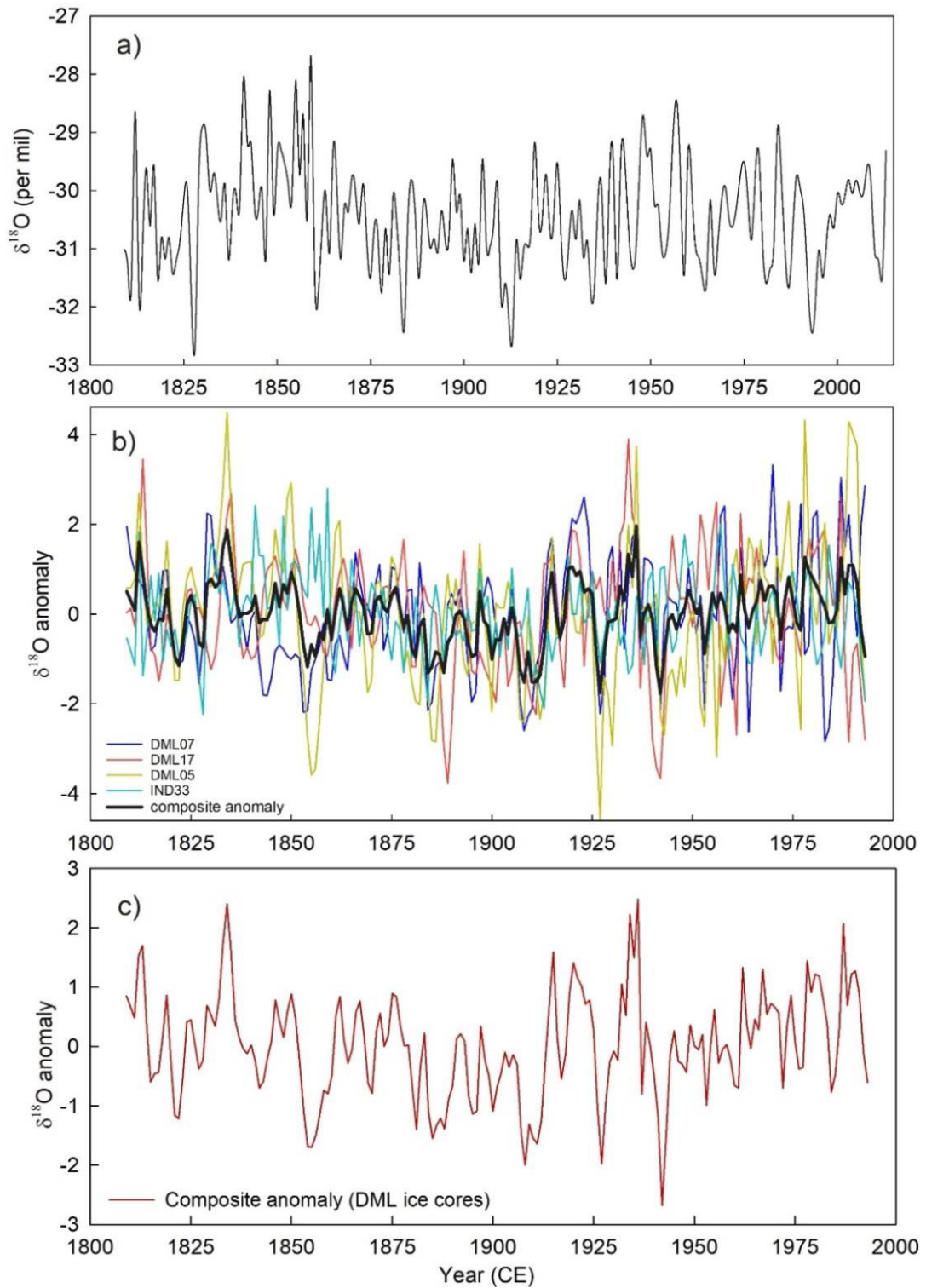


Figure 4.2. Ice core $\delta^{18}\text{O}$ record and anomaly in the selected $\delta^{18}\text{O}$ record from the DML region.

(a) The $\delta^{18}\text{O}$ record of IND33 core (1809–2013 CE). (b) The $\delta^{18}\text{O}$ records of other published ice cores (DML05, DML07, and DML17) along with that of IND33 within a

common time window (1809–1993 CE). The thick backline denotes a composite anomaly record of selected ice cores. (c) Composite $\delta^{18}\text{O}$ anomaly record of DML ice cores (DML05, DML07, and DML17) (1809–1993 CE), excluding the IND33.

In recent years, isotope-enabled climate models have been employed to decipher isotopic signal variations in global precipitation related to climate variables (Risi et al., 2012). The European Centre Hamburg Model (ECHAM5-wiso) is an atmospheric general circulation model enabled with stable water isotopes that capture global precipitation signals (Werner et al., 2011). Therefore, the large-scale spatio-temporal record of $\delta^{18}\text{O}$ record of Antarctic precipitation will help us to interpret the point source ice core $\delta^{18}\text{O}$ record in a longer time scale. We have compared our $\delta^{18}\text{O}$ records with the model simulation output performed at spectral truncation T106 (corresponds to grid resolution $\sim 1^\circ \times 1^\circ$) using monthly historical sea ice and sea surface temperature from Hadley Centre (HadISST) (Rayner et al., 2003) with boundary conditions for the period 1871–2011 CE (Steiger et al., 2017). Comparing the IND33 ice core $\delta^{18}\text{O}$ record with the ECHAM5-wiso model output at the core site shows good agreement in the long-term trends. However, several short-term excursions were not captured in the model output (Figure 4.3a). Further, the amplitude of the fluctuations in the IND33 $\delta^{18}\text{O}$ record show higher values than that of the ECHAM5-wiso model. But comparing a single record with ECHAM5-wiso output might be tricky because individual records could be influenced by the processes such as diffusion, sublimation, redistribution, extreme precipitation events, effects of topographic features, and other small-scale processes which are not accounted for the ECHAM5-wiso model (Goursaud et al., 2018).

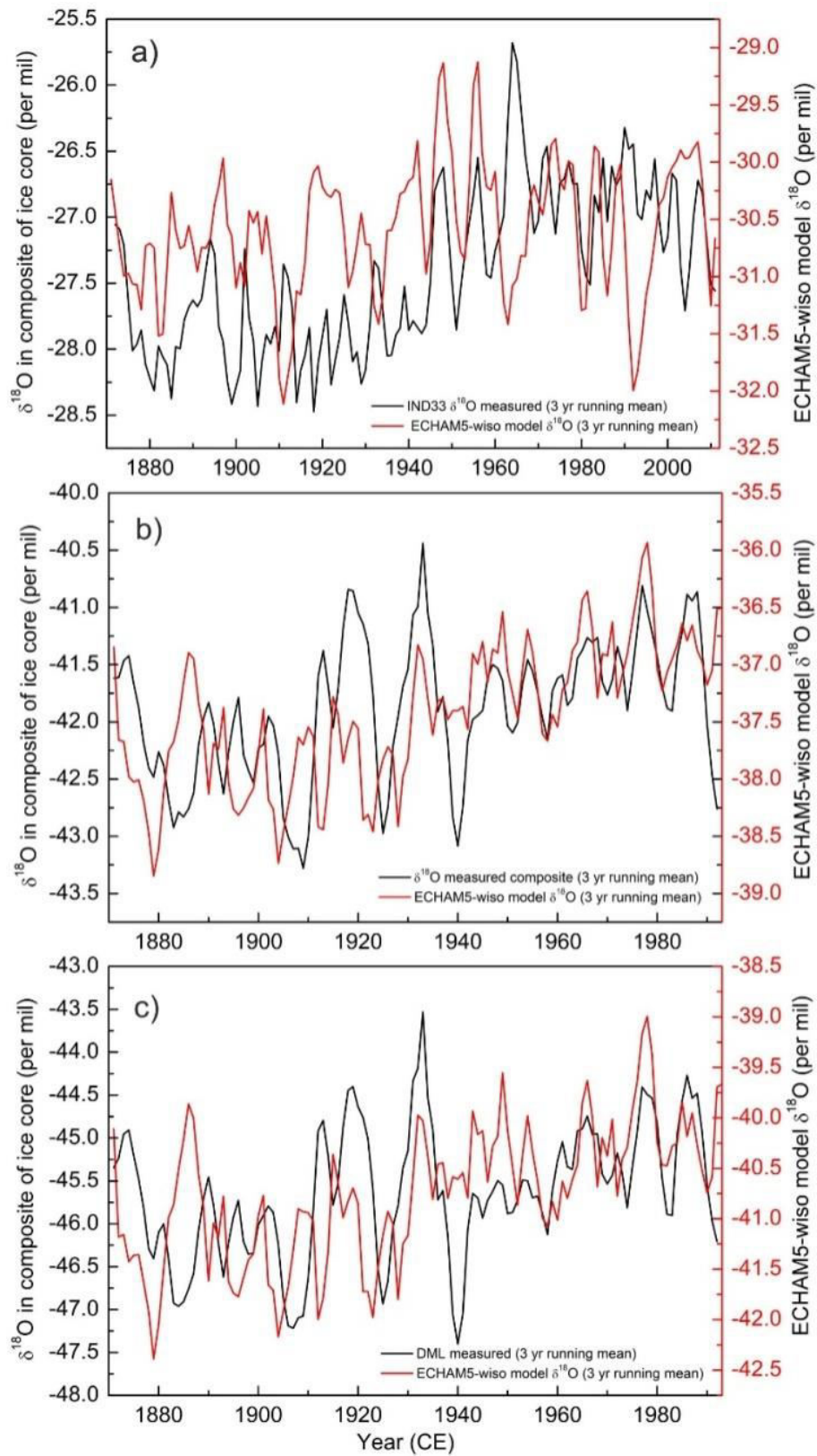


Figure 4.3. Comparison of ECHAM5-wiso model $\delta^{18}\text{O}$ record in precipitation and measured ice core $\delta^{18}\text{O}$ records.

Correlation of ECHAM5-wiso model $\delta^{18}\text{O}$ in precipitation with (a) $\delta^{18}\text{O}$ records of IND33 ($r=0.14$, $p>0.05$, $n=141$, 1871–2011 CE, lag = 1 year), (b) composite of all selected ice cores ($r=0.38$, $p<0.05$, $n=123$, 1871–1993 CE, lag = 1 year), (c) composite of DML ice core (DML05, DML07, and DML17) ($r=0.32$, $p<0.05$, $n=123$, 1871–1993 CE, lag = 1 year).

The model-derived $\delta^{18}\text{O}$ record compared with the composite anomaly record of four ice cores for the period of 1871–1993 CE (Figure 4.3b) shows a significant correlation ($r=0.38$, $n=123$, $p<0.05$, lag = 1 year). However, it is noteworthy that this correlation was improved ($r=0.64$, $n=43$, $p<0.05$) after the 1950s, possibly indicating reduced bias in the ECHAM5-wiso model. Further, we have also compared the ECHAM5-wiso model derived $\delta^{18}\text{O}$ record with the composite anomaly of ice cores after removing IND33 from composite (Figure 4.3c), which also shows a significant correlation ($r=0.32$, $p<0.05$, $n=123$, 1871–1993 CE, lag = 1 year) and improved further after the 1950s ($r=0.61$, $n=43$, $p<0.05$).

4.2.3 Factors controlling the $\delta^{18}\text{O}$ variability in DML ice core records

The $\delta^{18}\text{O}$ proxy records of Antarctic ice cores are controlled by various meteorological factors such as temperature, precipitation, sea ice extent, relative humidity, moisture source, and transport (Divine et al., 2009; Masson-Delmotte et al., 2008; Naik et al., 2010; Rahaman et al., 2019; Sinclair et al., 2012). These climate variables are also known to be modulated by dominant climate modes such as ENSO, PDO, and SAM and their phase relationships (Abram et al., 2013; Divine et al., 2009; Naik et al., 2010; Rahaman et al., 2019; Sinclair et al., 2012; Yu et al., 2017). Therefore, the DML ice core records could capture signals of any past changes in these oscillations and thus are ideally suitable for investigating the role of ENSO and PDO in modulating the DML climate and sea ice conditions in the proximal oceanic sectors.

4.2.3.1 $\delta^{18}\text{O}$ –temperature variability in the ice core record

Previous studies from the DML region (Masson-Delmotte et al., 2008; Naik et al., 2010; Rahaman et al., 2019) have demonstrated that the temperature is among all the meteorological parameters the dominant factor that explains maximum variability in ice core $\delta^{18}\text{O}$ records. To investigate the role of surface air temperature in $\delta^{18}\text{O}$ variability, we first compared multiple $\delta^{18}\text{O}$ records across the DML region (IND33, DML05, DML07, and DML17) with the ERA5 reanalysis data of surface air temperature of the core sites. The individual ice core $\delta^{18}\text{O}$ records do not show any significant correlation with ERA5 surface air temperature (Figure 4.4), suggesting that multiple factors other than temperature did influence $\delta^{18}\text{O}$ records at variable extents. Therefore, it is crucial to deconvolute the signal of dominant factors from the ice core composite signal of various atmospheric and oceanic parameters. The predominant climate signals recorded in the DML region were extracted based on principal component analysis (PCA) of multiple $\delta^{18}\text{O}$ ice core records (Chapter 2, Section 2.7.1), following the approach of Rahaman et al. (2019). The first and second components (PC1 and PC2) derived from PCA analysis of the composite $\delta^{18}\text{O}$ record were found to be significant (Eigenvalues >1); together, they explain ~60% of the total variability in $\delta^{18}\text{O}$ records (Chapter-2, Table 2.7).

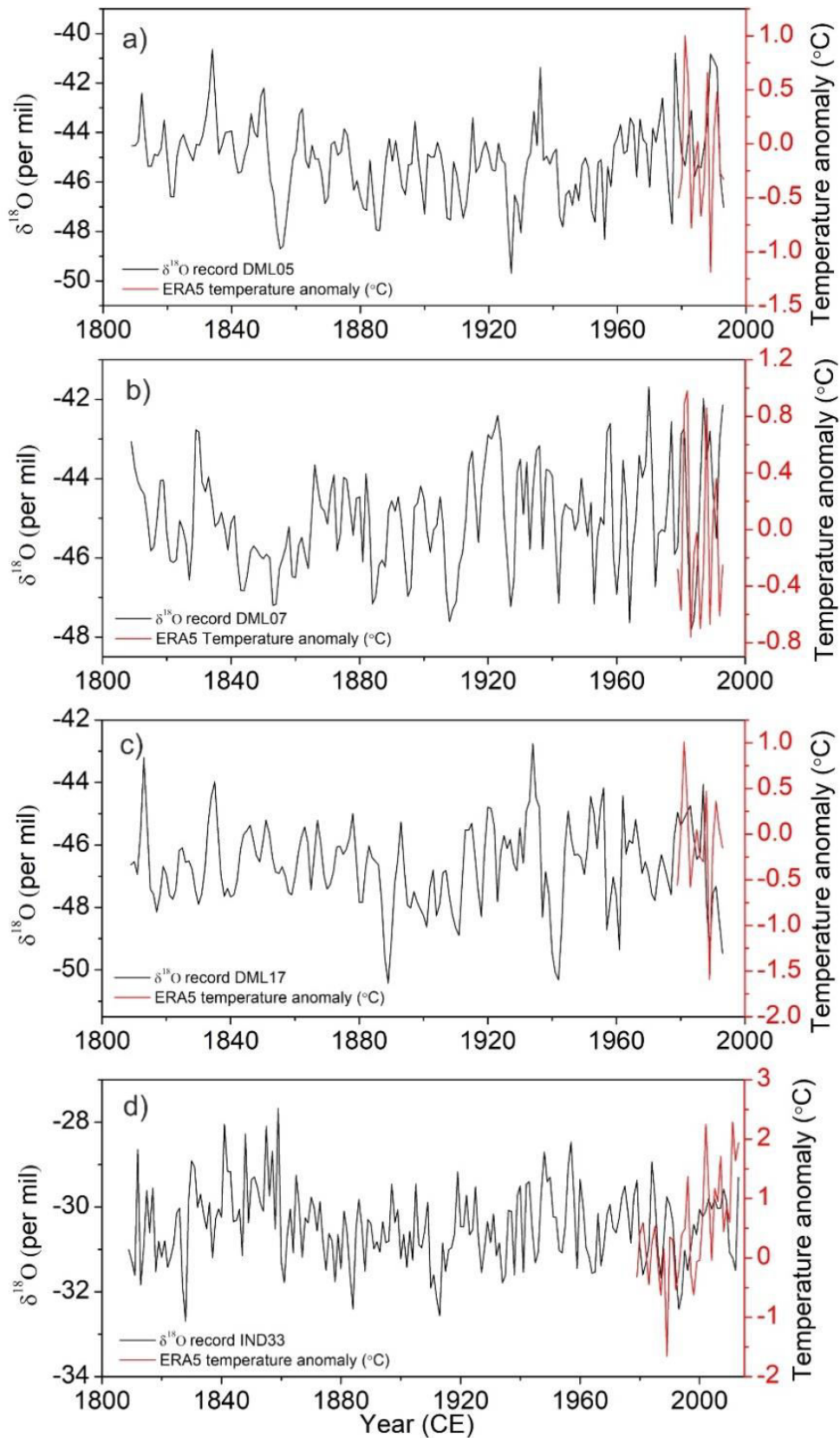


Figure 4.4. $\delta^{18}\text{O}$ ice core records from ice cores used in the present study and their correlation with ERA5 surface air temperature.

Annual variability of $\delta^{18}\text{O}$ records and its correlation to ERA5 surface air temperature (2m t) of selected ice core sites (a) DML05 ($r = 0.08$, $n=15$, 1979–1993 CE) (b) DML07 ($r = 0.02$, $n=15$, 1979–1993 CE) (c) DML17 ($r = 0.24$, $n=15$, 1979–1993 CE) and (d) IND33 ($r = 0.11$, $n=35$, 1979–2013 CE).

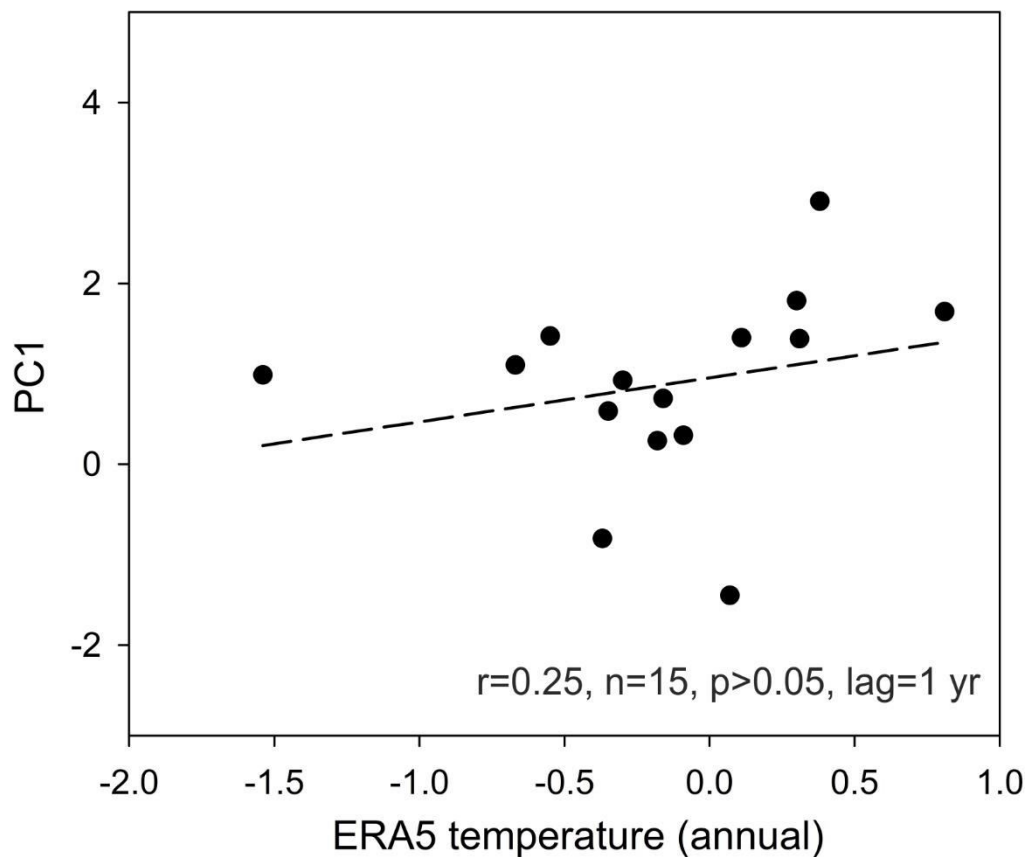


Figure 4.5. PC1 correlation with ERA5 annual surface air temperature.

Correlation of PC1 with annual ERA5 reanalysis surface air temperature ($r = 0.25$, $n=15$, $p<0.05$, 1979–1993 CE, lag = 1 year).

The first component (PC1) alone explains maximum variability up to ~32%, which represents the signal of the surface air temperature of the DML region, as previously demonstrated by (Rahaman et al., 2019). The inland DML ice cores contribute up to ~95% to PC1, whereas the coastal IND33 ice core contributes only ~5%. This implies that inland DML $\delta^{18}\text{O}$ records are primarily influenced by temperature. This observation is consistent with earlier reports (Goursaud et al., 2019). The PC1 shows weak correlation ($r=0.25$, $n=15$, $p>0.05$, 1979–1993 CE, lag=1year)

with annual SAT records (Figure 4.5). However, a significant correlation is observed in the PC1 time series, and seasonal (Oct-Nov-Dec) surface air temperature averaged across the grid box (71.5°S to 75.5°S; 11.0°E to 5°W) derived from ERA5 reanalysis ($r=0.74$, $n=15$, $p<0.05$ 1979–1993 CE, lag= 1 year) (Figure 4.6.a). It is important to investigate the possible reasons for a strong correlation between PC1 and spring temperature but a weak correlation between PC1 and mean annual temperature.

The stronger correlation of the ice core $\delta^{18}\text{O}$ signal with spring temperature is consistent with the earlier report (Rahaman et al., 2019). The lagged correlation between the ice core-derived temperature signal and ERA5 temperature is difficult to resolve because of a similar uncertainty range in the chronology estimate, i.e., ± 1 year. However, as discussed later, the mean annual temperature derived from the ice core $\delta^{18}\text{O}$ is biased by seasonal signal and could be one of the reasons for the lagged correlation. A detailed investigation is required to resolve unequivocally based on the multiple $\delta^{18}\text{O}$ records from short cores in the coastal regions with higher precipitation/accumulation sites. The problem of seasonal bias in ice core stable isotope-based temperature reconstruction has already been highlighted for the Antarctica Peninsula by Sime et al. (2009). They have demonstrated that the sensitivity of ice core $\delta^{18}\text{O}$ to the temperature change across the Peninsula is highly variable. The large-scale synoptic variability in $\delta^{18}\text{O}$ changes across Antarctica is primarily controlled by local changes in condensation temperature (Sime et al., 2009). Therefore, it is essential to investigate the potential impact of changes in the relationship between temperature during precipitation events (condensation temperature) and mean temperature. The RACMO2 model (van Wessem et al., 2018) monthly mean precipitation over the DML region (71.5°S to 75.5°S; 11.0°E to 5°W) for the period 1979–2013 CE shows two seasons of higher precipitation, i.e., April-May-Jun (fall

season) and Oct-Nov-Dec (spring to early summer season) (Chapter-3, Figure 3.3). This suggests that DML ice core $\delta^{18}\text{O}$ records register the seasonal temperature signal during periods of higher precipitation. It is unclear why ice core $\delta^{18}\text{O}$ records the temperature of early spring but not the fall season despite higher precipitation. Further, a recent study has demonstrated that more than 40% of the mean annual precipitations are associated with extreme precipitation events (EPs); therefore, temperature signals recorded in ice core $\delta^{18}\text{O}$ records could be biased toward the temperature during the EPs (Turner et al., 2019). To quantify the seasonal and EPs biases in the mean annual ice core signal, a more detailed investigation is required, which is beyond the scope of the present study.

We used a regression equation derived from the correlation plot between PC1 and ERA5 to reconstruct the temperature anomaly record for 1809–1993 CE (Figure 4.6a). The temperature reconstruction based on the regression equations shows a long-term cooling in the 19th century ($1.02 \pm 0.28^\circ\text{C}$), followed by a long-term warming trend ($1.0 \pm 0.37^\circ\text{C}$) in the 20th century (Figure 4.6b). Our observation in the present study is consistent with the findings of a systematic continent-wide cooling during the 19th century and significant warming in regions like DML during the last century (Stenni et al., 2017). In a previous study, Rahaman et al. (2019) investigated DML temperature variability and the role of ENSO, PDO, and SAM. Therefore, in the following section, we have primarily focused on the second PCA component (PC2), which has been identified as a factor related to sea ice variability.

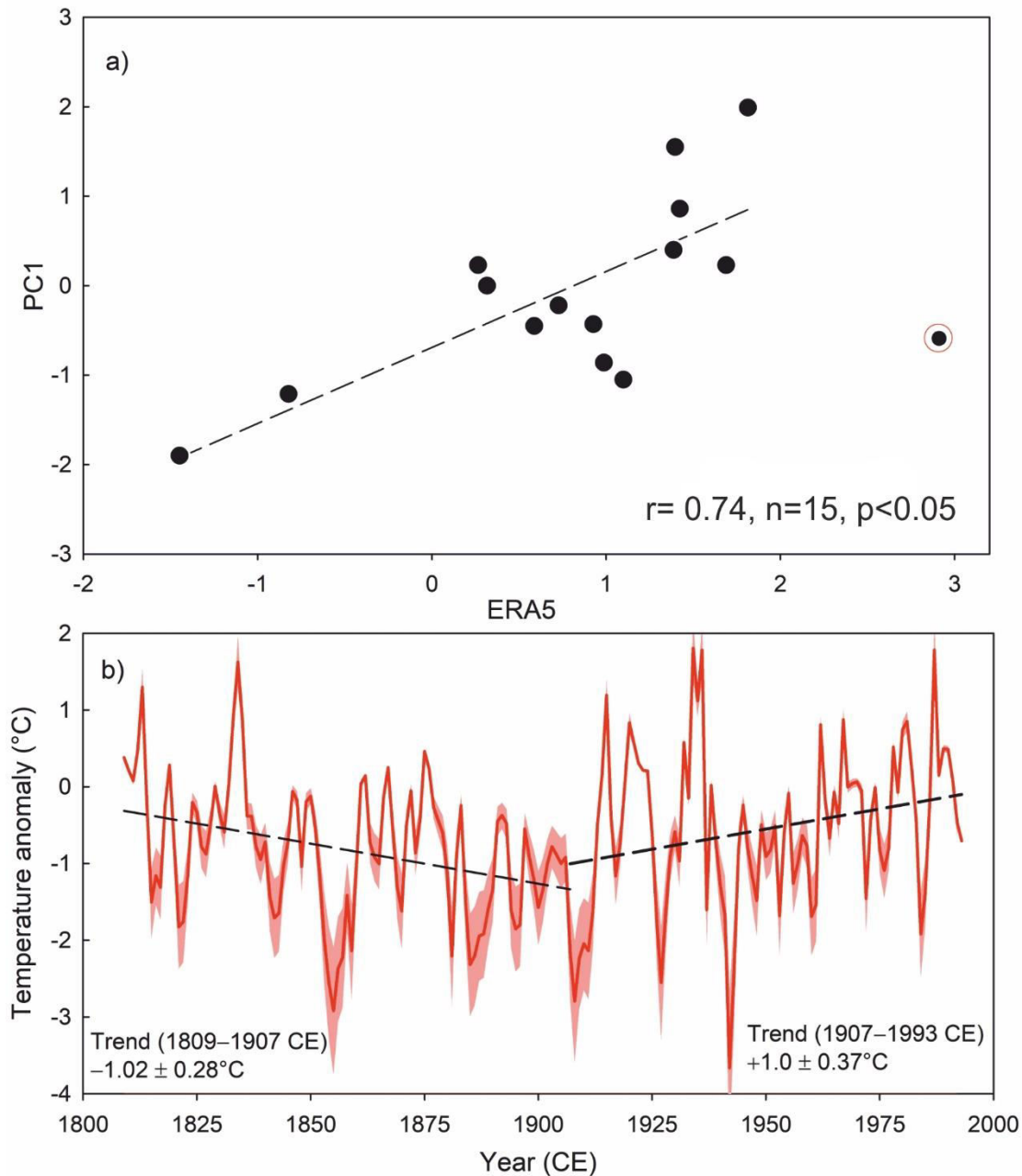


Figure 4.6. Correlation of PC1 with surface air temperature and temperature reconstruction.

(a) Correlation plot of PC1 with ERA5 reanalysis surface air temperature (Oct–Nov–Dec) ($r = 0.74$, $n = 15$, 1979–1993, lag = 1 year), the year 1988 is treated as an outlier and hence excluded in correlation (shown in red outlined circle). (b) Temperature anomaly record derived from PC1 using the regression equation of ERA5 temperature and PC1 shown in panel (a). The light shade represents error envelopes derived from the regression equation's uncertainty in the slope and intercept.

4.2.3.2 $\delta^{18}\text{O}$ –sea ice variability in the DML ice core record

Previous studies have demonstrated that sea ice variability and atmospheric circulation influence moisture source and transport processes, thereby controlling $\delta^{18}\text{O}$ variability in coastal Antarctic cores (Sinclair et al., 2012). To investigate the dominant sources of moisture in DML core sites, backward wind trajectory analysis was carried out for different seasons using HYSPLIT (<http://ready.arl.noaa.gov/HYSPLIT.php>). The backward trajectories indicate that moisture sources for the precipitation over the DML core sites are predominantly derived from the surrounding oceanic sectors (Figure 4.7). Therefore, any changes in SIC and sea ice extent (SIE) in these oceanic sectors would affect the moisture source and its supply for precipitation over the DML region. Previous studies have shown that these changes will be reflected in the stable water isotope compositions of the precipitation (Rahaman et al., 2016). During the winter, sea ice cover increases several folds, shifting the moisture source away from the coast, and the opposite happens during the summer months. Similarly, reduction in ice cover in the past allowed the local moisture from open seawater to supply isotopically enriched moisture to coastal Antarctica; on the contrary, when sea ice cover increased, moisture was supplied from distant sources with relatively depleted $\delta^{18}\text{O}$ due to distillation of heavier isotopes through successive precipitation/moisture loss during transportation.

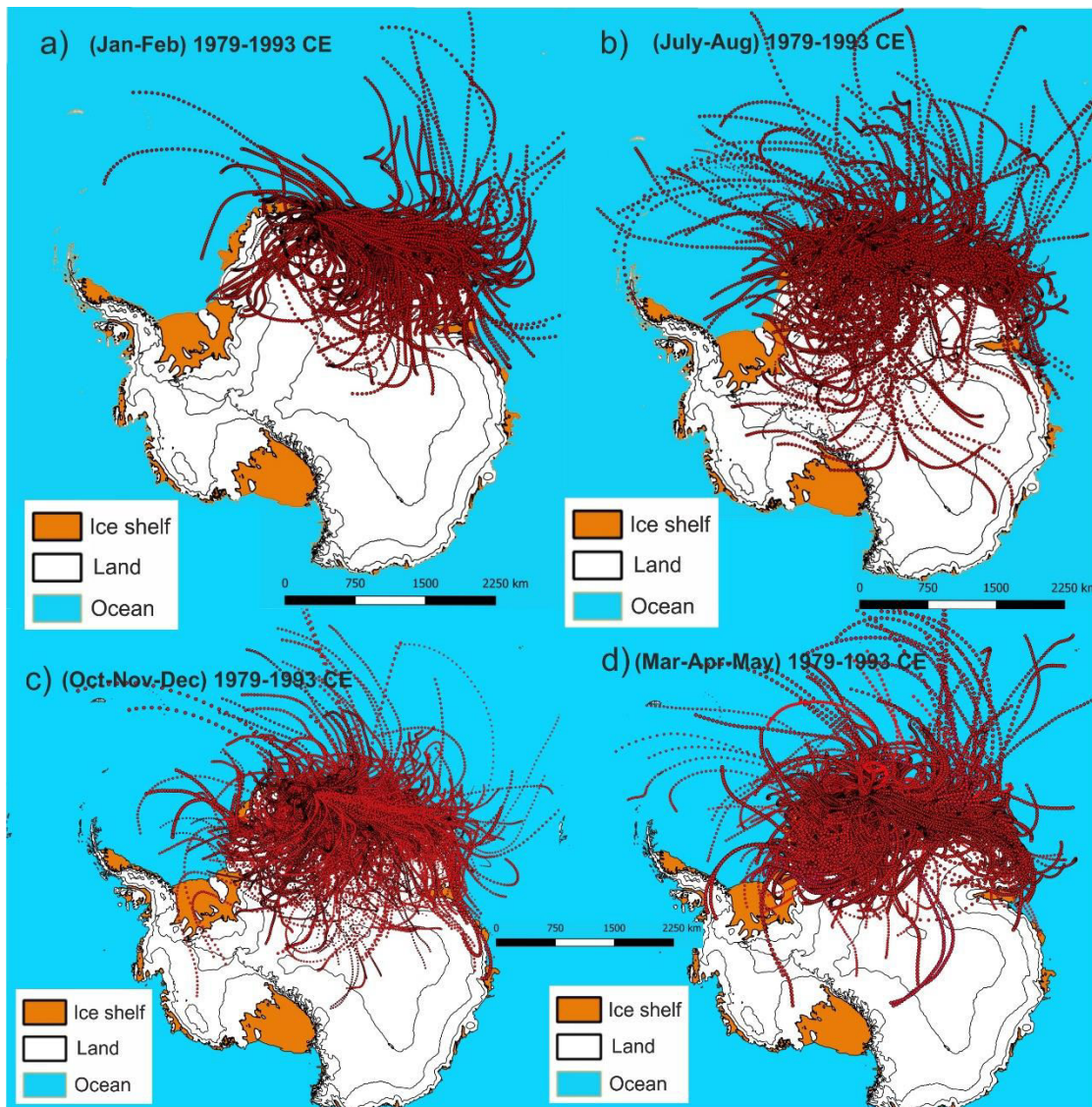


Figure 4.7. Seasonal backward wind trajectories analysis for the DML region.

Backward wind trajectory for (a) peak summer (Jan–Feb), (b) peak winter months (July–Aug), and for periods of maximum precipitation in DML (c) Apr–May–Jun and (d) Oct–Nov–Dec during 1979–1993 CE. The wind trajectories were calculated using the air parcel circulation model HYSPLIT (https://www.ready.noaa.gov/HYSPLIT_traj.php). The model is run for a 5-day backward trajectory of every precipitation event at the core location at 1000 m AGL.

We have investigated the second dominant factor, PC2, to explore its linkages with sea ice variations and wind conditions (strength and directions) for moisture transport and precipitation over the core sites. A spatial correlation of the National Snow and Ice Data Center (NSIDC) SIC record (Peng et al., 2013) with PC2 (1979–1993 CE)

reveals a significant positive correlation over the Western Indian Ocean Sector (WIOS) of Antarctica (Figure 4.8a). The PC2 was also correlated with Z500 geopotential height and wind vectors which shows a positive correlation over the Weddell Sea sector (high-pressure field), and the opposite is observed over the WIOS region (low-pressure area) (Figure 4.8a). We observe that the coastal IND33 core alone contributes a maximum (up to 60%) to PC2 variability and the remaining contributions come from the three inland DML ice cores (up to 40 %) (Chapter 2, Table 2.8). The spatial correlation of the IND33 $\delta^{18}\text{O}$ record with the SIC record shows a significant positive correlation over the same region (Figure 4.8b). This further confirms that the PC2 signal is primarily controlled by $\delta^{18}\text{O}$ variability in the IND33 coastal ice core, which is related to the changes in the sea ice cover and shifts in moisture transport. This finding is consistent with the previous report (Noone and Simmonds, 2004), which has suggested that the ice cores from coastal Antarctica are more sensitive to sea ice changes than those from interior Antarctica (Thomas and Bracegirdle, 2015). Based on the earlier studies, we expected an inverse correlation between sea ice and stable water isotopic records in the Antarctic ice core; an increase in sea ice can shift the moisture source (i.e., open sea) away from the core site, deplete the $\delta^{18}\text{O}$ during the moisture transport. Earlier studies also supported this (Masson-Delmotte et al., 2008; Rahaman et al., 2016). However, it is intriguing that the WIOS sea ice record is linearly correlated with the $\delta^{18}\text{O}$ record derived from ice cores. In the following section, we have investigated the potential factors responsible for the observed positive relation between the ice core $\delta^{18}\text{O}$ record and the sea ice variability in the WIOS region.

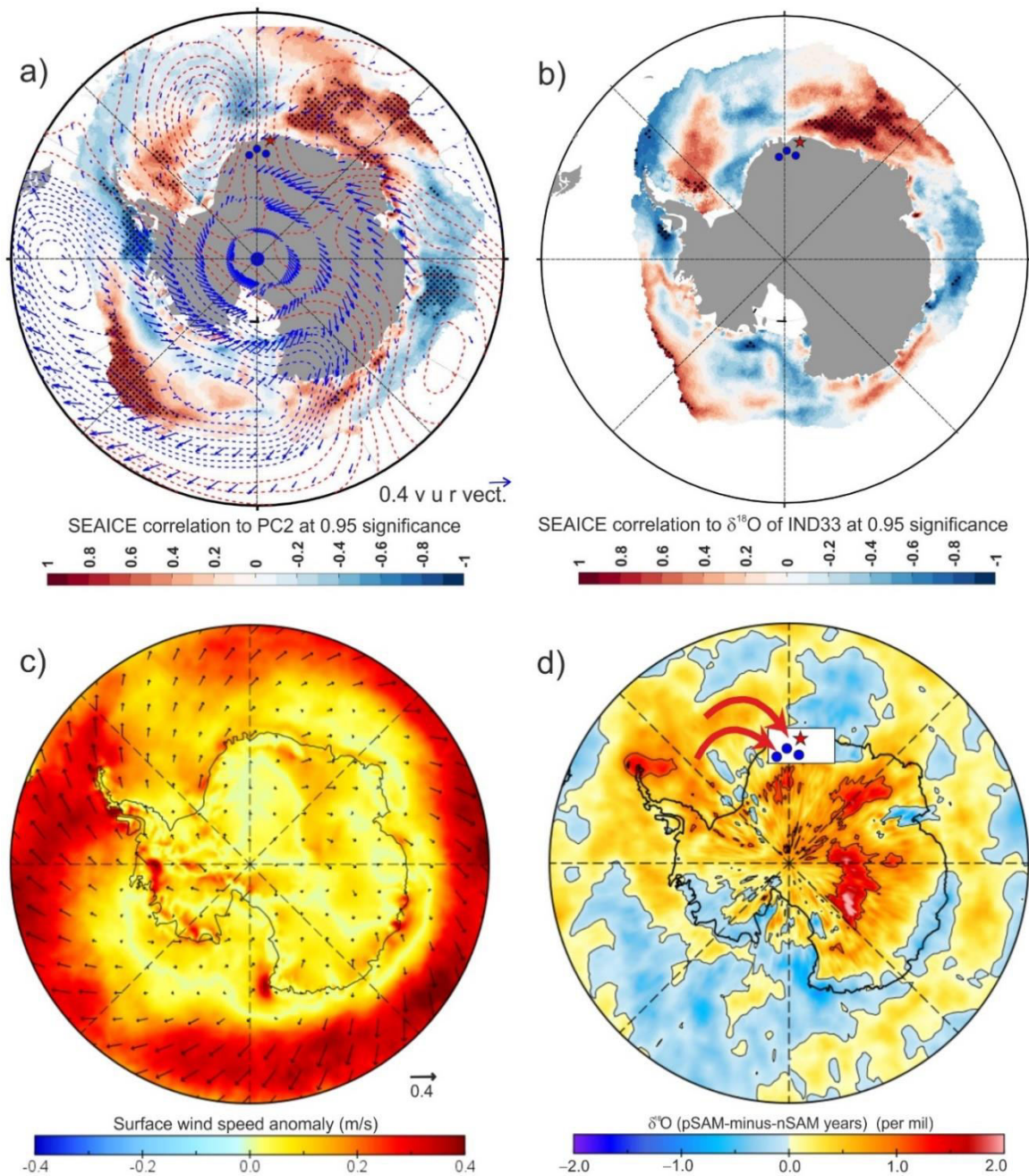


Figure 4.8. Spatial plots describing the correlation and mechanism for sea ice variability with $\delta^{18}\text{O}$ record.

(a) The PC2 was correlated with NSIDC sea ice concentration (shading: significant regions at 95% confidence level are highlighted in the black dots), ERA5 Z500 (dashed contours: red contours positive correlation and blue contours negative correlation), and ERA5 winds at 850-hPa level (vectors) during 1979–1993 CE. (b) IND33 $\delta^{18}\text{O}$ record is correlated with NSIDC SIC (1979–1993 CE); correlation is shown in the color code. Black dots highlight the regions of significant correlation at 95% confidence

level. (c) Composite anomaly maps of ERA5 surface wind speed (m/s) during positive SAM years. (d) Anomaly map of ECHAM5-wiso model $\delta^{18}\text{O}$ based on the difference between the positive and negative SAM years for the period (1979–2011).

During increased sea ice cover over the WIOS region, moisture availability and supply from this sector get reduced. On the contrary, strong and favourable wind conditions drive sea ice away from the Weddell Sea sector to the WIOS, leading to increased open water or less ice cover, making the Weddell Sea a dominant source. The stronger westerlies (Figure 4.8c) would thus increase the moisture supply from the Weddell Sea for precipitation over the IND33 core site, which is isotopically enriched, as shown in the ECHAM5-wiso modelled $\delta^{18}\text{O}$ anomaly plot (Figure 4.8d). Therefore, we suggest that the stable isotope variability at DML and the sea ice variability over WIOS respond to large-scale atmospheric circulation in this sector. Wind strength is the common driving force that causes changes in both moisture supplies to the study region and the sea ice transport from the Weddell Sea to the WIOS region. Since the Westerly winds around Antarctica are a robust system stable over a more extended period, the relationship between the PC2 and the SIC over the WIOS region could be established through the variability in the wind forcing, at least during the past few centuries. The SIC averaged across the grid box over the WIOS (60°S to 70°S, 15°E to 60°E) (Figure 4.9a) shows a strong correlation with PC2 ($r=0.81$, $n=15$, $p<0.05$) during the period 1979–1993 CE (Figure 4.9b). This empirical relation can be extended beyond 1979 to reconstruct the annual SIC record of the WIOS, with a reasonable assumption that this linear relationship has been stable over the entire record. Our high-resolution long-term sea ice record reconstructed based on an array of ice core records thus provides a unique opportunity to investigate the controlling factors for modulating annual to multi-decadal variability in SIC over the WIOS and deciphering its long-term trend during the past two centuries (Figure 4.9c).

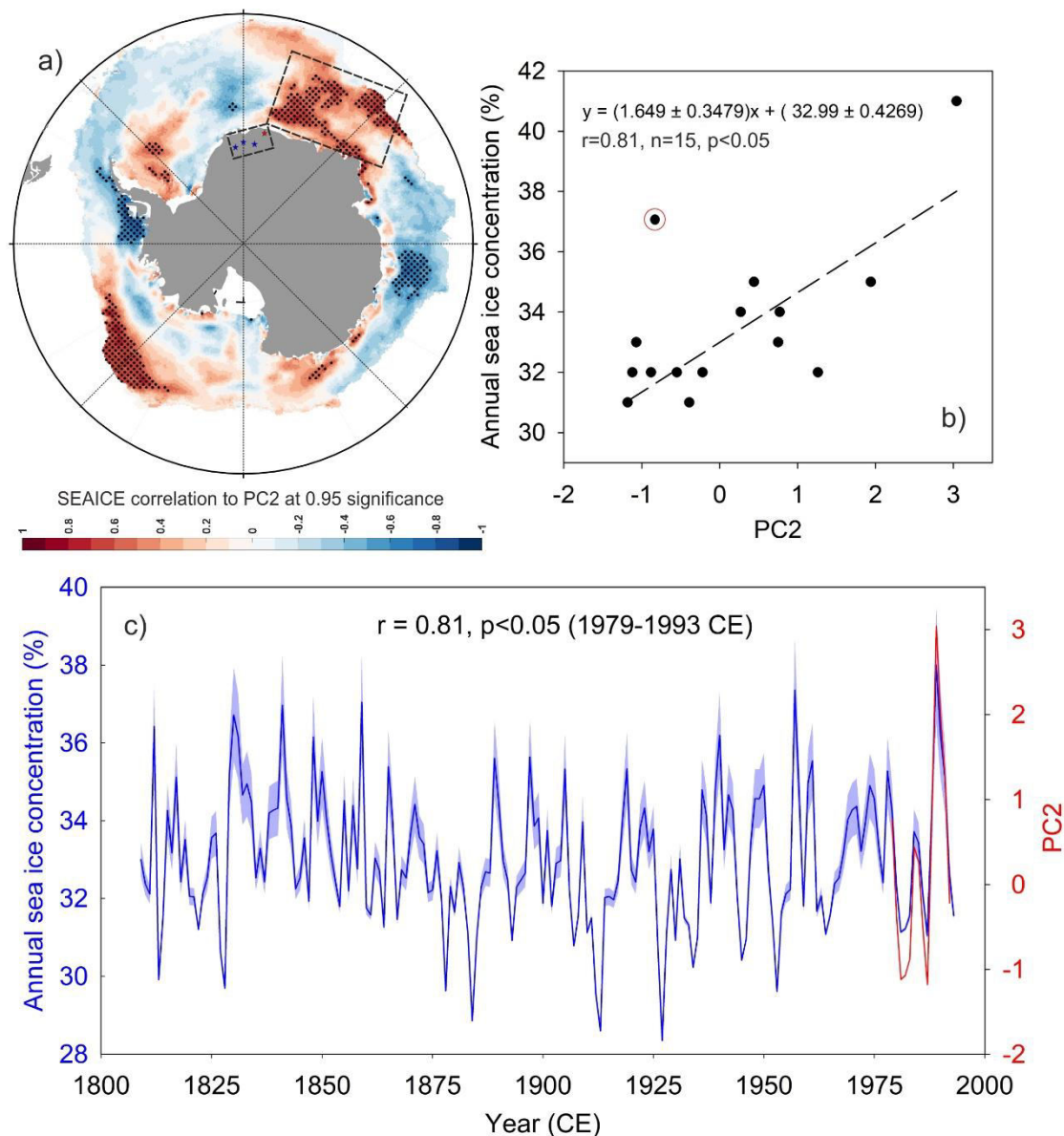


Figure 4.9. Correlation plots of PC2 with sea ice and reconstruction of sea ice concentration of WIOS.

(a) The PC2 is correlated with NSIDC SIC for 1979–1993 CE; correlation is shown in the colour code. Black dots highlight the regions of significant correlation at 95% confidence level, (b) PC2 shows a significant correlation with NSIDC sea ice concentration ($r = 0.81, n = 15, p < 0.05$) over the WIOS (60°S to 70°S , 15°E to 60°E) for the period 1979–1993 CE, the year 1988 is treated an outlier and excluded in the correlation (shown in red outlined circle). (c) The reconstructed annual sea ice concentration record over the WIOS is based on the regression equation between PC2 and the annual sea ice concentration record for 1979–1993 CE.

The following section shows the assessment of forcing factors and their relative roles in modulating sea ice variability in the WIOS for the past two centuries.

4.2.4 Sea ice trends and variability in the Western Indian Ocean Sector (WIOS)

Our reconstructed SIC record (1809–1993 CE) of the WIOS, together with the instrumental record (1994–2019 CE), enables us to discern the long-term trend and variability and investigate potential forcing factors and climate modes influencing sea ice variability at annual to decadal-scale during the past two centuries (1809–2019 CE). To identify a significant trend in the SIC record, we performed the Mann-Kendall test (Kendall, 1975) and determined the breaking points of the trend in the sea ice record (Supplementary Table S4). Based on the Mann-Kendall test, the reconstructed long-term sea ice record reveals a discernible declining trend in the 19th century (1830–1885CE) with a rate of $-0.58 \pm 0.12\%$ decade⁻¹ followed by a significant increasing trend with a rate of $+0.24 \pm 0.11\%$ decade⁻¹ in the 20th century during the period 1927–1993 CE (Figure 4.10). Further, to discern the recent trend of the last two decades from the long-term perspective, we have combined the satellite SIC record (1994–2019 CE) from National Snow and Ice Data Center (NSIDC) with the reconstructed record (Figure 4.10). The recent (1994–2014 CE) SIC record from NSIDC shows the highest increasing trend in the past two centuries with a rate of $+2.59 \pm 0.86\%$ decade⁻¹ followed by a sharp decrease during 2015–2016, associated with the extreme El Niño event of 2016 (Ionita et al., 2018; Stuecker et al., 2017).

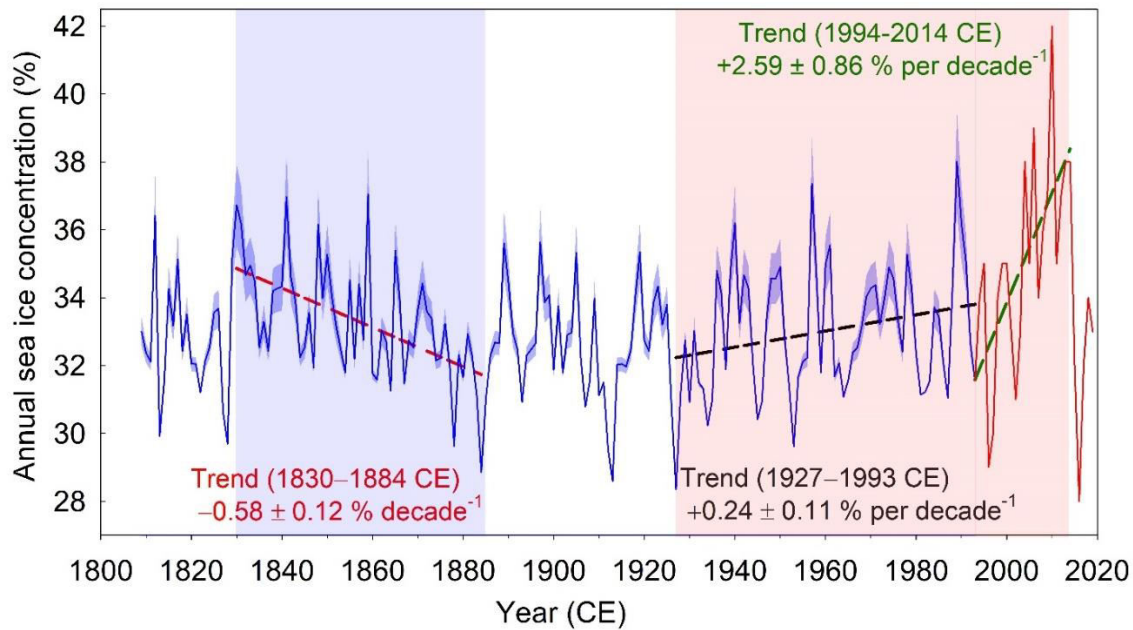


Figure 4.10. Sea ice variability and trends in WIOS, East Antarctica.

Trend analysis of the annual sea ice record of Antarctica's Western Indian Ocean Sector. A significant ($r=0.56$, $n=55$, $p<0.05$) declining trend is evident during 1830–1884 CE, followed by a significant ($r=0.25$, $n=67$, $p=0.058$) increasing trend during 1927–1993 CE. The observed NSIDC SIC record shows a significant increasing trend (red line) during 1994–2014 CE ($r=0.63$, $n=21$, $p<0.05$).

To understand variability in the sea ice record, power spectrum analysis (Schulz and Mudelsee, 2002) of the combined sea ice record (1809–2019 CE, Figure 4.11a) was performed, which shows significant (at 95% χ^2 level) periodicities of 2.8, 3.5, 8, 10 and 17.5 years (Figure 4.11b). These periodicities indicate strong interannual to decadal variability in sea ice concentration in the WIOS region during the past two centuries. Further, wavelet analysis (Torrence and Compo, 1998) demonstrates how these periodicities evolved in the past two centuries at various frequency bands ranging from interannual to decadal scales (Figure 4.11c). This shows significant periodicities at 2–8 years band at discrete intervals, which have become more dominant in recent decades (Figure 4.11c). We also observe periodicities at the decadal band (16–24 years) which became more dominant since the beginning of the 20th century. Scaled average variance

at ENSO band (2–8 years) shows a dramatic increase after ~1970 CE (Figure 4.11d). The variance at 16–24 years band shows an overall increasing trend since ~1800 CE with two prominent peaks during ~1890–1950 and ~1980–2019 CE (Figure 4.11d).

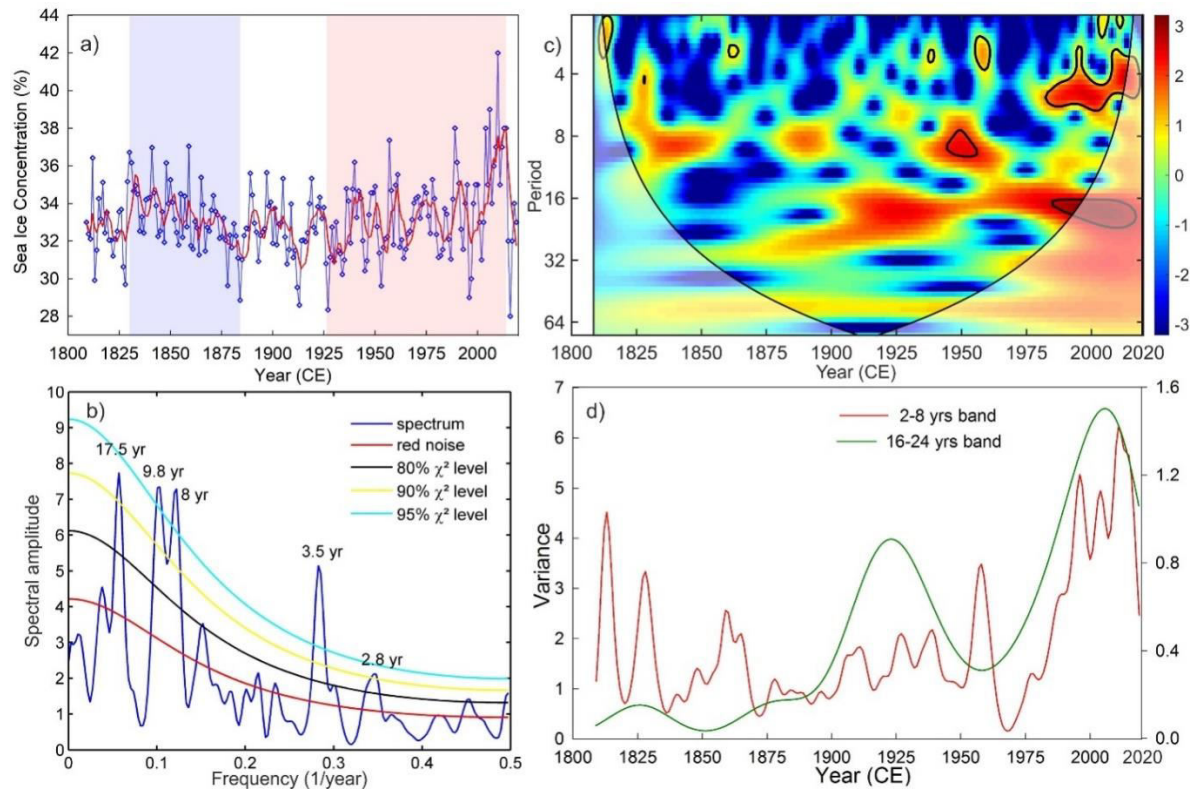


Figure 4.11. Time series analysis for the reconstructed sea ice concentration record.

(a) SIC record of the Western Indian Ocean Sector (1809–2019 CE) (blue shaded region show decreasing trend while red shaded region shows an increasing trend in SIC). (b) The power spectrum analysis of sea ice records shows significant periodicities of 2.8, 3.5, 8.0, 9.8, and 17.5 years at 90% χ^2 level. (c) Wavelet analysis of the reconstructed SIC record highlights significant periodicities in the colour band. (d) Scaled average variance analysis of reconstructed SIC at two specific frequency bands, 2–8 years and 16–24 years.

In the following section, we have investigated how the climate modes influence sea ice variability, particularly ENSO teleconnections and their interaction with SAM.

4.2.5 Influence of SAM and ENSO teleconnections on sea ice dynamics

SAM is known to influence Antarctic SIC through the changes in wind conditions due to the changes in sea level pressure (Holland et al., 2017). Wind-driven changes in sea ice advection are the dominant driver of sea ice variability around much of West Antarctica, whereas wind-driven thermodynamic changes dominate elsewhere (Holland and Kwok, 2012). The PC2 correlated with Z500 geopotential height shows a SAM-like pattern (Isaacs et al., 2021), positive correlation over the Weddell Sea sector (high-pressure field) and negative over the WIOS region (low-pressure area) (Figure 4.8a). This indicates that the climatic factors modulated by SAM influence sea ice variability in the WIOS. To investigate the influence of SAM on sea-ice variability over the WIOS, the NSIDC Antarctic SIC record is correlated with the Marshall SAM index (Marshall, 2003). This spatial correlation map highlights a significant (95% level) positive correlation over the WIOS (15°E to 60°E) during 1979–2013 CE (Figure 4.12a). This demonstrates the possible role of SAM in influencing sea ice cover in the WIOS.

Further, to examine this linear relationship on a longer time scale, reanalysis 20CRV2c SAM-Index (1851–2019 CE) was compared with the reconstructed sea ice record, which shows that both the records broadly co-vary throughout the period (Figure 4.12b). The wavelet coherence analysis performed between the sea ice record and 20CRV2c SAM-Index (1851–2019 CE) highlights significant in-phase relation during 1865–1884 CE and 1979–2013 CE at 4–8 years frequency band (Figure 4.12c). We observed that the sea ice increase in the recent decades, except for the last five years (2015–2019), is concomitant with the shifting of SAM to a positive phase. The higher interannual sea ice variability coincides with in-phase relation with SAM during the above intervals suggesting larger control of SAM on sea ice variability. Switching of SAM phases modulates pressure distribution over the Southern Ocean and Antarctica

and thus the wind conditions (speed and directions). Sea ice variability over the high southern latitudes is strongly controlled by changes in the westerly wind system, ocean surface current, and drifting of sea ice associated with the modulation of SAM (Deb et al., 2017; Hall and Visbeck, 2002). During positive SAM, low pressure over Antarctica intensifies the westerlies. Intensification of surface westerlies over the circumpolar ocean ($\sim 60^\circ\text{S}$) associated with the shifting of SAM to a positive phase leads to a significant zonal sea ice drift from the Weddell Sea toward the WIOS (Dickens et al., 2019; Lefebvre et al., 2004). Shifting SAM towards the positive phase thus resulted in increased piling of sea ice over the WIOS. This mechanism could explain the increase in sea ice over the western Indian Ocean (around 60°S) during the positive SAM years (Deb et al., 2017). Thus, we suggest that such a dynamic link between SAM and SIC over the WIOS has existed for the past two centuries. Our analysis of surface wind speed and SIC has demonstrated that the positive SAM years impacted the surface wind system and, thereby, changes in sea ice over the WIOS region (Figure 4.13). During positive SAM years, the circumpolar westerly wind became more vital in the Weddell Sea region (shown in wind vectors) that drifted the sea ice away from the Weddell Sea Sector and transported to the WIOS (Figure 4.13a & b). Further, such stronger wind conditions may also help to form more sea ice in the WIOS. An increase in westerlies will enhance the heat exchange, i.e., heat loss from the surface water to the atmosphere due to temperature gradient (cooler atmosphere and warmer ocean) and an increase in sea ice formation (Deb et al., 2017; Raphael, 2003; Simmonds and Xingren, 1993).

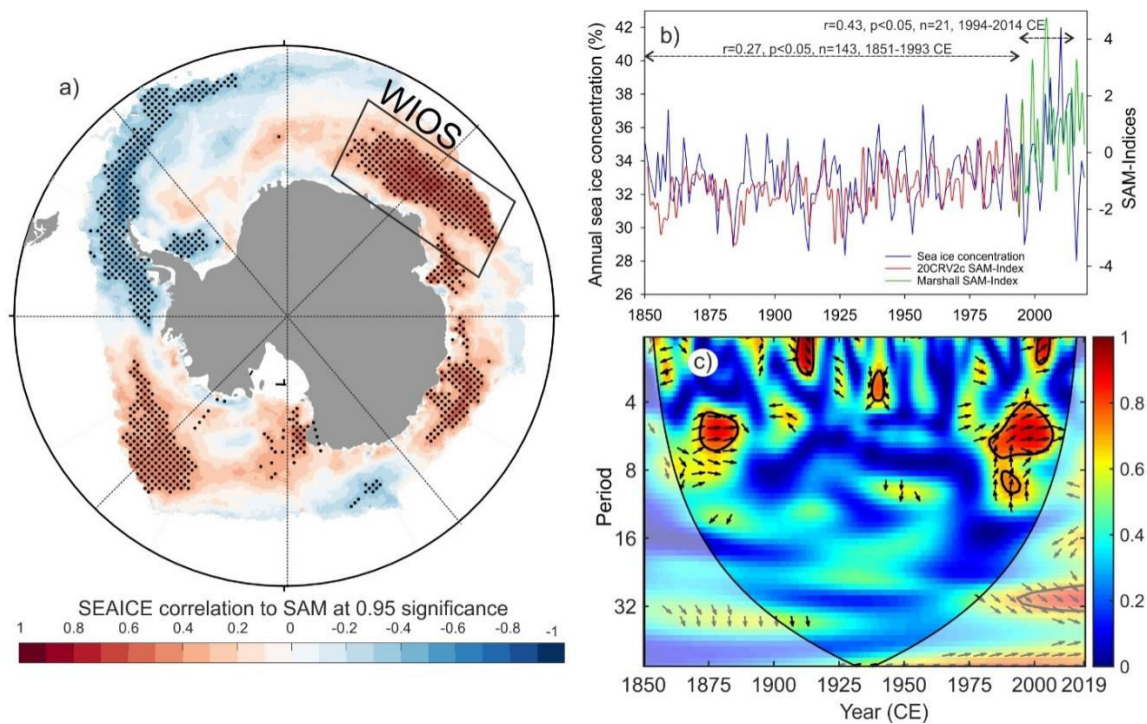


Figure 4.12. Correlation and time series analysis of sea ice concentration with SAM indices.

(a) NSIDC SIC record (1979–2013 CE) is correlated with Marshall SAM Index (Marshall, 2003). The regions of significant (95% significance level) correlations are highlighted in black dots. (b) Correlation between the reconstructed SIC record (PC2) (1809–1993 CE) combined with the instrumental record (1994–2019 CE) and SAM records (Gong and Wang, 1999; Marshall, 2003). The reconstructed SIC shows an overall weak correlation ($r=0.27, p<0.05, n=143, 1851-1993$ CE) with the long-term SAM Index (Gong & Wang, 1999); however, the correlation is improved during 1865–1885 CE ($r=0.77, p<0.05, n=20$) and coincides with decreasing SIC trend. (c) Wavelet coherence analysis of reconstructed and instrumental SIC with combined 20CRV2c SAM Index (Gong and Wang, 1999) for 1851–1993 and Marshall SAM Index (Marshall, 2003) for 1994–2019 CE. The thick black contours indicate 95% of confidence, based on a red noise model. The thin black line indicates the cone of influence. The relative phase relationship is shown as arrows (with in-phase pointing right, anti-phase pointing left, SIC leading SAM by 90° pointing straight down, and vice versa). The significant in-phase correlation is highlighted during 1865–1885 and 1979–2013 CE time intervals, associated with decreasing and increasing trends in SIC.

Therefore, stronger westerlies could increase sea ice cover in the WIOS by transporting and forming new sea ice. However, at this stage, it is difficult to quantify the role of these two individual factors. While the reconstructed and instrumental SIC record over the WIOS demonstrates an overall increasing trend associated with a positive shift of SAM during 1960–2014 CE, a dramatic decrease in the NSIDC SIC was observed during 2015–2016.

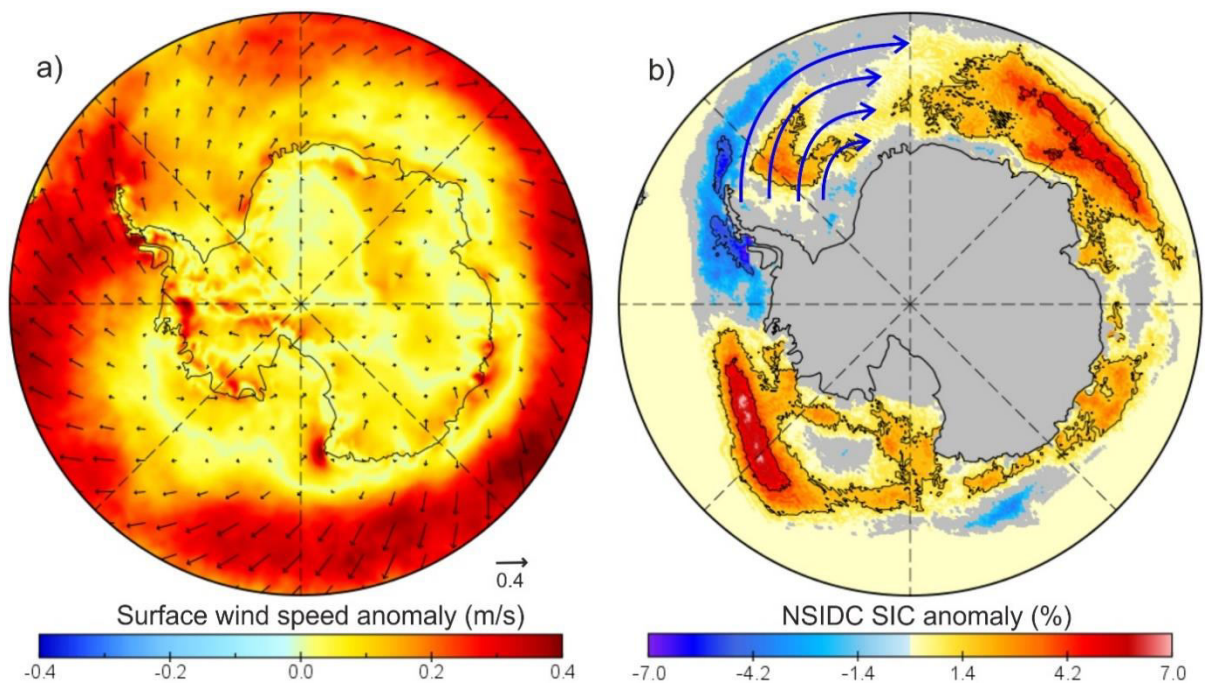


Figure 4.13. Surface winds and sea ice anomaly plots during the positive SAM years.

Composite anomaly maps of (a) ERA5 surface wind speed (m/s) and (b) NSIDC SIC (%) for the positive SAM periods during the interval 1979–2019. However, during the interval, 1979–2019 CE, strong positive SAM years with anomaly >1 were selected for composite anomaly plots: twenty such positive SAM years were identified and used for composite wind speed and NSIDC SIC anomaly plots. The anomaly plots show an increase in SIC over the WIOS region concurrent with wind-related sea ice transport from the Weddell Sea sector. The blue arrows shown in panel (b) highlight the movement of sea ice from the Weddell Sea sector to the Indian Ocean Sector, resulting in an increase in SIC over the WIOS.

This abrupt decrease in SIC over the WIOS region is associated with the extreme El Niño event of 2015–2016 (Ionita et al., 2018; Stuecker et al., 2017). The influence of ENSO is known to affect sea ice formation and transport, leading to some variability between ENSO and sea ice concentration (Kwok and Comiso, 2002b; Liu et al., 2004; Renwick, 2002; Stammerjohn et al., 2008; Yuan, 2004). To investigate the influence of ENSO on sea ice variation in space and time, the NSIDC SIC record is correlated with the Southern Oscillation Index (SOI) index (Figure 4.14a), which highlights a significant positive correlation over the WIOS during 1979–2019 CE. This suggests that ENSO is important in modulating SIC over the WIOS.

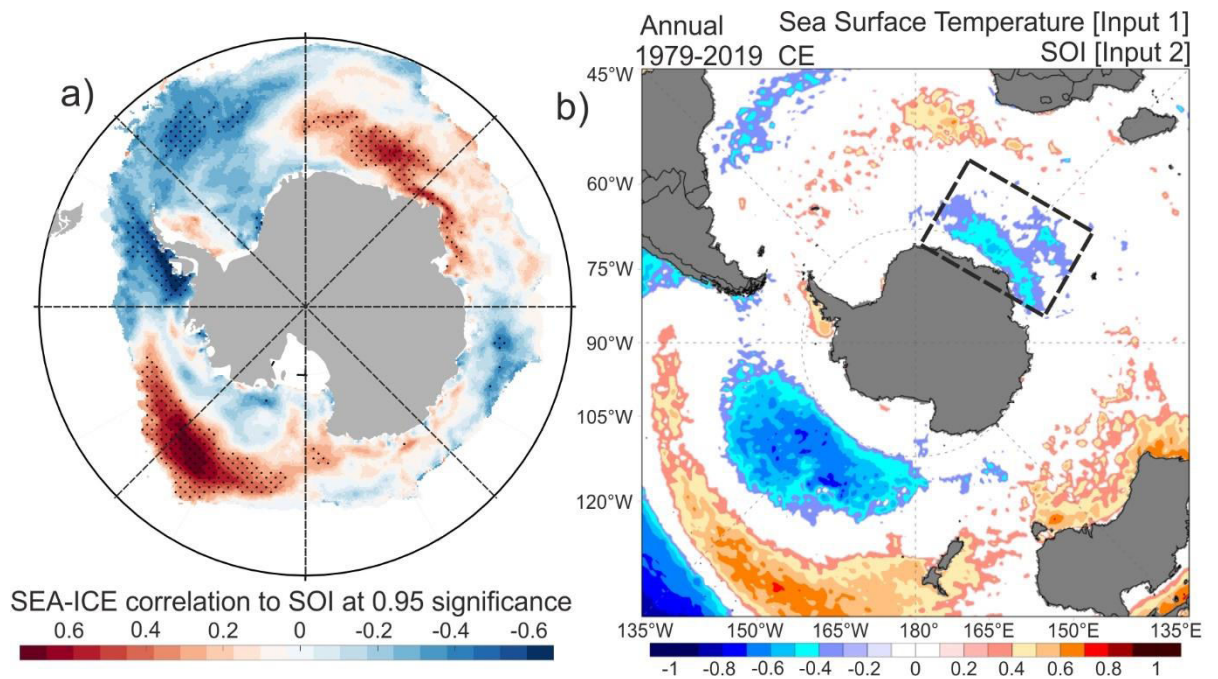


Figure 4.14. Sea ice correlation with SOI and surface air temperature.

(a) The annual NSIDC SIC record is correlated with the annual records of the Southern Oscillation Index (SOI) (1979,–2019 CE) (Ropelewski and Jones, 1987). Regions of significant correlation (at 95 % confidence level) are highlighted with black dots; (b) ERA5 annual Sea Surface Temperature (SST) is correlated with SOI (Ropelewski and Jones, 1987) (1979–2019 CE). The color code highlights regions of significant correlation (at 95 % confidence level).

Studies have shown that the SST and related variability in the SIC over the Southern Ocean are controlled through ENSO-related climate teleconnections through alteration of the surface energy fluxes (Ciasto and England, 2011; Simpkins et al., 2012; Yeo and Kim, 2015). The spatial correlation plot between ERA5 SST and SOI (1979–2019 CE) reveals a significant (at 95 % confidence level) inverse relation in the WIOS (Figure 4.14b). To understand the role of SST variation on SIC over the Southern Ocean, the ERA5 SST was correlated with SIC, which shows a significant inverse correlation (at 95% confidence level) in WIOS (Figure 4.15).

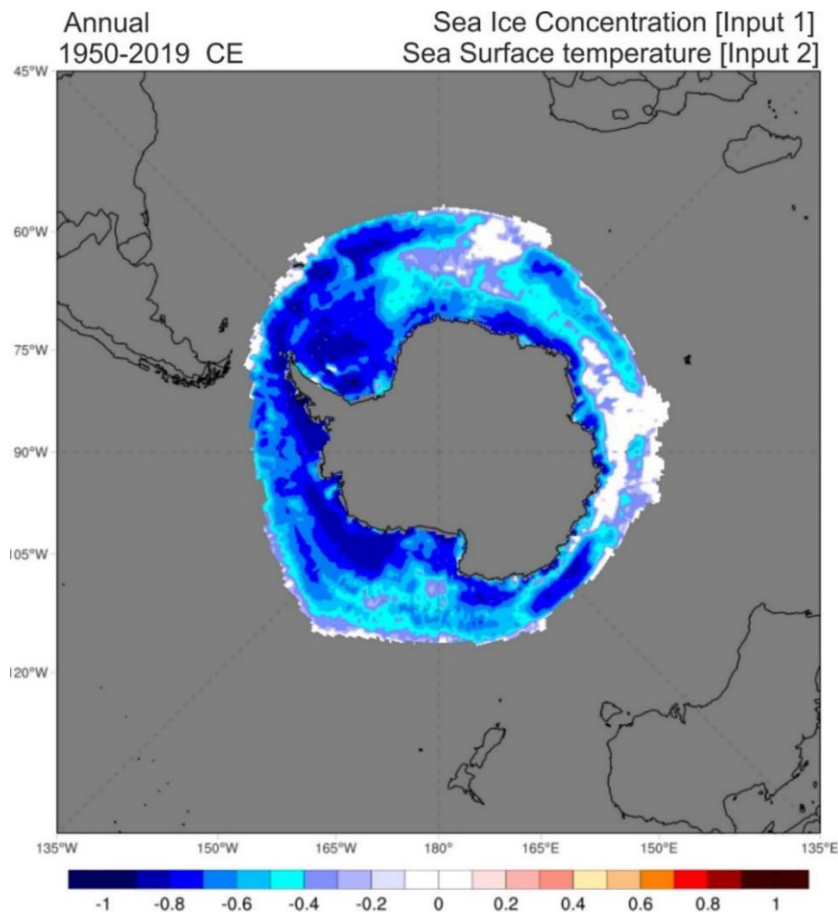


Figure 4.15. Sea ice correlation with ERA5 annual SST.

Correlation of sea ice concentration with ERA5 SST during 1950–2019 CE. The regions of significant correlation (at 95 % confidence level) are highlighted in the colour code. A significant inverse correlation is observed over the WIOS.

Further, to demonstrate how ENSO influences sea ice variability, we have plotted surface temperature anomaly maps of a few selected strong El Niño and La Niña years and compared them with the anomaly maps of NSIDC SIC corresponding to these ENSO events (Figure 4.16). During strong El Niño years (1987, 2016), we have observed a positive temperature anomaly (Figure 4.16a, b) over the WIOS region, which exactly coincides with the negative sea ice anomaly (Figure 4.16e, f), and the opposite is observed during strong La Niña years (1989, 2010), i.e., negative temperature (Figure 4.16c, d) and positive sea ice anomaly over the WIOS region (Figure 4.16g, h). This suggests the role of ENSO-driven SST changes on sea ice variability in the WIOS.

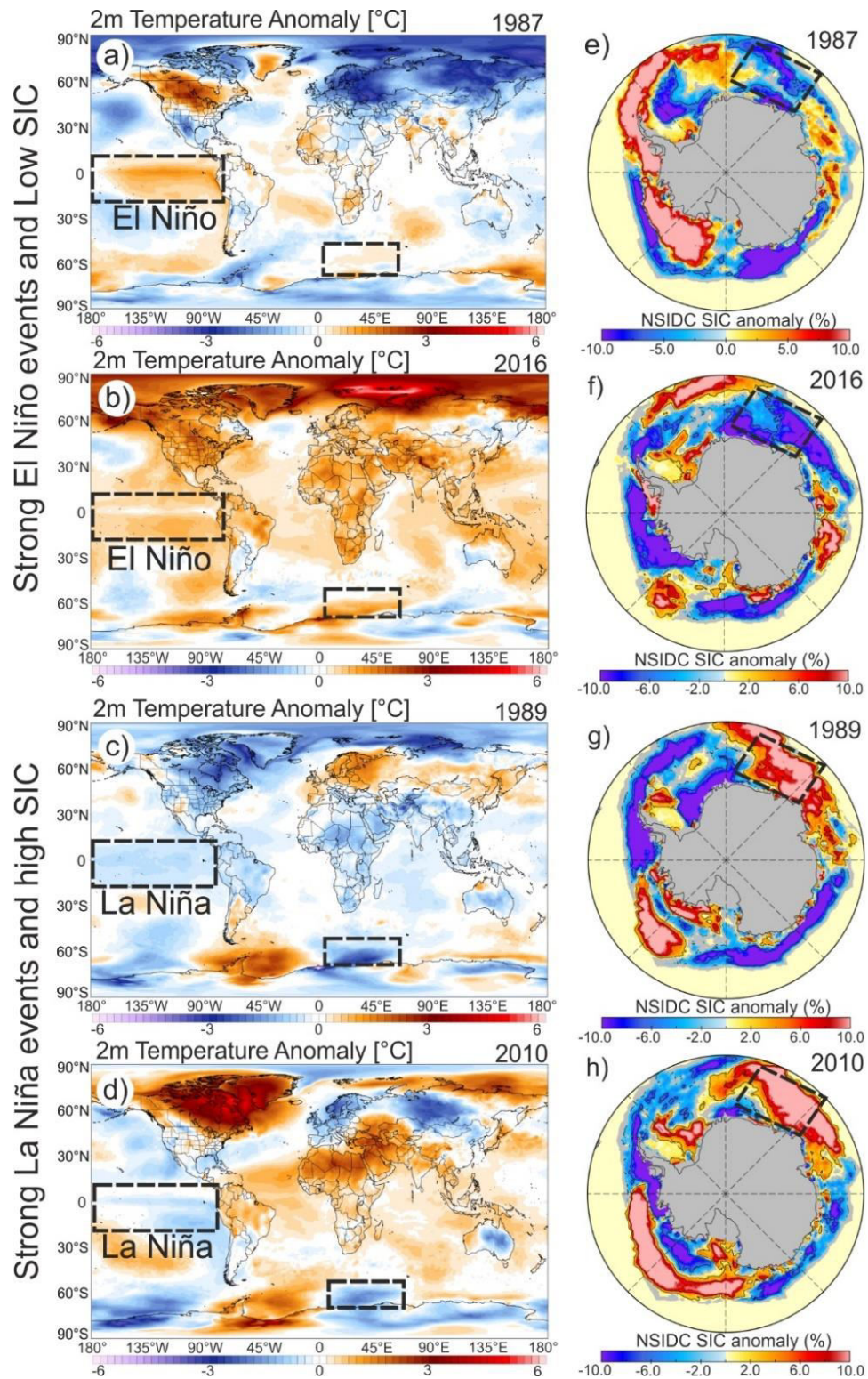


Figure 4.16. Spatial anomaly plots of surface air temperature and sea ice concentration during El Niño and La Niña.

Spatial anomaly plots during strong El Niño events (a-b) ERA5 2m temperature, (e-f) NSIDC sea ice concentration. Similar plots during strong La Niña events (c-d) ERA5 2m temperature (g-h) NSIDC sea ice concentration.

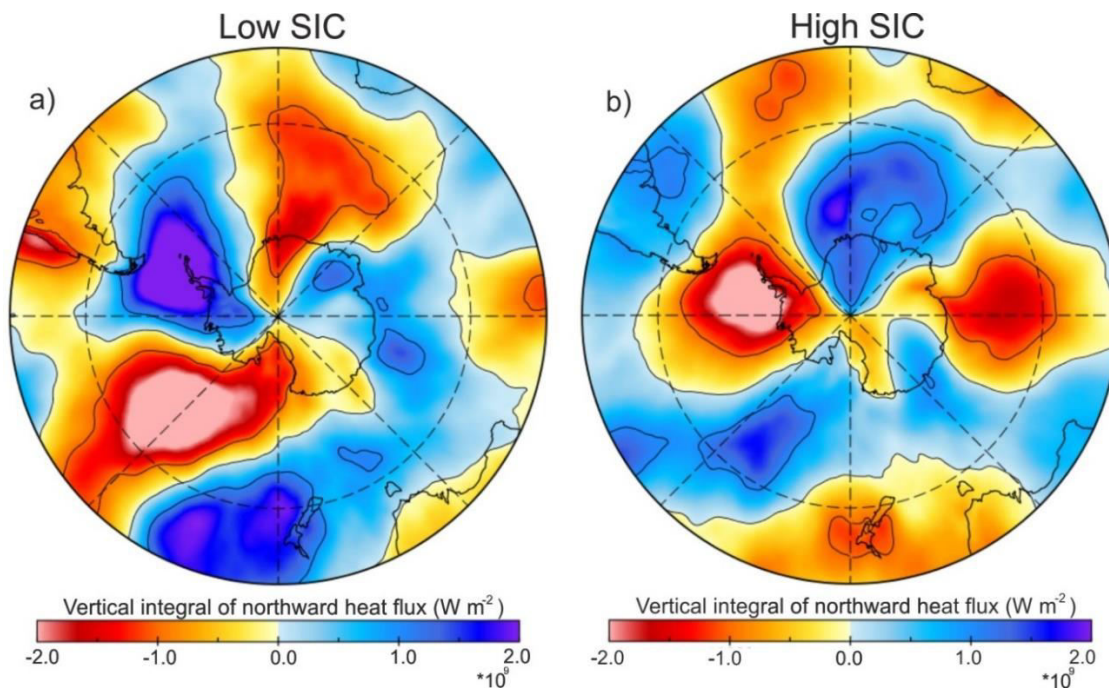


Figure 4.17. Heat flux anomaly plots during El Niño (low sea ice) and La Niña (high sea ice) years

Anomaly composites mean of ERA5 vertical integral of the northward heat flux (W m^{-2}) during (a) low sea ice concentration and El Niño years, (b) high sea ice concentration and La Niña years over 1979–2019 CE.

A recent study of sea ice concentration around the DML region observed a strong correlation with the sea surface temperature (SST) anomalies in the tropical Pacific. It attributed it to an atmospheric wave train pattern extending from the South Pacific (Isaacs et al., 2021). Such a southward-propagating atmospheric wave train could alter sea ice concentration by enhancing the meridional airflow. Since WIOS falls within the above study region, a similar mechanism can explain sea ice variability. To demonstrate how remote Pacific teleconnections influence the sea ice variability, we have investigated the role of northward heat flux (W m^{-2}) during strong El Niño (low SIC) and La Niña (high SIC) years. During the El Niño year, a strong negative northward heat flux anomaly is observed over the WIOS region, which coincides with low SIC, suggesting increased southward heat transport towards the WIOS region (Figure 4.17a) and opposite during the La Niña years (Figure 4.17b). This demonstrates

how remote Pacific teleconnections influence the sea ice variability through northward heat transport during the ENSO events.

Although both SAM and ENSO influence sea ice variability around Antarctica, their phase relation decides the extent of variability. ENSO teleconnections are stronger when El Niño coincides with the negative SAM phase and La Niña with positive SAM (Fogt and Bromwich, 2006; Fogt et al., 2011; Stammerjohn et al., 2008). Wavelet coherency of SOI and SAM shows significant anti-phase relation after the 1940s at the decadal band (16–32 years), coinciding with the increase in sea ice trend and variability (Figure 4.18a, b). In conclusion, increasing ENSO frequencies coupled with shifting of SAM to positive phase and their anti-phase relation resulted in an increase in sea ice variability and trend in the recent decades.

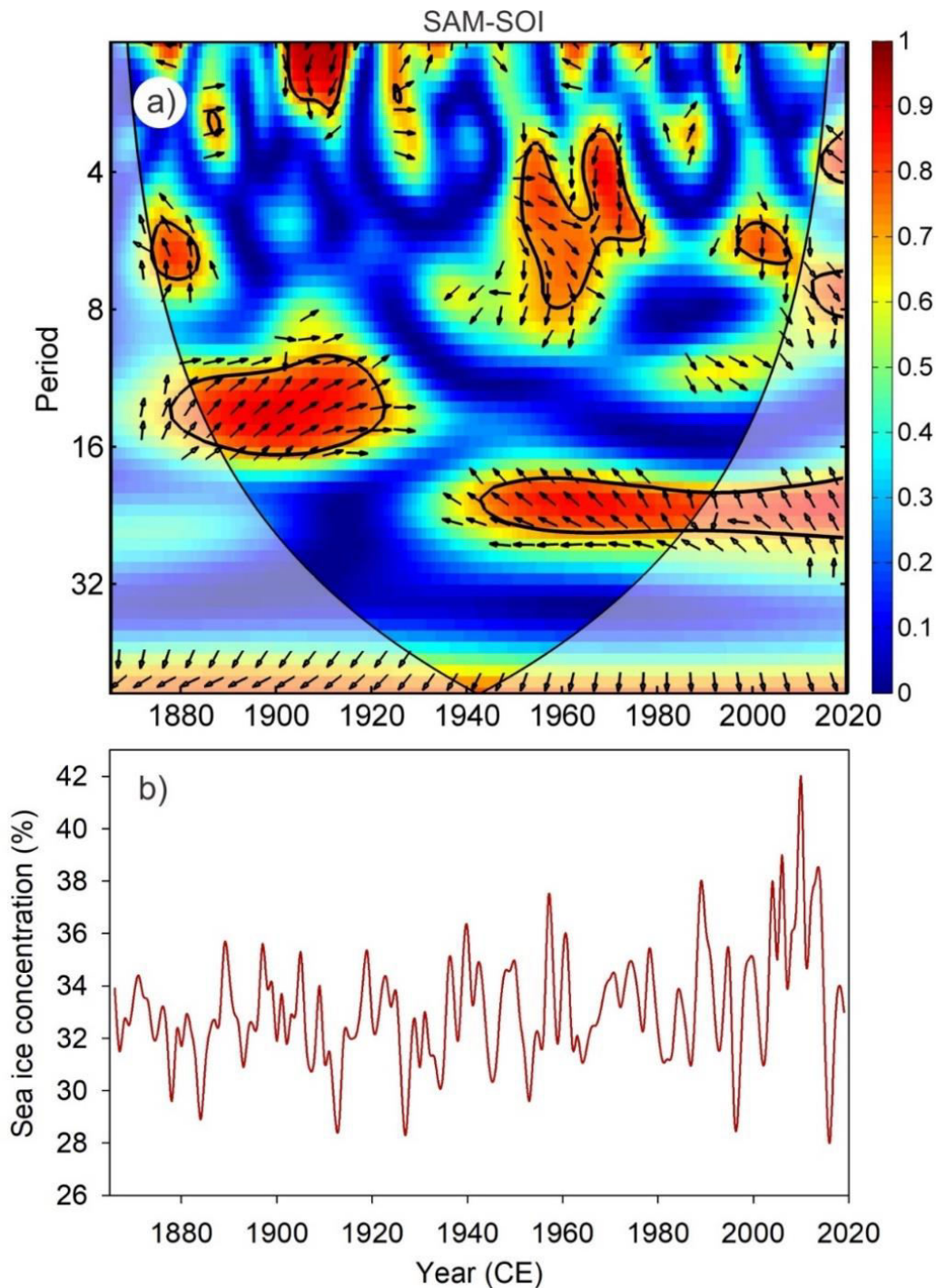


Figure 4.18. Wavelet coherence analysis of SAM and SOI.

(a) Wavelet coherence analysis of SAM (Gong and Wang, 1999; Marshall, 2003) and SOI (Ropelewski and Jones, 1987) during 1866–2019 CE. Based on a red noise model, the thick black contours indicate 95% confidence. The thin black line indicates the cone of influence. The relative phase relationship is shown as arrows (with in-phase pointing right, anti-phase pointing left, SAM leading SOI by 90° pointing straight up, and vice versa). (b) Annual variation in sea ice concentration during 1866–2019 CE.

4.3 Conclusions

A high resolution (at seasonal scale) ice core $\delta^{18}\text{O}$ record (1809–2013 CE) from the coastal region integrated with published ice core records from Dronning Maud Land (DML) in East Antarctica enabled us to reconstruct past changes in temperature and sea ice record. Our study revealed that the $\delta^{18}\text{O}$ records of ice cores from inland (high elevation) regions represent mainly the past temperature changes, whereas $\delta^{18}\text{O}$ records from coastal (low elevation) sites are more sensitive to sea ice variations and thus offer an opportunity to reconstruct the past sea ice variability. The reconstructed sea ice record combined with satellite records provided the longest Antarctic Sea ice record (1809 to 2019) of the Western Indian Ocean Sector of Antarctica (WIOS) at an annual resolution which enabled us to investigate the factors that contributed to sea ice variability at annual to multi-decadal time scales.

The key findings in the present study are as follows:

1. Reconstructed sea ice revealed a significant decline during 1830–1884 CE with a rate of $0.58 \pm 0.12 \text{ \% decade}^{-1}$ followed by a moderate increasing trend with a rate of $0.24 \pm 0.11\% \text{ decade}^{-1}$ during 1927–1993 CE.
2. The observed NSIDC sea ice record over the WIOS region during the recent decades (1994–2014 CE) shows a dramatic increase in the past two centuries with a rate of $2.59 \pm 0.86 \text{ \% decade}^{-1}$.
3. Interannual to decadal sea-ice variability over the WIOS region is mainly controlled by wind-driven sea-ice dynamics associated with SAM modulations and teleconnections to the Pacific oscillations.

4. The increase in interannual sea ice variability and trend in recent decades over the WIOS region is attributed to the shifting of SAM to a positive phase and concurrent increase in ENSO frequency.

Chapter 5

Sea surface temperature variability over the western Indian Ocean sector of Antarctica during the past two centuries and its linkages to tropical-extratropical climate modes

5.1 Introduction

High-resolution coastal ice core records on an annual scale are comparable with instrumental records and can be used to reconstruct several parameters beyond the instrumental record. During the recent rapid evolution of global climate, it is imperative to quantify its regional impact on the Antarctic climate on an annual to seasonal scale. However, only a few ice-core records from low-elevation regions are available. After the 1990s, some shallow ice cores were retrieved from the Atlantic sector (Altnau et al., 2015; Graf et al., 2002; Isaksson and Karlén, 1994) and the Weddell Sea sector (Mulvaney et al., 2002) of coastal Dronning Maud Land. Some annually resolved ice core records are also available from Antarctic Peninsula (Fernandoy et al., 2018), the Ross sea sector (Bertler et al., 2011), Law Dome (Delmotte et al., 2000; Masson-Delmotte et al., 2003; Morgan et al., 1997), Adélie Land (Ciais et al., 1995; Goursaud et al., 2017; Yao et al., 1990) and Princess Elizabeth region (Ekaykin et al., 2017). Recent reconstructions of temperature (Stenni et al., 2017) and surface mass balance (Thomas et al., 2017) for the last 2000 years highlighted the need for more coastal ice core records from Dronning Maud Land.

Stable isotopes of water (δD and $\delta^{18}O$) from Antarctic ice cores are considered the most valuable tool to reconstruct past climate changes related to surface air temperature (Jouzel et al., 2003; Masson-Delmotte et al., 2008). Rayleigh fractionation model (Ciais and Jouzel, 1994) is closely applied to define the relation of δD and $\delta^{18}O$

with temperature variability of the site but is not strongly associated with the average source temperature (Masson-Delmotte et al., 2004). Whereas the second-order parameter deuterium excess, ($d - excess = \delta D - 8 * \delta^{18}O$) (Dansgaard, 1964) derived as a kinetic fractionation component and predominantly associated with the temperature at the source and hence can be used to decipher the variability and evolution of temperature at moisture source (Merlivat and Jouzel, 1979; Stenni et al., 2010). The spatial variation of $d-excess$ over the Antarctic continent is well documented with a compilation and synthesis of data, which shows an increasing value while moving from coast to interior land (Goursaud et al., 2018; Masson-Delmotte et al., 2008; Touzeau et al., 2016). However, the temporal variability of $d-excess$ on a seasonal to inter-annual scale is not documented from the coastal DML region of East Antarctica and remains poorly understood. Isotopic modeling based on theoretical studies suggests that $d-excess$ variability is mainly controlled through variation in relative humidity (RH) and sea surface temperature (SST) over the moisture source region (Ciais et al., 1995; Merlivat and Jouzel, 1979; Petit et al., 1991), further they preserve the vapor signal while moving towards the polar region (Bonne et al., 2015; Jouzel et al., 2013). Several studies have used different ice core records of $d-excess$ to reflect the past SST condition during glacial-interglacial changes (Stenni et al., 2004; Stenni et al., 2001; Stenni et al., 2010; Vimeux et al., 2001; Vimeux et al., 1999), whereas such studies from low elevation ice core are limited.

El Niño Southern Oscillation (ENSO) is a leading mode of ocean-atmospheric variability over the tropical Pacific and strongly influences global climate variability (Alexander et al., 2002; Karoly, 1989; Trenberth et al., 1998). ENSO variability is mainly associated with an anomalous change in SST over the tropical Pacific and firmly controls the SST over the Southern Hemisphere (SH) (Ciasto and England, 2011; Ciasto

and Thompson, 2008; Renwick, 2002; Verdy et al., 2006; Yuan, 2004). However, the heat transport from the equatorial Pacific to SH extra-tropics is associated with the Pacific South American (PSA) pattern, an extension of alternating wave train-like anomalous positive and negative geopotential height, from tropics towards the southeast Pacific near Antarctica-South America (Karoly, 1989). Pacific Decadal Oscillation (PDO) is considered to be a long-lived ENSO-like variability and a leading mode of SST variation over the North Pacific Ocean SST (Mantua and Hare, 2002; Mantua et al., 1997). This also influences the SH SST on a decadal time scale. A recent study Wang et al. (2019) shows coupled influence of ENSO–PDO, which further modulates SST over the Atlantic Ocean sector. ENSO-related atmospheric teleconnection dominantly controls the SST and sea-ice variability over the Southern Ocean through modulation of surface energy flux. Whereas the ENSO-PDO-related SST variation over the Western Indian Ocean sector (WIOS) of Antarctica and their possible influence on sea ice variation is poorly quantified.

Atmospheric circulation of extra-tropics over the SH is dominantly controlled by Southern Annular Mode (SAM), defined as a leading mode of the pressure difference between extra-tropics and Antarctica (Gong and Wang, 1999; Marshall, 2003; Simmonds, 2003; Thompson and Wallace, 2000; Turner et al., 2005). The positive mode of SAM is associated with negative pressure anomaly over the Antarctic region, which strengthens the SH westerlies (Hall and Visbeck, 2002; Thompson and Wallace, 2000). Modulation in the surface westerly winds greatly influences the Ekman transport and ocean-atmospheric fluxes, which further influences the SST variation over the Southern Ocean (Ciasto and Thompson, 2008; Screen et al., 2010; Verdy et al., 2006). Several studies suggest that modulation of SAM mode strongly influences the Antarctic sea ice (Hall and Visbeck, 2002; Holland et al., 2017) and surface air temperature

(Marshall, 2007; Schneider et al., 2004; Thompson and Solomon, 2002; Van Den Broeke and Van Lipzig, 2003). A recent positive shift in SAM mode resulted in wind-drifted sea ice over the WIOS region (Deb et al., 2017; Ejaz et al., 2021; Holland and Kwok, 2012), which further increases sea ice concentration. However, the long-term variability of sea ice concentration over the WIOS region and its associated inter-annual SST variation needs to be quantified. This study used a new coastal ice core record of *d-excess* and reconstructed the SST anomaly over the WIOS for the past two centuries (1809–2013 CE).

5.2 Results and Discussion

5.2.1 Temporal variation in $\delta^{18}\text{O}$, δD , and *d-excess* records

The temporal variations of $\delta^{18}\text{O}$ and δD at the IND33 ice core are shown in Figure 5.1a. This new ice core from the coastal DML region offers seasonal to annual scale records of $\delta^{18}\text{O}$ and δD . The second-order parameter *d-excess* is calculated as an effect of kinetic fractionation or deviation from the Global Meteoric Water Line (GMWL). The *d-excess* shows excellent variability throughout the record (1809–2013 CE) with anomalous high values during (1812, 1851, 1891, and 1969) and a sudden drop to a negative low during 1941 (Figure 5.2b). In this study, a negative trend is observed in the *d-excess* record during 1809–1967 CE, whereas a significant positive trend is observed during 1981–2013 CE.

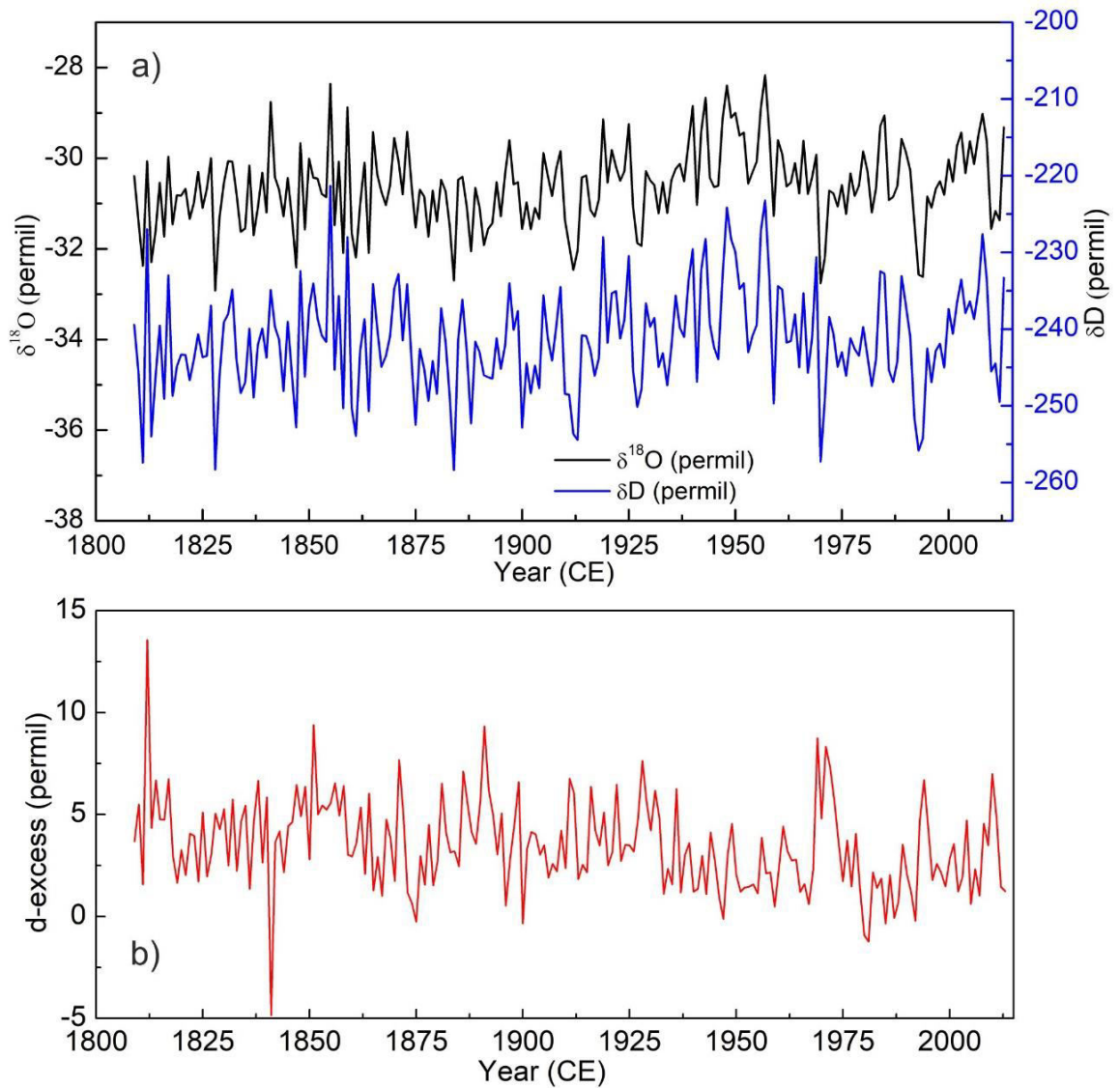


Figure 5.1. Annual variability of (a) $\delta^{18}\text{O}$ and δD records and (b) *d-excess* record from IND-33 ice core, derived from measured $\delta^{18}\text{O}$ and δD ice core record (1809–2013 CE).

In this study, a published *d-excess* record of IND25 is also compared with the IND33 record. The $\delta\text{D}-\delta^{18}\text{O}$ values of the IND33 ice core (1903–2006 CE) are found to be distributed along the regression line ($\delta\text{D} = 7.21 * \delta^{18}\text{O} - 20.49$; $r^2 = 0.90$), while $\delta\text{D}-\delta^{18}\text{O}$ of IND25 ice core (1903–2006 CE) shows a regression line ($\delta\text{D} = 8.17 * \delta^{18}\text{O} - 9.56$; $r^2 = 0.94$), which appears to be similar to GMWL (Figure 5.2a–b). Both ice cores reveal a significant difference in the slope of the regression line, although they

are ~100 km apart with a small latitudinal change. The δD - $\delta^{18}O$ slope of the IND33 ice core (m = 7.21 ± 0.16) is lower than the IND25 ice core (m = 8.17 ± 0.20). The trend in the *d-excess* record of both ice cores looks similar and shows a decreasing trend in their common time window (1903–2006 CE) (Figure 5.2c). This similarity may be due to small latitudinal changes in their location and the influence of common forcing factors.

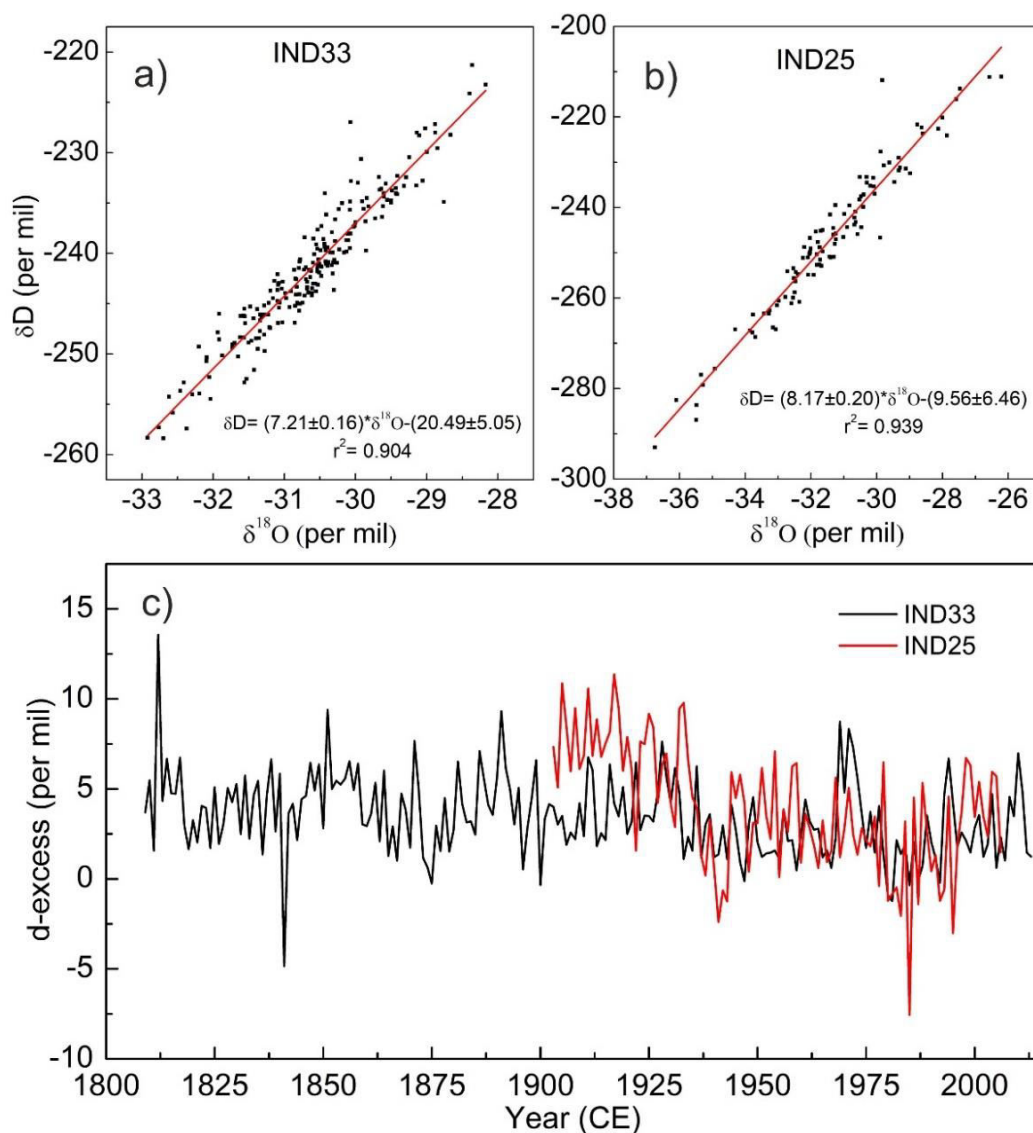


Figure 5.2. Correlation of δD with $\delta^{18}O$ ice core records used in this study and comparison of *d-excess* record.

δD vs. δ¹⁸O record from (a) IND33 (1809–2013 CE) and (b) IND25 (1903–2006 CE). (c) comparison of the d-excess record of the IND33 ice core with the published IND25 record.

5.2.2 Factors controlling the variability in *d-excess* and its relation to oceanic evaporation

The stable isotope of water (δD or $\delta^{18}O$) is extensively used as a surface air temperature proxy and thus gives a better understanding of past temperature changes (Jouzel et al., 2003; Masson-Delmotte et al., 2008; Mulvaney et al., 2012; Stenni et al., 2017; Thamban, 2017). However, the *d-excess* (non-equilibrium component) is mainly associated with the change in temperature at oceanic moisture sources or sea surface temperature (SST) and relative humidity (RH) (Merlivat and Jouzel, 1979; Stenni et al., 2010; Uemura et al., 2012; Uemura et al., 2008). The *d-excess* record is primarily anti-correlated with surface relative humidity and correlated with SST. However, the *d-excess* record of the IND33 ice core highlights an inverse correlation with the ERA5 Sea Surface Temperature Anomaly (SSTA) over the Western Indian Ocean Sector (WIOS) (Figure 5.3a). This suggests that some other factors are influencing the SST over the WIOS region. Therefore, it is required to identify the possible factors governing this anti-correlation between ice core-derived *d-excess* and ERA5 SST. Coastal Antarctic regions highlight several specific challenges related to the katabatic winds influencing the isotopic records. This suggests the large-scale wind circulation pattern is supposed to be the other possible influencing factor in controlling the *d-excess* record in the coastal ice cores. Since SAM is the dominant mode of climate variability in the southern hemisphere, shifting SAM to positive mode results in the strengthening of westerlies. Further analysis suggests wind-influenced sea-ice transport from the Weddell Sea sector to the Western Indian Ocean sector during the positive SAM years (Figure 5.3b). This accumulation and stacking of sea ice over the WIOS region result

in to drop in the SST. At the same time, the Weddell Sea sector observed a reduction in sea ice and an increase in SST in the open ocean system. This suggests a positive correlation of *d-excess* record with SST over the Weddell Sea sector and anti-correlation over the WIOS region of the Southern Ocean.

In order to verify this relationship and further establish the mechanism behind the anti-correlation (deviation from standard correlation), this study used a model-based *d-excess* record from ECHAM5-wiso (European Central Hamburg Model enabled with Water Isotope). ECHAM5 is an atmospheric general circulation model designed by the Max Planck Institute of Meteorology. The ECAHM5-wiso model produces outputs for the long term (Steiger et al., 2017) and the recent satellite era (Werner et al., 2011). Long-term simulations of the isotope-enabled ECHAM5-wiso model are available from 1871 to 2011 CE at T106 (1 degree) spatial resolution. The ECHAM5-wiso-derived *d-excess* is anti-correlated with ERA5 SST around the WIOS region and correlated over the Weddell Sea Sector (Figure 5.3c). The model-derived anti-correlation over the WIOS region is consistent with the ice core-derived derived relation of *d-excess* and ERA5 SST. Therefore, this anti-correlation can further extend back to reconstruct the WIOS SST, with a reasonable assumption that this relation also existed in the past. However, the Antarctic wind is robust and stable over a longer time interval. This suggests long-term wind-related sea ice drifting from Weddell Sea Sector to the WIOS region. This further strengthens the assumption to extend back the observed relation and reconstruction of SST over the WIOS.

The SSTA averaged across the WIOS region (60°S–70°S; 20°E–60°E) gives a significant anti-correlation with the *d-excess* ($r = -0.60$, $n=35$, 1979–2013 CE) (Figure 5.3d). Subsequently, this empirical relation extended beyond 1979 and reconstructed

the annual SSTA (1809–2013 CE) for the WIOS region (60°S–70°S; 20°E–60°E). However, the SSTA reconstruction is done with a reasonable assumption that such a linear relationship would be stationary for the entire reconstruction period (1809–2013 CE).

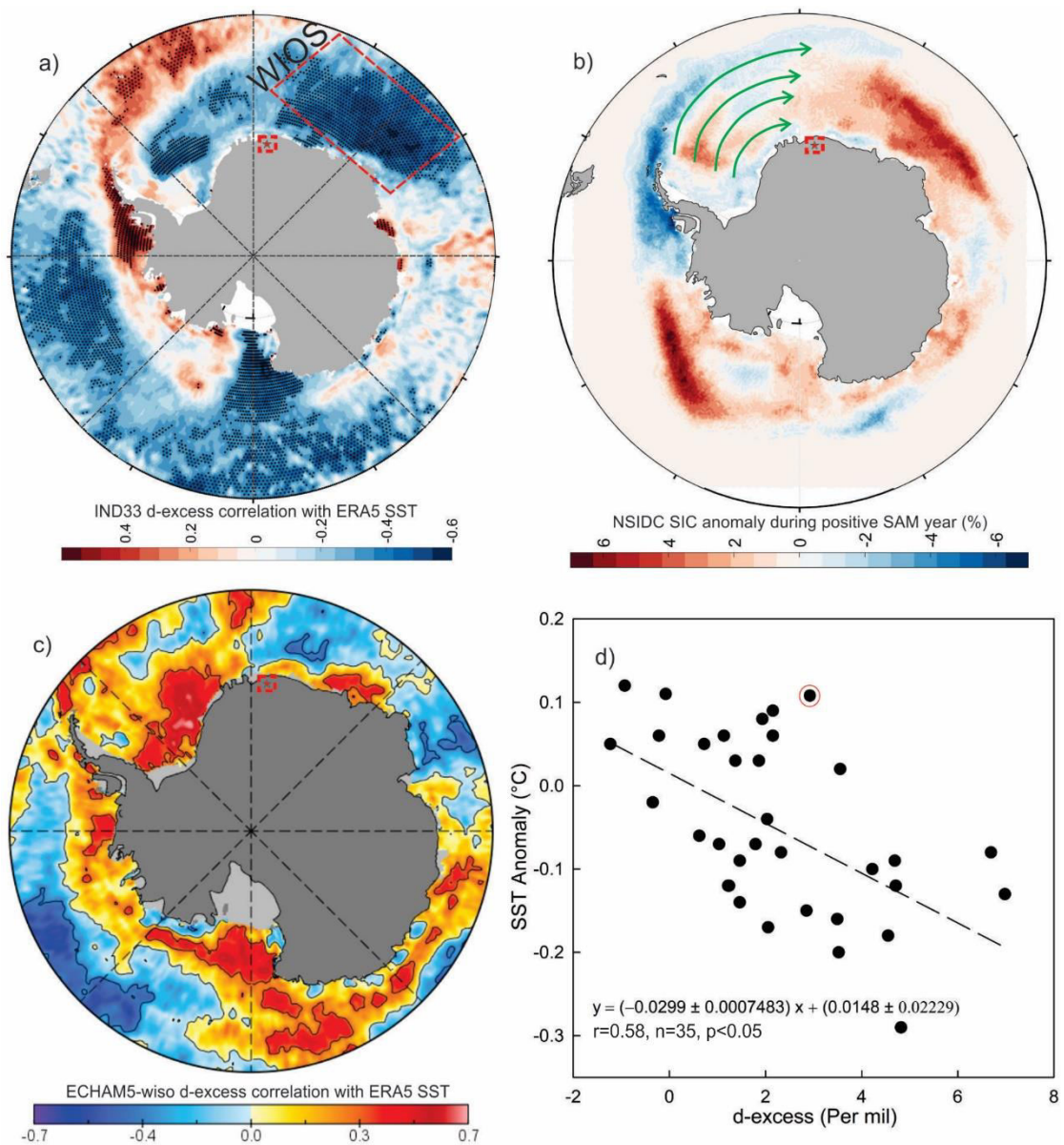


Figure 5.3. Correlation of ice core and ECHAM5-wiso model-based d -excess record with sea surface temperature and influence of wind drifted sea ice.

(a) Spatial correlation of IND33 d -excess record with ERA-5 Sea Surface Temperature Anomaly (SSTA) over the Western Indian Ocean Sector (WIOS) (1979–2013 CE). The regions of significant spatial correlations (at 95% confidence level) are highlighted in

black stipples (b) NSIDC SIC anomaly during the positive SAM years. (c) Spatial correlation of ECHAM5-wiso derived *d*-excess, and ERA-5 SST during 1979–2011 CE (d) *d*-excess record of IND33 shows significant anti-correlation with ERA5 SSTA ($r=-0.60$, $n=35$) over the WIOS ($60^{\circ}\text{S}-70^{\circ}\text{S}$; $20^{\circ}\text{E}-60^{\circ}\text{E}$).

This high-resolution reconstructed SSTA record on an annual scale gives a unique opportunity to discern its long-term trend and variability and further consideration for potential forcing factors and climate modes controlling the fluctuation in SSTA at the annual to decadal scale. The reconstructed SSTA record shows a long-term increasing trend with a rate of $+0.004 \pm 0.001$ ($^{\circ}\text{C decade}^{-1}$) during 1809–1967 CE. After that, a decreasing trend is observed with a rate of -0.028 ± 0.009 ($^{\circ}\text{C decade}^{-1}$) during 1981–2014 CE (Figure 5.4).

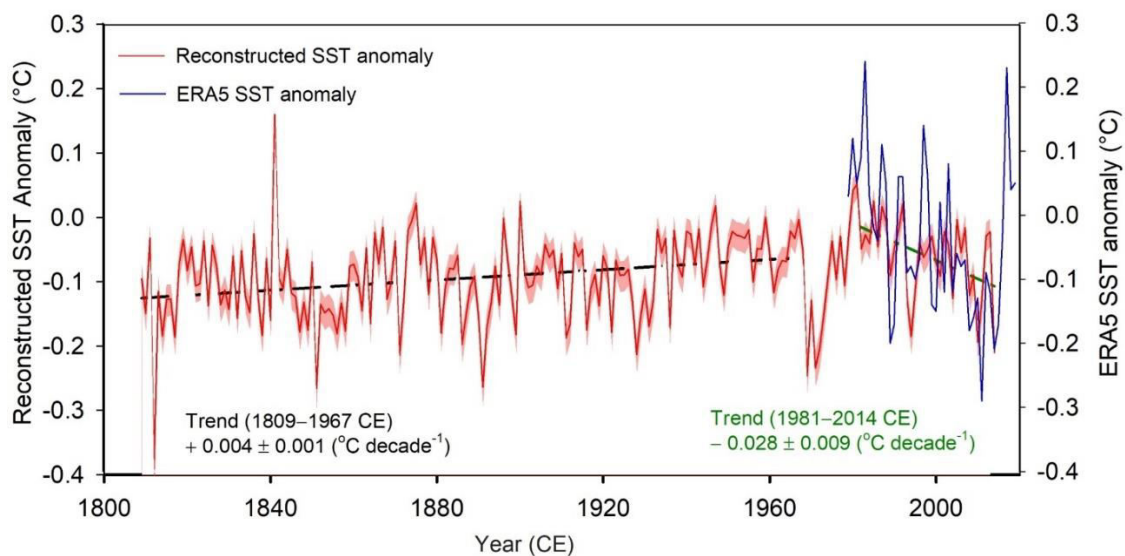


Figure 5.4. Reconstructed SSTA based on the *d*-excess ice core record.

*The reconstructed annual SSTA record over the WIOS was based on the regression equation derived from the correlation plot between *d*-excess and SSTA.*

Further, to investigate the dominant climate oscillations and their temporal evolution during 1809–2013 CE, this study used spectral analysis using Redfit software (Schulz

and Mudelsee, 2002) for the annual reconstructed SSTA of the WIOS region. The spectral analysis shows significant (90% χ^2 levels) periodicities of 2, 2.5, 3, 4, 20, and 40 years (Figure 5.5a). Wavelet analysis for reconstructed SSTA shows how these periodicities evolved over the past two centuries (Torrence and Compo, 1998) (Figure 5.5b). This indicates the complete dominance of decadal oscillation at 40 yr frequency band and a 20 yr oscillation during 1965–1990 CE, related to Pacific Decadal Oscillation (PDO). However, the periodicities within the El Niño Southern Oscillation (ENSO) band (2–8 yr) show their signal throughout the record.

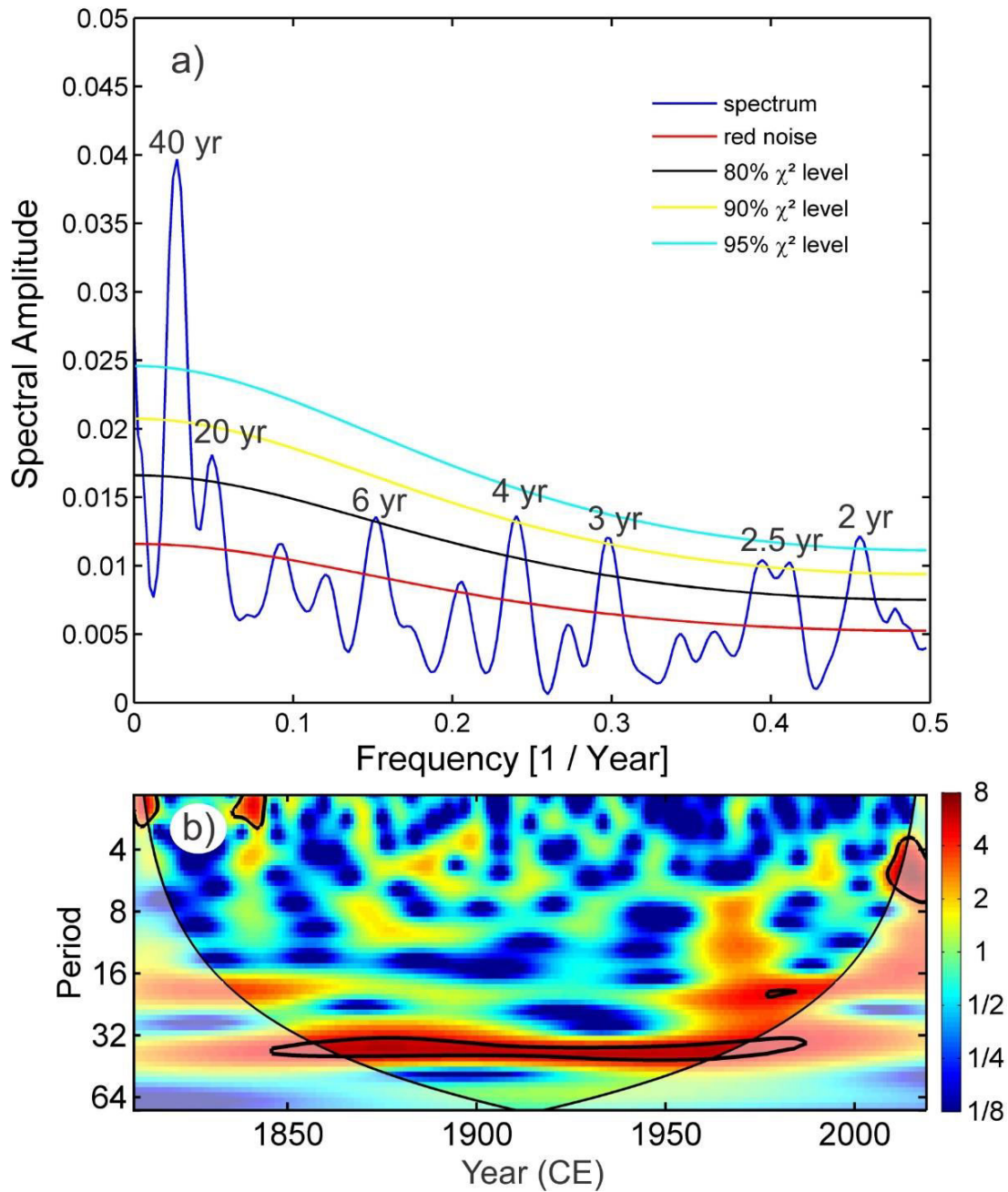


Figure 5.5. Power spectrum and wavelet transform analysis of reconstructed SSTA.

Spectral analysis of reconstructed SSTA for WIOS shows significant periodicities of 2, 2.5, 3, 4, 6, 20, and 40 yrs. (b) Continuous wavelet analysis of reconstructed SSTA shows the maximum power of decadal oscillation throughout the record.

To check the robustness of reconstructed SSTA, this study highlighted some strongest negative (1911, 1916, 1922, 1928, 1936, 1969, 1971, 1994, 2010, and 2011) and positive SSTA (1947, 1981, 1987, and 1992) from the 1900–2013 CE (Figure 5.6a). This study observed that except for 1922 and 1969, all the highlighted negative SSTA were associated with La Niña (cooling phase of ENSO). In comparison, the strong positive SSTA is associated with El Niño (warming phase of ENSO). However, to discern the spatial variation of SST over the WIOS during the extreme negative and positive values, this study used anomaly plots for ERA5 SST reanalysis data. The anomaly plots show negative SSTA over the WIOS region, corresponding to the strong negative reconstructed SSTA (1994, 2010, 2011, and 2014) period (Figure 5.6 b, c, d, e). In contrast, positive SSTA is observed over the WIOS region during the corresponding positive reconstructed SSTA (1947, 1981, 1987, and 1992) (Figure 5.6 f, g, h, i). This observed relation and spatial variation of SST over the WIOS region further increases the robustness of the reconstructed SSTA.

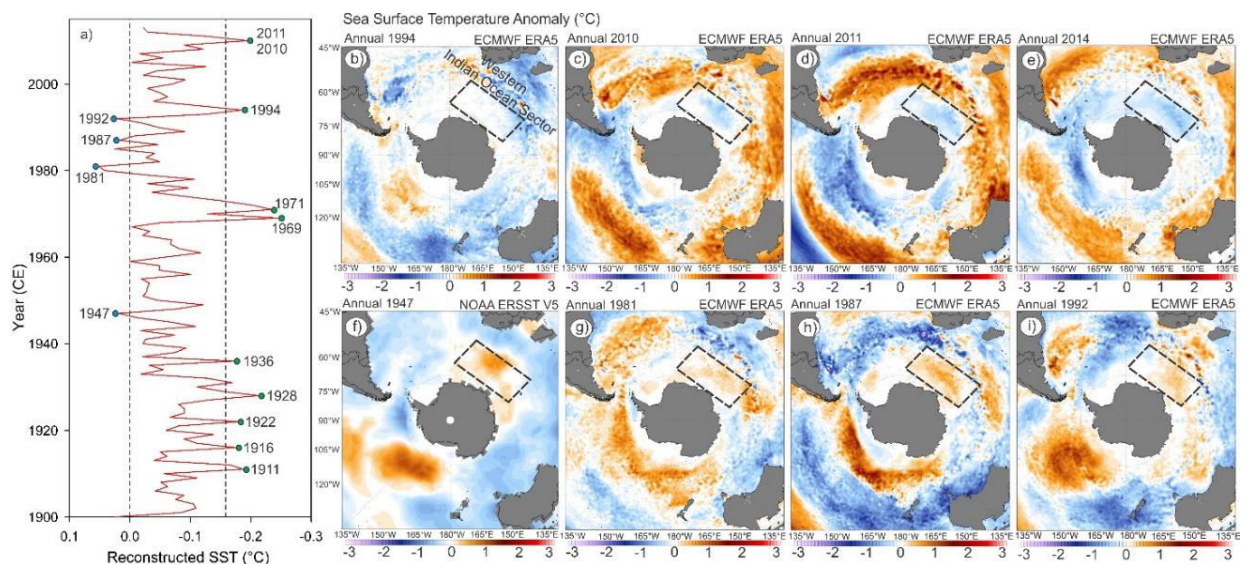


Figure 5.6. Temporal and spatial demonstration of maximum/minimum SSTA observed in the last century related to El Niño /La Niña, respectively.

(a) Reconstructed SSTA with a maximum and minimum anomaly in the last century. Spatial variation in SSTA over the WIOS region during the negative SSTA period (b) 1994 (c) 2010 (d) 2011 (e) 2014 and positive SSTA period (f) 1947 (g) 1981 (h) 1987 and (i) 1992

5.2.3 Role of tropical variability and its control on SSTA over the WIOS region

The anomalous variability in SST of tropics is mainly associated with ENSO and is considered the principal mode of atmosphere-ocean coupled variability on the inter-annual time scale and widely controls the global climate (Bjerknes, 1969; McPhaden et al., 2006; Neelin et al., 1998; Ropelewski and Halpert, 1986; Trenberth et al., 1998). The PDO is considered long-lived ENSO-like variability over the North Pacific Ocean SSTA and modulates the global climate on a decadal scale (Mantua and Hare, 2002; Wang et al., 2019). Their impact is not limited to the tropical region but also modulates the SSTA of the Southern Ocean surrounding the Antarctic continent. Further, to discern their relative role in modulating SST over the different oceanic sectors, the present study used a spatial correlation of Nino3.4 and PDO with the ERA-Interim annual SST record from 1979–2013 CE (Figure 5.7a–b). Both Nino3.4 and PDO show a positive correlation over the two oceanic sectors, (i) WIOS and (ii) Ross-Amundsen Sea in the Pacific Ocean Sector (Figure 5.7a–b). Compared to Nino3.4, the PDO shows a much stronger correlation over the WIOS.

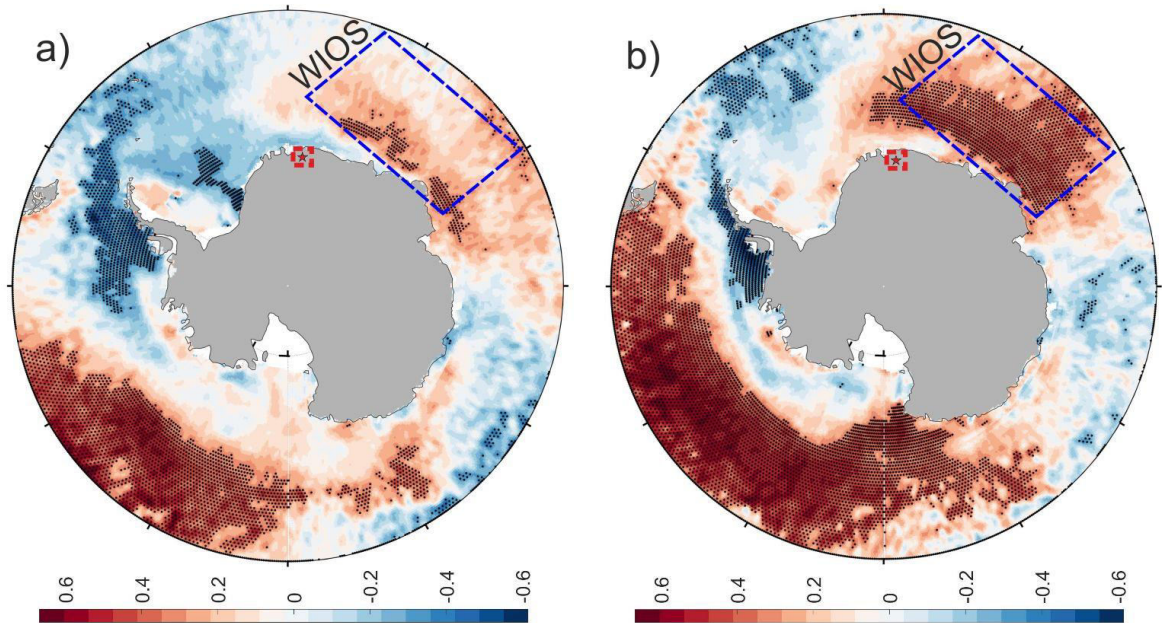


Figure 5.7. Spatial correlation of ERA5 SST with Nino3.4 and PDO.

Spatial correlation of ERA-5 SST with annual (a) Nino3.4 and (b) PDO record from tropical Pacific. The regions of significant spatial correlations (at 95% confidence level) are highlighted in black stipples.

This indicates that SST over the WIOS region is dominantly controlled by decadal climate variability. The cross-wavelet analysis of reconstructed SSTA with Nino3.4 and PDO index is used to highlight their influence on the annual to decadal band (Figure 5.8a–b). The observed result shows the common influence of ENSO at 2–4 yr during 1885–1990 CE and a complete in phase relation at 4–6 yr frequency band for a small-time window 1985–2000 CE (Figure 5.8c). The cross-wavelet analysis of reconstructed SSTA with PDO shows substantial control of the PDO signal. PDO mainly controls the long-term SSTA over the WIOS region at 32–40 yr frequency bands throughout the record (Figure 5.8d). However, a strong in-phase influence of PDO is observed at a higher frequency band of 20 yr from 1950–1980 CE. This indicates that SSTA over the WIOS region is mainly controlled by decadal variability.

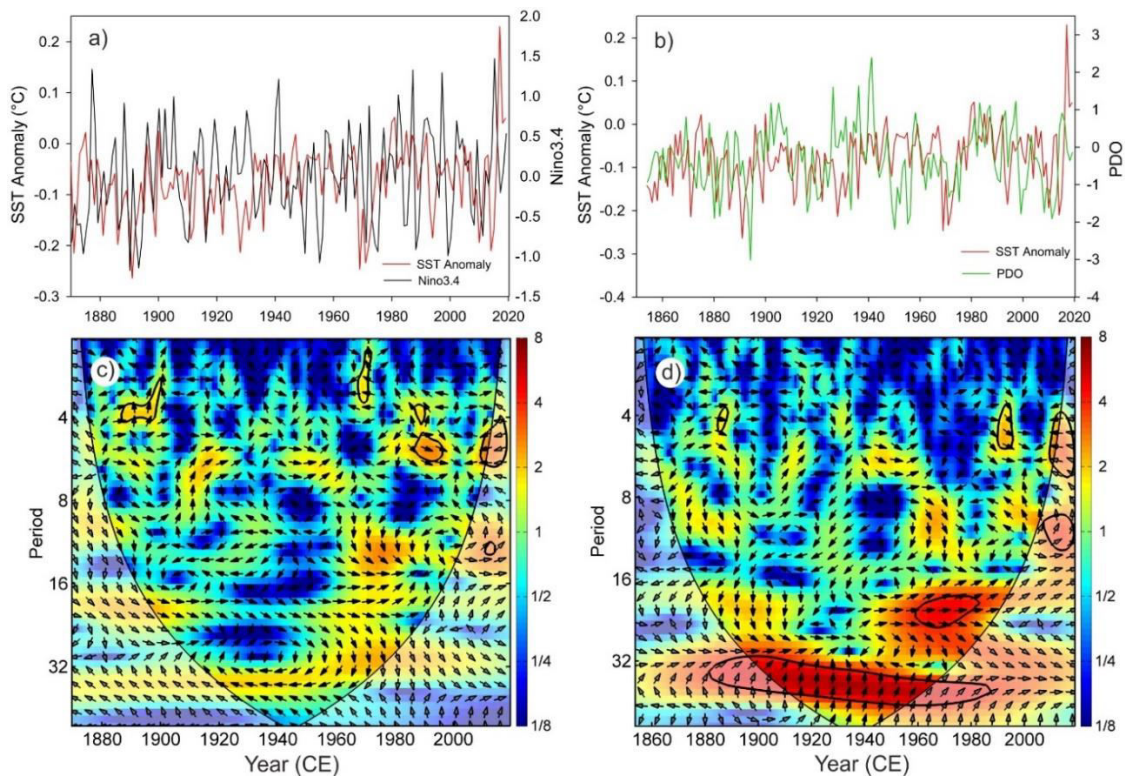


Figure 5.8 Cross wavelet transform analysis of reconstructed SSTA with Nino3.4 and PDO.

Annual variation of reconstructed SSTA with (a) Nino3.4 (1870–2019 CE) and (b) PDO (1854–2019 CE). Cross-wavelet analysis of reconstructed SSTA with (c) Nino 3.4 (1870–2019 CE) (d) PDO (1854–2019 CE). The thick black contours indicate 95% confidence based on a red noise model. The thick black line indicates a cone of influence. The relative phase relationship is shown as arrows (with in-phase pointing right, anti-phase pointing left, SSTA leading Nino3.4, and PDO by 90° pointing straight down and vice versa).

5.2.4 Role of SAM in controlling the SST variability over the WIOS region

Sea ice variability around the Antarctic region is dominantly controlled by ocean-atmospheric coupled oscillations and modulates the transfer mechanism of heat between ocean and atmosphere (Cerrone et al., 2017; Paolo et al., 2018; Renwick, 2002; Sen Gupta and England, 2006; Stammerjohn et al., 2008). Sea ice variability also significantly modulates the Antarctic climate change. The Southern Ocean's SST variation strongly influences the Antarctic sea ice concentration (Purich et al., 2016; Renwick, 2002). Spatial correlation between reconstructed SSTA and NSIDC SIC is used to examine the influence of SSTA on sea ice variability from 1979–2013 CE (Figure 5.9a). The observed result shows a strong inverse correlation over the WIOS region. Further, the average annual sea ice concentration over the WIOS region (60°S–70°S; 20°E–60°E) is compared with reconstructed SSTA and observed a strong inverse correlation ($r=-0.66$ with NSIDC SIC) (Figure 5.9b).

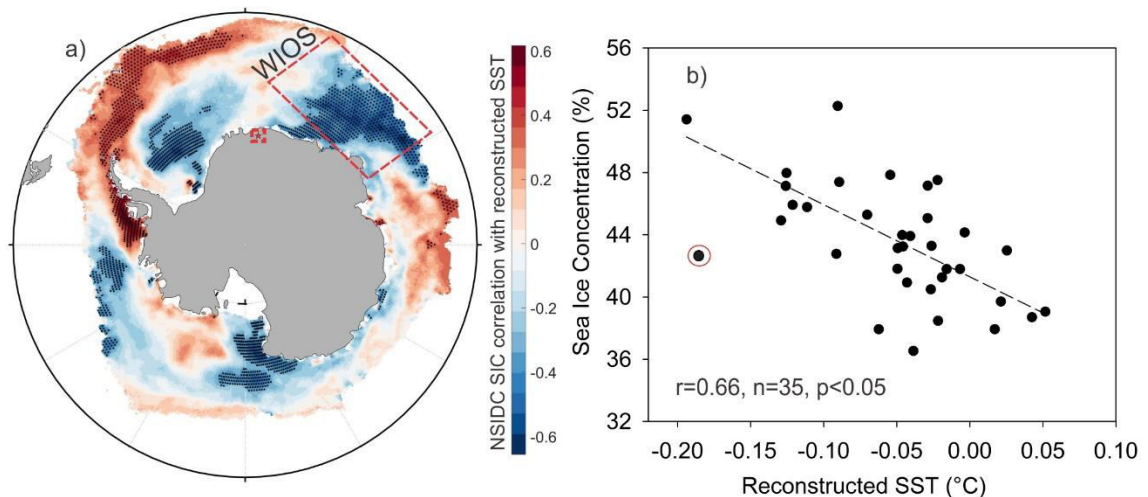


Figure 5.9. Correlation of sea ice concentration with reconstructed SSTA over the WIOS.

(a) Reconstructed SSTA of WIOS shows a significant spatial correlation with NSIDC sea ice concentration (1979–2013 CE). The regions of significant spatial correlations (at 95% confidence level) are highlighted in black stipples (b) Reconstructed SSTA show a significant correlation with NSIDC sea ice concentration ($r=-0.66$, $n=35$, 1979–2013 CE) over the WIOS region ($60^{\circ}\text{S}-70^{\circ}\text{S}$; $20^{\circ}\text{E}-60^{\circ}\text{E}$).

This indicates that modulation in SSTA associated with oceanic circulation and heat transport over the WIOS region controls the variability of sea ice concentration. However, the atmospheric circulation also controls the Antarctic Sea ice concentration and SST of the Southern Ocean. The atmospheric variability over the Southern Hemisphere (SH) is associated with SAM, which explains the maximum variability and exchange of air mass circulation between extra-tropics and high latitudes (Gong and Wang, 1999; Thompson and Wallace, 2000). However, to explore its influence on the WIOS region, this study used the annual Marshall SAM index for spatial correlation with ERA-5 annual SST from 1979–2013 CE, which shows an inverse correlation (Figure 5.10a). This suggests that the recent decrease in SST over the WIOS region is clearly associated with shifting SAM to positive mode. Further, a wavelet coherence analysis is used to establish this relationship with the reconstructed SSTA of the WIOS region. During 1975–2000 CE, wavelet coherence of Marshall SAM Index with reconstructed SSTA shows total anti-phase relation within 2–6 years frequency band and shifted to the annual frequency band between 2000–2013 CE (Figure 5.10b).

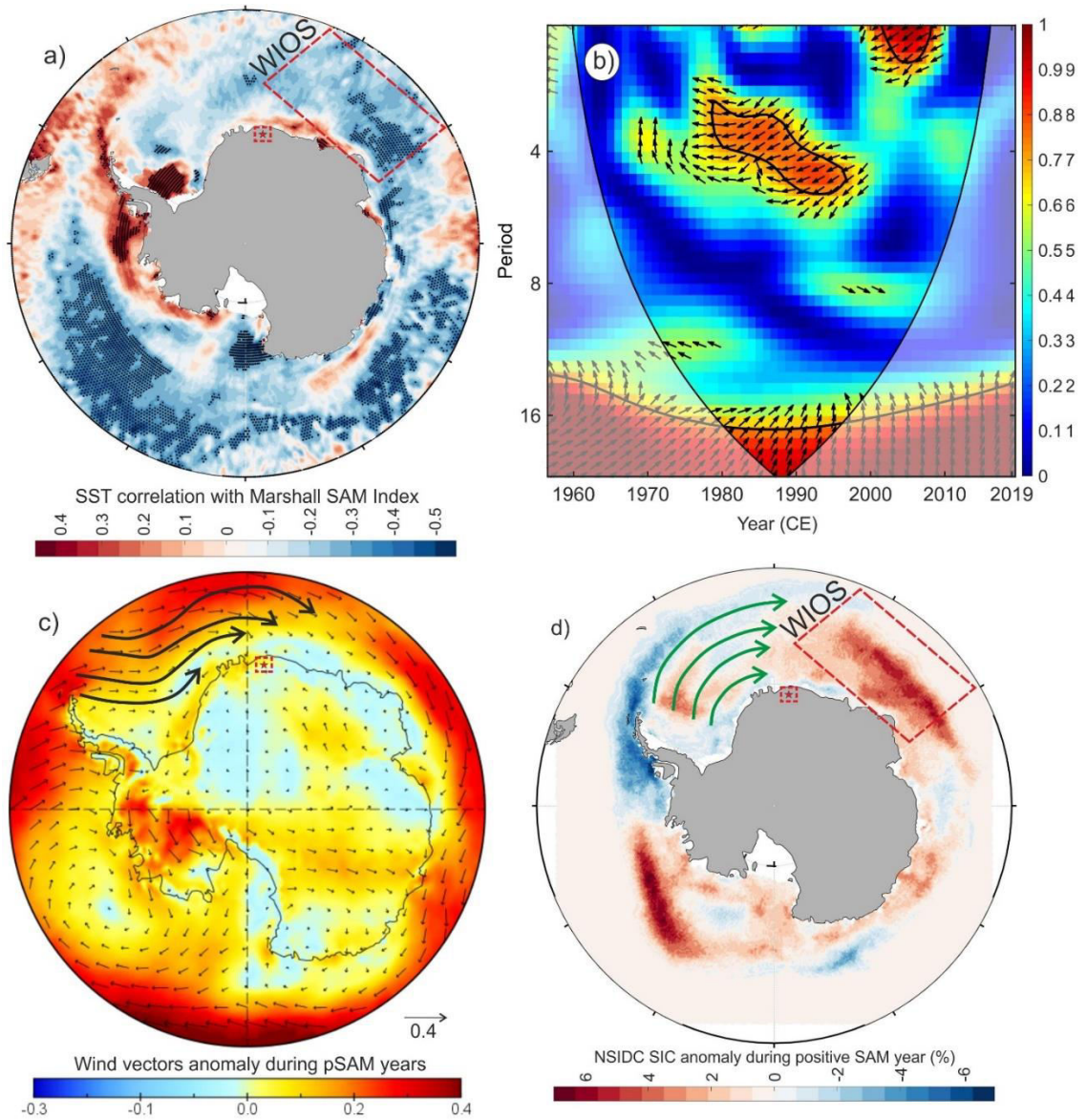


Figure 5.10. Spatial and wavelet coherence plots show a possible mechanism for variation in SSTA over the WIOS.

(a) Spatial variation of ERA-5 SST with Marshall SAM-Index (1979–2019 CE). (b) Wavelet coherence analysis of reconstructed SSTA with Marshall SAM-Index (1957–2019 CE). (c) Anomaly plot for winds (vectors) during the positive SAM years. (d) NSIDC SIC anomaly plot during the positive SAM years. Wind pattern during the positive SAM years suggests wind-driven sea-ice transport from the Weddell Sea sector to WIOS. The stacking of wind-driven sea ice over the WIOS region indicates a drop in the regional SST.

This highlights the role of SAM in modulating the SSTA of the WIOS region while shifting to positive mode. The positive shift in SAM appears to result in intensifying westerly winds over the Southern Ocean, bringing significant zonal sea ice drifting from the Weddell Sea to the WIOS region (Deb et al., 2017; Holland and Kwok, 2012). Based on an anomaly plot of wind vectors during positive SAM years, this study suggests that sea ice transport from the Weddell Sea sector to WIOS is strongly influenced by wind patterns (Figure 5.10c). As a result of this accumulating sea ice in the WIOS region during positive SAM years (Figure 5.10d), the SSTA decreases. This decreasing trend is observed in the reconstructed SSTA over WIOS from 1981–2014 CE, with a rate of $0.023 \pm 0.0002 \text{ }^\circ\text{C decade}^{-1}$.

5.3 Conclusions

This study used high-resolution (seasonal-annual scale) *d-excess* records (1809–2013 CE) from newly recovered ice cores from the DML coast of East Antarctica. It shows that ice core-based *d-excess* records in the coastal DML region are primarily related to past SST variation in the WIOS area. This study provided the first long-term SST records (1809–2019) with annual resolution around the West Indian Ocean Sector (WIOS) in Antarctica and allowed investigation of factors contributing to SST changes at annual to multi-decadal time scales. The key findings in the present study are as follows:

1. The ice core-based *d-excess* record from the DML coast revealed an excellent correlation with SST variation over the WIOS region. This enabled the reconstruction of long-term annual SST records based on *d-excess*.
2. The reconstructed SST anomaly record (SSTA) and the available ERA-5 SSTA allow identifying trends and long-term variability during 1809–2019 CE. The

SSTA shows an increasing trend with a rate of $+0.004 \pm 0.001$ °C decade⁻¹ during 1809–1967 CE, followed by a declining trend with a rate of -0.028 ± 0.009 °C decade⁻¹ during 1981–2014 CE.

3. The long-term decadal variability of SSTA over the WIOS is dominantly controlled through PDO, whereas inter-annual variability is mainly associated with ENSO.
4. The recent decline in SSTA over the WIOS is related to the strengthening of SAM. This decline in SSTA is mainly controlled by the accumulation of wind-driven sea ice brought from the Weddell Sea region due to the strengthening of SAM.

Chapter 6

Spatio-temporal variability of triple water isotopes in high accumulation regions of East Antarctica

6.1 Introduction

Atmospheric humidity has a substantial role in regulating the climate system of the Antarctic coast. The moisture availability is primarily related to precipitation and ice formation, hence, controlling the mass balance of the Antarctic ice sheet (Gettelman et al., 2006; Naakka et al., 2021). Further, atmospheric moisture also has vast implications in modulating the seasonal and spatial variability of Antarctic sea ice (Naakka et al., 2021). Therefore, it is essential to understand the relative humidity and moisture condition in the past and their recent trend. The satellite-based instrumental data of atmospheric conditions is available only from 1979; however, scientists must rely on proxy-based studies from Antarctic ice core records beyond the satellite era.

Snow and ice cores from polar ice caps provide a wealth of information on past climate with potentially higher temporal resolution than any other climate proxies and comparable to instrumental records at seasonal to decadal time scales. Stable water isotopes ($\delta^{18}\text{O}$ and δD) have played an important role in ice core-based paleoclimate studies ever since Dansgaard (1964) explained the relationship between the isotopic composition and the temperature of the cloud at the condensation site. The variation of $\delta^{18}\text{O}$ and δD is predominantly caused by the disparity in the saturation vapor pressure between the lighter and heavier isotopes, leading to equilibrium fractionation. Moreover, the higher diffusivity of lighter isotopes than heavier ones lead to kinetic fractionation that contributes to the formation of snowflakes and evaporation. Compared with the δD record, the kinetic

fractionation substantially influences $\delta^{18}\text{O}$ (Merlivat, 1978), resulting in the deviation from the Global Meteoric Water Line (GMWL). This deviation from GMWL is considered a second-order effect, measured by *d-excess* (deuterium-excess) (Dansgaard, 1964).

The *d-excess* in the vapor over the ocean generally increases with decreasing humidity, therefore considered a tracer for the past moisture source in the polar records (Jouzel et al., 1982). The transportation of air masses from the evaporative sources from the southern ocean to Antarctica experience significant isotope fractionations due to successive precipitation during the moisture transport, therefore *d-excess* account for both the processes, i.e., condensation and source temperatures (Petit et al., 1991; Stenni et al., 2001; Vimeux et al., 1999). Model studies have also demonstrated that the relative humidity signal of the source region in the polar *d-excess* could be inundated by the variation in the sea surface temperature at the evaporative source (Vimeux et al., 1999). Therefore, *d-excess* can be used as a proxy to reconstruct the temperature at the source rather than relative humidity.

Recent advancements and new analytical techniques have enhanced the capability of accurately measuring the least abundant oxygen isotopic ratio, $^{17}\text{O}/^{16}\text{O}$ (Barkan and Luz, 2007; Landais et al., 2008). As a result, a new hydrological tracer known as *^{17}O -excess* has been introduced into the stable isotopic system. The *^{17}O -excess* record is strongly related to relative humidity (Angert et al., 2004; Schoenemann et al., 2014), but unlike the *d-excess*, it is not affected by the temperature and isotope composition of the surface waters (Landais et al., 2008). Therefore, the *^{17}O -excess* record in the ice/snow core can be used as a more robust and reliable proxy for the reconstruction of relative humidity and related meteorological parameters. However, the *^{17}O -excess* records from the Antarctic ice/snow

cores are very limited, especially from the high accumulation of east Antarctica. Further, model-based studies are associated with several complexities, such as the sensitivity of water isotope ratios in precipitation with variation in atmospheric circulation (Schoenemann and Steig, 2016). Due to these challenges in quantification, the ice/snow core record can be used to understand the evolution of the moisture source and relative humidity over the DML region of East Antarctica.

In this study, a snow core transect from the DML region (coast to inland) of east Antarctica is used to understand the spatial variability of *d-excess* and *¹⁷O-excess* in the DML region and investigate the meteorological/geographical control over the DML region. The model-derived stable isotopes from ECHAM5-wiso (Steiger et al., 2017; Werner et al., 2018) are also used to compare with the snow core transect. Further, an attempt has been made to reconstruct the first long-term relative humidity for the past two centuries (1809–2013 CE) based on the *¹⁷O-excess* ice core record from the DML region.

6.2 Results and Discussion

6.2.1 Spatial distribution of triple water isotopes in Antarctica and factors controlling their variability

The interpretation of Antarctic ice core stable isotopic records requires a precise assessment of δD and $\delta^{18}O$ distributions in surface snow. The evaluation, however, requires sufficient in situ observations. A recent study by Masson-Delmotte et al. (2008) has compiled a stable isotopic record of the surface snow from various locations in the Antarctic. The compilation constitutes an almost complete database of stable isotopic records from several observation sites since the 1960s. Even though the DML region still shows data gaps due to the introduction of new proxies. For the first time in the DML

region, spatial variability of triple-oxygen isotopes (^{18}O , ^{17}O , and ^{16}O) in modern snow along a transect was used to delineate the processes and their paleoclimatic interpretations. The stable isotopes ($\delta^{18}\text{O}$, $\delta^{17}\text{O}$, and δD) from the snow core transect aided our understanding of spatial variations and investigated the influences of meteorological and geographical controls. In this study, isotope-enabled ECHAM5-wiso model data of stable isotopes are used to compare with surface snow core transect data. The ECHAM5 (European Central Hamburg Model) is an atmospheric general circulation model developed at the Max Planck Institute for Meteorology. When enabled with a stable water isotope, this model simulation is called ECHAM5-wiso. The ECAHM5-wiso model outputs are available at long-term time scales (Steiger et al., 2017) and in the recent satellite era (Werner et al., 2018). The long-term model simulation of the ECHAM5-wiso model results is available from 1871 to 2011 at T106 (1 degree) spatial resolution. The boundary conditions used in the long-term ECHAM5-wiso simulations were taken from HadISST fields. The ECHAM5-wiso model derived δD and $\delta^{18}\text{O}$ distribution map for the year 2008, is shown in Figure 6.1a-b which clearly shows significant spatial variability. The spatial distribution plots show a decline of δD and $\delta^{18}\text{O}$ from the coast to inland due to the fractionation of heavier isotopes from the moisture moving towards inland Antarctica (Figure 6.1a-b). It has been shown earlier by Masson-Delmotte et al. (2008) that the change in isotopic values is associated with condensation temperature along the snow core from coastal to inland, which is influenced by factors such as latitude, distance from the coast, and elevation. The isotopic signature in the snow core is consistent with the model-derived results and earlier studies from Masson-Delmotte et al. (2008). Surface snow core records from the Mountain region show steep isotopic gradients (Figure 6.1d-e) due to rapid cooling and continentality (Wang et al., 2009).

Further, to understand the spatial variation in the relative humidity, the *d-excess* record is derived from the ECHAM5-wiso model (Figure 6.1c). Spatial distribution plots of model-based *d-excess* show a continuous increase from the coast to the inland region. The snow core transects also show an increasing trend in *d-excess* from coast to inland (Figure 6.1f). However, the relative humidity increases from coast to inland of the Antarctic; therefore, *d-excess* should ideally indicate a decreasing trend towards inland Antarctica. The results show deviation in the model and observed *d-excess* record. This deviation is possibly due to the influence of Sea Surface Temperature and relative humidity in the *d-excess* record (Bonne et al., 2019; Schlosser et al., 2008).

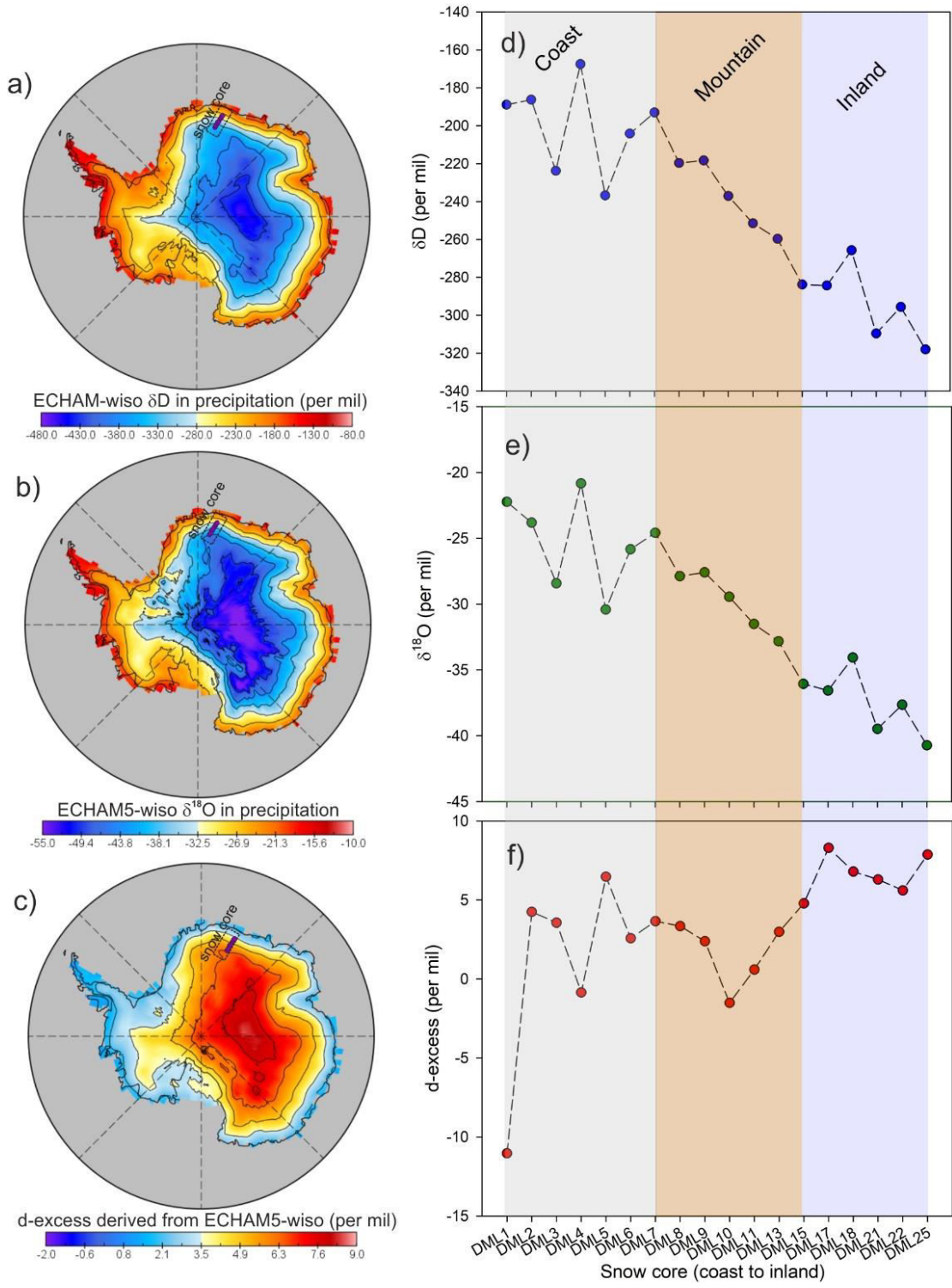


Figure 6.1. Spatial variation of stable isotope derived from the ECHAM5-wiso model and surface snow core transect.

Spatial variation of ECHAM5-wiso model derived (a) δD (b) $\delta^{18}O$ and (c) d -excess record (per mil) in precipitation. Surface snow core stable isotopic record of (d) δD (b) $\delta^{18}O$ and (c) d -excess record (per mil) in precipitation. Light grey, brown, and blue shaded colours denote the coast, mountain, and inland snow samples.

6.2.2 Spatial variation in the ^{17}O -excess record over the DML region

Recently, the advent of new technology and, thus, improvement in the measurement precisions of $\delta^{17}O$ and $\delta^{18}O$ enabled us to derive ^{17}O -excess and introduce a new proxy for more accurate reconstruction of past relative humidity and moisture transport history. The deviation from the GMWL in the $\delta^{18}O$ and $\delta^{17}O$ plots is calculated as ^{17}O -excess. The variation in the ^{17}O -excess is small and hence calculated on the logarithmic scale (Barkan and Luz, 2005), unlike the d -excess record, described on the linear scale. The correlation between the $\delta^{18}O$ and $\delta^{17}O$ records of the snow core transect is shown in Figure 6.2a. Excellent correlation is observed between $\delta^{18}O$ and $\delta^{17}O$ along the snow core transect with slope ($m=0.537$). The ^{17}O -excess record from the surface snow core transect shows a decreasing trend from coast to inland (Figure 6.2b). However, three sharp increases in the ^{17}O -excess record are observed (DML03-DML05, DML07-DML13, and DML18-DML20), which might be due to a sharp rise in elevation while moving toward inland.

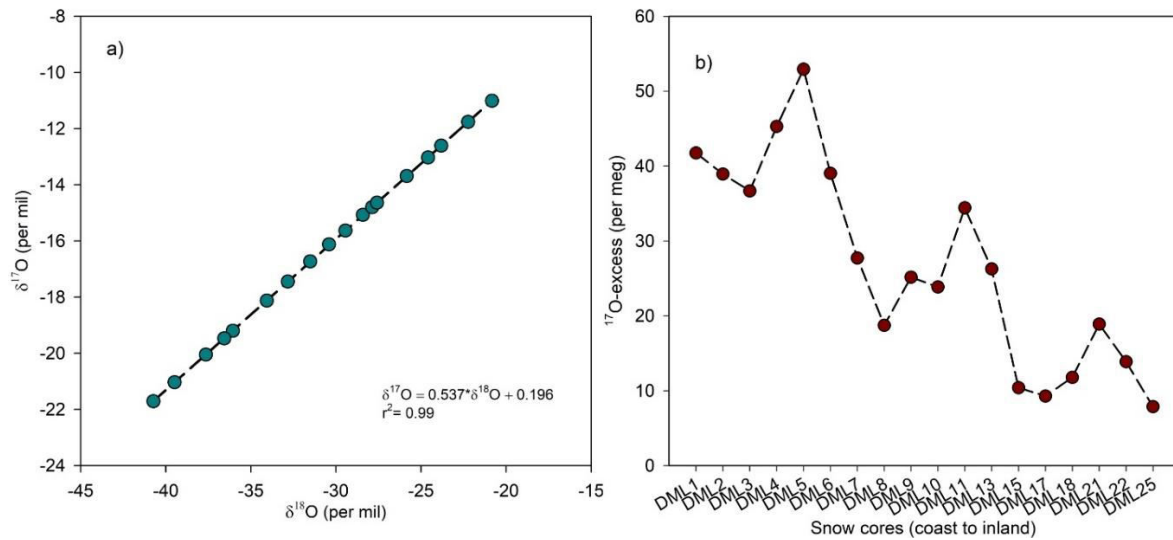


Figure 6.2. Relationship between $\delta^{17}\text{O}$ and $\delta^{18}\text{O}$ in DML surface snow core transect and the variation of ^{17}O -excess (per meg).

A linear relationship between (a) $\delta^{17}\text{O}$ (per mil) and $\delta^{18}\text{O}$ (per mil) record in DML surface snow core transect, dotted black line denotes the Global Meteoric Water Line. (b) Variation of ^{17}O -excess record in the surface snow core transect.

In this study, ERA5 relative humidity data is used to investigate the role of relative humidity on the *d-excess* and ^{17}O -excess records. The *d-excess* record shows a positive correlation with relative humidity ($r=0.52$, $n=18$) (Figure 6.3a); however, an inverse relationship is expected to be observed based on the empirical relation. The *d-excess* may have a mixed signal of sea surface temperature, thereby deviating from the typical correlation. The ^{17}O -excess record, used as a robust proxy for the relative humidity (Landais et al., 2012; Uemura et al., 2010), shows an inverse correlation along the snow core transect. The correlation between the ^{17}O -excess and ERA5 relative humidity is significant over the DML region ($r= -0.77$, $n=18$) (Figure 6.3b). This suggests that the newly derived proxy ^{17}O -excess is strongly influenced by the variation in relative humidity over the DML region.

However, geographical factors also indirectly control the variability in the ^{17}O -excess record due to the modulation of relative humidity. The snow core record in the mountain region (DML07–DML13) shows a sharp increase in the ^{17}O -excess due to lower relative humidity in the mountain region.

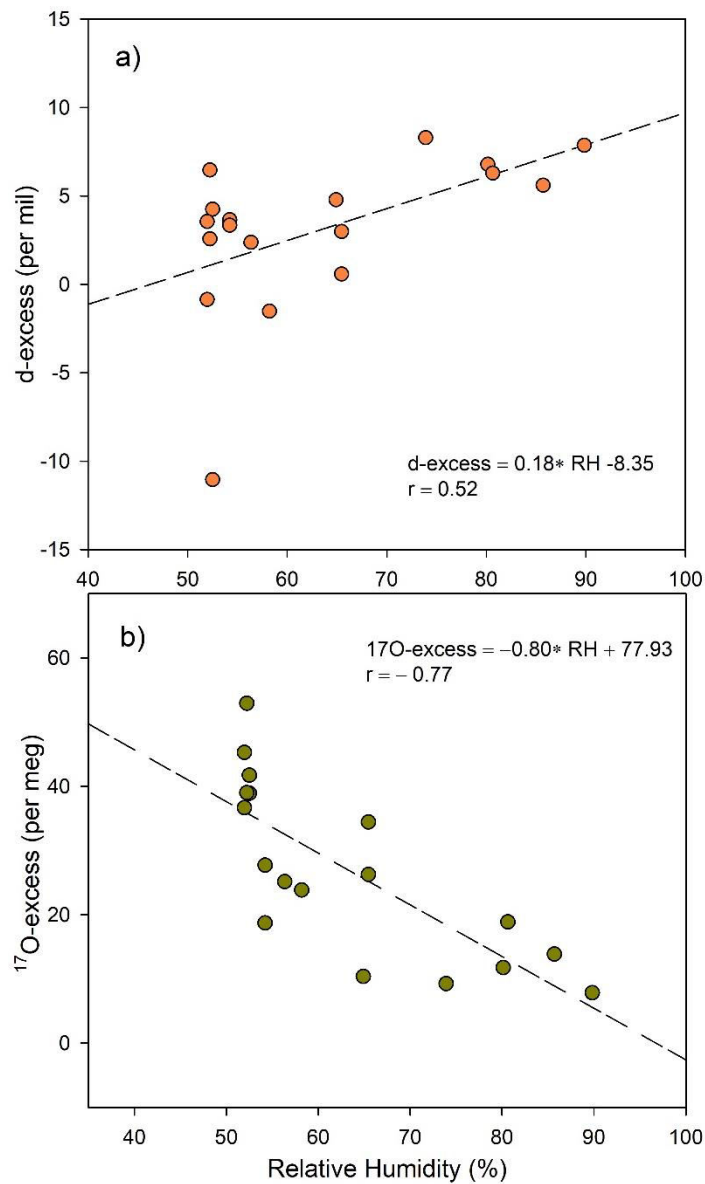


Figure 6.3. Correlation of relative humidity (%) with (a) d -excess (per mil) and (b) ^{17}O -excess (per meg).

The ^{17}O -excess and relative humidity show a significant inverse correlation due to the negligible influence of temperature. Therefore, ^{17}O -excess shows a more promising proxy for reconstructing past relative humidity using the ice core ^{17}O -excess record from the DML region. In this study, an attempt has been made to obtain a high-resolution form of stable oxygen isotope ratio with a primary focus on the ^{17}O -excess record-based IND33 ice core from the DML region. The isotopic measurement was made at an interval of ~50-70 cm resolution (one sample per core run) of the total core length. A total of 186 runs were made for the IND33 ice core (intact ice core sample retrieved from R1–R186). In this study, one sample is measured from each intact ice core and processed to obtain the data for deriving the ^{17}O -excess. Details of the sampling, measurement technique and methods are discussed in previous Chapter 2 (see Section 2.3). The age-depth model has already been discussed elsewhere by Ejaz et al. (2021) and is used for the chronology of ^{17}O -excess.

6.2.3 Temporal variation of ^{17}O -excess in ice core record and controlling factors

The ice core record of ^{17}O -excess shows significant variability in the last 200 years (1809–2013 CE), ranging from -8 to 78 per meg with an average value of ~31 per meg (Figure 6.4). This high variability in the ^{17}O -excess record is possibly due to a change in the supply of moisture from the Weddell Sea during low and high ice conditions (Ejaz et al., 2021; Rahaman et al., 2016). However, the other factor controlling such large variability in the ^{17}O -excess record is related to wind strength, which contains moisture transport. The ^{17}O -excess is not showing any discernible trends during the 19th century (Figure 6.4). An increasing trend is observed at the beginning of the 20th century, followed by a rapid decrease during 1993–1996 CE (Figure 6.4).

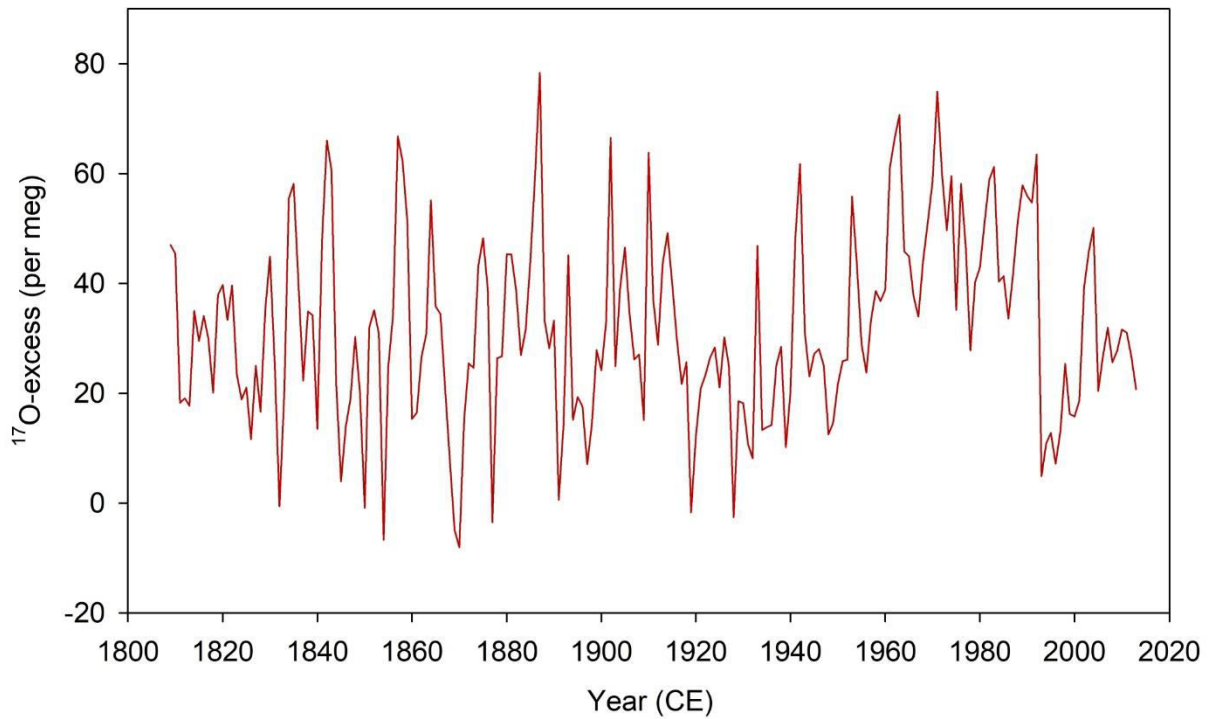


Figure 6.4. Annual variation of the ^{17}O -excess (per meg) in the IND33 ice core.

To investigate possible influencing factors that control the variability in the ^{17}O -excess, here we used a spatial correlation of ^{17}O -excess with the ERA5 relative humidity (%) for the period 1979–2013 CE (Figure 6.5a). It was observed that ^{17}O -excess and ERA5 relative humidity is inversely correlated over the DML region. However, a linear regression equation is derived from the correlation observed between ERA5 relative humidity and ^{17}O -excess record during the period 1979–2013 CE. This linear equation observed between the ERA5 relative humidity, and ^{17}O -excess can be used to derive the relative humidity for the past two centuries with an underlying assumption that these relationships were stationary for the entire ice core record (Figure 6.5b). Studies have suggested that relative humidity largely influences radiative energy transfer and mass balance of the Antarctic ice sheet (Gettelman et al., 2002; Gettelman et al., 2006; Naakka et al., 2021). Therefore, this

study attempts to reconstruct the relative humidity over the DML region for a better understanding of the precipitation and ice sheet mass balance.

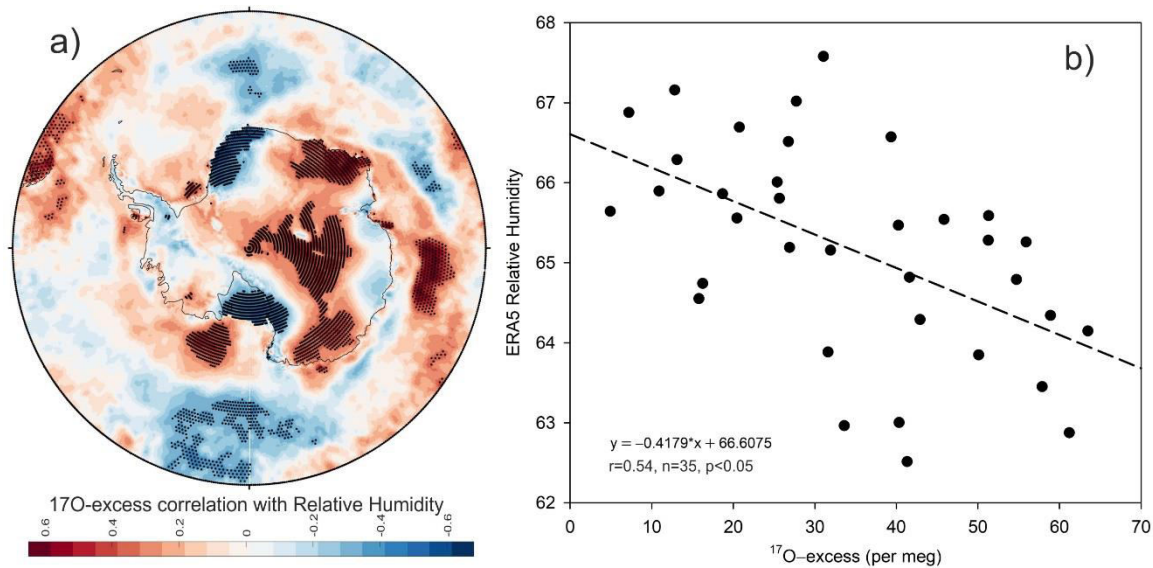


Figure 6.5. (a) Correlation of IND33 ice core ^{17}O -excess record with ERA5 Relative Humidity (%). (b) Linear regression of ^{17}O -excess with ERA5 Relative Humidity (%) during 1979–2013 CE.

Black dots in Figure 6.5a highlight the regions of significant correlation at 95% confidence level.

6.2.4 Reconstruction of relative humidity and its role in Antarctic climate variability

The regression equation derived from the relation between ^{17}O -excess vs. relative humidity (%) was used to reconstruct the record of the relative humidity (%) for the past two centuries (1809–2013 CE). The reconstruction assumes that this correlation has been consistent over the past two centuries. The reconstructed relative humidity (%) shows significant annual variation ranging from ~ 63 – 67 % (Figure 6.6a). The variation in the

relative humidity largely controls the total precipitation of the region and, therefore, significantly influences the variability of the Antarctic sea ice and ice-sheet mass balance (Gettelman et al., 2006). To investigate the evolution and relation of relative humidity with other factors such as precipitation, sea ice, and Antarctic ice sheet mass balance. This study used a spatial correlation of reconstructed relative humidity with ERA5 Total Precipitation and NSIDC sea ice (Peng et al., 2013) during the 1979–2013 CE.

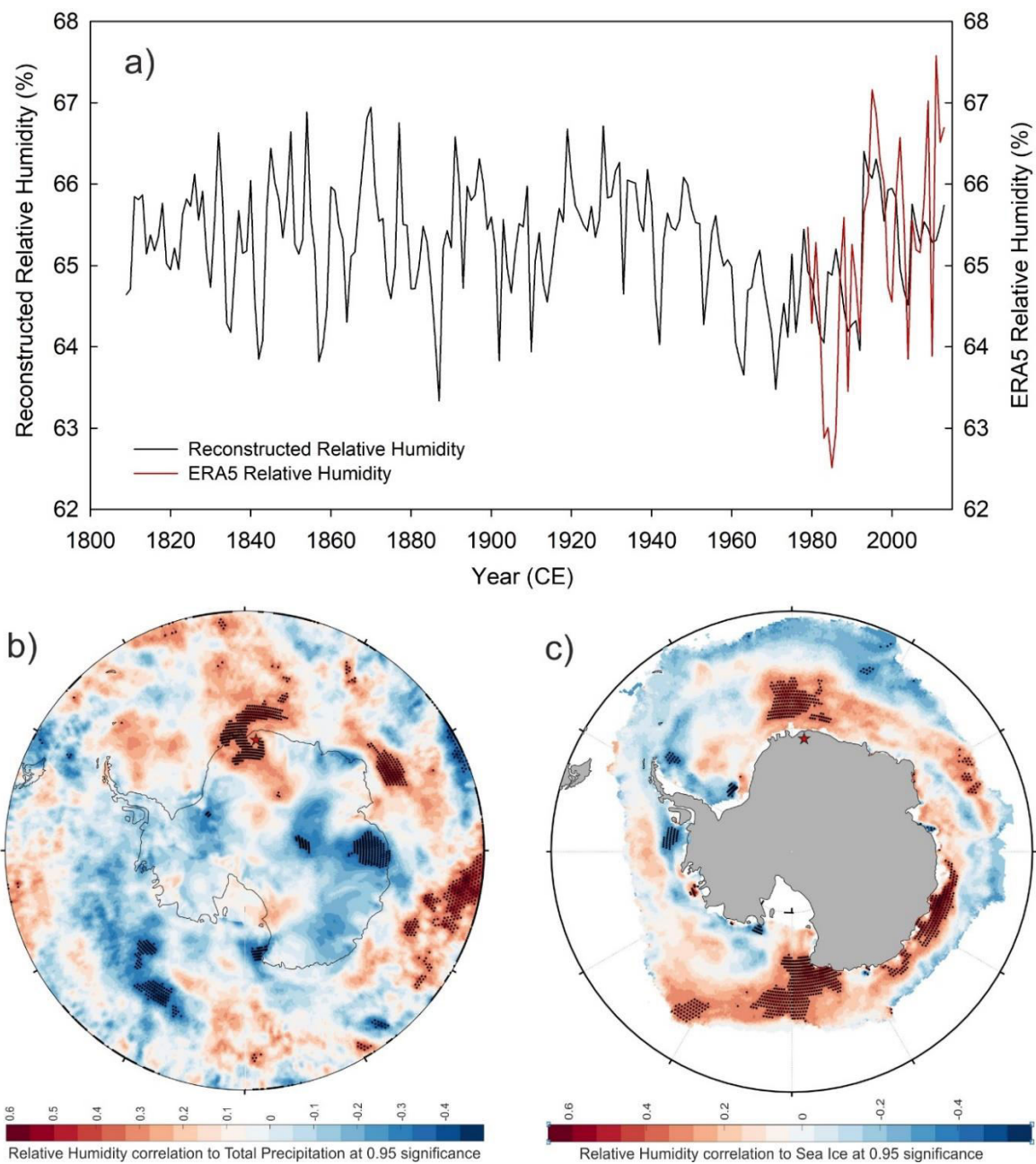


Figure 6.6. (a) Reconstructed relative humidity for the past two centuries (1809–2013 CE) based on the ^{17}O -excess record. Spatial correlation of reconstructed relative humidity with (b) ERA5 Total Precipitation and (c) NSIDC sea ice Concentration during 1979–2013 CE.

The black line denotes the reconstructed relative humidity, and the red line represents the ERA5 relative humidity (%). Black dots highlight the regions of significant correlation at 95% confidence level. The red star denotes the IND33 ice core location.

The reconstructed relative humidity significantly correlates with total precipitation in the DML region (Figure 6.6b). Additionally, a significant correlation is also observed between relative humidity and NSIDC sea ice in the proximal oceanic sector of the DML region (Figure 6.6c). Therefore, it is suggested that the variation in the relative humidity and moisture supply controls the precipitation, ice sheet mass balance, and sea ice variability in the Antarctic region. However, different modes of climate variability in the tropical and extra-tropical regions control the Antarctic climate variability. Therefore, it is essential to understand the role of these climate modes on the variability of reconstructed relative humidity for the past two centuries.

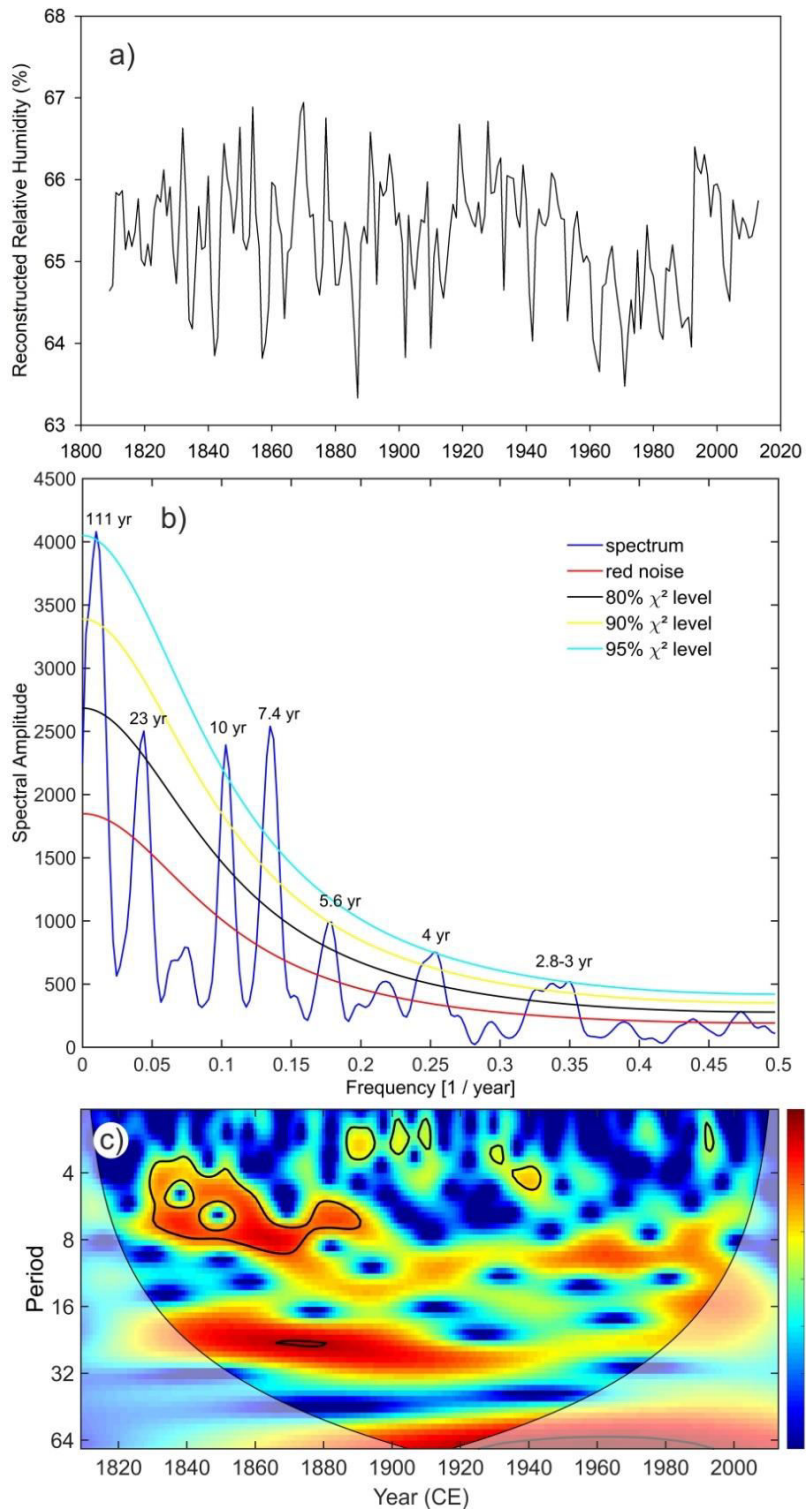


Figure 6.7. (a) Reconstructed relative humidity (%) (1809–2013 CE) based on the linear regression equation derived from the correlation plot between ^{17}O -excess and ERA5

relative humidity (%). (b) Spectral analysis of reconstructed relative humidity (%). (c) Wavelet transform analysis of reconstructed relative humidity (%).

6.2.5 Relative humidity variability and influence of different climate modes

To identify the influence of these climate modes in the reconstructed relative humidity over the DML region, a power spectrum analysis was performed (Figure 6.7b), which shows significant periodicities in the 3-8 yr frequency band. This interannual variability in the relative humidity could be due to the influence of El Niño Southern Oscillation (ENSO). ENSO variability has a larger role in controlling the relative humidity and related tropical precipitation (Todd et al., 2018). However, tropical variability also influences the Antarctic coastal region. The details of ENSO teleconnection in controlling the DML climate are discussed in chapters 3 and 4. Additionally, decadal periodicities of 10 yr and 23 yr are also observed in the relative humidity record, suggesting the influence of decadal oscillation such as Interdecadal Pacific Oscillation (IPO) (Figure 6.7b). A wavelet transform analysis is performed on reconstructed relative humidity to infer the evolution of ENSO and IPO-related variability (Figure 6.7c). The wavelet transforms show a significant ENSO signal of 3-8 yr frequency band during 1830–1890 CE and a decadal signal of 22–23-year frequency band during ~1865–1885 CE (Figure 6.7c). However, it is important to understand the relation of these climate modes to the variability of relative humidity in the DML and its proximal oceanic sectors.

To understand the role of these climate modes, spatial correlation of relative humidity is performed with Southern Oscillation Index (SOI), IPO, and Southern Annular Mode (SAM) during 1979–2013 CE. SOI is an ENSO index derived from the pressure

difference between the western and eastern tropical pacific during El Niño and La Niña (Trenberth, 1984). Studies suggested that the extended period of negative (positive) SOI coincides with the warm (cold) oceanic water condition in the tropical pacific (Ropelewski and Jones, 1987; Trenberth, 1984; Trenberth and Caron, 2000). SOI and relative humidity show an inverse correlation over the DML region (Figure 6.8a). This inverse correlation suggests that during the El Niño (warm) oceanic water condition, the DML region observed an increase in the relative humidity and vice versa. However, the correlation is weak, possibly due to interference of interannual variability from SAM. The IPO is regarded as PDO-like climate variability over the Pacific region, with decadal cyclicity of 20–30 years (Henley et al., 2015; Vance et al., 2022). The positive and negative phase of IPO is related to the warm and cold ocean water condition. The IPO and relative humidity were significantly correlated over the DML region (Figure 6.8b). This suggests that during the positive phase of IPO, the DML region observed an increase in relative humidity.

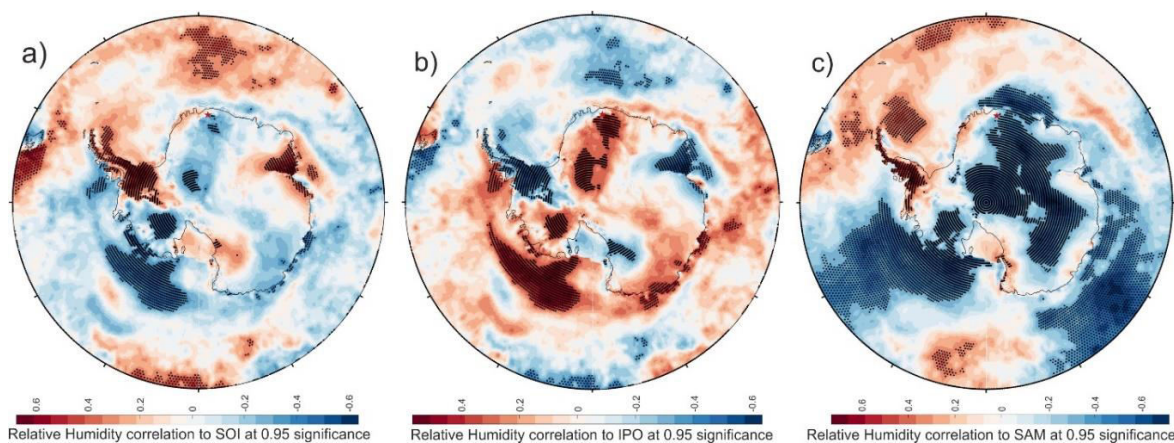


Figure 6.8. Spatial correlation of ERA5 relative humidity with (a) SOI, (b) IPO, and (c) SAM during 1979–2013 CE.

Black dots highlight the regions of significant correlation at 95% confidence level.

Wind is one of the most prominent climate variables that control the relative humidity and moisture supply variability. The relative humidity is dominantly controlled by the variability of wind speed (Xu et al., 2021). Therefore, the climate modes controlling the wind, such as SAM, have a more prominent role in controlling the variability of relative humidity. SAM is the leading mode of pressure differences between the extra-tropics and Antarctica (Gong and Wang, 1999; Marshall, 2003; Simmonds et al., 2003; Thompson and Wallace, 2000; Turner et al., 2005). It has been demonstrated in several studies that the SAM dominates extratropical atmospheric circulation over the SH. During the positive mode of SAM, negative pressure anomalies are present over the Antarctic region, thereby strengthening the westerly wind (Hall and Visbeck, 2002; Thompson and Wallace, 2000). As a result of the strengthening of westerlies, the relative humidity may show a considerable variation in the DML region and its proximal oceanic sectors of East Antarctica. Therefore, an attempt has been made to understand the relationship between SAM and relative humidity over the DML region. The SAM index and relative humidity show a significant inverse correlation (Figure 6.8c). This suggests that during the positive mode of SAM, westerlies are intensified; therefore, the DML region and nearby oceanic sector observed a reduction in the relative humidity during 1979–2013 CE.

6.3 Conclusion

This study attempts to understand the spatial variability of the triple oxygen and hydrogen isotope in the DML region of East Antarctica for the first time and further understand the variability of the relative humidity in the past two centuries. It was found that the isotopic variation in the surface snow transect from coast to inland follows a similar trend as observed in the ECHAM5-wiso model-derived stable isotopes. Model and surface snow

core shows a depletion of heavier isotopic from coast to inland due to the removal of heavier isotopes in the successive precipitation events during the transport from coast to inland. The $\delta^{18}\text{O}$ and δD in the mountain region show a monotonic decreasing trend due to a rapid drop in the temperature with elevation and continentality. The ^{17}O -excess from surface snow shows a decreasing trend while moving from coast to inland and is inversely related to relative humidity.

Additionally, this study reconstructed the first long-term relative humidity record from the DML region based on the ^{17}O -excess ice core record. The relative humidity has large-scale implications on regulating the Antarctic precipitation, sea ice variability, and ice sheet mass balance. This study observed a significant correlation between relative humidity and precipitation in the DML region. This suggests that increasing relative humidity brings more precipitation, resulting in increased accumulation on the Antarctic ice sheet. Further, the sea ice variability in the proximal oceanic sector of the DML region is primarily controlled by the variation in relative humidity. Increased relative humidity provides more moisture for sea ice formation. However, the variability in the relative humidity is largely controlled by different climate modes, which modulate the Antarctic climate. It was found that ENSO is dominantly controlling the Interannual variability of the reconstructed relative humidity. The spatial correlation between SOI and relative humidity suggests that during the warm ocean condition, relative humidity increases in the DML region. This study also shows that IPO controls the decadal relative humidity variability and is positively correlated with the DML region. Furthermore, SAM has a more significant role in controlling wind-related variability in the relative humidity of the DML region. The

study suggests that positive SAM results in the strengthening of westerly wind and a reduction in relative humidity during 1979–2013 CE.

Chapter 7

Summary and Future Perspectives

This thesis deals with the long-term reconstruction of annual surface air temperature, sea ice concentration, sea surface temperature, and associated atmospheric parameters based on annually resolved stable water isotopic parameters ($\delta^{18}\text{O}$, δD , *d-excess*, and $^{17}\text{O-excess}$) of ice cores retrieved from the Dronning Maud Land (DML) region of East Antarctica. The $\delta^{18}\text{O}$ ice core records were used to reconstruct the surface air temperature of the DML region and the sea ice concentration variability of the Western Indian Ocean Sector of Antarctica (WIOS) region. The present study provides the first long-term reconstruction of the annual variability of sea ice concentration for the past two centuries. Second-order proxies like *d-excess* and $^{17}\text{O-excess}$ were used to reconstruct the sea surface temperature over the WIOS region and relative humidity in the DML region, respectively. The reconstructed records for the past two centuries show excellent variability and trends that enable us to assess the roles of different climate modes and forcings factors.

Further, several snow cores (~1 m each) collected along a coast-to-inland transect in DML, representing at least one year of snow accumulation, were used to generate spatial records of triple oxygen and hydrogen isotopes comparable to model-derived records. The key findings of the doctoral study are summarized in the following sections.

7.1 Surface air temperature of the DML region during the past two centuries

A high-resolution (annually resolved), nearly two centuries long (1809–1993 CE) surface air temperature record was reconstructed utilizing the $\delta^{18}\text{O}$ profile of an ice core

record (IND33) from the DML region of East Antarctica. The temperature signals from this previously collected ice cores from the DML region were extracted using a principal component analysis (PCA) to reconstruct the DML surface air temperature record from 1809–1993 CE. The ERA5 (fifth generation ECMWF atmospheric reanalysis of the global climate) temperature anomaly record (1994–2019 CE) combined with ice core-based surface air temperature reconstruction (1809–1993 CE) enables us to examine the long-term trends, variability, and links to various climate modes such as SAM (Southern Annular Mode), ENSO (El Niño Southern Oscillation), and IPO (Interdecadal Pacific Oscillation). A significant cooling trend is observed with a rate of -0.164 ± 0.045 °C decade⁻¹ during 1809–1907 CE, followed by a significant warming trend at a rate of $+0.452 \pm 0.056$ °C decade⁻¹ during the recent decades (1942–2019 CE). The present study revealed that ENSO, coupled with SAM, is the primary factor modulating surface air temperature variability. The ENSO band temperature signals have been persistent during the past two centuries, and since the 1940s, a significant shift from low-frequency (12–18 years band) to high-frequency (2–8 years band) oscillations has been observed. The dramatic warming in the recent decades in DML has been attributed to the effect of SAM shifting to a positive phase, coupled with increasing ENSO influence in this region of Antarctica.

7.2 Sea ice concentration, trends, and variability during the last two centuries

Antarctic sea ice plays a vital role in modulating the global climate. It is one of the least studied but critical climate variables for understanding past and future climate changes. The present study provides the first long-term (1809 to 2019) sea ice reconstruction of the WIOS region based on multiple annually resolved stable isotope ice core records combined with satellite data from the DML region. This enables us to

determine the factors contributing to sea ice variability on an annual to multidecadal time scale. Sea ice record revealed a significant decline during 1830–1884 CE with a rate of 0.58 ± 0.12 % decade⁻¹, followed by a moderately increasing trend with a rate of 0.24 ± 0.11 % decade⁻¹ during 1927–1993 CE. The observed NSIDC sea ice record over the WIOS region during the recent decades (1994–2014 CE) shows a dramatic increase in the past two centuries with a rate of 2.59 ± 0.86 % decade⁻¹. The study found that the sea-ice variability in the WIOS region is predominantly influenced by wind-driven sea-ice dynamics, mainly through SAM modulation and teleconnection to Pacific oscillations. Further, interannual sea ice variability and trend have increased in recent decades over the WIOS region due to the shift in the SAM phase and concurrent increase in ENSO frequency.

7.3 Sea surface temperature variability in WIOS and control of different climate modes

Sea surface temperature (SST) is a crucial component of the ocean system in understanding the response to climate change. The SST variation in the proximal oceanic sectors has a more prominent role in controlling the coastal Antarctic climate. However, SST records on annual scale resolution are not available on a longer time scale. Annually resolved *d-excess* records (1809–2013 CE) from the IND33 ice core were used to reconstruct the SST variation during the past two centuries. The results of this study show that *d-excess* records based on ice cores are mainly related to past SST variations in the WIOS area and can be used to reconstruct past SST anomalies (SSTA). Together with the reconstructed SSTA records (1809–2013 CE) and the available ERA5 SSTA, we provided the first long-term reconstructed SST record (1809–2019) with the annual resolution for WIOS. Our reconstructed SSTA record and available ERA-5 SSTA allow us to identify long-term trends and variability. Over 1809–1967 CE, the

SSTA shows an increasing trend of $+0.004\text{ }^{\circ}\text{C decade}^{-1}$, followed by a declining trend of $-0.028\text{ }^{\circ}\text{C decade}^{-1}$ during 1981–2014 CE. It was found that the tropical variability related to PDO (Pacific Decadal Oscillation) has a dominant role in controlling the decadal variability of SSTA over the WIOS. However, the recent decline in SSTA over the WIOS can be attributed to the wind-driven sea ice accumulation caused by the strengthening of SAM.

7.4 Spatial and temporal variability of triple water isotopes in coastal East Antarctica

This study addressed the spatial variability of triple oxygen and hydrogen isotopes along a transect of snow cores retrieved from the DML region. The isotopic variation in the snow followed a similar coast-to-inland trend obtained from the ECHAM5-wiso model. It was found that both surface snow cores and the model outputs show depletion of heavier isotopes from coast to inland due to the fractionation of heavier isotopes in precipitation events. However, the mountain region shows a monotonic decreasing trend in $\delta^{18}\text{O}$ and δD due to rapid temperature drops with height and the effect of the polar plateau. The ^{17}O -*excess* record shows a decreasing trend from coast to inland and is inversely correlated with relative humidity.

Additionally, this study reconstructed the first long-term relative humidity record from the DML region based on the ^{17}O -*excess* ice core record. It was found that the reconstructed relative humidity has large-scale implications for regulating the Antarctic precipitation in the DML region and sea ice variability in the proximal oceanic sector. This study also observed the role of different climate modes, such as ENSO, IPO, and SAM, in controlling the variability of relative humidity in the DML region.

7.5 Future Perspectives

The present study using proxy records of Antarctic ice cores retrieved from the DML region, provided annually resolved records of surface air temperature, sea ice concentration, and sea surface temperature for the past two centuries. Studies of coastal ice rises have demonstrated that coastal DML from Antarctica offers excellent sites for obtaining annually resolved reconstruction of Antarctic climate, sea ice, westerly wind strength controlled global and regional climatic modes, and atmospheric-ocean interactions. The Southern Hemisphere westerly winds and sea ice have a critical role in the global climate system through their influence on Southern Ocean (SO) circulation, upwelling, and carbon exchange with the deeper ocean. Stronger winds (and reduced sea ice) will enhance ventilation and increase carbon transfer from the ocean into the atmosphere, resulting in an accelerated global mean temperature rise through an enhanced greenhouse effect. However, an unequivocal link between SO upwelling and atmospheric CO₂ remains elusive mainly due to the limited observational data and limitations of models. Therefore, reconstructing westerlies, sea ice, and resultant gas fluxes across the ocean surface over several hundred and thousands of years from coastal Antarctica using ice cores is critically important in understanding the tipping points in the climate system. The study of decadal climate variability, which has strong regional characteristics and modulates long-term global warming trends, is critical to understand the recent climate variability and its societal implications. Establishing the long-term relationships between westerly winds, sea ice, and various climatic modes/oscillations on a long-term basis would also help in understanding the potential extratropical/tropical linkages. Therefore, future ice core studies from the DML region should focus on quantifying the extent to which the SO will act as a source or sink of CO₂ in the future.

Bibliography

- Abram, N.J., Mulvaney, R., Vimeux, F., Phipps, S.J., Turner, J., England, M.H., 2014. Evolution of the Southern Annular Mode during the past millennium. *Nature Climate Change* 4, 564-569.
- Abram, N.J., Mulvaney, R., Wolff, E.W., Mudelsee, M., 2007. Ice core records as sea ice proxies: An evaluation from the Weddell Sea region of Antarctica. *Journal of Geophysical Research: Atmospheres* 112, D15101.
- Abram, N.J., Mulvaney, R., Wolff, E.W., Triest, J., Kipfstuhl, S., Trusel, L.D., et al., 2013. Acceleration of snow melt in an Antarctic Peninsula ice core during the twentieth century. *Nature Geoscience* 6, 404.
- Abram, N.J., Thomas, E.R., McConnell, J.R., Mulvaney, R., Bracegirdle, T.J., Sime, L.C., et al., 2010. Ice core evidence for a 20th century decline of sea ice in the Bellingshausen Sea, Antarctica. *Journal of Geophysical Research: Atmospheres* 115.
- Alexander, M.A., Bladé, I., Newman, M., Lanzante, J.R., Lau, N.-C., Scott, J.D., 2002. The Atmospheric Bridge: The Influence of ENSO Teleconnections on Air–Sea Interaction over the Global Oceans. *Journal of Climate* 15, 2205-2231.
- Altnau, S., Schlosser, E., Isaksson, E., Divine, D., 2015. Climatic signals from 76 shallow firn cores in Dronning Maud Land, East Antarctica. *The Cryosphere* 9, 925-944.
- Angert, A., Cappa, C.D., DePaolo, D.J., 2004. Kinetic ^{17}O effects in the hydrologic cycle: Indirect evidence and implications. Associate editor: J. Horita. *Geochimica et Cosmochimica Acta* 68, 3487-3495.

- Bamber, J.L., Riva, R.E.M., Vermeersen, B.L.A., LeBrocq, A.M., 2009. Reassessment of the Potential Sea-Level Rise from a Collapse of the West Antarctic Ice Sheet. *Science* 324, 901-903.
- Barkan, E., Luz, B., 2005. High precision measurements of $^{17}\text{O}/^{16}\text{O}$ and $^{18}\text{O}/^{16}\text{O}$ ratios in H_2O . *Rapid Communications in Mass Spectrometry* 19, 3737-3742.
- Barkan, E., Luz, B., 2007. Diffusivity fractionations of HO/HO and HO/HO in air and their implications for isotope hydrology. *Rapid Communications in Mass Spectrometry* 21, 2999-3005.
- Berman, E.S., Levin, N.E., Landais, A., Li, S., Owano, T., 2013. Measurement of $\delta^{18}\text{O}$, $\delta^{17}\text{O}$, and ^{17}O -excess in water by off-axis integrated cavity output spectroscopy and isotope ratio mass spectrometry. *Analytical chemistry* 85, 10392-10398.
- Bertler, N.A.N., Mayewski, P.A., Carter, L., 2011. Cold conditions in Antarctica during the Little Ice Age — Implications for abrupt climate change mechanisms. *Earth and Planetary Science Letters* 308, 41-51.
- Bintanja, R., van Oldenborgh, G.J., Drijfhout, S.S., Wouters, B., Katsman, C.A., 2013. Important role for ocean warming and increased ice-shelf melt in Antarctic sea-ice expansion. *Nature Geoscience* 6, 376-379.
- Bjerknes, J., 1969. Atmospheric Teleconnections from the Equatorial PACIFIC1. *Monthly Weather Review* 97, 163.
- Bonne, J.-L., Behrens, M., Meyer, H., Kipfstuhl, S., Rabe, B., Schönike, L., et al., 2019. Resolving the controls of water vapour isotopes in the Atlantic sector. *Nature Communications* 10, 1632.

- Bonne, J.-L., Steen-Larsen, H.C., Risi, C., Werner, M., Sodemann, H., Lacour, J.-L., et al., 2015. The summer 2012 Greenland heat wave: In situ and remote sensing observations of water vapor isotopic composition during an atmospheric river event. *Journal of Geophysical Research: Atmospheres* 120, 2970-2989.
- Cappa, C.D., Hendricks, M.B., DePaolo, D.J., Cohen, R.C., 2003. Isotopic fractionation of water during evaporation. *Journal of Geophysical Research: Atmospheres* 108.
- Carleton, A.M., 1989. Antarctic sea-ice relationships with indices of the atmospheric circulation of the Southern Hemisphere. *Climate Dynamics* 3, 207-220.
- Cauquoin, A., Jean-Baptiste, P., Risi, C., Fourré, É., Landais, A., 2016. Modeling the global bomb tritium transient signal with the AGCM LMDZ-iso: A method to evaluate aspects of the hydrological cycle. *Journal of Geophysical Research: Atmospheres* 121, 6126-6126.
- Cerrone, D., Fusco, G., Simmonds, I., Aulicino, G., Budillon, G., 2017. Dominant Covarying Climate Signals in the Southern Ocean and Antarctic Sea Ice Influence during the Last Three Decades. *Journal of Climate* 30, 3055-3072.
- Chakraborty, S., Goswami, B.N., Dutta, K., 2012. Pacific coral oxygen isotope and the tropospheric temperature gradient over the Asian monsoon region: a tool to reconstruct past Indian summer monsoon rainfall. *Journal of Quaternary Science* 27, 269-278.
- Chen, L., Li, T., Yu, Y., Behera, S.K., 2017. A possible explanation for the divergent projection of ENSO amplitude change under global warming. *Climate Dynamics* 49, 3799-3811.

- Chen, N., Majda, A.J., 2017. Simple stochastic dynamical models capturing the statistical diversity of El Niño Southern Oscillation. *Proceedings of the National Academy of Sciences* 114, 1468-1473.
- Ciais, P., Jouzel, J., 1994. Deuterium and oxygen 18 in precipitation: Isotopic model, including mixed cloud processes. *Journal of Geophysical Research: Atmospheres* 99, 16793-16803.
- Ciais, P., White, J.W.C., Jouzel, J., Petit, J.R., 1995. The origin of present-day Antarctic precipitation from surface snow deuterium excess data. *Journal of Geophysical Research: Atmospheres* 100, 18917-18927.
- Ciasto, L.M., England, M.H., 2011. Observed ENSO teleconnections to Southern Ocean SST anomalies diagnosed from a surface mixed layer heat budget. *Geophysical Research Letters* 38.
- Ciasto, L.M., Thompson, D.W.J., 2008. Observations of Large-Scale Ocean–Atmosphere Interaction in the Southern Hemisphere. *Journal of Climate* 21, 1244-1259.
- Clem, K.R., Fogt, R.L., 2013. Varying roles of ENSO and SAM on the Antarctic Peninsula climate in austral spring. *Journal of Geophysical Research: Atmospheres* 118, 411,481-411,492.
- Clem, K.R., Renwick, J.A., McGregor, J., Fogt, R.L., 2016. The relative influence of ENSO and SAM on Antarctic Peninsula climate. *Journal of Geophysical Research: Atmospheres* 121, 9324-9341.

- Cobb, K.M., Charles, C.D., Cheng, H., Edwards, R.L., 2003. El Niño/Southern Oscillation and tropical Pacific climate during the last millennium. *Nature* 424, 271-276.
- Convey, P., 2003. Maritime Antarctic Climate Change: Signals from Terrestrial Biology, Antarctic Peninsula Climate Variability: Historical and Paleoenvironmental Perspectives, pp. 145-158.
- Cook, A.J., Fox, A.J., Vaughan, D.G., Ferrigno, J.G., 2005. Retreating Glacier Fronts on the Antarctic Peninsula over the Past Half-Century. *Science* 308, 541-544.
- Coplen, T.B., De Bièvre, P., Krouse, H.R., Vocke, R.D., Gröning, M., Rozanski, K., 1996. Ratios for light-element isotopes standardized for better interlaboratory comparison. *Eos, Transactions American Geophysical Union* 77, 255-255.
- Curran, M.A.J., van Ommen, T.D., Morgan, V.I., Phillips, K.L., Palmer, A.S., 2003. Ice Core Evidence for Antarctic Sea Ice Decline Since the 1950s. *Science* 302, 1203-1206.
- D'Arrigo, R., Wilson, R., Deser, C., Wiles, G., Cook, E., Villalba, R., et al., 2005. Tropical–North Pacific Climate Linkages over the Past Four Centuries. *Journal of Climate* 18, 5253-5265.
- Dansgaard, W., 1964. Stable isotopes in precipitation. *Tellus* 16, 436-468.
- Dansgaard, W., Johnsen, S.J., Clausen, H.B., Dahl-Jensen, D., Gundestrup, N.S., Hammer, C.U., et al., 1993. Evidence for general instability of past climate from a 250-kyr ice-core record. *Nature* 364, 218-220.

- Dansgaard, W., Johnsen, S.J., Møller, J., Langway, C.C., 1969. One Thousand Centuries of Climatic Record from Camp Century on the Greenland Ice Sheet. *Science* 166, 377-380.
- Deb, P., Dash, M.K., Dey, S.P., Pandey, P.C., 2017. Non-annular response of sea ice cover in the Indian sector of the Antarctic during extreme SAM events. *International Journal of Climatology* 37, 648-656.
- Delmotte, M., Masson, V., Jouzel, J., Morgan, V.I., 2000. A seasonal deuterium excess signal at Law Dome, coastal eastern Antarctica: A southern ocean signature. *Journal of Geophysical Research: Atmospheres* 105, 7187-7197.
- Dickens, W.A., Kuhn, G., Leng, M.J., Graham, A.G.C., Dowdeswell, J.A., Meredith, M.P., et al., 2019. Enhanced glacial discharge from the eastern Antarctic Peninsula since the 1700s associated with a positive Southern Annular Mode. *Scientific reports* 9, 14606.
- Ding, Q., Steig, E.J., Battisti, D.S., Küttel, M., 2011. Winter warming in West Antarctica caused by central tropical Pacific warming. *Nature Geoscience* 4, 398-403.
- Ding, Q., Steig, E.J., Battisti, D.S., Wallace, J.M., 2012. Influence of the Tropics on the Southern Annular Mode. *Journal of Climate* 25, 6330-6348.
- Divine, D.V., Isaksson, E., Kaczmarek, M., Godtlielsen, F., Oerter, H., Schlosser, E., et al., 2009. Tropical Pacific–high latitude south Atlantic teleconnections as seen in $\delta^{18}\text{O}$ variability in Antarctic coastal ice cores. *Journal of Geophysical Research* 114.

- Eayrs, C., Holland, D., Francis, D., Wagner, T., Kumar, R., Li, X., 2019. Understanding the Seasonal Cycle of Antarctic Sea Ice Extent in the Context of Longer-Term Variability. *Reviews of Geophysics* 57, 1037-1064.
- Eichler, A., Schwikowski, M., Gäggeler, H.W., Furrer, V., Synal, H.-A., Beer, J., et al., 2000. Glaciochemical dating of an ice core from upper Grenzgletscher (4200 m a.s.l.). *Journal of Glaciology* 46, 507-515.
- Ejaz, T., Rahaman, W., Laluraj, C.M., Mahalinganathan, K., Thamban, M., 2021. Sea Ice Variability and Trends in the Western Indian Ocean Sector of Antarctica During the Past Two Centuries and Its Response to Climatic Modes. *Journal of Geophysical Research: Atmospheres* 126, e2020JD033943.
- Ekaykin, A.A., Vladimirova, D.O., Lipenkov, V.Y., Masson-Delmotte, V., 2017. Climatic variability in Princess Elizabeth Land (East Antarctica) over the last 350 years. *Clim. Past* 13, 61-71.
- EPICA community members, 2004. Eight glacial cycles from an Antarctic ice core. *Nature* 429, 623–628.
- Epstein, S., Mayeda, T., 1953. Variation of O18 content of waters from natural sources. *Geochimica et Cosmochimica Acta* 4, 213-224.
- Etheridge, D.M., Steele, L.P., Langenfelds, R.L., Francey, R.J., Barnola, J.-M., Morgan, V.I., 1996. Natural and anthropogenic changes in atmospheric CO₂ over the last 1000 years from air in Antarctic ice and firn. *Journal of Geophysical Research: Atmospheres* 101, 4115-4128.

- Fernandoy, F., Tetzner, D., Meyer, H., Gacitúa, G., Hoffmann, K., Falk, U., et al., 2018. New insights into the use of stable water isotopes at the northern Antarctic Peninsula as a tool for regional climate studies. *The Cryosphere* 12, 1069-1090.
- Ferrari, R., Jansen, M.F., Adkins, J.F., Burke, A., Stewart, A.L., Thompson, A.F., 2014. Antarctic sea ice control on ocean circulation in present and glacial climates. *Proceedings of the National Academy of Sciences* 111, 8753-8758.
- Fogt, R.L., Bromwich, D.H., 2006. Decadal Variability of the ENSO Teleconnection to the High-Latitude South Pacific Governed by Coupling with the Southern Annular Mode. *Journal of Climate* 19, 979-997.
- Fogt, R.L., Bromwich, D.H., Hines, K.M., 2011. Understanding the SAM influence on the South Pacific ENSO teleconnection. *Climate Dynamics* 36, 1555-1576.
- Foster, A.F.M., Curran, M.A.J., Smith, B.T., Van Ommen, T.D., Morgan, V.I., 2006. Covariation of Sea ice and methanesulphonic acid in Wilhelm II Land, East Antarctica. *Annals of Glaciology* 44, 429-432.
- Fowler, A.M., Boswijk, G., Lorrey, A.M., Gergis, J., Pirie, M., McCloskey, S.P.J., et al., 2012. Multi-centennial tree-ring record of ENSO-related activity in New Zealand. *Nature Climate Change* 2, 172-176.
- Fretwell, P., Pritchard, H.D., Vaughan, D.G., Bamber, J.L., Barrand, N.E., Bell, R., et al., 2013. Bedmap2: improved ice bed, surface and thickness datasets for Antarctica. *The Cryosphere* 7, 375-393.
- Fujita, K., Abe, O., 2006. Stable isotopes in daily precipitation at Dome Fuji, East Antarctica. *Geophysical Research Letters* 33.

- Gettelman, A., Seidel, D.J., Wheeler, M.C., Ross, R.J., 2002. Multidecadal trends in tropical convective available potential energy. *Journal of Geophysical Research: Atmospheres* 107, ACL 17-11-ACL 17-18.
- Gettelman, A., Walden, V.P., Miloshevich, L.M., Roth, W.L., Halter, B., 2006. Relative humidity over Antarctica from radiosondes, satellites, and a general circulation model. *Journal of Geophysical Research: Atmospheres* 111.
- Gong, D., Wang, S., 1999. Definition of Antarctic Oscillation index. *Geophysical Research Letters* 26, 459-462.
- Goodwin, B.P., Mosley-Thompson, E., Wilson, A.B., Porter, S.E., Sierra-Hernandez, M.R., 2016. Accumulation Variability in the Antarctic Peninsula: The Role of Large-Scale Atmospheric Oscillations and Their Interactions*. *Journal of Climate* 29, 2579-2596.
- Goosse, H., Braida, M., Crosta, X., Mairesse, A., Masson-Delmotte, V., Mathiot, P., et al., 2012. Antarctic temperature changes during the last millennium: evaluation of simulations and reconstructions. *Quaternary Science Reviews* 55, 75-90.
- Goursaud, S., Masson-Delmotte, V., Favier, V., Orsi, A., Werner, M., 2018. Water stable isotope spatio-temporal variability in Antarctica in 1960–2013: observations and simulations from the ECHAM5-wiso atmospheric general circulation model. *Clim. Past* 14, 923-946.
- Goursaud, S., Masson-Delmotte, V., Favier, V., Preunkert, S., Fily, M., Gallée, H., et al., 2017. A 60-year ice-core record of regional climate from Adélie Land, coastal Antarctica. *The Cryosphere* 11, 343-362.

- Goursaud, S., Masson-Delmotte, V., Favier, V., Preunkert, S., Legrand, M., Minster, B., et al., 2019. Challenges associated with the climatic interpretation of water stable isotope records from a highly resolved firn core from Adélie Land, coastal Antarctica. *The Cryosphere* 13, 1297-1324.
- Graf, W., Oerter, H., Reinwarth, O., Stichler, W., Wilhelms, F., Miller, H., et al., 2002. Stable-isotope records from Dronning Maud Land, Antarctica. *Annals of Glaciology* 35, 195-201.
- Gregory, S., Noone, D., 2008. Variability in the teleconnection between the El Niño–Southern Oscillation and West Antarctic climate deduced from West Antarctic ice core isotope records. *Journal of Geophysical Research: Atmospheres* 113.
- Grinsted, A., Moore, J.C., Jevrejeva, S., 2004. Application of the cross wavelet transform and wavelet coherence to geophysical time series. *Nonlinear Processes in Geophysics* 11, 561–566.
- Hall, A., Visbeck, M., 2002. Synchronous Variability in the Southern Hemisphere Atmosphere, Sea Ice, and Ocean Resulting from the Annular Mode*. *Journal of Climate* 15, 3043-3057.
- Henley, B.J., Gergis, J., Karoly, D.J., Power, S., Kennedy, J., Folland, C.K., 2015. A Tripole Index for the Interdecadal Pacific Oscillation. *Climate Dynamics* 45, 3077-3090.
- Hersbach, H., Bell, B., Berrisford, P., Hirahara, S., Horányi, A., Muñoz-Sabater, J., et al., 2020. The ERA5 global reanalysis. *Quarterly Journal of the Royal Meteorological Society* 146, 1999-2049.

- Hobbs, W.R., Massom, R., Stammerjohn, S., Reid, P., Williams, G., Meier, W., 2016. A review of recent changes in Southern Ocean sea ice, their drivers and forcings. *Global and Planetary Change* 143, 228-250.
- Hoffmann, G., Werner, M., Heimann, M., 1998. Water isotope module of the ECHAM atmospheric general circulation model: A study on timescales from days to several years. *Journal of Geophysical Research: Atmospheres* 103, 16871-16896.
- Holland, Kwok, R., 2012. Wind-driven trends in Antarctic sea-ice drift. *Nature Geoscience* 5, 872-875.
- Holland, M.M., Landrum, L., Kostov, Y., Marshall, J., 2017. Sensitivity of Antarctic sea ice to the Southern Annular Mode in coupled climate models. *Climate Dynamics* 49, 1813-1831.
- Holloway, M.D., Sime, L.C., Allen, C.S., Hillenbrand, C.-D., Bunch, P., Wolff, E., et al., 2017. The Spatial Structure of the 128 ka Antarctic Sea Ice Minimum. *Geophysical Research Letters* 44, 11,129-111,139.
- Holloway, M.D., Sime, L.C., Singarayer, J.S., Tindall, J.C., Bunch, P., Valdes, P.J., 2016. Antarctic last interglacial isotope peak in response to sea ice retreat not ice-sheet collapse. *Nature Communications* 7, 12293.
- Hoskins, B.J., Ambrizzi, T., 1993. Rossby Wave Propagation on a Realistic Longitudinally Varying Flow. *Journal of Atmospheric Sciences* 50, 1661-1671.
- Ionita, M., Scholz, P., Grosfeld, K., Treffeisen, R., 2018. Moisture transport and Antarctic sea ice: austral spring 2016 event. *Earth Syst. Dynam.* 9, 939-954.

- IPCC, 2013. *Climate Change 2013: The Physical Science Basis. Contribution of Working Group I to the Fifth Assessment Report of the Intergovernmental Panel on Climate Change*. Cambridge University Press, 1535.
- Isaacs, F.E., Renwick, J.A., Mackintosh, A.N., Dadic, R., 2021. ENSO Modulates Summer and Autumn Sea Ice Variability Around Dronning Maud Land, Antarctica. *Journal of Geophysical Research: Atmospheres* 126, e2020JD033140.
- Isaksson, E., Karlén, W., 1994. Spatial and temporal patterns in snow accumulation, western Dronning Maud Land, Antarctica. *Journal of Glaciology* 40, 399-409.
- Jena, B., Kumar, A., Ravichandran, M., Kern, S., 2018. Mechanism of sea-ice expansion in the Indian Ocean sector of Antarctica: Insights from satellite observation and model reanalysis. *PLOS ONE* 13, e0203222.
- Jin, D., Kirtman, B.P., 2009. Why the Southern Hemisphere ENSO responses lead ENSO. *Journal of Geophysical Research: Atmospheres* 114.
- Jones, J.M., Gille, S.T., Goosse, H., Abram, N.J., Canziani, P.O., Charman, D.J., et al., 2016. Assessing recent trends in high-latitude Southern Hemisphere surface climate. *Nature Climate Change* 6, 917-926.
- Jouzel, J., 2013. A brief history of ice core science over the last 50 yr. *Clim. Past* 9, 2525-2547.
- Jouzel, J., Delaygue, G., Landais, A., Masson-Delmotte, V., Risi, C., Vimeux, F., 2013. Water isotopes as tools to document oceanic sources of precipitation. *Water Resources Research* 49, 7469-7486.

- Jouzel, J., Masson-Delmotte, V., Cattani, O., Dreyfus, G., Falourd, S., Hoffmann, G., et al., 2007. Orbital and Millennial Antarctic Climate Variability over the Past 800,000 Years. *Science* 317, 793-796.
- Jouzel, J., Merlivat, L., 1984. Deuterium and oxygen 18 in precipitation: Modeling of the isotopic effects during snow formation. *Journal of Geophysical Research: Atmospheres* 89, 11749-11757.
- Jouzel, J., Merlivat, L., Lorius, C., 1982. Deuterium excess in an East Antarctic ice core suggests higher relative humidity at the oceanic surface during the last glacial maximum. *Nature* 299, 688-691.
- Jouzel, J., Vimeux, F., Caillon, N., Delaygue, G., Hoffmann, G., Masson-Delmotte, V., et al., 2003. Magnitude of isotope/temperature scaling for interpretation of central Antarctic ice cores. *Journal of Geophysical Research: Atmospheres* 108.
- Karoly, D.J., 1989. Southern Hemisphere Circulation Features Associated with El Niño-Southern Oscillation Events. *Journal of Climate* 2, 1239-1252.
- Kavanaugh, J.L., Cuffey, K.M., 2003. Space and time variation of $\delta^{18}\text{O}$ and δD in Antarctic precipitation revisited. *Global Biogeochemical Cycles* 17.
- Kendall, M.G., 1975. Rank correlation methods. Griffin, Oxford, England.
- Kwok, R., Comiso, J.C., 2002a. Southern Ocean Climate and Sea Ice Anomalies Associated with the Southern Oscillation. *Journal of Climate* 15, 487-501.
- Kwok, R., Comiso, J.C., 2002b. Spatial patterns of variability in Antarctic surface temperature: Connections to the Southern Hemisphere Annular Mode and the Southern Oscillation. *Geophysical Research Letters* 29, 50-51-50-54.

Lachlan-Cope, T., Connolley, W., 2006. Teleconnections between the tropical Pacific and the Amundsen-Bellinghausens Sea: Role of the El Niño/Southern Oscillation. *Journal of Geophysical Research: Atmospheres* 111.

Laluraj, C.M., Rahaman, W., Thamban, M., Srivastava, R., 2020. Enhanced Dust Influx to South Atlantic Sector of Antarctica During the Late-20th Century: Causes and Contribution to Radiative Forcing. *Journal of Geophysical Research: Atmospheres* 125, e2019JD030675.

Laluraj, C.M., Thamban, M., Naik, S.S., Redkar, B.L., Chaturvedi, A., Ravindra, R., 2010. Nitrate records of a shallow ice core from East Antarctica: Atmospheric processes, preservation and climatic implications. *The Holocene* 21, 351-356.

Laluraj, C.M., Thamban, M., Naik, S.S., Redkar, B.L., Chaturvedi, A., Ravindra, R., 2011. Nitrate records of a shallow ice core from East Antarctica: Atmospheric processes, preservation and climatic implications. *The Holocene* 21, 351-356.

Laluraj, C.M., Thamban, M., Satheesan, K., 2014. Dust and associated geochemical fluxes in a firn core from coastal East Antarctica and its linkages with Southern Hemisphere climate variability over the last 50 years. *Atmospheric Environment* 90, 23-32.

Landais, A., Barkan, E., Luz, B., 2008. Record of $\delta^{18}\text{O}$ and ^{17}O -excess in ice from Vostok Antarctica during the last 150,000 years. *Geophysical Research Letters* 35.

Landais, A., Casado, M., Prié, F., Magand, O., Arnaud, L., Ekaykin, A., et al., 2017. Surface studies of water isotopes in Antarctica for quantitative interpretation of deep ice core data. *Comptes Rendus Geoscience* 349, 139-150.

- Landais, A., Ekaykin, A., Barkan, E., Winkler, R., Luz, B., 2012. Seasonal variations of $\delta^{17}\text{O}$ -excess and $\delta^2\text{H}$ -excess in snow precipitation at Vostok station, East Antarctica. *Journal of Glaciology* 58, 725-733.
- Landais, A., Risi, C., Bony, S., Vimeux, F., Descroix, L., Falourd, S., et al., 2010. Combined measurements of $\delta^{17}\text{O}$ -excess and $\delta^2\text{H}$ -excess in African monsoon precipitation: Implications for evaluating convective parameterizations. *Earth and Planetary Science Letters* 298, 104-112.
- Leduc, M., Matthews, H.D., de Elía, R., 2016. Regional estimates of the transient climate response to cumulative CO_2 emissions. *Nature Climate Change* 6, 474-478.
- Lefebvre, W., Goosse, H., Timmermann, R., Fichefet, T., 2004. Influence of the Southern Annular Mode on the sea ice–ocean system. *Journal of Geophysical Research: Oceans* 109.
- Li, S., Levin, N.E., Chesson, L.A., 2015. Continental scale variation in $\delta^{17}\text{O}$ -excess of meteoric waters in the United States. *Geochimica et Cosmochimica Acta* 164, 110-126.
- Li, X., Cai, W., Meehl, G.A., Chen, D., Yuan, X., Raphael, M., et al., 2021. Tropical teleconnection impacts on Antarctic climate changes. *Nature Reviews Earth & Environment* 2, 680-698.
- Lim, E.-P., Hendon, H.H., 2015. Understanding and predicting the strong Southern Annular Mode and its impact on the record wet east Australian spring 2010. *Climate Dynamics* 44, 2807-2824.

- Liu, J., Curry, J.A., Martinson, D.G., 2004. Interpretation of recent Antarctic sea ice variability. *Geophysical Research Letters* 31.
- Lüthi, D., Le Floch, M., Bereiter, B., Blunier, T., Barnola, J.-M., Siegenthaler, U., et al., 2008. High-resolution carbon dioxide concentration record 650,000–800,000 years before present. *Nature* 453, 379-382.
- Luz, B., Barkan, E., 2010. Variations of $^{17}\text{O}/^{16}\text{O}$ and $^{18}\text{O}/^{16}\text{O}$ in meteoric waters. *Geochimica et Cosmochimica Acta* 74, 6276-6286.
- MacDonald, G.M., Case, R.A., 2005. Variations in the Pacific Decadal Oscillation over the past millennium. *Geophysical Research Letters* 32.
- Mahalinganathan, K., Thamban, M., 2016. Potential genesis and implications of calcium nitrate in Antarctic snow. *The Cryosphere* 10, 825-836.
- Mann, M.E., Zhang, Z., Rutherford, S., Bradley, R.S., Hughes, M.K., Shindell, D., et al., 2009. Global Signatures and Dynamical Origins of the Little Ice Age and Medieval Climate Anomaly. *Science* 326, 1256-1260.
- Mantua, N.J., Hare, S.R., 2002. The Pacific Decadal Oscillation. *Journal of Oceanography* 58, 35-44.
- Mantua, N.J., Hare, S.R., Zhang, Y., Wallace, J.M., Francis, R.C., 1997. A Pacific Interdecadal Climate Oscillation with Impacts on Salmon Production**. *Bulletin of the American Meteorological Society* 78, 1069-1080.
- Marshall, 2007. Half-century seasonal relationships between the Southern Annular mode and Antarctic temperatures. *International Journal of Climatology* 27, 373-383.

- Marshall, A.G., Hudson, D., Wheeler, M.C., Hendon, H.H., Alves, O., 2012. Simulation and prediction of the Southern Annular Mode and its influence on Australian intra-seasonal climate in POAMA. *Climate Dynamics* 38, 2483-2502.
- Marshall, G.J., 2003. Trends in the Southern Annular Mode from Observations and Reanalyses. *Journal of Climate* 16, 4134-4143.
- Marshall, G.J., Orr, A., van Lipzig, N.P.M., King, J.C., 2006. The Impact of a Changing Southern Hemisphere Annular Mode on Antarctic Peninsula Summer Temperatures. *Journal of Climate* 19, 5388-5404.
- Marshall, G.J., Stott, P.A., Turner, J., Connolley, W.M., King, J.C., Lachlan-Cope, T.A., 2004. Causes of exceptional atmospheric circulation changes in the Southern Hemisphere. *Geophysical Research Letters* 31.
- Masson-Delmotte, V., Delmotte, M., Morgan, V., Etheridge, D., van Ommen, T., Tartarin, S., et al., 2003. Recent southern Indian Ocean climate variability inferred from a Law Dome ice core: new insights for the interpretation of coastal Antarctic isotopic records. *Climate Dynamics* 21, 153-166.
- Masson-Delmotte, V., Hou, S., Ekaykin, A., Jouzel, J., Aristarain, A., Bernardo, R.T., et al., 2008. A Review of Antarctic Surface Snow Isotopic Composition: Observations, Atmospheric Circulation, and Isotopic Modeling. *Journal of Climate* 21, 3359-3387.
- Masson-Delmotte, V., Stenni, B., Jouzel, J., 2004. Common millennial-scale variability of Antarctic and Southern Ocean temperatures during the past 5000 years reconstructed from the EPICA Dome C ice core. *The Holocene* 14, 145-151.

- McPhaden, M.J., Zebiak, S.E., Glantz, M.H., 2006. ENSO as an Integrating Concept in Earth Science. *Science* 314, 1740-1745.
- Medley, B., McConnell, J.R., Neumann, T.A., Reijmer, C.H., Chellman, N., Sigl, M., et al., 2018. Temperature and Snowfall in Western Queen Maud Land Increasing Faster Than Climate Model Projections. *Geophysical Research Letters* 45, 1472-1480.
- Meredith, M.P., King, J.C., 2005. Rapid climate change in the ocean west of the Antarctic Peninsula during the second half of the 20th century. *Geophysical Research Letters* 32.
- Merlivat, L., 1978. Molecular diffusivities of H₂¹⁶O, HD¹⁶O, and H₂¹⁸O in gases. *Journal of Chemical Physics* 69, 2864-2871.
- Merlivat, L., Jouzel, J., 1979. Global climatic interpretation of the deuterium-oxygen 18 relationship for precipitation. *Journal of Geophysical Research: Oceans* 84, 5029-5033.
- Mills, S.C., Le Brocq, A.M., Winter, K., Smith, M., Hillier, J., Ardakova, E., et al., 2019. Testing and application of a model for snow redistribution (Snow_Blow) in the Ellsworth Mountains, Antarctica. *Journal of Glaciology* 65, 957-970.
- Mo, K.C., Higgins, R.W., 1998. The Pacific–South American Modes and Tropical Convection during the Southern Hemisphere Winter. *Monthly Weather Review* 126, 1581-1596.

- Morgan, V.I., Wookey, C.W., Li, J., van Ommen, T.D., Skinner, W., Fitzpatrick, M.F., 1997. Site information and initial results from deep ice drilling on Law Dome, Antarctica. *Journal of Glaciology* 43, 3-10.
- Mott, R., Vionnet, V., Grünewald, T., 2018. The Seasonal Snow Cover Dynamics: Review on Wind-Driven Coupling Processes. *Frontiers in Earth Science* 6.
- Mulvaney, R., Abram, N.J., Hindmarsh, R.C.A., Arrowsmith, C., Fleet, L., Triest, J., et al., 2012. Recent Antarctic Peninsula warming relative to Holocene climate and ice-shelf history. *Nature* 489, 141.
- Mulvaney, R., Oerter, H., Peel, D.A., Graf, W., Arrowsmith, C., Pasteur, E.C., et al., 2002. 1000 year ice-core records from Berkner Island, Antarctica. *Annals of Glaciology* 35, 45-51.
- Münch, Kipfstuhl, S., Freitag, J., Meyer, H., Laepple, T., 2016. Regional climate signal vs. local noise: a two-dimensional view of water isotopes in Antarctic firn at Kohnen Station, Dronning Maud Land. *Clim. Past* 12, 1565-1581.
- Naakka, T., Nygård, T., Vihma, T., 2021. Air Moisture Climatology and Related Physical Processes in the Antarctic on the Basis of ERA5 Reanalysis. *Journal of Climate* 34, 4463-4480.
- Naik, S.S., Thamban, M., Laluraj, C.M., Redkar, B.L., Chaturvedi, A., 2010. A century of climate variability in central Dronning Maud Land, East Antarctica, and its relation to Southern Annular Mode and El Niño-Southern Oscillation. *Journal of Geophysical Research* 115.
- Nardin, R., Severi, M., Amore, A., Becagli, S., Burgay, F., Caiazzo, L., et al., 2021. Dating of the GV7 East Antarctic ice core by high-resolution chemical records

- and focus on the accumulation rate variability in the last millennium. *Clim. Past* 17, 2073-2089.
- Neelin, J.D., Battisti, D.S., Hirst, A.C., Jin, F.-F., Wakata, Y., Yamagata, T., et al., 1998. ENSO theory. *Journal of Geophysical Research: Oceans* 103, 14261-14290.
- Nicolas, J.P., Bromwich, D.H., 2014. New Reconstruction of Antarctic Near-Surface Temperatures: Multidecadal Trends and Reliability of Global Reanalyses. *Journal of Climate* 27, 8070-8093.
- Noone, D., Simmonds, I., 2002. Annular variations in moisture transport mechanisms and the abundance of $\delta^{18}\text{O}$ in Antarctic snow. *Journal of Geophysical Research: Atmospheres* 107, ACL 3-1-ACL 3-11.
- Noone, D., Simmonds, I., 2004. Sea ice control of water isotope transport to Antarctica and implications for ice core interpretation. *Journal of Geophysical Research: Atmospheres* 109.
- Ohshima, K.I., Fukamachi, Y., Williams, G.D., Nihashi, S., Roquet, F., Kitade, Y., et al., 2013. Antarctic Bottom Water production by intense sea-ice formation in the Cape Darnley polynya. *Nature Geoscience* 6, 235-240.
- Okumura, Y.M., Schneider, D., Deser, C., Wilson, R., 2012. Decadal–Interdecadal Climate Variability over Antarctica and Linkages to the Tropics: Analysis of Ice Core, Instrumental, and Tropical Proxy Data. *Journal of Climate* 25, 7421-7441.
- Otto-Bliesner, B.L., Brady, E.C., Fasullo, J., Jahn, A., Landrum, L., Stevenson, S., et al., 2016. Climate Variability and Change since 850 CE: An Ensemble Approach with the Community Earth System Model. *Bulletin of the American Meteorological Society* 97, 735-754.

- Overpeck, J.T., Cole, J.E., 2006. Abrupt Change in Earth's Climate System. *Annual Review of Environment and Resources* 31, 1-31.
- PAGES 2k Consortium, 2013. Continental-scale temperature variability during the past two millennia. *Nature Geoscience* 6, 339–346.
- Pang, H., Hou, S., Landais, A., Masson-Delmotte, V., Prie, F., Steen-Larsen, H.C., et al., 2015. Spatial distribution of ^{17}O -excess in surface snow along a traverse from Zhongshan station to Dome A, East Antarctica. *Earth and Planetary Science Letters* 414, 126-133.
- Paolo, F.S., Padman, L., Fricker, H.A., Adusumilli, S., Howard, S., Siegfried, M.R., 2018. Response of Pacific-sector Antarctic ice shelves to the El Niño/Southern Oscillation. *Nature Geoscience* 11, 121-126.
- Peng, G., Meier, W.N., Scott, D.J., Savoie, M.H., 2013. A long-term and reproducible passive microwave sea ice concentration data record for climate studies and monitoring. *Earth Syst. Sci. Data* 5, 311-318.
- Peter, H., Carl, W., 2004. A depth-derived Pleistocene age model: Uncertainty estimates, sedimentation variability, and nonlinear climate change. *Paleoceanography* 19.
- Petit, J.R., Jouzel, J., Raynaud, D., Barkov, N.I., Barnola, J.M., Basile, I., et al., 1999. Climate and atmospheric history of the past 420,000 years from the Vostok ice core, Antarctica. *Nature* 399, 429-436.
- Petit, J.R., White, J.W.C., Young, N.W., Jouzel, J., Korotkevich, Y.S., 1991. Deuterium excess in recent Antarctic snow. *Journal of Geophysical Research: Atmospheres* 96, 5113-5122.

- Picciotto, E., De Maere, X., Friedman, I., 1960. Isotopic Composition and Temperature of Formation of Antarctic Snows. *Nature* 187, 857.
- Porter, S.E., Parkinson, C.L., Mosley-Thompson, E., 2016. Bellingshausen Sea ice extent recorded in an Antarctic Peninsula ice core. *Journal of Geophysical Research: Atmospheres* 121, 886-813,900.
- Purich, A., England, M.H., Cai, W., Chikamoto, Y., Timmermann, A., Fyfe, J.C., et al., 2016. Tropical Pacific SST Drivers of Recent Antarctic Sea Ice Trends. *Journal of Climate* 29, 8931-8948.
- Rahaman, W., Chatterjee, S., Ejaz, T., Thamban, M., 2019. Increased influence of ENSO on Antarctic temperature since the Industrial Era. *Scientific reports* 9, 6006.
- Rahaman, W., Thamban, M., Laluraj, C.M., 2016. Twentieth-century sea ice variability in the Weddell Sea and its effect on moisture transport: Evidence from a coastal East Antarctic ice core record. *The Holocene* 26, 338-349.
- Raphael, M.N., 2003. Impact of observed sea-ice concentration on the Southern Hemisphere extratropical atmospheric circulation in summer. *Journal of Geophysical Research: Atmospheres* 108.
- Rayner, N.A., Parker, D.E., Horton, E.B., Folland, C.K., Alexander, L.V., Rowell, D.P., et al., 2003. Global analyses of sea surface temperature, sea ice, and night marine air temperature since the late nineteenth century. *Journal of Geophysical Research: Atmospheres* 108, n/a-n/a.
- Renwick, J.A., 2002. Southern Hemisphere Circulation and Relations with Sea Ice and Sea Surface Temperature. *Journal of Climate* 15, 3058-3068.

- Risi, C., Landais, A., Bony, S., Jouzel, J., Masson-Delmotte, V., Vimeux, F., 2010a. Understanding the $\delta^{18}O$ excess glacial-interglacial variations in Vostok precipitation. *Journal of Geophysical Research* 115.
- Risi, C., Landais, A., Bony, S., Jouzel, J., Masson-Delmotte, V., Vimeux, F., 2010b. Understanding the $\delta^{18}O$ excess glacial-interglacial variations in Vostok precipitation. *Journal of Geophysical Research: Atmospheres* 115.
- Risi, C., Noone, D., Worden, J., Frankenberg, C., Stiller, G., Kiefer, M., et al., 2012. Process-evaluation of tropospheric humidity simulated by general circulation models using water vapor isotopologues: 1. Comparison between models and observations. *Journal of Geophysical Research: Atmospheres* 117.
- Ropelewski, C.F., Halpert, M.S., 1986. North American Precipitation and Temperature Patterns Associated with the El Niño/Southern Oscillation (ENSO). *Monthly Weather Review* 114, 2352-2362.
- Ropelewski, C.F., Jones, P.D., 1987. An Extension of the Tahiti–Darwin Southern Oscillation Index. *Monthly Weather Review* 115, 2161-2165.
- Röthlisberger, R., Crosta, X., Abram, N.J., Armand, L., Wolff, E.W., 2010. Potential and limitations of marine and ice core sea ice proxies: an example from the Indian Ocean sector. *Quaternary Science Reviews* 29, 296-302.
- Scambos, T.A., Hulbe, C., Fahnestock, M., Bohlander, J., 2017. The link between climate warming and break-up of ice shelves in the Antarctic Peninsula. *Journal of Glaciology* 46, 516-530.

- Schlosser, E., Oerter, H., Masson-Delmotte, V., Reijmer, C., 2008. Atmospheric influence on the deuterium excess signal in polar firn: implications for ice-core interpretation. *Journal of Glaciology* 54, 117-124.
- Schmidt, G.A., Jungclauss, J.H., Ammann, C.M., Bard, E., Braconnot, P., Crowley, T.J., et al., 2012. Climate forcing reconstructions for use in PMIP simulations of the Last Millennium (v1.1). *Geosci. Model Dev.* 5, 185-191.
- Schneider, D.P., Steig, E.J., Comiso, J.C., 2004. Recent Climate Variability in Antarctica from Satellite-Derived Temperature Data. *Journal of Climate* 17, 1569-1583.
- Schneider, D.P., Steig, E.J., Van Ommen, T., 2017. High-resolution ice-core stable-isotopic records from Antarctica: towards interannual climate reconstruction. *Annals of Glaciology* 41, 63-70.
- Schoenemann, S.W., Schauer, A.J., Steig, E.J., 2013. Measurement of SLAP2 and GISP $\delta^{17}\text{O}$ and proposed VSMOW-SLAP normalization for $\delta^{17}\text{O}$ and ^{17}O excess. *Rapid Communications in Mass Spectrometry* 27, 582-590.
- Schoenemann, S.W., Steig, E.J., 2016. Seasonal and spatial variations of ^{17}O excess and dexcess in Antarctic precipitation: Insights from an intermediate complexity isotope model. *Journal of Geophysical Research: Atmospheres* 121, 11,215-211,247.
- Schoenemann, S.W., Steig, E.J., Ding, Q., Markle, B.R., Schauer, A.J., 2014. Triple water-isotopologue record from WAIS Divide, Antarctica: Controls on glacial-interglacial changes in ^{17}O excess of precipitation. *Journal of Geophysical Research: Atmospheres* 119, 8741-8763.

- Schulz, M., Mudelsee, M., 2002. REDFIT: estimating red-noise spectra directly from unevenly spaced paleoclimatic time series. *Computers & Geosciences* 28, 421-426.
- Schytt, V., 1954. Journeys of the glaciological party 1950–51. In: Giaever, J. The white desert: the official account of the Norwegian–British–Swedish Antarctic expedition. London: Chatto & Windus: , 232–244.
- Screen, J.A., Gillett, N.P., Karpechko, A.Y., Stevens, D.P., 2010. Mixed Layer Temperature Response to the Southern Annular Mode: Mechanisms and Model Representation. *Journal of Climate* 23, 664-678.
- Sen Gupta, A., England, M.H., 2006. Coupled Ocean–Atmosphere–Ice Response to Variations in the Southern Annular Mode. *Journal of Climate* 19, 4457-4486.
- Shepherd, A., Ivins, E., Rignot, E., Smith, B., van den Broeke, M., Velicogna, I., et al., 2018. Mass balance of the Antarctic Ice Sheet from 1992 to 2017. *Nature* 558, 219-222.
- Sigl, M., McConnell, J.R., Toohey, M., Curran, M., Das, S.B., Edwards, R., et al., 2014. Insights from Antarctica on volcanic forcing during the Common Era. *Nature Climate Change* 4, 693-697.
- Sigl, M., Winstrup, M., McConnell, J.R., Welten, K.C., Plunkett, G., Ludlow, F., et al., 2015. Timing and climate forcing of volcanic eruptions for the past 2,500 years. *Nature* 523, 543-549.
- Sigmond, M., Fyfe, J.C., 2014. The Antarctic Sea Ice Response to the Ozone Hole in Climate Models. *Journal of Climate* 27, 1336-1342.

- Sime, L.C., Marshall, G.J., Mulvaney, R., Thomas, E.R., 2009. Interpreting temperature information from ice cores along the Antarctic Peninsula: ERA40 analysis. *Geophysical Research Letters* 36.
- Simmonds, I., 2003. Modes of atmospheric variability over the Southern Ocean. *Journal of Geophysical Research: Oceans* 108, SOV 5-1-SOV 5-30.
- Simmonds, I., Keay, K., Lim, E.-P., 2003. Synoptic Activity in the Seas around Antarctica. *Monthly Weather Review* 131, 272-288.
- Simmonds, I., Xingren, W., 1993. Cyclone behaviour response to changes in winter southern hemisphere sea-ice concentration. *Quarterly Journal of the Royal Meteorological Society* 119, 1121-1148.
- Simpkins, G.R., Ciasto, L.M., Thompson, D.W.J., England, M.H., 2012. Seasonal Relationships between Large-Scale Climate Variability and Antarctic Sea Ice Concentration. *Journal of Climate* 25, 5451-5469.
- Sinclair, K.E., Bertler, N.A.N., van Ommen, T.D., 2012. Twentieth-Century Surface Temperature Trends in the Western Ross Sea, Antarctica: Evidence from a High-Resolution Ice Core. *Journal of Climate* 25, 3629-3636.
- Sloyan, B.M., 2006. Antarctic bottom and lower circumpolar deep water circulation in the eastern Indian Ocean. *Journal of Geophysical Research: Oceans* 111.
- Sneed, S.B., Mayewski, P.A., Dixon, D.A., 2011. An emerging technique: multi-ice-core multi-parameter correlations with Antarctic sea-ice extent. *Annals of Glaciology* 52, 347-354.

- Sorge, E., 1933. The Scientific Results of the Wegener Expeditions to Greenland. The Geographical Journal 81, 333-344.
- Spence, P., Fyfe, J.C., Montenegro, A., Weaver, A.J., 2010. Southern Ocean Response to Strengthening Winds in an Eddy-Permitting Global Climate Model. Journal of Climate 23, 5332-5343.
- Stammerjohn, S.E., Martinson, D.G., Smith, R.C., Yuan, X., Rind, D., 2008. Trends in Antarctic annual sea ice retreat and advance and their relation to El Niño–Southern Oscillation and Southern Annular Mode variability. Journal of Geophysical Research: Oceans 113.
- Steen-Larsen, H.C., Masson-Delmotte, V., Hirabayashi, M., Winkler, R., Satow, K., Prié, F., et al., 2014. What controls the isotopic composition of Greenland surface snow? Clim. Past 10, 377-392.
- Steiger, N.J., Steig, E.J., Dee, S.G., Roe, G.H., Hakim, G.J., 2017. Climate reconstruction using data assimilation of water isotope ratios from ice cores. Journal of Geophysical Research: Atmospheres 122, 1545-1568.
- Stenni, B., Curran, M.A.J., Abram, N.J., Orsi, A., Goursaud, S., Masson-Delmotte, V., et al., 2017. Antarctic climate variability on regional and continental scales over the last 2000 years. Clim. Past 13, 1609-1634.
- Stenni, B., Jouzel, J., Masson-Delmotte, V., Röthlisberger, R., Castellano, E., Cattani, O., et al., 2004. A late-glacial high-resolution site and source temperature record derived from the EPICA Dome C isotope records (East Antarctica). Earth and Planetary Science Letters 217, 183-195.

- Stenni, B., Masson-Delmotte, V., Johnsen, S., Jouzel, J., Longinelli, A., Monnin, E., et al., 2001. An Oceanic Cold Reversal During the Last Deglaciation. *Science* 293, 2074-2077.
- Stenni, B., Masson-Delmotte, V., Selmo, E., Oerter, H., Meyer, H., Röthlisberger, R., et al., 2010. The deuterium excess records of EPICA Dome C and Dronning Maud Land ice cores (East Antarctica). *Quaternary Science Reviews* 29, 146-159.
- Stuecker, M.F., Bitz, C.M., Armour, K.C., 2017. Conditions leading to the unprecedented low Antarctic sea ice extent during the 2016 austral spring season. *Geophysical Research Letters* 44, 9008-9019.
- Swithinkbank, C., 1957. The morphology of the ice shelves of western Dronning Maud Land. In: *Norwegian–British–Swedish Antarctic Expedition 1949–52: scientific results*. Oslo: Norsk Polarinstitut 3A, 1–37.
- Thamban, M., 2017. Antarctic Palaeoclimate Reconstruction Using Ice Cores: Indian Initiatives during 2008-2016. *Proceedings of the Indian National Science Academy* 90.
- Thamban, M., Chaturvedi, A., Rajakumar, A., Naik, S.S., D'Souza, W., Singh, A., et al., 2006. Aerosol perturbations related to volcanic eruptions during the past few centuries as recorded in an ice core from the Central Dronning Maud Land, Antarctica. *Current science* 91, 1200-1207.
- Thamban, M., Laluraj, C.M., Mahalinganathan, K., Redkar, B.L., Naik, S.S., Shrivastava, P.K., 2010. Glaciochemistry of surface snow from the Ingrid

- Christensen Coast, East Antarctica, and its environmental implications. *Antarctic Science* 22, 435-441.
- Thamban, M., Naik, S.S., Laluraj, C.M., Chaturvedi, A., Ravindra, R., 2013. Antarctic Climate Variability During the Past Few Centuries Based on Ice Core Records from Coastal Dronning Maud Land and Its Implications on the Recent Warming, in: Sinha, R., Ravindra, R. (Eds.), *Earth System Processes and Disaster Management*. Springer Berlin Heidelberg, Berlin, Heidelberg, pp. 51-66.
- Thamban, M., Rahaman, W., Laluraj, C.M., 2020. Millennial to quasi-decadal variability in Antarctic climate system as evidenced from high-resolution ice core records. *Current Science* 119, 255-264.
- Thomas, E.R., Abram, N.J., 2016. Ice core reconstruction of sea ice change in the Amundsen-Ross Seas since 1702 A.D. *Geophysical Research Letters* 43, 5309-5317.
- Thomas, E.R., Allen, C.S., Etourneau, J., King, A.C.F., Severi, M., Winton, V.H.L., et al., 2019. Antarctic Sea Ice Proxies from Marine and Ice Core Archives Suitable for Reconstructing Sea Ice over the Past 2000 Years. *Geosciences* 9, 506.
- Thomas, E.R., Bracegirdle, T.J., 2015. Precipitation pathways for five new ice core sites in Ellsworth Land, West Antarctica. *Climate Dynamics* 44, 2067-2078.
- Thomas, E.R., Bracegirdle, T.J., Turner, J., Wolff, E.W., 2013. A 308 year record of climate variability in West Antarctica. *Geophysical Research Letters* 40, 5492-5496.

- Thomas, E.R., van Wessem, J.M., Roberts, J., Isaksson, E., Schlosser, E., Fudge, T.J., et al., 2017. Regional Antarctic snow accumulation over the past 1000 years. *Climate of the Past* 13, 1491-1513.
- Thompson, D.W.J., Solomon, S., 2002. Interpretation of Recent Southern Hemisphere Climate Change. *Science* 296, 895-899.
- Thompson, D.W.J., Solomon, S., Kushner, P.J., England, M.H., Grise, K.M., Karoly, D.J., 2011. Signatures of the Antarctic ozone hole in Southern Hemisphere surface climate change. *Nature Geoscience* 4, 741.
- Thompson, D.W.J., Wallace, J.M., 2000. Annular Modes in the Extratropical Circulation. Part I: Month-to-Month Variability*. *Journal of Climate* 13, 1000-1016.
- Tian, C., Wang, L., Kaseke, K.F., Bird, B.W., 2018. Stable isotope compositions ($\delta^2\text{H}$, $\delta^{18}\text{O}$ and $\delta^{17}\text{O}$) of rainfall and snowfall in the central United States. *Scientific reports* 8, 6712.
- Todd, A., Collins, M., Lambert, F.H., Chadwick, R., 2018. Diagnosing ENSO and Global Warming Tropical Precipitation Shifts Using Surface Relative Humidity and Temperature. *Journal of Climate* 31, 1413-1433.
- Torrence, C., Compo, G.P., 1998. A Practical Guide to Wavelet Analysis. *Bulletin of the American Meteorological Society* 79, 61-78.
- Touzeau, A., Landais, A., Stenni, B., Uemura, R., Fukui, K., Fujita, S., et al., 2016. Acquisition of isotopic composition for surface snow in East Antarctica and the links to climatic parameters. *The Cryosphere* 10, 837-852.

- Trenberth, K.E., 1984. Signal Versus Noise in the Southern Oscillation. *Monthly Weather Review* 112, 326-332.
- Trenberth, K.E., Branstator, G.W., Karoly, D., Kumar, A., Lau, N.-C., Ropelewski, C., 1998. Progress during TOGA in understanding and modeling global teleconnections associated with tropical sea surface temperatures. *Journal of Geophysical Research: Oceans* 103, 14291-14324.
- Trenberth, K.E., Caron, J.M., 2000. The Southern Oscillation Revisited: Sea Level Pressures, Surface Temperatures, and Precipitation. *Journal of Climate* 13, 4358-4365.
- Turner, J., 2004. The El Niño–southern oscillation and Antarctica. *International Journal of Climatology* 24, 1-31.
- Turner, J., Colwell, S.R., Marshall, G.J., Lachlan-Cope, T.A., Carleton, A.M., Jones, P.D., et al., 2005. Antarctic climate change during the last 50 years. *International Journal of Climatology* 25, 279-294.
- Turner, J., Marshall, G.J., Clem, K., Colwell, S., Phillips, T., Lu, H., 2020. Antarctic temperature variability and change from station data. *International Journal of Climatology* 40, 2986-3007.
- Turner, J., Phillips, T., Marshall, G.J., Hosking, J.S., Pope, J.O., Bracegirdle, T.J., et al., 2017. Unprecedented springtime retreat of Antarctic sea ice in 2016. *Geophysical Research Letters* 44, 6868-6875.
- Turner, J., Phillips, T., Thamban, M., Rahaman, W., Marshall, G.J., Wille, J.D., et al., 2019. The Dominant Role of Extreme Precipitation Events in Antarctic Snowfall Variability. *Geophysical Research Letters* 46, 3502-3511.

- Uemura, R., Barkan, E., Abe, O., Luz, B., 2010. Triple isotope composition of oxygen in atmospheric water vapor. *Geophysical Research Letters* 37.
- Uemura, R., Masson-Delmotte, V., Jouzel, J., Landais, A., Motoyama, H., Stenni, B., 2012. Ranges of moisture-source temperature estimated from Antarctic ice cores stable isotope records over glacial–interglacial cycles. *Clim. Past* 8, 1109-1125.
- Uemura, R., Matsui, Y., Yoshimura, K., Motoyama, H., Yoshida, N., 2008. Evidence of deuterium excess in water vapor as an indicator of ocean surface conditions. *Journal of Geophysical Research: Atmospheres* 113.
- Urban, F.E., Cole, J.E., Overpeck, J.T., 2000. Influence of mean climate change on climate variability from a 155-year tropical Pacific coral record. *Nature* 407, 989-993.
- Van Den Broeke, M.R., Van Lipzig, N.P.M., 2003. Response of Wintertime Antarctic Temperatures to the Antarctic Oscillation: Results of a Regional Climate Model, *Antarctic Peninsula Climate Variability: Historical and Paleoenvironmental Perspectives*, pp. 43-58.
- van Wessem, J.M., van de Berg, W.J., Noël, B.P.Y., van Meijgaard, E., Amory, C., Birnbaum, G., et al., 2018. Modelling the climate and surface mass balance of polar ice sheets using RACMO2 – Part 2: Antarctica (1979–2016). *The Cryosphere* 12, 1479-1498.
- Vance, T.R., Kiem, A.S., Jong, L.M., Roberts, J.L., Plummer, C.T., Moy, A.D., et al., 2022. Pacific decadal variability over the last 2000 years and implications for climatic risk. *Communications Earth & Environment* 3, 33.

- Verdy, A., Marshall, J., Czaja, A., 2006. Sea Surface Temperature Variability along the Path of the Antarctic Circumpolar Current. *Journal of Physical Oceanography* 36, 1317-1331.
- Vimeux, F., Masson, V., Delaygue, G., Jouzel, J., Petit, J.R., Stievenard, M., 2001. A 420,000 year deuterium excess record from East Antarctica: Information on past changes in the origin of precipitation at Vostok. *Journal of Geophysical Research: Atmospheres* 106, 31863-31873.
- Vimeux, F., Masson, V., Jouzel, J., Stievenard, M., Petit, J.R., 1999. Glacial–interglacial changes in ocean surface conditions in the Southern Hemisphere. *Nature* 398, 410-413.
- Wang, S., Huang, J., He, Y., Guan, Y., 2014. Combined effects of the Pacific Decadal Oscillation and El Niño–Southern Oscillation on Global Land Dry–Wet Changes. *Scientific reports* 4, 6651.
- Wang, Y.-L., Hsu, Y.-C., Lee, C.-P., Wu, C.-R., 2019. Coupling Influences of ENSO and PDO on the Inter-Decadal SST Variability of the ACC around the Western South Atlantic. *Sustainability* 11, 4853.
- Wang, Y., Hou, S., Masson-Delmotte, V., Jouzel, J., 2009. A new spatial distribution map of $\delta^{18}\text{O}$ in Antarctic surface snow. *Geophysical Research Letters* 36.
- Welch, K.A., Mayewski, P.A., Whitlow, S.I., 1993. Methanesulfonic acid in coastal Antarctic snow related to sea-ice extent. *Geophysical Research Letters* 20, 443-446.

- Werner, M., Jouzel, J., Masson-Delmotte, V., Lohmann, G., 2018. Reconciling glacial Antarctic water stable isotopes with ice sheet topography and the isotopic paleothermometer. *Nature Communications* 9, 3537.
- Werner, M., Langebroek, P.M., Carlsen, T., Herold, M., Lohmann, G., 2011. Stable water isotopes in the ECHAM5 general circulation model: Toward high-resolution isotope modeling on a global scale. *Journal of Geophysical Research* 116.
- Winski, D.A., Fudge, T.J., Ferris, D.G., Osterberg, E.C., Fegyveresi, J.M., Cole-Dai, J., et al., 2019. The SP19 chronology for the South Pole Ice Core – Part 1: volcanic matching and annual layer counting. *Clim. Past* 15, 1793-1808.
- Winstrup, M., Svensson, A.M., Rasmussen, S.O., Winther, O., Steig, E.J., Axelrod, A.E., 2012. An automated approach for annual layer counting in ice cores. *Clim. Past* 8, 1881-1895.
- Xiao, C., Dou, T., Sneed, S.B., Li, R., Allison, I., 2015. An ice-core record of Antarctic sea-ice extent in the southern Indian Ocean for the past 300 years. *Annals of Glaciology* 56, 451-455.
- Xu, M., Yu, L., Liang, K., Vihma, T., Bozkurt, D., Hu, X., et al., 2021. Dominant role of vertical air flows in the unprecedented warming on the Antarctic Peninsula in February 2020. *Communications Earth & Environment* 2, 133.
- Yabuki, T., Suga, T., Hanawa, K., Matsuoka, K., Kiwada, H., Watanabe, T., 2006. Possible source of the antarctic bottom water in the Prydz Bay Region. *Journal of Oceanography* 62, 649-655.

- Yan, Y., Bender, M.L., Brook, E.J., Clifford, H.M., Kemeny, P.C., Kurbatov, A.V., et al., 2019. Two-million-year-old snapshots of atmospheric gases from Antarctic ice. *Nature* 574, 663-666.
- Yao, T.D., Petit, J.R., Jouzel, J., Lorius, C., Duval, P., 1990. Climatic Record From an Ice Margin Area in East Antarctica. *Annals of Glaciology* 14, 323-327.
- Yeh, S.-W., Cai, W., Min, S.-K., McPhaden, M.J., Dommenges, D., Dewitte, B., et al., 2018. ENSO Atmospheric Teleconnections and Their Response to Greenhouse Gas Forcing. *Reviews of Geophysics* 56, 185-206.
- Yeo, S.-R., Kim, K.-Y., 2015. Decadal changes in the Southern Hemisphere sea surface temperature in association with El Niño–Southern Oscillation and Southern Annular Mode. *Climate Dynamics* 45, 3227-3242.
- Yu, L., Zhong, S., Winkler, J.A., Zhou, M., Lenschow, D.H., Li, B., et al., 2017. Possible connections of the opposite trends in Arctic and Antarctic sea-ice cover. *Scientific reports* 7, 45804.
- Yuan, X., 2004. ENSO-related impacts on Antarctic sea ice: a synthesis of phenomenon and mechanisms. *Antarctic Science* 16, 415-425.
- Yuan, X., Kaplan, M.R., Cane, M.A., 2018. The Interconnected Global Climate System—A Review of Tropical–Polar Teleconnections. *Journal of Climate* 31, 5765-5792.

List of Publications

1. Rahaman, W., Chatterjee, S., **Ejaz, T.** and Thamban, M. (2019). Increased influence of ENSO on Antarctic temperature since the Industrial Era. *Scientific Reports* **9**, 6006. DOI: 10.1038/s41598-019-42499-x (**Impact Factor: 4.99**)
2. **Ejaz, T.**, Rahaman, W., Laluraj, C. M., Mahalinganathan, K., and Thamban, M. (2021). Sea ice variability and trends in the Western Indian Ocean sector of Antarctica during the past two centuries and its response to climatic modes. *Journal of Geophysical Research: Atmospheres*, 126. DOI: [10.1029/2020JD033943](https://doi.org/10.1029/2020JD033943) (**Impact Factor: 4.26**)
3. **Ejaz, T.**, Rahaman, W., Laluraj, C. M., Mahalinganathan, K., and Thamban, M. (2022). Rapid warming over east Antarctica since ~1940s caused by increasing influence of ENSO and SAM. *Frontiers in Earth Science*. DOI: 10.3389/feart.2022.799613 (**Impact Factor: 3.66**)
4. Mahalinganathan, K., Thamban, M., **Ejaz, T.**, Srivastava, R., Redkar, B L., and Laluraj, CM., (2022). Spatial variability and post-depositional diffusion of stable isotopes in high accumulation regions of East Antarctica. *Frontiers in Earth Science*. DOI: 10.3389/feart.2022.925447 (**Impact Factor: 3.66**)

Conference Presentations

1. **Ejaz, T.**, Rahaman, W., Laluraj, C. M., Mahalinganathan, K., and Thamban, M (2019). “Influence of extra-tropical climate modes and solar forcing on Antarctic ice core temperature during the last two centuries”, *International Conference on Climate Change Impacts, Vulnerabilities, and Adaptation*, IIT Kharagpur during 26th February – 02nd March 2019. (**Oral Presentation**)
2. **Ejaz, T.**, Rahaman, W., Laluraj, C. M., Mahalinganathan, K., and Thamban, M (2019). “Influence of extra-tropical climate modes and solar forcing on

Antarctic ice core temperature during the last two centuries”. *National Conference of Polar Sciences at NCPOR*, from 20th–22nd August 2019. **(Poster Presentation)**

3. **Ejaz, T.**, Rahaman, W., Laluraj, C. M., Mahalinganathan, K., and Thamban, M (2022). “Enhanced warming over Dronning Maud Land during the recent decades caused by coupled interactions between ENSO and SAM”, *10th SCAR Open Science Conference*, organized virtually during 01st–10th August 2022. **(Oral Presentation)**

4. **Ejaz, T.**, Rahaman, W., Laluraj, C. M., Mahalinganathan, K., Redkar B.L., and Thamban, M (2022). “Sea surface temperature variability over the western Indian Ocean sector of Antarctica during the past two centuries and its linkages to tropical-extratropical climate modes”. *3rd IPICS Open Science Conference* organized at **Crans-Montana, Switzerland** during 02nd–07th October 2022. **(Poster Presentation)**